UNIVERSITAT POLITÈCNICA
DE CATALUNYA

Feedback of Channel State Information in Multi-Antenna Systems Based on Quantization of Channel Gram Matrices

PhD Dissertation

Daniel Francisco Sacristán Murga

Centre Tecnològic de Telecomunicacions de Catalunya (CTTC)

e-mail: daniel.sacristan@cttc.es

Thesis Advisor: Dr. Antonio Pascual Iserte

Associate Professor

Universitat Politècnica de Catalunya (UPC)

e-mail: antonio.pascual@upc.edu

July 2012

This work was partially funded by the Centre Tecnològic de Telecomunicacions de Catalunya.

A mi familia,

Abstract

This dissertation deals with the proper design of efficient feedback strategies for Multiple-Input Multiple-Output (MIMO) communication systems. MIMO systems outperform single antenna systems in terms of achievable throughput and are more resilient to noise and interference, which are becoming the limiting factors in the current and future communications. Apart from the clear performance advantages, MIMO systems introduce an additional complexity factor, since they require knowledge of the propagation channel in order to be able to adapt the transmission to the propagation channel's characteristics and achieve optimum performance. This channel knowledge, also known as Channel State Information (CSI), is estimated at the receiver and sent to the transmitter through a limited feedback link.

In this dissertation, first, the minimum channel information necessary at the transmitter for the optimum precoding design is identified. This minimum information for the optimum design of the system corresponds to the channel Gram matrix. It is essential for the design of optimized systems to avoid the transmission of redundant feedback information. Following this idea, a quantization algorithm that exploits the differential geometry of the set of Gram matrices and the correlation in time present in most propagation channels is developed in order to greatly improve the feedback performance. This scheme is applied first to single-user MIMO communications, then to some particular multiuser scenarios, and finally it is extended to general multiuser broadcast communications. To conclude, the feedback link sizing is studied. An analysis of the tradeoff between size of the forward link and size of the feedback link is

formulated and the radio resource allocation problem, in terms of transmission energy, time, and bandwidth of the forward and feedback links is presented.

Resumen

En un mundo cada vez más interconectado, donde hay una clara tendencia hacia un mayor número de comunicaciones inalámbricas simultáneas (comunicaciones M2M: *Machine to Machine*, redes de sensores, etc.) y en el que las necesidades de capacidad de transmisión de los enlaces de comunicaciones aumentan de manera vertiginosa (audio, video, contenidos multimedia, alta definición, etc.) el problema de la interferencia se convierte en uno de los factores limitadores de los enlaces junto con los desvanecimientos del nivel de señal y las pérdidas de propagación. Por este motivo los sistemas que emplean múltiples antenas tanto en la transmisión como en la recepción (los llamados sistemas MIMO: *Multiple-Input Multiple-Output*) se presentan como una de las soluciones más interesantes para satisfacer los crecientes requisitos de capacidad y comportamiento relativo a interferencias.

Los sistemas MIMO permiten obtener un mejor rendimiento en términos de tasa de transmisión de información y a su vez son más robustos frente a ruido e interferencias en el canal. Esto significa que pueden usarse para aumentar la capacidad de los enlaces de comunicaciones actuales o para reducir drásticamente el consumo energético manteniendo las mismas prestaciones. Por otro lado, además de estas claras ventajas, los sistemas MIMO introducen un punto de complejidad adicional puesto que para aprovechar al máximo las posibilidades de estos sistemas es necesario tener conocimiento de la información de estado del canal (CSI: *Channel State Information*) tanto en el transmisor como en el receptor. Esta CSI se obtiene mediante estimación de canal en el receptor y posteriormente se envía al transmisor a través de un canal

de realimentación.

Esta tesis trata sobre el diseño del canal de realimentación para la transmisión de CSI, que es un elemento fundamental de los sistemas de comunicaciones del presente y del futuro. Las técnicas de transmisión que consideran activamente el efecto de la interferencia y el ruido requieren adaptarse al canal y, para ello, la realimentación de CSI es necesaria.

En esta tesis se identifica, en primer lugar, la mínima información sobre el estado del canal necesaria para implementar un diseño óptimo en el transmisor, con el fin de evitar transmitir información redundante y obtener así un sistema más eficiente. Esta información es la matriz de Gram del canal MIMO. Seguidamente, se desarrolla un algoritmo de cuantificación adaptado a la geometría diferencial del conjunto que contiene la información a cuantificar y que además aprovecha la correlación temporal existente en los canales de propagación inalámbricos. Este algoritmo se implementa y evalúa primero en comunicaciones MIMO punto a punto entre dos usuarios, después se implementa para algunos casos particulares con múltiples usuarios, y finalmente se amplía para el caso general de sistemas *broadcast* multi-usuario. Adicionalmente, esta tesis también estudia y optimiza el dimensionamiento del canal de realimentación en función de la cantidad de recursos radio disponibles, en términos de ancho de banda, tiempo y potencia de transmisión. Para ello presenta el problema de la distribución óptima de dichos recursos radio entre el enlace de transmisión de datos y el enlace de realimentación para transmisión de información sobre estado del canal como un problema de optimización.

Contents

List of Figures

Notation

Throughout this dissertation, boldface lowercase denote column vectors, bold uppercase denote matrices, and lowercase italics represent scalars. Besides, the following notation is used:

$\mathbb{R}, \mathbb{C}$	The set of real and complex numbers, respectively.
$\mathbb{R}^+$	The set of all strictly positive real numbers.
$\mathbb{R}^{N\times M}, \mathbb{C}^{N\times M}$	The set of $N \times M$ matrices with real- and complex-valued entries, respectively.
$f(x)\|_{x=a}$	Function $f(x)$ evaluated at x = a.
$\mathbb{E}\{\cdot\}$	Statistical expectation. When used with a subindex, it specifies the distribution over which the expectation is taken, e.g., $\mathbb{E}_x\{\cdot\}$ is the expectation over the distribution of a random variable x.
$\mathrm{tr}\{\mathbf{A}\}$	Trace of the matrix $\mathbf{A}$.
$\lvert\mathbf{A}\rvert$ or $\det(\mathbf{A})$	Determinant of the matrix $\mathbf{A}$.
$\mathfrak{Re}\{\cdot\}$	Real part operator.
$\mathfrak{Im}\{\cdot\}$	Imaginary part operator.
$\lVert\cdot\rVert_F$	Frobenius norm.

$\mathbf{A} \succ 0$	Matrix $\mathbf{A}$ is positive definite.
$\mathbf{A}^T$	Transpose of $\mathbf{A}$.
$\mathbf{A}^H$	Conjugate transpose (Hermitian) of $\mathbf{A}$.
$\mathbf{A}^{1/2}$	Hermitian square root of the positive semidefinite matrix $\mathbf{A}$, i.e., $\mathbf{A}^{1/2}\mathbf{A}^{1/2} = \mathbf{A}$.
$\mathbf{A}^{-1}$	Inverse of matrix $\mathbf{A}$.
$(\mathbf{A})^+$	Pseudo-inverse of matrix $\mathbf{A}$.
$a^\star$	Optimal value of variable a in an optimization problem.
$[\mathbf{A}]_{n,m}$	Matrix element located in row n and column m.
$\mathbf{D}_n$	Duplication matrix.
$\mathbf{C}_n$	Antiduplication matrix, defined as the unique matrix such that, for all $\mathbf{X} \in \mathbb{R}^{n\times n}$, $\mathsf{vec}(\mathbf{X} - \mathbf{X}^T) = \mathbf{C}_n\mathsf{veci}(\mathbf{X} - \mathbf{X}^T)$.
$\lambda_{\max}(\mathbf{A}), \lambda_i(\mathbf{A})$	Maximum eigenvalue and i-th eigenvalue (sorted in decreasing order), respectively, of matrix $\mathbf{A}$.
$\mathbf{u}_{\max}(\mathbf{A}), \mathbf{u}_i(\mathbf{A})$	Unitary eigenvector associated to the maximum and to the i-th eigenvalue, respectively, of matrix $\mathbf{A}$.
$\mathcal{P}(\mathbf{A}, N)$	Positive semidefinite projection operator, defined as: $\mathcal{P}(\mathbf{A}, N) \triangleq \sum_{i=1}^{N} \lambda_i(\mathbf{A})\mathbf{u}_i(\mathbf{A})\mathbf{u}_i(\mathbf{A})^H$, where $\mathbf{A}$ is an Hermitian matrix.
$\mathrm{vec}(\mathbf{A})$	Vector constructed by stacking the columns of matrix $\mathbf{A}$ from left to right.
$\mathrm{veci}(\mathbf{A})$	Vector constructed by stacking the elements of each column of matrix $\mathbf{A}$ that lie strictly below the main diagonal.
$\mathrm{vech}(\mathbf{A})$	Vector constructed by stacking the elements of each column of matrix $\mathbf{A}$ that lie on or below the main diagonal.

$\widetilde{\mathsf{vec}}\,(\cdot)$	$\left[\mathsf{vech}(\Re\mathrm{e}(\cdot))^T \mathsf{veci}(\Im\mathrm{m}(\cdot))^T\right]^T$.
arg	Argument.
$\min, \max$	Minimum and maximum, respectively.
$\frac{\partial f(\mathbf{x})}{\partial x_i}$	Partial derivative of function $f(\mathbf{x})$ with respect to the variable x_i.
$\frac{\partial f(\mathbf{x})}{\partial \mathbf{x}}$ or $\nabla_{\mathbf{x}} f(\mathbf{x})$	Gradient of function $f(\mathbf{x})$ with respect to vector $\mathbf{x}$.
$\mathbf{I}, \mathbf{I}_n$	Identity matrix and identity matrix of size n, respectively.
$\mathrm{blockdiag}(\{\mathbf{A_k}\})$	Block-diagonal matrix with diagonal blocks given by the set $\{\mathbf{A_k}\}$.
$\mathrm{diag}(a_1, ..., a_n)$	Diagonal matrix with the main diagonal given by $a_1, ..., a_n$.
α	Equal up to a scaling factor (proportional).
$\triangleq$	Defined as.
$\simeq$	Approximately equal.
$\mathsf{log}(\cdot)$	Natural logarithm.
$\mathsf{log}_a(\cdot)$	Base-a logarithm.
$\exp(\cdot)$	Exponential function.
$\mathrm{sign}(x)$	Sign function: $\mathrm{sign}(x) = \begin{cases} 1 & x > 0 \\ -1 & x < 0 \\ 0 & x = 0 \end{cases}$.
δ_{mj}	Kronecker delta: $\delta_{mj} = \begin{cases} 1 & m = j \\ 0 & m \neq j \end{cases}$.

$\mathcal{CN}(\mathbf{m}, \mathbf{C})$ Complex circularly symmetric Gaussian vector distribution with mean $\mathbf{m}$ and covariance matrix $\mathbf{C}$.

$\otimes$ Kronecker product. If $\mathbf{A}$ is $m \times n$, then

$$\mathbf{A} \otimes \mathbf{B} \triangleq \begin{pmatrix} [\mathbf{A}]_{1,1}\,\mathbf{B} & \dots & [\mathbf{A}]_{1,m}\,\mathbf{B} \\ \vdots & \ddots & \vdots \\ [\mathbf{A}]_{n,1}\,\mathbf{B} & \dots & [\mathbf{A}]_{n,m}\,\mathbf{B} \end{pmatrix}.$$

Acronyms

ABS	Access Base Station
AWGN	Additive White Gaussian Noise
BC	Broadcast Channel
BCH	Broadcast Data Channel
BD	Block Diagonalization
BER	Bit Error Rate
BLAST	Bell-Labs Layered Space-Time
BPSK	Binary Phase Shift Keying
BS	Base Station
CRC	Cyclic Redundancy Check
CSI	Channel State Information
CSIT	Channel State Information at the Transmitter
DPC	Dirty Paper Coding
DPCM	Differential Pulse Code Modulation
D-BLAST	Diagonal-BLAST

EMOS Eurecom MIMO Openair Sounder

FDD Frequency Division Duplex

HBS Hub Base Station

i.i.d. independent and identically distributed

LOS Line of Sight

MAC Multiple Access Channel

MI Mutual Information

MIMO Multiple-Input Multiple-Output

MISO Multiple-input Single-output

ML Maximum Likelihood

MRC Maximal Ratio Combining

MS Mobile Station

MSE Mean Square Error

MMSE Minimum Mean Square Error

NLOS Non-Line of Sight

OFDM Orthogonal Frequency-Division Multiplexing

QPSK Quadrature Phase Shift Keying

RF Radio Frequency

SCH Synchronization Symbol

SER Symbol Error Rate

SINR	Signal to Interference Plus Noise Ratio
SNR	Signal to Noise Ratio
STBC	Space-Time Block Code
STTC	Space-Time Trellis Code
SVD	Singular Value Decomposition
TDD	Time Division Duplex
UE	User Equipment
V-BLAST	Vertical-BLAST
vs.	versus

Chapter 1

Introduction

1.1 Motivation

We live in a world which is increasingly interconnected, and there is a clear trend towards more simultaneous wireless communications. There are not only human to human communications, but also machine to machine communications, wireless sensor networks, and a plethora of new services that require wireless transmission of some kind. The capacity requirements of the wireless connections are also rapidly growing, as services transmit increasing amounts of data (audio, video, high definition, etc.). In this context, Multiple-Input Multiple-Output (MIMO) communications, based on the simultaneous use of multiple antennas at the transmitter and the receiver, are considered one of the most suitable solutions due to the increased system capacity they can provide and their behavior against interference.

MIMO communication channels are known to provide significant gains in terms of system capacity [Tel99, Fos98] and resilience to fading [Ala98, Tar99a]. These gains depend strongly on the quantity and quality of the Channel State Information (CSI) which is available during the design, as studied in [Gol06, Mol11]. Obviously, the best performance is achieved when such CSI is complete and perfect, but this is a non-realistic solution, especially at the transmitter [Gol03]. In scenarios where channel

reciprocity does not hold, a feedback link with limited capacity can be used to send the CSI from the receiver to the transmitter, as depicted in Figure 1.1. The design of the feedback link is a fundamental element in current and future communication systems, and is the focus of this dissertation.

The use of a feedback link requires the digitalization and quantization of the information to be sent through it. In this sense, proper quantization procedures to be applied to the channel estimates have to be designed. Following this idea, and for the scenario of point-to-point MIMO communications, extensive work has been done over the Grassmannian manifold, which consists of points that represent the subspaces spanned by transmit beamforming matrices [Ede98]. Under the constraint of uniform power allocation among beams, quantization in this manifold as described in [Lov03, Rag07] is optimum for several criteria.

In more general cases where the power allocation is not constrained to be uniform, the optimum linear signalling scheme at the transmitter depends on the MIMO propagation channel matrix $\mathbf{H}$ through the MIMO channel Gram matrix, which is defined as $\mathbf{R}_H = \mathbf{H}^H\mathbf{H}$, for any quality measure such as Mutual Information (MI), Mean Square Error (MSE), Signal to Noise Ratio (SNR), or Bit Error Rate (BER), among others [Gol06, Mon10, Jaf01, Pal03b]. Note that in this case, the design is determined by the right singular vectors of the propagation channel matrix $\mathbf{H}$ (and not only on the subspace spanned by them, as happens when the power allocation is constrained to be uniform) in addition to the singular values. Taking this into account, the quantization to be applied prior to the feedback transmission should be performed over the set of Gram-like matrices, i.e., Hermitian and positive definite matrices (such as $\mathbf{R}_H$), instead of the Grassmannian manifold.

This dissertation presents a feedback technique based on a differential quantization algorithm to be applied to the channel Gram matrix as a whole, exploiting the intrinsic differential geometry of the set of positive definite Hermitian matrices and using geodesic curves. Each channel Gram matrix corresponds to a point in such

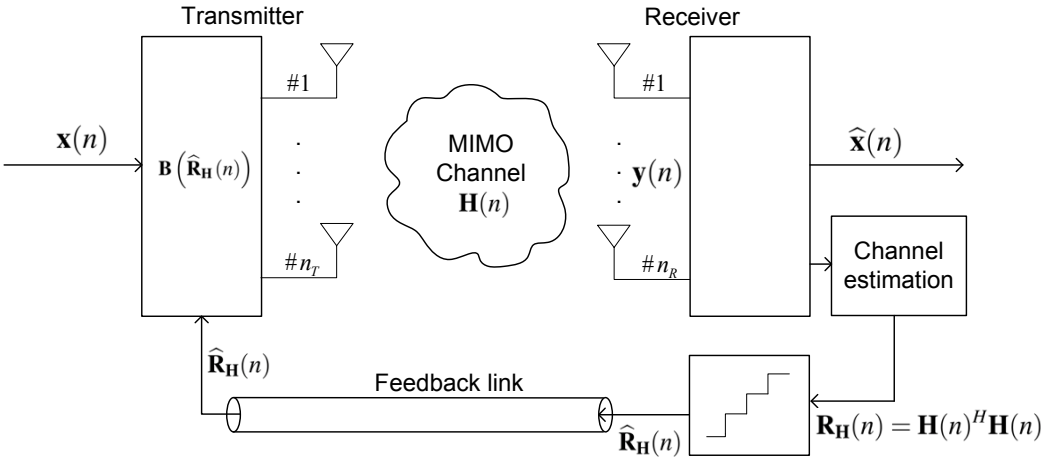

Figure 1.1: A feedback link with limited capacity is used to send the CSI from the receiver to the transmitter.

set and the variations at consecutive time instants are modeled to be along geodesic curves. One of the benefits of the feedback technique proposed in this dissertation is that the number of feedback bits required is independent of the number of antennas. Additionally, this strategy can be applied to any system configuration concerning the number of antennas at the transmitter and the receiver, even when the feedback load is constrained to a single bit.

The motivation for the development of feedback strategies is originally the single-user, point-to-point MIMO scenario. However, working in this topic suggested that the algorithms could be extended to other system topologies such as multi-user scenarios. Following this idea, a feedback algorithm for the multi-user Broadcast Channel (BC) featuring Block Diagonalization (BD) is also studied in this thesis. In the proposed scheme for the BC, the transmitter only needs to know the individual channel Gram matrices of each of the users. Another scenario with application of channel Gram matrix feedback deals with a network topology consisting of a radio-backhauling link and a wireless access link featuring aggressive frequency reuse. A system is considered, in which the radio-backhaul link has to be completely transparent to the access link, i.e., it should cause no interference to the access link while using the same frequencies

simultaneously. This can be achieved with the use of two different types of CSI sent through the feedback links, which correspond to the channel information and to the noise plus interference covariance matrix at the receiver. It is shown that the CSI required in both cases corresponds to a positive definite and Hermitian matrix which can be quantized using the approach developed in this thesis.

Furthermore, the proposed feedback architecture is then extended for its implementation in the general scenario of multiuser MIMO BC. This involves an additional linear transformation at the receiver in order to obtain an equivalent channel which is also known at the transmitter.

A numerical comparison with other feedback techniques is presented for the different simulation scenarios, including realistic propagation channels obtained through real measurements and also synthetic generated channels. Although the noise and delay of the feedback link are not considered in the system model and design, simulations of the effect that these factors would have on the performance are also presented.

Finally, an analysis on the distribution of radio resources between the feedback and the data communication links is presented. In practice, the radio resources allocated to the transmission of feedback are taken from the resources that are available for the forward data link. While the use of feedback improves the design of the transceiver increasing the performance, having less resources for the data link decreases the performance of the system. This tradeoff is presented and the resource allocation that maximizes the overall performance is derived for the case of point-to-point MIMO communications.

1.2 Outline of the dissertation

As commented previously, this dissertation deals with the design and optimization of the feedback link in MIMO wireless systems, and is structured as follows. This introductory chapter presents the motivation that led to this dissertation and enumerates

the research results of the dissertation.

Chapter 2 presents a general overview of MIMO communications and a brief description of the state of the art in CSI feedback techniques. It also provides the basic concepts that are used later during the dissertation.

Chapter 3 describes the proposed differential geodesic quantization and feedback algorithm for point-to-point MIMO communications, which exploits the time correlation of the propagation channel and the geometry of the set of Gram matrices. This algorithm is evaluated numerically through simulations and compared to other feedback schemes in the literature. The simulations consider both computer generated channel models and real channel measurements. The effect of CSI delay and transmission errors in the feedback link over the system performance is also studied.

Chapter 4 extends the application of the feedback algorithm to the case of multiuser MIMO systems, specifically: (i) the BC scenario featuring BD, and; (ii) a scenario which emerges from actual network planning in an all-wireless environment with aggressive frequency reuse. It is shown that these system designs allow the use of channel Gram matrix feedback in order to carry out the optimum precoder design. Simulations show a performance comparison with respect to other feedback schemes proposed in the literature.

Chapter 5 derives a generic transceiver design framework based on an equivalent channel computation. The proposed framework allows the application of the channel Gram matrix feedback technique to generic MIMO BC scenarios and also to systems that feature robust transceiver designs. This chapter presents an analytical study of the quantization error in order to obtain a model which allows the implementation of robust transceiver designs. Numerical simulations of the performance are also conducted and analyzed.

Chapter 6 studies a very important issue in wireless MIMO systems design with feedback, which is the feedback link sizing. The performance gains obtained by using feedback are compared to the cost of such feedback in terms of radio resources

(transmission time, power, and bandwidth). This comparison shows that there is a tradeoff between the forward data link and the feedback link regarding the radio resource allocation. This resource allocation tradeoff between the forward and feedback links is studied in order to optimally allocate the radio resources among the different communication phases: training and channel estimation, CSI feedback, and data transmission.

Finally, chapter 7 concludes the dissertation and describes some lines for future research.

1.3 Research contributions

This dissertation deals with the quantization and feedback of CSI in MIMO communication systems. The main contributions are the derivation of a differential quantization algorithm for channel Gram matrices based on geodesic curves, its applications to different scenarios, including point-to-point MIMO and multiuser MIMO, and an analysis of the feedback link sizing with respect to the forward data transmission link. These contributions have led to the following publications.

Chapter 3

This chapter deals with the point-to-point MIMO scenario with channel Gram matrix feedback. The main results are a differential quantization algorithm for Gram matrices based on geodesic curves and a performance analysis in scenarios based on real channel measurements and also synthetic channel models. This research led to the publication of three conference papers and one journal paper:

- D. Sacristán-Murga, F. Kaltenberger, A. Pascual-Iserte, and A. I. Pérez-Neira, "Differential feedback in MIMO communications: performance with delay and real channel measurements", in *Proceedings of the International ITG Workshop on Smart Antennas (WSA 2009)*, February 2009.

- D. Sacristán-Murga and A. Pascual-Iserte, "Differential feedback of MIMO channel correlation matrices based on geodesic curves", in *Proceedings of the IEEE International Conference Acoustics, Speech, Signal Processing (ICASSP 2009)*, April 2009.

- F. Kaltenberger, D. Sacristán-Murga, A. Pascual-Iserte, and A. I. Pérez-Neira, "Low-rate differential feedback for real measured temporally correlated MIMO channels", in *Proc. NEWCOM++ - ACoRN Joint Workshop*, April 2009.

- D. Sacristán-Murga and A. Pascual-Iserte, "Differential feedback of MIMO channel Gram matrices based on geodesic curves", *IEEE Trans. on Wireless Communications*, vol. 9, no. 12, pp. 3714–3727, December 2010.

Chapter 4

This chapter deals with some BC scenarios in which the feedback of the MIMO channel Gram matrix can be applied in a simple manner. The results from this chapter have been published in two conference papers:

- D. Sacristán-Murga and A. Pascual-Iserte, "Differential feedback of channel Gram matrices for block diagonalized multiuser MIMO systems", in *Proceedings of the IEEE International Conference on Communications (ICC 2010)*, May 2010.

- D. Sacristán-Murga and A. Pascual-Iserte, "Precoding and feedback schemes for a MIMO backhaul link in the presence of interference", in *Proceedings of the IEEE International Symposium on Personal, Indoor and Mobile Radio Communications (PIMRC 2010)*, September 2010.

Chapter 5

The fifth chapter contributes a general framework for the multiuser MIMO BC with feedback, and extends the application of the channel Gram matrix feedback presented in the previous chapter through the use of a novel equivalent channel transformation

applied at the receivers. These results have been published in one conference paper and one journal paper:

- D. Sacristán-Murga, M. Payaró, A. Pascual-Iserte, "Robust linear precoding for MSE minimization in MIMO broadcast systems with channel Gram matrix feedback", in *Proceedings of the IEEE International Workshop on Signal Processing Advances for Wireless Communications (SPAWC 2011)*, June 2011.

- D. Sacristán-Murga, M. Payaró and A. Pascual-Iserte, "Transceiver design framework for multiuser MIMO-OFDM broadcast systems with channel Gram matrix feedback", accepted for publication in *IEEE Trans. on Wireless Communications*, 2012.

Chapter 6

This chapter deals with the problem of resource allocation in terms of feedback link sizing. The tradeoff in performance due to the resource allocation among data and feedback links is analyzed and the effect of energy consumption in the base band is also evaluated. These research results have been published in three conference papers and a journal paper is under preparation:

- D. Sacristán-Murga and A. Pascual-Iserte, "Trade-off between feedback load for the channel state information and system performance in MIMO communications", in *Proceedings of the International ICST Conference on Mobile Lightweight Wireless Systems (MOBILIGHT 2010)*, May 2010.

- D. Sacristán-Murga, A. Pascual-Iserte and P. Tradacete, "Resource allocation between feedback and forward links: impact on system performance and CSI", in *Proceedings of the 19th European Signal Processing Conference (EUSIPCO 2011)*, September 2011.

- D. Sacristán-Murga, A. Pascual-Iserte and V. P. Gil Jiménez, "Resource allocation between feedback and forward MIMO links and energy consumption", in

Proceedings of the IEEE 76th Vehicular Technology Conference (VTC2012-Fall 2012), September 2012.

Chapter 2

Channel state information in MIMO communications

It is widely known that CSI is required both at the transmitter and at the receiver in order to fully exploit the potential, in terms of increased achievable throughput and resilience to fading, of MIMO communication channels [Gol03, Mol11, Jae09, PI05]. This CSI can be estimated at the receiver and then sent to the transmitter through a dedicated feedback link with limited capacity. In order to optimize the feedback transmission, the first task is to identify the content to be fed back, i.e., the CSI that is required at the transmitter, and then to derive a proper and efficient quantization procedure.

This chapter presents first a brief introduction to the MIMO wireless linear channel model considered in this dissertation, in order to identify the elements that could be subject to be CSI feedback. Then, it is shown that the specific required CSI depends on the type of transceiver design and system power constraints. According to this, in this chapter, the linear transceiver designs with no Channel State Information at the Transmitter (CSIT), with perfect CSIT, and with imperfect or partial CSIT are commented. Next, the effect in terms of performance degradation due to the use of imperfect CSIT is described. Finally, an overview of the state of the art in

quantization and feedback techniques for both the single-user point-to-point and the multiuser MIMO scenarios is presented.

2.1 The wireless linear MIMO channel

MIMO channels are present in both wired and wireless scenarios. However, this dissertation will focus only on the wireless case. In wired MIMO communications the characteristics of the physical propagation channel are usually time invariant and, therefore, the transmission schemes do not suffer from the challenges dealt with in this dissertation.

The MIMO channel is characterized by its transition probability density function, which describes the probability of receiving vector $\mathbf{y}$ conditioned on the fact that vector $\mathbf{x}$ was transmitted. This characterization is usually difficult to work with, and other simpler models are commonly used. One of the most broadly considered models is the linear MIMO channel. In this case, the output of the channel is modeled to be a linear function of the input. Additionally, the thermal noise which is present in the communication front-ends is modeled through a noise term $\mathbf{w}$. The transmit vector is handled at the transmitter through the linear precoding matrix $\mathbf{B}$. This results in the system model depicted in Figure 2.1, with an input-output relation given by

$$\mathbf{y} = \mathbf{HBx} + \mathbf{w} \in \mathbb{C}^{n_R}, \tag{2.1}$$

where $\mathbf{H} \in \mathbb{C}^{n_R \times n_T}$ represents the response of a channel with n_T and n_R transmit and receive antennas, respectively, such that the element $[\mathbf{H}]_{ij}$ denotes the channel path gain between the j-th transmit antenna and the i-th receive antenna, $\mathbf{x} \in \mathbb{C}^{n_S}$ are the n_S symbols to be transmitted, $\mathbf{B} \in \mathbb{C}^{n_T \times n_S}$ is the linear transmitter precoding matrix, $\mathbf{y} \in \mathbb{C}^{n_T}$ contains the symbols received at the receiver's antennas, and $\mathbf{w} \in \mathbb{C}^{n_R}$ is the noise term at the receiver.

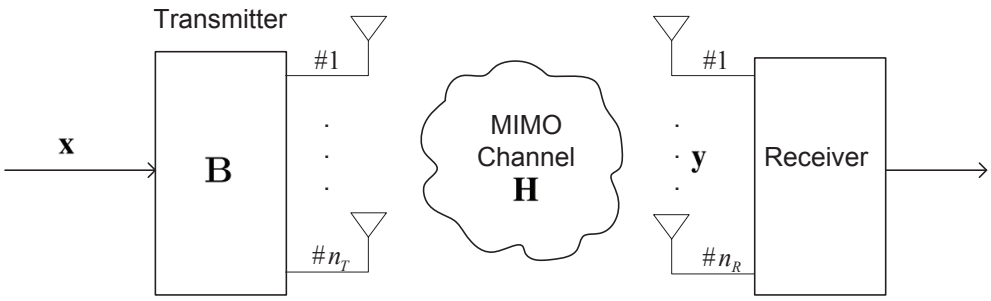

Figure 2.1: Linear MIMO channel model.

2.2 On the content and availability of CSI

The specific CSI to be fed back to the transmitter depends on the transmitter design, i.e., the optimality criterion used in the design of the transmit precoding matrix $\mathbf{B}$, which in fact depends on the quality criterion and the design constraints considered for the transceiver architecture. In works such as [Sca02, Lov05a, Lov05b] a peak power constraint is considered at the transmitter ($\lambda_{\max}(\mathbf{B}\mathbf{B}^H) \leq P_T$, where $\lambda_{\max}(\cdot)$ corresponds to the largest eigenvalue and P_T is the power constraint). As shown there, for many quality criteria, the columns of the resulting optimum transmission matrix are mutually orthogonal and have the same norm, i.e., the optimum power allocation is uniform. In this situation, [Sca02,Lov05a,Lov05b] show that the optimum codebook design for non-differential channel quantization and feedback is one where the codewords are the subspaces generated by the columns of the transmission matrices $\mathbf{B}$ and not by the matrices themselves. Following this idea, extensive work has been done over the Grassmannian manifold, which consists of points that represent the subspaces spanned by transmit beamforming matrices.

On the other hand, it is also of interest to consider a mean power constraint (i.e., the transmission matrix $\mathbf{B}$ is such that $\|\mathbf{B}\|_F^2 \leq P_T$), as in [Bog12, Pay09b] and references therein, for example [Shi08, Ral98]. In this case the resulting optimum precoder $\mathbf{B}$ depends on the singular values of the channel matrix $\mathbf{H}$ and also on the right singular vectors, but not on the left singular vectors (this is a direct consequence from the fact

that the most usual quality criteria[1], and consequently also the optimum transmit precoder $\mathbf{B}$, depend on the channel through its Gram matrix $\mathbf{R}_H = \mathbf{H}^H\mathbf{H}$). As also shown in those references, the optimum power allocation at the transmitter is in general not uniform [Bog12, Shi08]. This means that the channel Gram matrix is the element that contains the minimum required information for the optimum precoder design (i.e., both the eigenvectors and the eigenvalues of $\mathbf{R}_H$, see [Bou06])[2]. Following this criterion, the quantization should be applied over the set of Gram-like matrices, instead of the Grassmannian manifold.

Depending on the amount and quality of the CSI available at the transmitter and receiver, there are different transmission strategies that can be implemented. The most common scenario corresponds to the case where the receiver has perfect CSI, because the channel estimation process is conducted at the receiver. Regarding the CSIT there are three possible scenarios:

- No CSIT: There is not any knowledge of any parameter concerning the interference or the propagation channel at the transmitter. In this case, the best transmitter strategy consists in employing space-time codes [Bel05, Par08, Tar99b, Gan01].

- Perfect CSIT: There is full knowledge of the instantaneous channel realization and of the interference characteristics at the transmitter. In this case the potential of MIMO strategies can be exploited completely. There are many possible transceiver strategies [Ber08, Mol11, Pal03a] depending on the system design criterion or the system performance metric.

[1]Some of these quality criteria are mutual information, MSE, SNR, or BER, among others [Bog12, Shi08, Pay09b, Tel99, Ral98, Yan94].

[2]Note that decoupling the feedback in feedback of the power allocation and a feedback of the beamforming, this last being based on the Grassmann manifold, is not possible since, when non-uniform power allocation is applied, knowledge of the subspace spanned by the dominant right singular vectors is not enough (see [Shi08, Bog12, Pal03b, Tel99, Bou06]).

- Imperfect or partial CSIT: There is inaccurate or partial knowledge about the parameters describing the channel at the transmitter. This occurs, for example, due to the CSI quantization prior to the feedback transmission, or if there are transmission errors in the feedback link. In this case, the transmitter strategy depends on the quality and type of CSI available at the transmitter as shown in [NM11, Ron05, Tar09].

2.3 Transceiver designs

This section presents a brief background of some of the most relevant communication strategies for MIMO communications, for the different degrees of accuracy of the CSI available at the transmitter.

- Designs with no CSIT: From a conceptual perspective there are two approaches to transceiver designs. One option is to increase the transmission rate by exploiting the multiplexing gain. The other philosophy is that of the transmission schemes which are optimized to take advantage of the diversity gain provided by MIMO channels.

  Regarding the strategies that are focused on maximizing the multiplexing gain, the Bell-Labs Layered Space-Time (BLAST) family [Fos96] is among the most known. The most relevant from these are the Vertical-BLAST (V-BLAST) [Loz02] and the Diagonal-BLAST (D-BLAST) [Fos96]. In the V-BLAST scheme, different data streams are transmitted through each antenna. Each data stream is independently coded, and consequently the transmitter can send multiple data streams simultaneously and the final rate is increased. D-BLAST, on the other hand, also allows for coding across subchannels.

  Concerning the techniques that are focused on the diversity gain, the most significant strategies are Space-Time Block Codes (STBCs), which are decoded with

optimum performance if perfect CSI is available at the receiver. The first contribution in this field was given by Alamouti in [Ala98], who proposed a rate one orthogonal STBC for two transmit antennas. The main interest of orthogonal STBCs is that the optimum Maximum Likelihood (ML) detector can be decoupled into a set of parallel ML detectors with extremely reduced complexity based only on linear operations. This work was further generalized to any number of transmit antennas in [Tar99a, Gan01, Gan02, Sto02]. In these works it is shown that rate one orthogonal STBCs exist only for the case of two transmitting antennas. Either the rate one or the orthogonality properties must be dropped to be able to obtain a suitable STBC design in a scenario with a different number of antennas.

Finally, Space-Time Trellis Codes (STTCs) are codes that provide both coding and diversity gain. STTCs are based on transmission of redundant copies of a convolutional code distributed over time and over the number of transmit antennas [Tar98, Jaf03, Saf04]. They provide a very good performance at the cost of higher signal processing computational complexity, since they rely on a Viterbi decoder at the receiver while the STBCs need only linear processing. For this reason the STTCs are seldom adopted in current wireless communication systems.

- Designs with perfect CSIT: This case has been extensively studied by the research community [Gol06, Ber08, Mol11]. The case of linear transmitters and receivers has been generalized, under the framework of convex optimization, in [Pal03b]. With perfect CSI at the transmitter, typical objective functions, such as the minimization of the trace of the MSE matrix or the maximization of the mutual information, fall into two categories extracted from majorization theory: Schur-convex and Schur-concave functions [Mar79]. Following this idea, the design of any MIMO communications system can be framed, in a unified way,

into the powerful of theory of convex optimization and consequently, the design problem can be solved very efficiently.

- Designs with imperfect CSIT: In this situation, the imperfections in the available CSIT can be modeled and taken into account in the design process. This leads to the so called robust designs, such as [NM11, Ron06, Zha08, Bog11, PI06, Pay07]. In this case the transmitter can be designed, for example, following a worst-case approach, which optimizes the performance for the worst possible situation of the channel among the ones that are compatible with the CSIT; or designed following a Bayesian approach, which optimizes the best mean performance averaged over the unknown parameters of the CSIT.

2.4 Performance degradation with imperfect CSI at the transmitter

There are multiple studies on the system performance degradation caused by imperfect CSIT when compared to the case of perfect CSIT [Bas12, Zha09, MN08, Cho02a, Zho11]. The case where the transmitter applies a beamforming design assuming that the CSIT available is perfect is studied in [Cho02a, Cho02b] for a Rayleigh fading channel. The performance degradation is analyzed from a purely statistical Bayesian perspective [Kay93] in terms of the increase of the mean Chernoff upper bound of the probability of error averaged over the statistics of the actual channel conditioned to the channel estimate, taking into account the statistical behavior of the error in the CSI. This analysis concludes that there is a loss in the diversity order. Additionally, the following types of error are identified and described: noise from the own estimation process, quantization errors, and delay in the feedback of the channel estimate. The main conclusion is that depending on the quality of the CSI, it may be more adequate to follow a space-time coding strategy with no CSIT instead of a beamforming design

based on imperfect CSIT. The work in [MN08] presents an analytical study of the impact of feedback link transmission errors in terms of BER of combined beamforming and Maximal Ratio Combining (MRC) in slow Rayleigh fading channels, while [Zha09] focuses on the performance degradation caused by errors in the channel estimation process. A similar analysis is also carried out in [Bha02], which presents a degradation analysis in terms of outage mutual information in three different situations: imperfect CSI at the receiver and no CSI at the transmitter, perfect CSI at the receiver and quantized CSI at the transmitter, and imperfect CSI at the receiver and quantized CSI at the transmitter. The impact of CSI delay is studied analytically in [Bas12], and [Dab06] studies the performance loss and derives a bound on the capacity loss when using Gram matrix feedback with random codebooks and a fixed number of feedback bits.

2.5 Feedback strategies for point-to-point MIMO communications

In this section, a brief overview of the current research in quantization and feedback algorithms for MIMO communications is presented.

Quantization algorithms in the literature can be classified fundamentally according to two different criteria: if they exploit temporal correlation of the parameter to be quantized (i.e., differential versus non-differential quantization) and according to the objective of the quantization, which depends on the design criterion (for example, if the complete channel response matrix is to be sent through the feedback link or only the Gram of the channel matrix, or even just the subspace spanned by the dominant right singular vectors of the channel matrix).

Under a transmitter design constraint of uniform power allocation among beams, quantization in the Grassmannian manifold, which consists of points that represent the

subspaces spanned by transmit beamforming matrices, is optimum for several criteria [Lov03].

In more flexible designs where the power allocation is not constrained to be uniform, the optimum linear signalling scheme at the transmitter depends on the MIMO channel Gram matrix, i.e., $\mathbf{R}_H = \mathbf{H}^H\mathbf{H}$, for any quality measure such as mutual information, MSE, SNR, or BER, among others [Mol11, Bog11, Jaf01, Pal03b].[3] Note that in this case, the design is determined by the right singular vectors of the channel matrix $\mathbf{H}$ (and not only on the subspace spanned by them) in addition to the singular values. Taking this into account, the quantization should be applied over the set of Gram matrices, i.e., the set of Hermitian and positive definite matrices (such as $\mathbf{R}_H$).

2.5.1 Non-differential quantization techniques

Strategies based on non-differential quantization make use of a codebook, which is a collection of codewords or quantization candidates selected to maximize the distance between each other according to a design criterion. Each codeword corresponds to a possible precoding matrix for the system. The codebook is designed off-line and is known to both the transmitter and the receiver. If the statistics of the channel are known beforehand, they can be exploited to improve the design of the codebook. The receiver evaluates all the codewords with the current known channel and sends to the transmitter the index of the codeword that maximizes the system design criterion according to the current channel. The transmitter will then apply the precoder associated to such selected codeword.

Following this idea, extensive work has been done over the Grassmannian manifold. [Lov03] proposes a quantization technique called Grassmannian beamforming, which is based on codebooks built to maximize the distance between codewords belonging

[3] According to [Pal03b], any quality magnitude such as the MI, MSE, SNR, or BER can be expressed as a function of the MSE matrix $\mathbf{E} = \left(\mathbf{I} + \frac{1}{\sigma_w^2}\mathbf{B}^H\mathbf{R}_H\mathbf{B}\right)^{-1}$, where the covariance matrix of the zero-mean circularly symmetric complex Gaussian noise is given by $\mathbf{R}_\mathbf{w} = \mathbb{E}\{\mathbf{w}\mathbf{w}^H\} = \sigma_w^2\mathbf{I}$.

to the Grassmannian manifold [Ede98]. In [Roh06] the authors present an iterative method for constructing codebooks of also beamforming matrices with uniform power allocation that are optimized to minimize mutual information loss for a given SNR for general channel distributions.

While these techniques are conceptually simple and they usually require the lowest computational complexity, they have a fundamental drawback for the use in real systems. They are designed and optimized under the assumption that the CSI at consecutive time instants is independent, which is usually not true. Measurements show that there is a strong correlation in time of the parameters to be tracked, and some approaches have been developed based on hierarchical codebooks for progressive refinement of the quantization [Hea09] and also on feedback compression to reduce the redundancy of CSI fed back at consecutive time instants [Tar09, Hua06b, Ino09]. In [Pan07], different interpolation approaches and cluster-based precoding are performed in the Grassmannian manifold to exploit correlation in the propagation channel of OFDM subcarriers that are close in frequency.

2.5.2 Differential quantization techniques

Differential quantization techniques are based on exploiting the correlation in time present in the physical parameters of the propagation channel. Each feedback update sends quantized information on the difference between the last fed back estimate and the current channel. This means that the accuracy of the CSI at the transmitter improves with each feedback update, until it reaches an upper bound determined by the correlation factor of the channel and the feedback rate. Another advantage of differential feedback techniques is that they adapt easily to variable feedback rates, since most require only a minimum of 1 bit per feedback use.

In [Xia09] a CSI feedback scheme is presented which is based on Differential Pulse Code Modulation (DPCM) on each element of the matrix and the quantization is

related to the MIMO channel matrix **H**.

In [Yan07] the constraint of uniform power allocation is considered and a differential quantization algorithm is proposed. The technique involves defining a random geodesic curve over the Grassmannian manifold [Ede98] and indicating through 1 bit of feedback the direction that minimizes the distance to the optimum beamforming matrix, which is also a point in the manifold.

The technique from [Roh07] performs a parametrization of the channel singular vectors prior to the quantization to obtain statistically independent parameters, but suffers from propagation of the quantization error when reversing the transformation at the transmitter. The parameters are quantized component-wise following differential quantization scheme based on DPCM, and element-wise quantization of power allocation information is also considered.

Other recent techniques based on codebooks built on the Grassmannian manifold that exploit channel temporal correlation are [Hea09], which uses progressive refinement codebooks, [Ino09], which features channel prediction to reduce the feedback rate, [Kim11], which uses a spherical cap codebook with variable radius, and [Abe07, Kim08b], which consider a rotation based differential feedback built on top of a codebook in the Grassmannian manifold.

2.6 Feedback strategies in multiuser communications

There is a large amount of literature about feedback strategies for multiuser MIMO systems, both for the BC and also for the Multiple Access Channel (MAC). However, most of them feature CSI quantization algorithms similar to those described for the point-to-point scenario. In this section, an overview of some of the most important ones is presented.

Regarding the BC, in [Cha08] the authors propose a quantization and feedback of the channel Gram matrix for the featuring a direct quantization of each element of matrix $\mathbf{R}_H$ separately. [Tan07] presents a scheduling and feedback strategy that achieves multiuser diversity gain without substantial feedback requirements. The transmission strategy features per-antenna scheduling at the Base Station (BS), which maps each transmit antenna at the BS (equivalently, a spatial channel) to a user that deploys a zero-forcing receiver. An opportunistic feedback protocol is proposed to reduce the feedback requirements. For the case where the users have different priorities and also different degrees of CSI feedback, the work in [Muk12] presents a variation of the waterfilling algorithm that guarantees a minimum performance to each user depending on the set of priorities.

Concerning MIMO MACs, it is known that CSI at the transmitters allows to improve system performance regardless of whether it is perfect or partial [Yu04, Jor03, Kim08b, Soy09]. Examples of techniques that require the full channel response matrix knowledge at the transmitters are [Yu04, Jor03], while some other techniques use only the channel covariance information [Kim08b, Soy09], or just channel mean information [Soy09]. Since no communication between the transmitters is considered, the quantization and feedback algorithms for this scenario are performed using the same strategies as in the single-user scenario.

2.7 Chapter summary

This chapter has tried to give a reasonable brief introduction to the use of CSI in the design of MIMO communication systems in order to describe the working environment for the next chapters. The different degrees of CSI knowledge at the transmitter have been described, the linear model for MIMO channels has been presented, and a general overview of the different strategies available in the literature for the cases of perfect CSI, imperfect CSI, and no CSI has been commented. Finally a general overview of

the types of feedback, including differential and non differential feedback, has been provided, and some particular algorithms from the literature have been described.

Chapter 3

Differential feedback of channel Gram matrices using geodesic curves

3.1 Introduction

The previous chapter showed the motivation for the development of a feedback scheme for MIMO communications based on the quantization of the channel Gram matrix. In the literature there are multiple works that focus on the feedback of such matrix. For example, in [Cha08] the authors propose the feedback of the channel Gram matrix featuring a direct quantization of each element of matrix $\mathbf{R}_H$ separately[1]. In [Dab06], a feedback based on channel Gram matrix quantization is assumed exploiting random codebooks and a bound in the capacity loss is derived. [Kim08a, Jaf01] also assume feedback of the channel Gram matrix for the design of the precoder for the sum-rate maximization criterion and derive the capacity region for the particular case of

[1] In [Cha08] a multi-user scenario is considered, where each channel Gram matrix is quantized and fed back independently for each user. The quantization procedure described in such work can also be applied to the single-user point to point MIMO case directly.

single beamforming transmission. The work in [Kim11] proposes a differential strategy featuring a spherical cap codebook with a radius that adapts to the statistics of the directional variation.

The technique presented in this chapter is based on a differential quantization algorithm to be applied to the channel Gram matrix as a whole, exploiting the intrinsic differential geometry of the set of positive definite Hermitian matrices and using geodesic curves. The work in [Bou06] also uses the concept of geodesic curves in the set of Gram-like matrices, but the application is for channel classification instead of differential quantization.

In the quantization technique proposed in this chapter each channel Gram matrix corresponds to a point in such set and the variations at consecutive time instants are modeled to be along geodesic curves. For each feedback transmission, the algorithm defines a set of random orthogonal geodesic curves centered at the point in the set corresponding to the last fed back channel Gram matrix, and identifies a set of points along these curves which are the quantization candidates. The number of candidates is determined by the number of feedback bits, and the selection of the point to be fed back depends on the cost function associated to the adopted quality criterion for the precoder design. One of the benefits of this technique is that the feedback overhead is independent of the number of antennas, even when the feedback load is constrained to 1 bit.

Since the generation of the geodesic curves has a random component, an analysis of the expectation and variance of the direction associated to the random route followed by the algorithm is also presented in this chapter. A numerical comparison with other feedback techniques is shown for different simulation scenarios, featuring both synthetic generated channels and real channel measurements.

This chapter is organized as follows. The system and signal models are given in section 3.2. Section 3.3 introduces the geometry of the space of Gram matrices, whereas the description of the algorithm follows in section 3.4. Section 3.5 is devoted

to the study of the expectation and variance of the directions taken by the algorithm compared to the gradient of the cost function associated to the design criterion. Simulations of the performance are shown in section 3.6, including the effect of delay and transmission errors in the feedback link. Finally, the last section summarizes the results of the chapter.

3.2 System and signal models

This chapter assumes the system model described in chapter 1 and depicted in Figure 1.1, which is reproduced here again as Figure 3.1, i.e., a flat fading MIMO channel with n_T and n_R transmit and receive antennas, respectively, represented at time instant n by $\mathbf{H}(n) \in \mathbb{C}^{n_R \times n_T}$. The n_R received signals at the same time instant, assuming a linear transmitter, can be modeled as

$$\mathbf{y}(n) = \mathbf{H}(n)\mathbf{B}\big(\widehat{\mathbf{R}}_H(n)\big)\mathbf{x}(n) + \mathbf{w}(n) \in \mathbb{C}^{n_R}, \tag{3.1}$$

where $\mathbf{x}(n) \in \mathbb{C}^{n_S}$ are the n_S streams of signals transmitted with $\mathbb{E}\left\{\mathbf{x}(n)\mathbf{x}^H(n)\right\} = \mathbf{I}$, and $\mathbf{B} \in \mathbb{C}^{n_T \times n_S}$ is the linear transmitter precoding matrix that must satisfy the mean transmit power constraint $\|\mathbf{B}\|_F^2 \leq P_T$. Note that it is explicitly expressed that $\mathbf{B}$ depends on the available estimate of the channel Gram matrix $\widehat{\mathbf{R}}_H(n)$, where the exact matrix is defined as $\mathbf{R}_H(n) = \mathbf{H}^H(n)\mathbf{H}(n)$. The Additive White Gaussian Noise (AWGN) at the receiver is represented by $\mathbf{w}(n) \in \mathbb{C}^{n_R}$ with $\mathbb{E}\big\{\mathbf{w}(n)\mathbf{w}^H(n)\big\} = \sigma_w^2\mathbf{I}$.

It is assumed that the receiver knows the current channel matrix $\mathbf{H}(n)$, and that the transmitter applies a naive design[2] of $\mathbf{B}$ assuming that the available CSI at its side, is perfect, as in [Mon06a, Mon06b, Sad06, Roh06, Roh07, Yan07, Hea09, Ino09,

[2]In this chapter a naive design is considered and not a robust design that takes into account explicitly the presence of noise or errors in the available CSI, since the scope of this chapter is on the feedback itself and not on the design of the transmitter. Note, however, that an extension to robust designs could also be considered by a proper definition of the cost function g, that will be defined next.

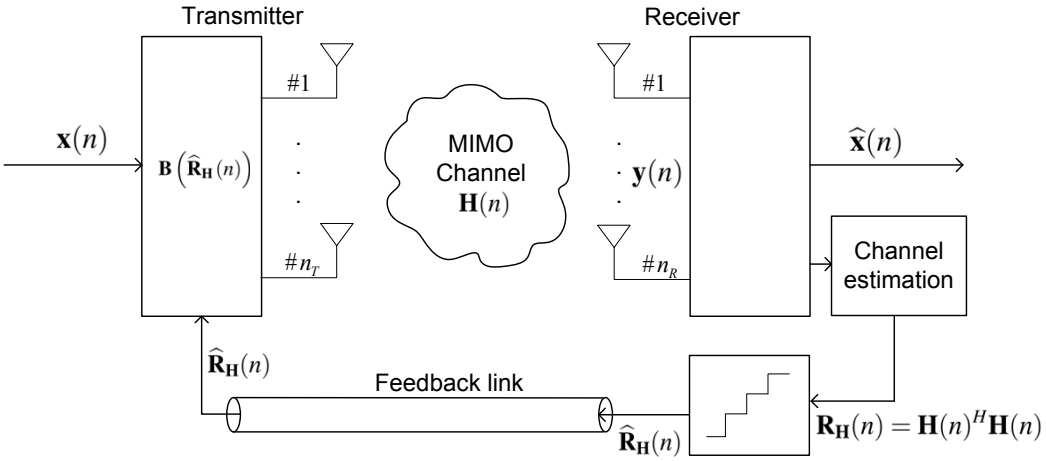

Figure 3.1: Point-to-point MIMO system model.

Cha08, Ban03a, Lov03, Hua06a][3]. The presence of errors and delay in the feedback link is not considered in the system model and the design, however, in order to give some insight into the effect that delay and noise in the feedback link would have on the system, numerical simulations are performed in section 3.6. The transmitter design can be performed according to different criteria, such as the maximization of the MI or the SNR, or the minimization of the MSE or the BER, among others. In all the cases, the optimum precoder matrix $\mathbf{B}$ has been shown to depend only on the channel Gram matrix $\mathbf{R}_H(n)$ [Pay09b,Pal03b]. For each design criterion a *cost function* $g\big(\widehat{\mathbf{R}}_H(n), \mathbf{H}(n)\big)$ can be defined, such that the design objective is its minimization. Some examples of cost functions are given next[4] (the dependency with respect to the time index n is dropped for the sake of clarity in the notation) [Pal03b, PI04]:

- *Maximization of the SNR with single beamforming ($n_S = 1$):*

$$g\big(\widehat{\mathbf{R}}_H(n), \mathbf{H}(n)\big) = -\frac{1}{\sigma_w^2}\left\|\mathbf{HB}\right\|_F^2, \tag{3.2}$$

[3]To the best of the author's knowledge this assumption is common to all work regarding limited feedback up to date. The generalization of this assumption is still an open research topic.

[4]Note that the focus of this thesis is not on the definition of the cost function, but on the minimization of *any* cost function g that depends simultaneously on the estimated channel Gram matrix available at the transmitter and the actual propagation channel.

and the optimum transmission matrix $\mathbf{B} \in \mathbb{C}^{n_T \times 1}$ is given by [Lo99]:

$$\mathbf{B}_{\text{SNR}}\big(\widehat{\mathbf{R}}_H(n)\big) = \sqrt{P_T}\mathbf{u}_{\max}\big(\widehat{\mathbf{R}}_H(n)\big), \tag{3.3}$$

where $\mathbf{u}_{\max}(\cdot)$ stands for the unit-norm eigenvector of maximum associated eigenvalue [Lo99].

- *Maximization of the mutual information:*

$$g\big(\widehat{\mathbf{R}}_H(n), \mathbf{H}(n)\big) = -\mathsf{log}_2 \left| \mathbf{I} + \frac{1}{\sigma_w^2}\mathbf{B}\mathbf{B}^H\mathbf{H}^H\mathbf{H} \right|, \tag{3.4}$$

and in this case the optimum transmission matrix $\mathbf{B} \in \mathbb{C}^{n_T \times n_S}$ is given by [Ral98, Cov06]:

$$\mathbf{B}_{\text{MI}}\big(\widehat{\mathbf{R}}_H(n)\big) = \widetilde{\mathbf{U}}(n)\mathbf{P}^{1/2}(n), \;\; \mathbf{P}(n) = \text{diag}(p_1, \ldots, p_{n_S}), \tag{3.5}$$

and the columns of $\widetilde{\mathbf{U}}(n)$ are the n_S orthonormal eigenvectors of $\widehat{\mathbf{R}}_H(n)$ associated to its n_S maximum eigenvalues $\{\lambda_i\}_{i=1}^{n_S}$. The power $\mathbf{P}(n)$ is allocated according to the waterfilling solution ($p_i = \max\{0, \mu - 1/\lambda_i\}$ where μ is a constant such that $\sum_{i=1}^{n_S} p_i = P_T$) [Ral98, Cov06].

Section 3.4 in this chapter is devoted to describing an algorithm for quantizing the actual channel Gram matrix $\mathbf{R}_H$ (instead of $\mathbf{H}$). Since $\mathbf{R}_H$ belongs to the set of Hermitian positive definite matrices[5] (i.e., $\mathbf{R}_H \succ \mathbf{0}$), exploiting the inherent geometry of this set will improve the performance of the quantization. Section 3.3 describes the main differential geometry concepts used in the algorithm.

[5]In the following it will be assumed that the channel Gram matrix is strictly positive definite. If this cannot be guaranteed because, for example, $n_R < n_T$, it is possible to work straightforwardly with extended Gram matrices defined as $\widetilde{\mathbf{R}}_H = \mathbf{H}^H\mathbf{H} + \epsilon\mathbf{I}$, for any $\epsilon > 0$, which are positive definite by construction. This is done by adding $\epsilon\mathbf{I}$ to the channel Gram matrix before the quantization is carried out at the receiver, and subtracting $\epsilon\mathbf{I}$ from the received feedback at the transmitter.

3.3 Geometry of the set of Hermitian positive definite matrices

One of the key advantages of the quantization algorithm presented in this dissertation is the fact that it exploits explicitly the specific geometry of the domain space, which is the set of Hermitian positive definite matrices. This section introduces the basic differential geometry concepts that are used in the derivations presented in next section.

The set of Hermitian positive definite matrices $\mathcal{S} = \left\{\mathbf{R} \in \mathbb{C}^{n\times n} : \mathbf{R}^H = \mathbf{R}, \mathbf{R} \succ \mathbf{0}\right\}$ has the geometry of a convex cone [Tal07], i.e., $\forall \mathbf{R}_1, \mathbf{R}_2 \in \mathcal{S}, \forall s \geq 0,\ \mathbf{R}_1 + s\mathbf{R}_2 \in \mathcal{S}$, whose vertex is the identity matrix. The characterization of this set is described properly by means of differential geometry, which states a set of definitions for the distance, scalar products, and routes within this set [Tal07, Pen06a][6]:

- *Scalar product and norm:* Consider the scalar product between two Hermitian matrices $\mathbf{A}$ and $\mathbf{B}$ at any point $\mathbf{R}$ (also named as *base point*) in this set $\mathcal{S}$. Following [Pen06b], the scalar product is required to be invariant by the action of any transformation: $\langle \mathbf{A}, \mathbf{B}\rangle_{\mathbf{R}} = \langle \mathbf{\Sigma A}, \mathbf{\Sigma B}\rangle_{\mathbf{\Sigma R}}$ for all $\mathbf{\Sigma}$ in the linear group GL_n. This is verified in particular by the following definition of scalar product, whose use has been proposed also in [Tal07] and [Pen06b]:

$$\begin{aligned} \langle \mathbf{A}, \mathbf{B}\rangle_{\mathbf{R}} &= \mathrm{tr}\left\{\mathbf{R}^{-1/2}\mathbf{A}\mathbf{R}^{-1}\mathbf{B}\mathbf{R}^{-1/2}\right\} \\ &= \mathrm{tr}\left\{\mathbf{R}^{-1}\mathbf{A}\mathbf{R}^{-1}\mathbf{B}\right\}. \end{aligned} \tag{3.6}$$

  From this definition of scalar product it follows that the norm is defined as $\|\mathbf{A}\|_{\mathbf{R}} = \sqrt{\mathrm{tr}\left\{\mathbf{R}^{-1}\mathbf{A}\mathbf{R}^{-1}\mathbf{A}\right\}}$.

[6] Actually, reference [Tal07] is devoted to the case of real symmetric positive definite matrices, although the results and conclusions can be extended directly to the complex case just by replacing the transpose operator with the Hermitian operator. An illustrative example of the use of such extension can be found in [Bou06].

- *Geodesic curve:* The geodesic curve $\mathbf{\Gamma}(t)$, which is the curve connecting two points $\mathbf{R}_1$ and $\mathbf{R}_2$ in the set $\mathcal{S}$ with minimum length and with all its points belonging to $\mathcal{S}$, is given by [Tal07]

$$\mathbf{\Gamma}(t) = \mathbf{R}_1^{1/2} \exp\big(t\mathbf{C}\big)\mathbf{R}_1^{1/2}, \tag{3.7}$$

where $\mathbf{C} = \mathbf{C}^H = \mathsf{log}\big(\mathbf{R}_1^{-1/2}\mathbf{R}_2\mathbf{R}_1^{-1/2}\big)$, $\mathbf{\Gamma}(0) = \mathbf{R}_1$, and $\mathbf{\Gamma}(1) = \mathbf{R}_2$. The derivative of the geodesic curve at $t = 0$, which is in fact the direction of such curve at $t = 0$, is given by the Hermitian matrix $\dot{\mathbf{\Gamma}}(0) = \mathbf{R}_1^{1/2}\mathbf{C}\mathbf{R}_1^{1/2}$, also called *velocity matrix*.

- *Geodesic distance:* The geodesic distance between any two points in $\mathcal{S}$ is given by the length of the geodesic arc that connects them. It can be shown that this distance is given by [Tal07]:

$$\mathrm{dist}_g(\mathbf{\Gamma}(0), \mathbf{\Gamma}(t)) = |t|\|\mathbf{C}\|_F, \;\Rightarrow\; \mathrm{dist}_g(\mathbf{R}_1, \mathbf{R}_2) = \|\mathbf{C}\|_F, \tag{3.8}$$

or, using an equivalent expression, $\mathrm{dist}_g(\mathbf{R}_1, \mathbf{R}_2) = \big(\sum_i |\mathsf{log}\lambda_i|^2\big)^{1/2}$, where $\{\lambda_i\}$ are the eigenvalues of matrix $\mathbf{R}_1^{-1/2}\mathbf{R}_2\mathbf{R}_1^{-1/2}$.

- *Orthogonality between two geodesic curves:* Consider two geodesic curves $\mathbf{\Gamma}_1(t) = \mathbf{R}^{1/2} \exp\big(t\mathbf{C}_1\big)\mathbf{R}^{1/2}$ and $\mathbf{\Gamma}_2(t) = \mathbf{R}^{1/2} \exp\big(t\mathbf{C}_2\big)\mathbf{R}^{1/2}$ that cut each other at point $\mathbf{R}$ at $t = 0$. We say that they are orthogonal if their directions at $t = 0$ are orthogonal, i.e., $\langle \dot{\mathbf{\Gamma}}_1(0), \dot{\mathbf{\Gamma}}_2(0)\rangle_{\mathbf{R}} = 0$, which, from the equation of the derivative and (3.6), can be written as:

$$\begin{aligned} \mathrm{tr}\left\{\mathbf{R}^{-1}\mathbf{R}^{1/2}\mathbf{C}_1\mathbf{R}^{1/2}\mathbf{R}^{-1}\mathbf{R}^{1/2}\mathbf{C}_2\mathbf{R}^{1/2}\right\} &= 0 \\ \iff \mathrm{tr}\left\{\mathbf{C}_1\mathbf{C}_2\right\} &= 0. \end{aligned} \tag{3.9}$$

3.4 Quantization and feedback algorithm

This section presents a feedback algorithm based on a differential quantization of the channel Gram matrix $\mathbf{R}_H(n)$. Its objective is to minimize the cost function g as

presented in section 3.2.[7]

The channel Gram matrices are points in the set of Hermitian positive definite matrices, and variations at consecutive time instants are modeled to be along geodesic curves in the set. Following this idea, the presented algorithm quantizes the geodesic trajectory connecting points in the set, as it is explained next.

3.4.1 Algorithm description

The proposed differential quantization algorithm for the feedback of the channel Gram matrix is composed of 4 steps, which are performed at every feedback update. The steps for feedback interval n are described as:

- ***Initial situation:*** The receiver has a perfect knowledge of the current channel matrix $\mathbf{H}(n)$. Both the transmitter and the receiver know which is the last quantization of the channel Gram matrix sent through the feedback channel $\widehat{\mathbf{R}}_H(n-1)$. At the first feedback transmission the algorithm starts from the cone vertex: $\widehat{\mathbf{R}}_H(0) = \mathbf{I}$.

- ***Step 1:*** Both the receiver and the transmitter use a common set of Q random Hermitian matrices $\{\tilde{\mathbf{C}}_i\}_{i=1}^{Q}$ that satisfy the following constraint: $\mathrm{tr}\left\{\tilde{\mathbf{C}}_m\tilde{\mathbf{C}}_j\right\} = \delta_{mj}$, as in (3.9). Then, each Hermitian matrix $\tilde{\mathbf{C}}_i$ is re-scaled individually by Δ, the quantization step[8]: $\mathbf{C}_i = \Delta\tilde{\mathbf{C}}_i$.

- ***Step 2:*** Both the receiver and the transmitter use the previous matrix $\widehat{\mathbf{R}}_H(n-1)$ to generate a common set of Q geodesic curves $\{\mathbf{\Gamma}_i(t)\}_{i=1}^{Q}$, all of them having

[7] The cost function g is related to the quality measure of the system. If the receiver does not know which is the design criterion that the transmitter will apply, an alternative cost function that can be used for the quantization is the geodesic distance between the actual channel Gram matrix and its fed back estimate, i.e., $g(\widehat{\mathbf{R}}_H(n), \mathbf{H}(n)) = \mathrm{dist}_g(\widehat{\mathbf{R}}_H(n), \mathbf{H}^H(n)\mathbf{H}(n))$.

[8] The quantization step Δ, known at the transmitter and the receiver, is constant, computed and optimized offline given the channel statistics. The choice of Δ and its impact on the performance is studied in section 3.6.1.

the same initial point $\widehat{\mathbf{R}}_H(n-1)$ and with orthogonal directions (note that the maximum number of orthogonal routes is given by the dimension of the set of Hermitian matrices, i.e., $Q \leq n_T^2$):

$$\mathbf{\Gamma}_i(t) = \widehat{\mathbf{R}}_H^{1/2}(n-1) \exp\left(t\mathbf{C}_i\right) \widehat{\mathbf{R}}_H^{1/2}(n-1). \tag{3.10}$$

- ***Step 3:*** Each of these geodesic curves is used to generate two candidates for the feedback:

$$\begin{cases} \widehat{\mathbf{R}}_H^{(2i-1)}(n) &= \mathbf{\Gamma}_i(-1), \qquad 1 \leq i \leq Q, \\ \widehat{\mathbf{R}}_H^{(2i)}(n) &= \mathbf{\Gamma}_i(1), \qquad 1 \leq i \leq Q. \end{cases} \tag{3.11}$$

- ***Step 4:*** The receiver, which is assumed to know $\mathbf{H}(n)$, evaluates the cost function for each of the candidates, selects the one that minimizes it, and sends the corresponding index i_{FB} through the feedback channel to the transmitter (therefore, the number of feedback bits has to be higher than or equal to $\mathsf{log}_2(2Q)$): $i_{FB} = \arg\min_i g(\widehat{\mathbf{R}}_H^{(i)}(n), \mathbf{H}(n)), \;\; 1 \leq i \leq 2Q$. The selected matrix will then be used for the transmitter design and as the starting point in the next feedback computation:

$$\widehat{\mathbf{R}}_H(n) = \widehat{\mathbf{R}}_H^{(i_{FB})}(n). \tag{3.12}$$

Figure 3.2 shows an illustrative example of the differential quantization process using 2 bits. Starting from $\widehat{\mathbf{R}}_H(n-1)$ (Figure 3.2.a), the algorithm generates 2 geodesic routes $\mathbf{\Gamma}_1(t)$ and $\mathbf{\Gamma}_2(t)$ with orthogonal velocity matrices $\dot{\mathbf{\Gamma}}_1(0)$ and $\dot{\mathbf{\Gamma}}_2(0)$, respectively (Figure 3.2.b,c). The four quantization candidates are: $\widehat{\mathbf{R}}_H^{(1)}(n) = \mathbf{\Gamma}_1(-1)$, $\widehat{\mathbf{R}}_H^{(2)}(n) = \mathbf{\Gamma}_1(1)$, $\widehat{\mathbf{R}}_H^{(3)}(n) = \mathbf{\Gamma}_2(-1)$, and $\widehat{\mathbf{R}}_H^{(4)}(n) = \mathbf{\Gamma}_2(1)$ (Figure 3.2.d). At the receiver, each candidate is evaluated in terms of the cost function and the one minimizing it is selected. In this case, and for illustrative purposes, the optimization criterion is the minimization of the geodesic distance to the actual channel Gram matrix and, therefore, candidate 3 is chosen (Figure 3.2.e). That is, the index $i_{FB} = 3$ is fed back to the transmitter and $\widehat{\mathbf{R}}_H(n) = \widehat{\mathbf{R}}_H^{(3)}(n)$. The quantization for the next feedback

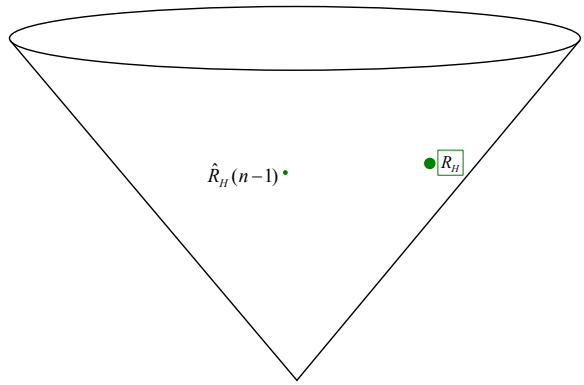

(a) Initial situation

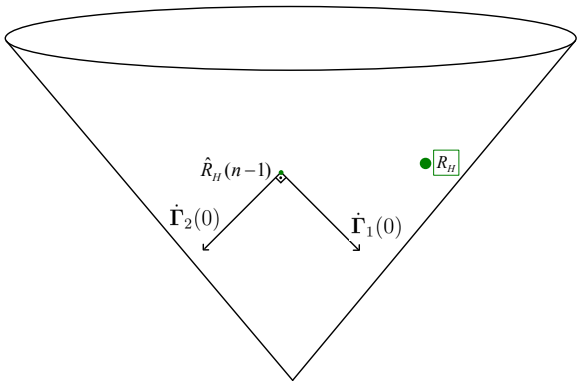

(b) Step 1

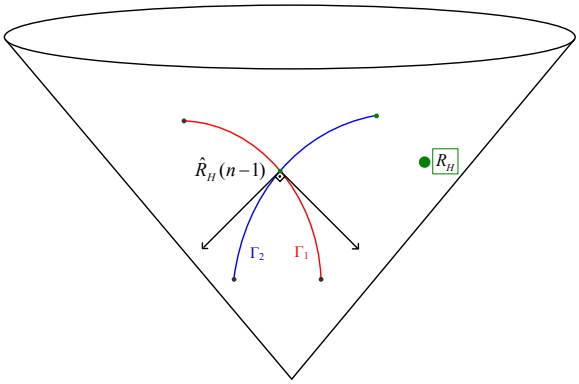

(c) Step 2

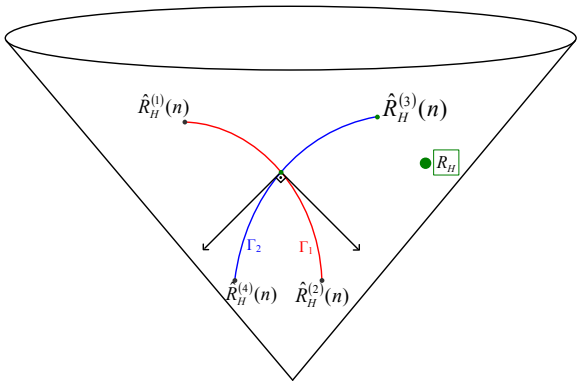

(d) Step 3

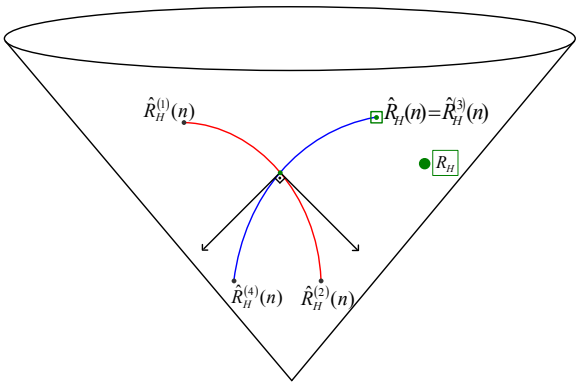

(e) Step 4

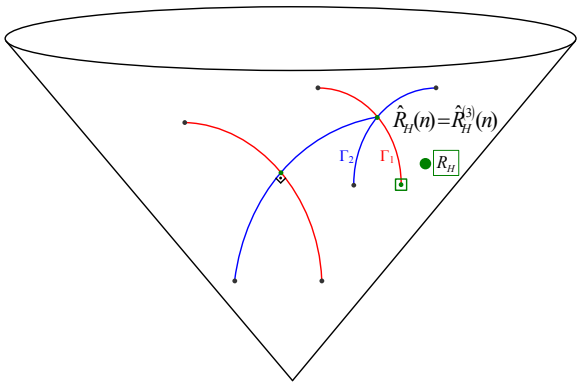

(f) Next time instant

Figure 3.2: Example of one feedback computation in a 2-bit differential quantization, using as optimization criterion the minimization of the geodesic distance to the actual channel Gram matrix.

update starts from this point, generates 2 orthogonal routes and four quantization candidates, selects the closest candidate to $\mathbf{R}_H$, and so on (Figure 3.2.f).

3.4.2 Computational complexity

In order to reduce the computational complexity required for the algorithm, matrices $\{\tilde{\mathbf{C}}_i\}$ can be conveyed from the transmitter to the receiver multiplexed with the data symbols, as suggested in [Yan07] and [Ban03a], or generated offline and stored in memory[9] at the receiver and the transmitter. Another option is to use 2 equal pseudo-random generators initialized, one at the transmitter and one at the receiver, using the same seed, and orthonormalizing the random matrices using the Gram-Schmidt procedure [Gol96]. Also, the matrix exponentials can be efficiently computed using Singular Value Decomposition (SVD) of the matrices $\{\tilde{\mathbf{C}}_i\}$, as also suggested in [Yan07]. The SVDs of $\{\tilde{\mathbf{C}}_i\}$ can be computed offline and stored in memory to decrease computational load at run time. The scaling due to the quantization step only needs to be performed on the singular values, not on the singular vectors.

This whole quantization process has a computational complexity that grows as $O(n_T^3)$. Step 1 implies no computational cost since the scaling by the quantization step can be applied together with later steps. Step 2 involves the square root of a matrix, which is an $O(n_T^3)$ operation [Gol96], and the exponential, which can be efficiently computed as described at the beginning of this subsection, with a complexity of $O(n_T)$. Step 3 is dominated by matrix multiplication, which is $O(n_T^3)$. Finally, the complexity of step 4 depends on the cost function of the system, which for the case of geodesic distances is governed by the computation of the eigenvalues of a matrix, and is $O(n_T^3)$. The computational complexity of other techniques will be commented in section 3.6.6, together with a brief description of each technique.

[9] In order to preserve the properties derived from randomness of the generated geodesics, the number of stored sets of matrices $\{\tilde{\mathbf{C}}_i\}_{i=1}^{Q}$ must be high. However, this is a matter of memory and not of computational complexity.

3.5 On the optimality of the algorithm

This section presents an analysis of the convergence behavior of the algorithm assuming that the channel matrix $\mathbf{H}$ is static. Consequently, the time index can be eliminated from the notation of $\mathbf{H}$ and $\mathbf{R}_H$. It is shown that, in the tracking phase and for the case of 1 bit of feedback, the expectation of the direction of the followed geodesic curve is proportional to the actual gradient of the cost function, which points in the direction of maximum increase/decrease of such cost function. The proof is derived for a generic design criterion or cost function g, and an expression of the variance in the direction of the selected routes with respect to the actual gradient is also provided. The author conjectures that the qualitative conclusion from this analysis would also be valid for the case of more than 1 bit of feedback[10].

3.5.1 Average direction of the geodesic routes

The average of the directions associated to the quantization routes followed in the tracking phase is studied in this section, for the case of 1 bit of feedback and any given cost function $g(\widehat{\mathbf{R}}_H(n), \mathbf{H})$; where $\mathbf{H}$ is the actual channel matrix and $\widehat{\mathbf{R}}_H(n)$ is the fed back channel Gram matrix at instant n.

As described in section 3.4, (see (3.10), (3.11), (3.12)), the geodesic quantization using 1 bit ($s[n] \in \{-1, 1\}$) has the following expression:

$$\widehat{\mathbf{R}}_H(n) = \widehat{\mathbf{R}}_H^{1/2}(n-1) \exp\big(s[n]\mathbf{C}\big)\widehat{\mathbf{R}}_H^{1/2}(n-1), \tag{3.13}$$

where the feedback bit $s[n]$ is calculated as:

$$s[n] = \text{sign}\left(g\big(\widehat{\mathbf{R}}_H^{(-1)}(n), \mathbf{H}\big) - g\big(\widehat{\mathbf{R}}_H^{(+1)}(n), \mathbf{H}\big)\right), \tag{3.14}$$

[10]The extension of the analysis for the case of more than 1 bit of feedback is a very complex open problem. To the best of the authors' knowledge there is only one similar analysis in the literature [Yan07] (which features a quantization in the Grassmannian manifold), and it is also for the case of 1 bit of feedback.

$\mathbf{C}$ is defined as explained in the footnote[11], and the two quantization candidates, $\widehat{\mathbf{R}}_H^{(-1)}(n)$ and $\widehat{\mathbf{R}}_H^{(+1)}(n)$, are defined as $\widehat{\mathbf{R}}_H^{(-1)}(n) = \widehat{\mathbf{R}}_H^{1/2}(n-1)\exp\big(-\mathbf{C}\big)\widehat{\mathbf{R}}_H^{1/2}(n-1)$ and $\widehat{\mathbf{R}}_H^{(+1)}(n) = \widehat{\mathbf{R}}_H^{1/2}(n-1)\exp\big(\mathbf{C}\big)\widehat{\mathbf{R}}_H^{1/2}(n-1)$.

The geodesic route associated to the quantization is written as:

$$\mathbf{\Gamma}_q(t) = \widehat{\mathbf{R}}_H^{1/2}(n-1)\exp\big(t\,\mathbf{C}\big)\widehat{\mathbf{R}}_H^{1/2}(n-1), \tag{3.15}$$

and the direction of $\mathbf{\Gamma}_q(t)$ is the derivative at $t=0$:

$$\dot{\mathbf{\Gamma}}_q(t)\Big|_{t=0} = \widehat{\mathbf{R}}_H^{1/2}(n-1)\mathbf{C}\widehat{\mathbf{R}}_H^{1/2}(n-1). \tag{3.16}$$

It is assumed that $\mathbf{H}$ and $\widehat{\mathbf{R}}_H(n-1)$ are such that function g is near a minimum (the algorithm is already in the tracking phase) and the quantization step is small, which implies that $\mathbf{C}$ is small and, consequently, $\widehat{\mathbf{R}}_H^{(-1)}(n)$ and $\widehat{\mathbf{R}}_H^{(+1)}(n)$ are close together. Then, using a first order Taylor approximation of the cost function with respect to the first variable, and after some manipulations described in appendix 3.A, results in (in the following, and for clarity reasons, the notation $\mathbf{B} = \widehat{\mathbf{R}}_H(n-1)$ will be used):

$$g\big(\widehat{\mathbf{R}}_H^{(-1)}(n),\mathbf{H}\big) - g\big(\widehat{\mathbf{R}}_H^{(+1)}(n),\mathbf{H}\big) = \operatorname{tr}\mathfrak{Re}\left[g_B^T\big(\widehat{\mathbf{R}}_H^{(-1)}(n) - \widehat{\mathbf{R}}_H^{(+1)}(n)\big)\right] + O\big(\|\mathbf{C}\|^2\big)\,, \tag{3.17}$$

where $[g_B]_{ij} = \frac{\partial g(\mathbf{B},\mathbf{H})}{\partial \mathbf{B}_{ij}}$ and $O\left(\|\mathbf{C}\|^2\right)$ denotes symbolically that the error in the Taylor approximation is bounded quadratically (error $\leq b\|\mathbf{C}\|^2$) for $\mathbf{C}$ small [Rud86].

Consequently, the direction towards the selected candidate is:

$$s[n]\;\dot{\mathbf{\Gamma}}_q(t)\Big|_{t=0} = \mathbf{B}^{1/2}\mathbf{C}\mathbf{B}^{1/2}\operatorname{sign}\left(g\big(\widehat{\mathbf{R}}_H^{(-1)}(n),\mathbf{H}\big) - g\big(\widehat{\mathbf{R}}_H^{(+1)}(n),\mathbf{H}\big)\right). \tag{3.18}$$

The average direction of the geodesic route used for quantization is

$$\mathbb{E}\left\{s[n]\dot{\mathbf{\Gamma}}_q(t)\Big|_{t=0}\right\} = \mathbb{E}\left\{\mathbf{B}^{1/2}s[n]\mathbf{C}\mathbf{B}^{1/2}\right\} = \mathbf{B}^{1/2}\mathbb{E}\left\{s[n]\mathbf{C}\right\}\mathbf{B}^{1/2}, \tag{3.19}$$

[11] Since the case of 1 bit of feedback is considered, there is only one generated direction and $\mathbf{C}$ can then be defined, for clarity in the equations, as $\mathbf{C} = c\,\mathbf{C_0}$ where c is related to the quantization step and $\mathbf{C_0}$ is random Hermitian and Gaussian. Because of the Hermitian property and for usefulness in the proof, $\mathbf{C_0}$ is modeled as $\mathbf{C_0} = \mathbf{A}^H + \mathbf{A}$, where $\mathbf{A}$ has i.i.d. components, each one following a Gaussian distribution $\mathcal{CN}(0,1)$.

where (see (3.17)):

$$\mathbb{E}\{s[n]\mathbf{C}\} = \mathbb{E}\left\{\text{sign}\left(\text{tr}\,\mathfrak{Re}\left[g_B^T\left(\widehat{\mathbf{R}}_H^{(-1)}(n) - \widehat{\mathbf{R}}_H^{(+1)}(n)\right)\right] + O\left(\|\mathbf{C}\|^2\right)\right)\mathbf{C}\right\}.$$

Substituting the expressions of $\widehat{\mathbf{R}}_H^{(-1)}(n)$ and $\widehat{\mathbf{R}}_H^{(+1)}(n)$, results in:

$$\widehat{\mathbf{R}}_H^{(-1)}(n) - \widehat{\mathbf{R}}_H^{(+1)}(n) = \mathbf{B}^{1/2}\exp\big(-\mathbf{C}\big)\mathbf{B}^{1/2} - \mathbf{B}^{1/2}\exp\big(\mathbf{C}\big)\mathbf{B}^{1/2}. \tag{3.20}$$

Following a third order Taylor approximation, (3.20) results in

$$\widehat{\mathbf{R}}_H^{(-1)}(n) - \widehat{\mathbf{R}}_H^{(+1)}(n) = -2\mathbf{B}^{1/2}\mathbf{C}\mathbf{B}^{1/2} + O\left(\|\mathbf{C}\|^3\right). \tag{3.21}$$

Combining all the previous results results in:

$$\mathbb{E}\{s[n]\mathbf{C}\} = \mathbb{E}\left\{\text{sign}\left(\text{tr}\,\mathfrak{Re}\left[-\mathbf{B}^{1/2}g_B^T\mathbf{B}^{1/2}\mathbf{C}\right] + O\left(\|\mathbf{C}\|^2\right)\right)\mathbf{C}\right\}. \tag{3.22}$$

Applying the corollary from (3.54) (see appendices 3.C and 3.D), it can be concluded that:

$$\mathbb{E}\left\{s[n]\,\dot{\mathbf{\Gamma}}_q(t)\Big|_{t=0}\right\} = \mathbf{B}^{1/2}\mathbb{E}\left\{s[n]\mathbf{C}\right\}\mathbf{B}^{1/2} = -\frac{2c}{\sqrt{\pi}}\frac{1}{\|\mathbf{B}^{1/2}g_B^T\mathbf{B}^{1/2}\|_F}\mathbf{B}g_B^T\mathbf{B} + O(c^2). \tag{3.23}$$

The derivations in appendix 3.B show that $g_B^T = \mathbf{B}^{-1}\nabla g\mathbf{B}^{-1}$. Substituting this expression in (3.23) yields:

$$\mathbb{E}\left\{s[n]\,\dot{\mathbf{\Gamma}}_q(t)\Big|_{t=0}\right\} = -\frac{2c}{\sqrt{\pi}}\frac{1}{\|\mathbf{B}^{1/2}g_B^T\mathbf{B}^{1/2}\|_F}\nabla g + O(c^2), \tag{3.24}$$

which means that the expectation of the geodesic route has the same direction as the gradient of the cost function (the minus sign is consistent with the goal of minimizing the cost function). The error term $O(c^2)$ is at least one order smaller than the nominal part of the expression.

3.5.2 Variance analysis

In section 3.5.1 it was proved that in average the algorithm points in the direction of the gradient of the cost function. However it would be interesting to calculate the

variance of the difference between the selected direction and the actual gradient. In order to study the variance, the error matrix $\mathbf{E}$ is defined as:

$$\mathbf{E} \triangleq s[n]\dot{\mathbf{\Gamma}}_q(0) - \mathbb{E}\left\{s[n]\dot{\mathbf{\Gamma}}_q(0)\right\}. \tag{3.25}$$

The error matrix $\mathbf{E}$ has a covariance given by $\mathbb{E}\left\{\mathbf{e}\mathbf{e}^H\right\}$, where $\mathbf{e} = \text{vec}(\mathbf{E})$ (the operator vec($\mathbf{E}$) returns the vector constructed by stacking the columns of matrix $\mathbf{E}$ from left to right).

As shown in (3.18)-(3.20), the direction towards the selected candidate can be written as:

$$s[n]\dot{\mathbf{\Gamma}}_q(0) = \mathbf{B}^{1/2}s[n]\mathbf{C}\mathbf{B}^{1/2} = \mathbf{B}^{1/2}\text{sign}\left(\text{tr}\,\mathfrak{Re}\left[\mathbf{X}\mathbf{C}\right] + O\left(\|\mathbf{C}\|^2\right)\right)\mathbf{C}\mathbf{B}^{1/2}, \tag{3.26}$$

where $\mathbf{X} = -\mathbf{B}^{1/2}g_B^T\mathbf{B}^{1/2}$ is Hermitian. (3.26) is written in vector form as (see Theorem 13.26 in [Lau05]):

$$\begin{aligned}\text{vec}(\mathbf{B}^{1/2}&\text{sign}\left(\text{tr}\,\mathfrak{Re}\left[\mathbf{X}\mathbf{C}\right] + O\left(\|\mathbf{C}\|^2\right)\right)\mathbf{C}\mathbf{B}^{1/2}) \\ &= \left(\mathbf{B}^{1/2^T} \otimes \mathbf{B}^{1/2}\right)\text{vec}\left(\text{sign}\left(\text{tr}\,\mathfrak{Re}\left[\mathbf{X}\mathbf{C}\right] + O\left(\|\mathbf{C}\|^2\right)\right)\mathbf{C}\right).\end{aligned} \tag{3.27}$$

As proved in appendix 3.E, the covariance of vec $(\text{sign}\left(\text{tr}\,\mathfrak{Re}\left[\mathbf{X}\mathbf{C}\right] + O\left(\|\mathbf{C}\|^2\right)\right)\mathbf{C})$ is:

$$\text{cov}\left(\text{vec}\left(\text{sign}\left(\text{tr}\,\mathfrak{Re}\left[\mathbf{X}\mathbf{C}\right] + O\left(\|\mathbf{C}\|^2\right)\right)\mathbf{C}\right)\right) = c^2\left(2\mathbf{I} - \frac{4}{\pi}\frac{\mathbf{x}^*\mathbf{x}^T}{\|\mathbf{x}\|^2}\right) + O\left(c^3\right), \tag{3.28}$$

where $\mathbf{x}$ is the result of stacking the columns of $\mathbf{X}^T$.

Consequently, the covariance of the directions followed by the algorithm is:

$$\mathbb{E}\left\{\mathbf{e}\mathbf{e}^H\right\} = c^2\left(\mathbf{B}^{1/2^T} \otimes \mathbf{B}^{1/2}\right)\left(2\mathbf{I} - \frac{4}{\pi}\frac{\mathbf{x}^*\mathbf{x}^T}{\|\mathbf{x}\|^2}\right)\left(\mathbf{B}^{1/2^T} \otimes \mathbf{B}^{1/2}\right)^H + O\left(c^3\right). \tag{3.29}$$

From this equation it can be observed that the covariance depends on $\widehat{\mathbf{R}}_H(n-1)$ (i.e., the previous fed back value) and on the gradient of the cost function. The error term $O(c^3)$ is at least one order smaller than the nominal part of the expression.

3.5.3 Particular case: geodesic distance as cost function

This subsection presents an analysis, as an example, of the particular case in which the optimization criterion is the minimization of the geodesic distance between the Gram matrix $\widehat{\mathbf{R}}_H$ fed back through the feedback link, and the Gram matrix of the actual channel realization $\mathbf{R}_H$. For the sake of simplicity in the notation, in this subsection the error terms are not given, however they are the same as presented for the general case in the previous sections, since this is just a particular case. In this particular case the optimization of the cost function is associated, by definition, to the geodesic route from $\widehat{\mathbf{R}}_H(n-1)$ to $\mathbf{R}_H$ (the notation $\mathbf{R} = \mathbf{R}_H$, $\mathbf{B} = \widehat{\mathbf{R}}_H(n-1)$ will be used for clarity reasons):

$$\mathbf{\Gamma}_{opt}(t) = \mathbf{B}^{1/2} \exp\left(t \log\left(\mathbf{B}^{-1/2}\mathbf{R}\mathbf{B}^{-1/2}\right)\right) \mathbf{B}^{1/2}. \tag{3.30}$$

The direction of the optimum geodesic route at $t = 0$ is given by:

$$\dot{\mathbf{\Gamma}}_{opt}(t)\Big|_{t=0} = \mathbf{B}^{1/2} \log\left(\mathbf{B}^{-1/2}\mathbf{R}\mathbf{B}^{-1/2}\right) \mathbf{B}^{1/2}. \tag{3.31}$$

Since $\mathbf{R}_H$ and $\widehat{\mathbf{R}}_H(n-1)$ are close together (the algorithm is already locked, that means, in the tracking phase), it makes sense to use a first order Taylor approximation of the logarithm ($\log(\mathbf{I} + \mathbf{B}^{-1/2}\mathbf{R}\mathbf{B}^{-1/2} - \mathbf{I}) \approx \mathbf{B}^{-1/2}\mathbf{R}\mathbf{B}^{-1/2} - \mathbf{I}$), which results in:

$$\dot{\mathbf{\Gamma}}_{opt}(t)\Big|_{t=0} \simeq \mathbf{R} - \mathbf{B}. \tag{3.32}$$

On the other hand, the direction of the random geodesic route $\mathbf{\Gamma}_q(t)$ is the derivative at $t = 0$ in the direction of the selected candidate (see (3.7)):

$$s[n]\,\dot{\mathbf{\Gamma}}_q(t)\Big|_{t=0} = s[n]\mathbf{B}^{1/2}\mathbf{C}\mathbf{B}^{1/2}. \tag{3.33}$$

where $s[n]$ can be written as:

$$\begin{aligned} s[n] =& \operatorname{sign}\left(\operatorname{dist}_g\left(\mathbf{R}, \widehat{\mathbf{R}}_H^{(-1)}(n)\right)^2 - \operatorname{dist}_g\left(\mathbf{R}, \widehat{\mathbf{R}}_H^{(+1)}(n)\right)^2\right) \\ =& \operatorname{sign}\left(\left\|\log\left(\mathbf{R}^{-1/2}\mathbf{B}^{1/2}\exp\left(-\mathbf{C}\right)\mathbf{B}^{1/2}\mathbf{R}^{-1/2}\right)\right\|_F^2\right. \\ & \left. - \left\|\log\left(\mathbf{R}^{-1/2}\mathbf{B}^{1/2}\exp\left(\mathbf{C}\right)\mathbf{B}^{1/2}\mathbf{R}^{-1/2}\right)\right\|_F^2\right). \end{aligned} \tag{3.34}$$

Using a first order Taylor approximation it follows that

$$s[n] \approx \text{sign}\left(\text{tr}\,\mathfrak{Re}\left(\left(\mathbf{B}^{1/2}\mathbf{R}^{-1}\mathbf{B}^{1/2} - \mathbf{B}^{1/2}\mathbf{R}^{-1}\mathbf{B}\mathbf{R}^{-1}\mathbf{B}^{1/2}\right)\mathbf{C}\right)\right). \tag{3.35}$$

From (3.33) and (3.34), the average direction of the geodesic route used for quantization is:

$$\mathbb{E}\left\{s[n]\,\dot{\mathbf{\Gamma}}_q(t)\Big|_{t=0}\right\} = \mathbb{E}\left\{\mathbf{B}^{1/2}s[n]\mathbf{C}\mathbf{B}^{1/2}\right\} = \mathbf{B}^{1/2}\mathbb{E}\left\{s[n]\mathbf{C}\right\}\mathbf{B}^{1/2}, \tag{3.36}$$

where

$$\mathbb{E}\left\{s[n]\mathbf{C}\right\} \simeq \mathbb{E}\left\{\text{sign}\left(\text{tr}\,\mathfrak{Re}\left\{\left(\left(\mathbf{B}^{1/2}\mathbf{R}^{-1}\mathbf{B}^{1/2} - \mathbf{B}^{1/2}\mathbf{R}^{-1}\mathbf{B}\mathbf{R}^{-1}\mathbf{B}^{1/2}\right)\mathbf{C}\right)\right\}\right)\mathbf{C}\right\}. \tag{3.37}$$

On substituting $\mathbf{P}$ in the corollary proved in appendix 3.C (3.54) with $\mathbf{C}$, and $\mathbf{G}$ with $\mathbf{B}^{1/2}\mathbf{R}^{-1}\mathbf{B}^{1/2} - \mathbf{B}^{1/2}\mathbf{R}^{-1}\mathbf{B}\mathbf{R}^{-1}\mathbf{B}^{1/2}$, it follows that

$$\mathbb{E}\left\{s[n]\mathbf{C}\right\} \simeq \alpha\left(\mathbf{B}^{1/2}\mathbf{R}^{-1}\mathbf{B}^{1/2} - \mathbf{B}^{1/2}\mathbf{R}^{-1}\mathbf{B}\mathbf{R}^{-1}\mathbf{B}^{1/2}\right), \tag{3.38}$$

where $\alpha = \frac{2}{\sqrt{\pi}}\frac{c}{\left\|\ \mathbf{B}^{1/2}\mathbf{R}^{-1}\mathbf{B}^{1/2} - \mathbf{B}^{1/2}\mathbf{R}^{-1}\mathbf{B}\mathbf{R}^{-1}\mathbf{B}^{1/2}\right\|_F}$, and

$$\mathbb{E}\left\{s[n]\,\dot{\mathbf{\Gamma}}_q(t)\Big|_{t=0}\right\} = \mathbf{B}^{1/2}\mathbb{E}\left\{s[n]\mathbf{C}\right\}\mathbf{B}^{1/2} \simeq \alpha\mathbf{B}\mathbf{R}^{-1}\left(\mathbf{R} - \mathbf{B}\right)\mathbf{R}^{-1}\mathbf{B}. \tag{3.39}$$

Since $\mathbf{R}$ and $\mathbf{B}$ are very close together (tracking phase), the following first order approximation can be made: $\mathbf{B}\mathbf{R}^{-1} \simeq \mathbf{R}^{-1}\mathbf{B} \simeq \mathbf{I}$. Consequently, (3.39) can be written as:

$$\mathbb{E}\left\{s[n]\,\dot{\mathbf{\Gamma}}_q(t)\Big|_{t=0}\right\} \simeq \alpha\left(\mathbf{R} - \mathbf{B}\right). \tag{3.40}$$

From (3.24), (3.32), and (3.40) it follows directly that, as mentioned before, the average direction of the random geodesic route used for quantization, which is parallel to the gradient of the cost function, has the same direction as the optimum geodesic route:

$$\mathbb{E}\left\{s[n]\,\dot{\mathbf{\Gamma}}_q(t)\Big|_{t=0}\right\} \propto \dot{\mathbf{\Gamma}}_{opt}(t)\Big|_{t=0}. \tag{3.41}$$

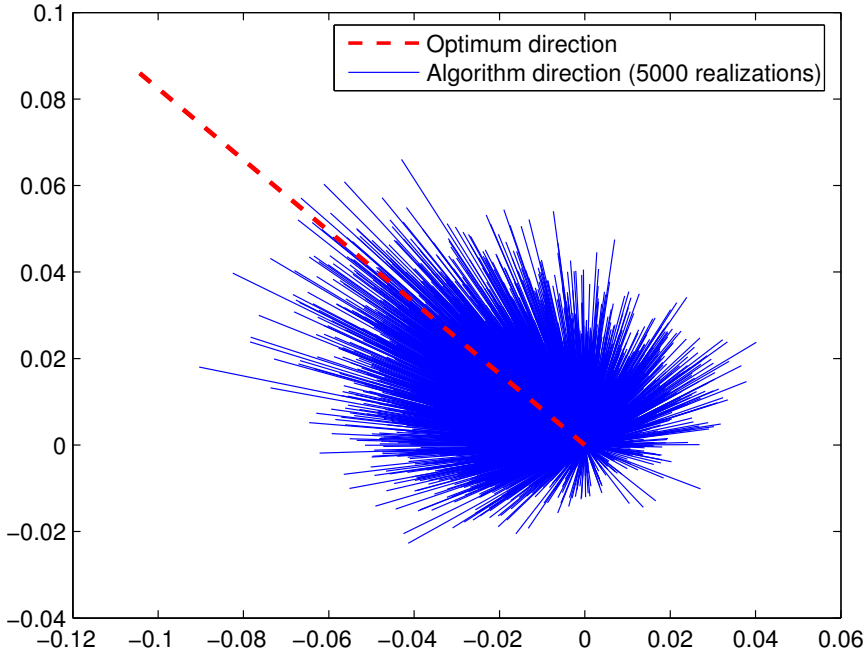

Figure 3.3: Real part of the first column of the directions followed by the quantization in the tracking phase.

In Figure 3.3 a single realization of a channel ($n_T = 3, n_R = 3$) with the feedback algorithm in the tracking phase is considered. The setup is simulated for 1 bit of feedback, which means that 2 quantization candidates are generated randomly and the best one is selected as the quantization result. The random generation of candidates was performed 5000 times taking the same initial point. The continuous lines correspond to the directions followed by the 5000 routes associated to the selected candidates (they represent the real part of the first column of the direction matrix $s[n]\dot{\mathbf{\Gamma}}_q(0)$ of the selected candidates). The dashed line corresponds to the value of $\mathbf{R}(n) - \widehat{\mathbf{R}}(n-1)$ and coincides with the average of the continuous lines. This is consistent with the result from section 3.5.1.

3.6 Simulations

This section presents numerical simulations for the analysis of the performance of the algorithm in both time varying and constant (i.e., time invariant) channels. In the constant channel, the behavior of the algorithm in terms of stable-state error (i.e., once the feedback has converged) can be observed, whereas in the time-varying case the tracking capabilities of the technique are evaluated. A random MIMO channel is considered, following a first-order autoregressive time variation model, which is described by the expression:

$$\mathbf{H}(n) = \rho\mathbf{H}(n-1) + \sqrt{1-\rho^2}\,\mathbf{N}(n), \tag{3.42}$$

where matrices $\mathbf{H}(0)$ and $\mathbf{N}(n)$ are assumed to be independent and composed of i.i.d. zero-mean complex Gaussian entries with unit variance. The time correlation factor ρ models the variability of the channel and depends on the Doppler frequency f_D caused by the movement of the transmitter/receiver through the expression $\rho = J_0\big(2\pi f_D \tau\big)$ [Ste99], where J_0 is the zeroth-order Bessel function of the first kind and τ corresponds to the time difference between consecutive feedback instants. Note that the case of an invariant channel corresponds to $\rho = 1$. The time correlation factor is usually expressed in terms of the normalized Doppler frequency $f_D\tau$, or f_D/f_{FB}, where f_{FB} is the frequency of feedback messages. The values for this parameter usually considered in the literature are $0.004 < f_D/f_{FB} < 0.01$ (see references [Yan07, Ino09, Roh07, Ban03a, Hua06b]), which correspond to $0.999 < \rho < 1$.

Regarding the precoding schemes used in the specific simulations shown in this chapter, single transmit-receive beamforming (3.3) or spatial multiplexing (3.5) have been exploited coming as a result of the optimum design criterion applied in each simulation, i.e., SNR and MI maximization, respectively. In the simulations evaluating BER, the single beamforming approach under maximum SNR was taken. Note that the presented feedback technique can be applied to any linear precoding scheme under any optimization and quality criterion and that the number of streams, the expression

of $\mathbf{B}$, etc. depend on such particular adopted criterion.

3.6.1 Optimization of the quantization step

The quantization step Δ, presented in section 3.4, is the geodesic distance between the last value of the quantized Gram matrix $\widehat{\mathbf{R}}_H(n-1)$ and the new quantization candidates. The choice of this parameter has a direct effect on the behavior of the algorithm, due to the tradeoff between convergence rate (i.e., ability to track the channel variations) and stable-state error. Fast varying channels require a larger Δ to be able to track the channel, while slow varying channels can use a smaller Δ to increase the accuracy. The optimum value of Δ depends on the correlation factor of the channel, the antenna configuration (n_T, n_R), the number of feedback bits, and the design criterion used at the transmitter. In the simulations the optimum Δ was computed numerically[12] for each case, for minimum mean performance loss calculated in a window of 40 time intervals. As an example, Figure 3.4 shows the average geodesic distance between the quantization result $\hat{\mathbf{R}}_H$ of the proposed algorithm and the exact $\mathbf{R}_H$ versus the quantization step Δ for the case of 3 bits of feedback in 2x2 and 3x3 MIMO channels. For the other techniques used in the simulations that have an equivalent parameter to Δ, this has also been optimized numerically for each case in order to provide a fair comparison.

3.6.2 Performance of the algorithm

In this subsection the algorithm is evaluated and its performance is compared to other feedback techniques, some of them differential [Roh07,Yan07] and some non-differential

[12]To the best of the authors' knowledge, the analytical optimization of the quantization step in the set of positive definite Hermitian matrices is still an open topic. In [Yan07] the authors tackled this issue by performing a numerical optimization for different values of the Doppler frequency. The same method has been followed in this thesis.

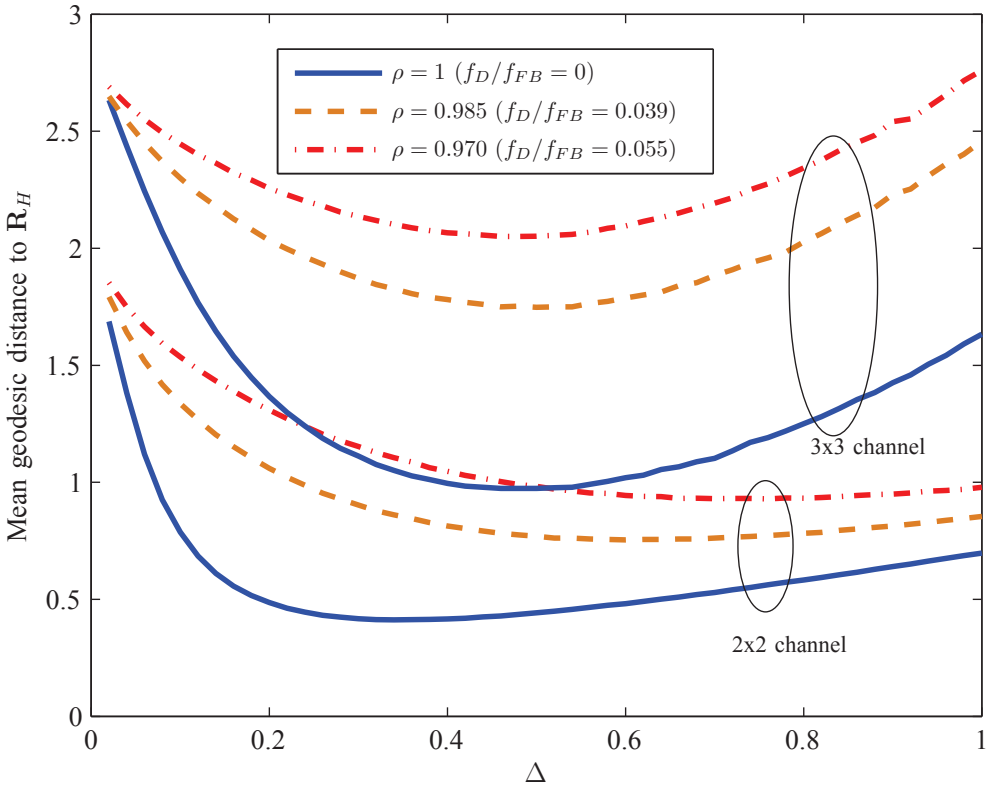

Figure 3.4: Mean geodesic distance between the quantization result $\hat{\mathbf{R}}_H$ *and the actual* $\mathbf{R}_H$ *vs. the quantization step* Δ.

[Lov03, Roh06, Roh07, Cha08]. For the simulations of non-differential techniques we consider the performance averaged over several channel realizations.

Figure 3.5 shows the SNR achieved in a constant channel for the proposed tracking algorithm, a tracking algorithm of channel response matrices[13], a differential algorithm based on 1-bit subspace tracking [Yan07], a non-differential feedback strategy which uses Grassmannian codebooks [Lov03], a non-differential quantization algorithm based on the parametrization of the channel singular vectors [Roh07], a non-differential

[13]The tracking algorithm of the channel response matrices is also a differential quantization strategy applied to $\mathbf{H}(n)$ instead of $\mathbf{R}_H(n)$, where the quantization candidates are also obtained through orthogonal routes. Note that in this case, the orthogonal routes are simple straight lines in the space of channel matrices $\mathbf{H}(n)$ and that the quantization step has also been optimized in order to optimize the performance and for a fair comparison with the proposed algorithm.

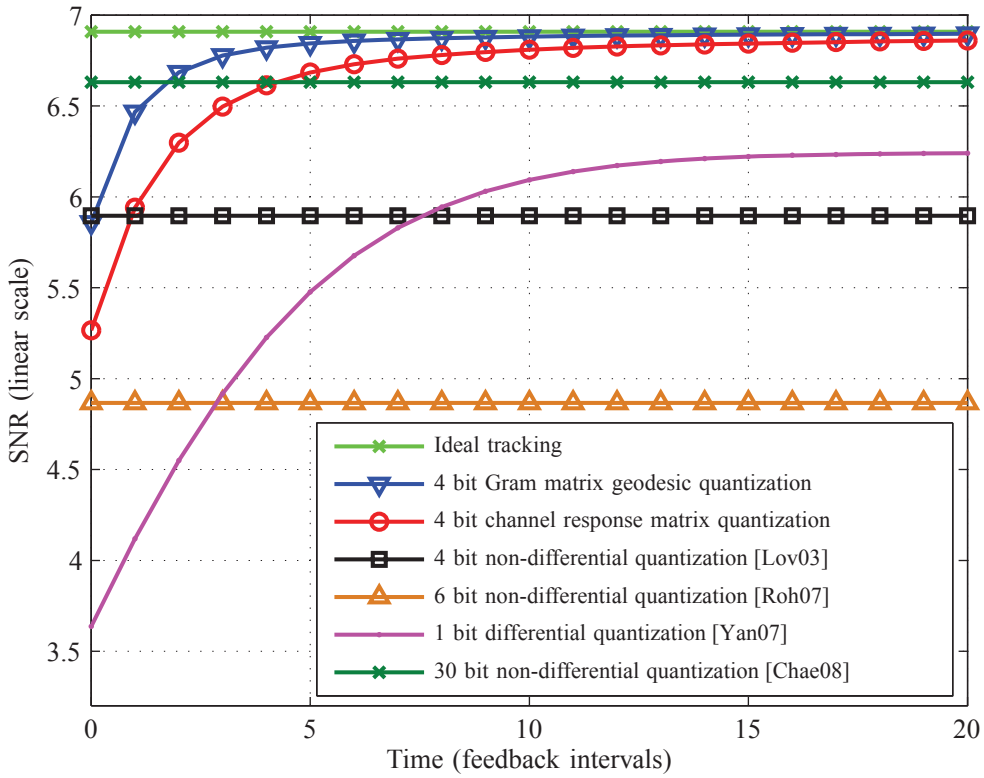

Figure 3.5: SNR achieved using different feedback techniques in a 3x3 time invariant channel.

quantization algorithm based on the quantization of the elements of the channel Gram matrix [Cha08], and ideal tracking using perfect CSI at the transmitter. The results have been averaged over 200 channel realizations and a normalized transmit power was considered. The algorithm proposed in this chapter shows faster convergence and smaller stable-state error than the other differential algorithms, even when using fewer bits of feedback. The gain is due to the use of geodesic routes on the space of Gram matrices. The non-differential techniques present a floor in the performance since they do not exploit the time-correlation of the channel.

In Figure 3.6, the behavior of the proposed algorithm is compared, in terms of achievable mutual information in a time variant channel, to the differential and non-differential algorithms from [Roh07], to the algorithm based on differential quantization of the channel response matrix, and to the performance with perfect CSI. The sim-

ulation considers a random realization of a propagation channel with $f_D/f_{FB} = 0.01$ (which corresponds to $\rho = 0.999$), and $n_T = 3$, $n_R = 3$ antennas. 500 realizations of the algorithms were averaged over that channel realization, using $P_T = 0.3$. The proposed algorithm offers a better tracking than the differential algorithms and also better performance than the non differential ones. The techniques from [Roh07] perform a parametrization of the channel singular vectors prior to quantization, and suffer from propagation of the quantization error when reversing the transformation at the transmitter. After the first intervals, the performance of the differential algorithm in [Roh07] using 14 feedback bits is similar to that of the proposed algorithm using only 4 bits. The non-differential feedback technique in [Roh07] results in uniform power allocation among transmission modes at the transmitter since the information of the channel singular values is not considered in such technique.

Figure 3.7 shows the BER achieved by the different techniques after 10 feedback updates using a Quadrature Phase Shift Keying (QPSK) modulation in a constant channel. The curves are averaged over 500 channel realizations and show that the differential algorithm based on geodesic curves achieves a lower BER even with fewer bits of feedback than the other algorithms and approaches the BER of the case with perfect CSI at the transmitter.

3.6.3 Effect of feedback delay

In real systems there is a delay introduced in the feedback link due to the estimation, processing, and transmission of the feedback information over the channel to the transmitter. This delay produces a mismatch between the CSI available at the transmitter and the current channel. Throughout this thesis, and in the literature in general [Mon06a, Mon06b, Sad06, Roh06, Roh07, Yan07, Hea09, Ino09, Cha08, Ban03a, Lov03, Hua06a], this effect was not considered. This subsection is devoted to describe numerically through simulations the performance degradation caused by this delay.

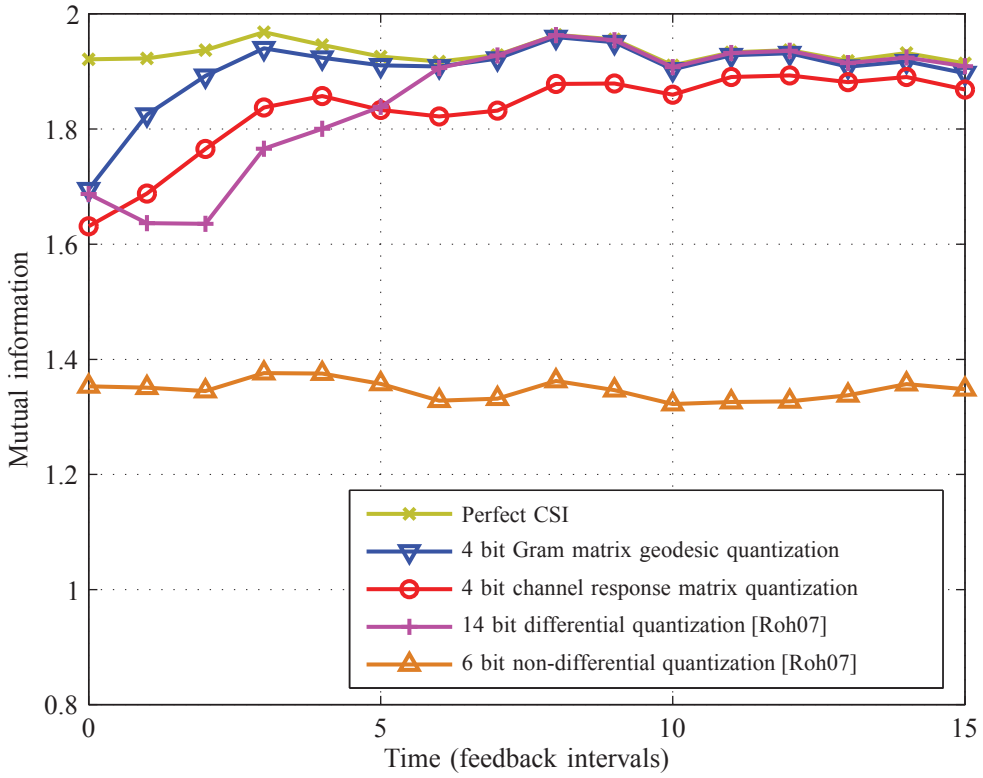

Figure 3.6: Mutual information achieved using different feedback techniques in a 3x3 time variant channel.

The topic of the effect of feedback delay is also treated in [Hua06a], for the strategy described in [Hua06b] which features a differential feedback scheme based on Markov chain theory[14].

The simulations in Figure 3.8 and Figure 3.9 show the impact of feedback delay on the performance of the system for high mobility and low mobility scenarios (f_D/f_{FB} of 0.05 and 0.001, respectively) versus the delay measured in feedback intervals. The average SNR achieved with the proposed technique as a function of the delay in the feedback link is compared to the cases of ideal tracking and delay-free feedback. It can be observed that the performance rapidly decreases in the high mobility scenario

[14]Note that the approach followed in [Hua06a] can not be pursued here because our proposed algorithm considers a continuous space of channel states as opposed to the discrete and finite number of channel states from the Markov chain in [Hua06b].

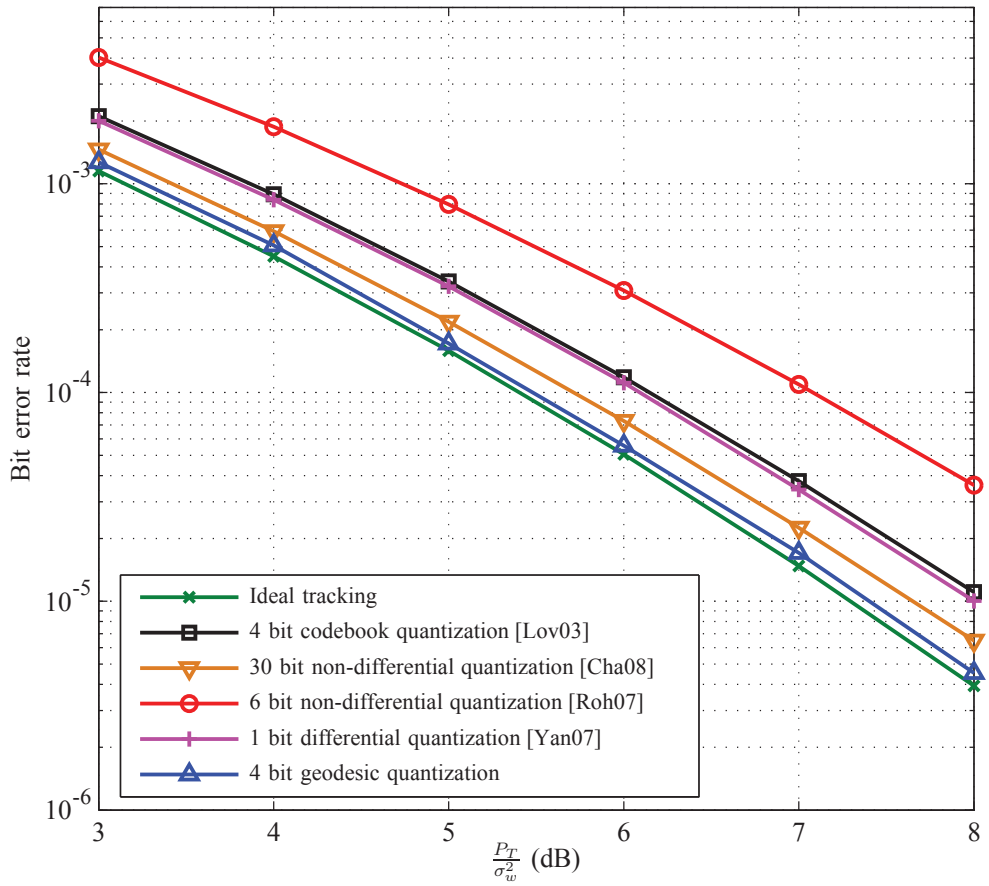

Figure 3.7: BER for different feedback techniques in a 3x3 system using a QPSK modulation.

while the effect is much smaller in the low mobility case.

3.6.4 Effect of transmission errors in the feedback link

Another effect that is present in real systems is the noise and errors in the feedback link. This specially affects differential algorithms, since they are based on the information transmitted in previous time instants. This subsection illustrates numerically this effect.

Figure 3.10 shows the average SNR achieved using the presented algorithm for the case of error-free feedback and also for the cases where the feedback link has a 10%

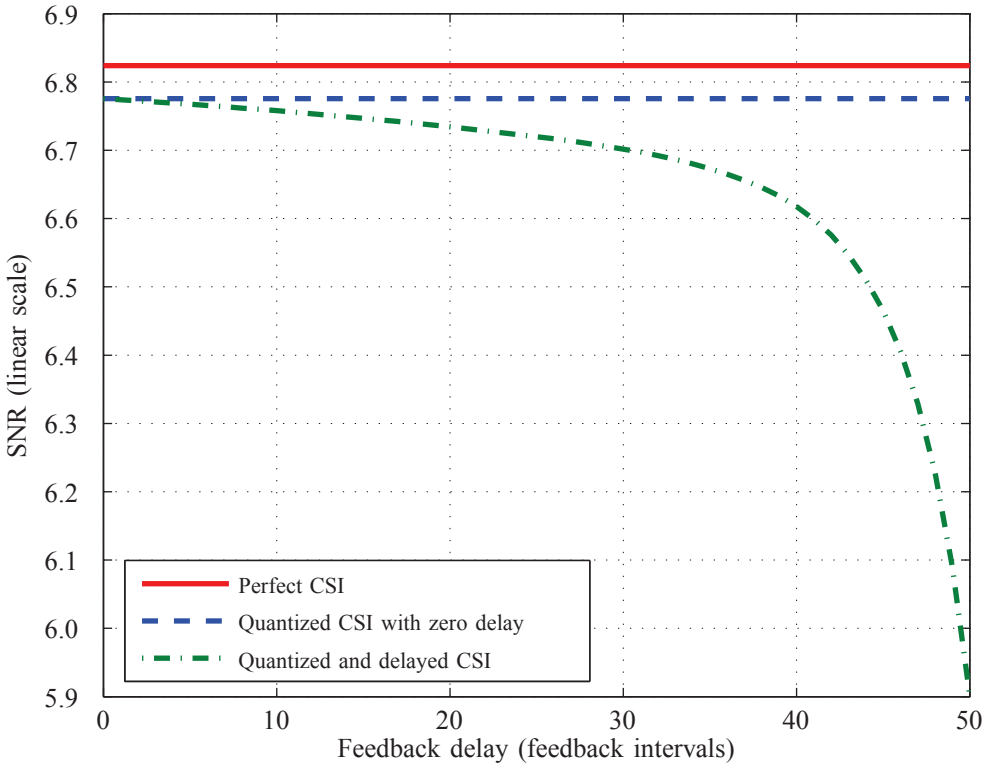

Figure 3.8: Effects of feedback delay in a low mobility scenario ($f_D/f_{FB} = 0.001$, *which corresponds to* $\rho = 0.9999$).

and a 5% error rate, which would correspond to a SNR in the feedback link of approximately 0dB and 1.8dB, respectively, if using a QPSK modulation and assuming a Gaussian feedback channel with no fading. The results are averaged over 200 channel realizations. The feedback strategy based on codebooks [Roh06] and the case of ideal tracking are plotted for comparison. Figure 3.11 shows the BER for the same techniques in a 3x3 time variant channel with $f_D/f_{FB} = 0.005$.

Both simulations show that the loss in performance tends to a constant value after some feedback intervals. Note that the Gram matrix geodesic feedback, even with errors and fewer bits in the feedback link, performs better than the codebook based technique [Roh06] without errors.

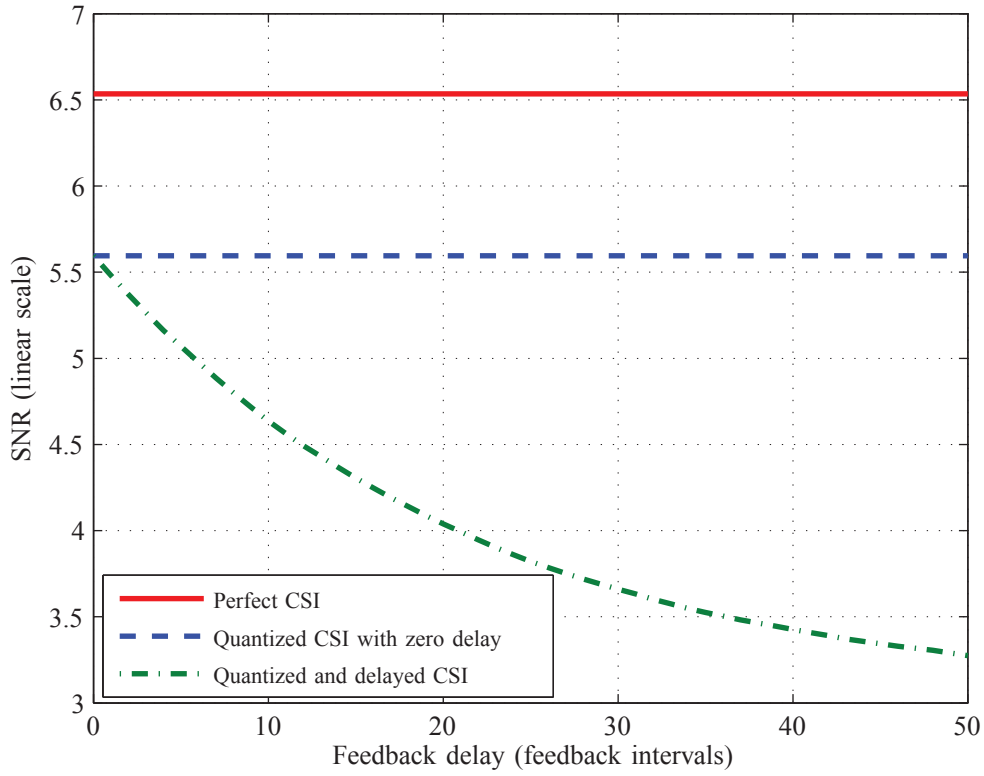

Figure 3.9: Effects of feedback delay in a high mobility scenario ($f_D/f_{FB} = 0.05$, *which corresponds to* $\rho = 0.9755$).

3.6.5 Performance in real channels

All the previous simulations and numerical evaluations have been obtained using the analytic channel model described in (3.42). A more realistic evaluation and the actual validation of the gains obtained by the use of the feedback technique presented in this chapter would require the use of real channel measurements. In this sense, in this subsection, the realistic MIMO channel measurements obtained with the Eurecom MIMO Openair Sounder (EMOS) [Kal08b,Kal08c] are used. The channel measurement data used have been made publicly available at www.openairinterface.org.

The EMOS is based on the OpenAirInterface hardware/software development platform at Eurecom. It operates at 1.900-1.920 GHz with 5 MHz channels and can perform real-time channel measurements between a BS and multiple users synchronously. The

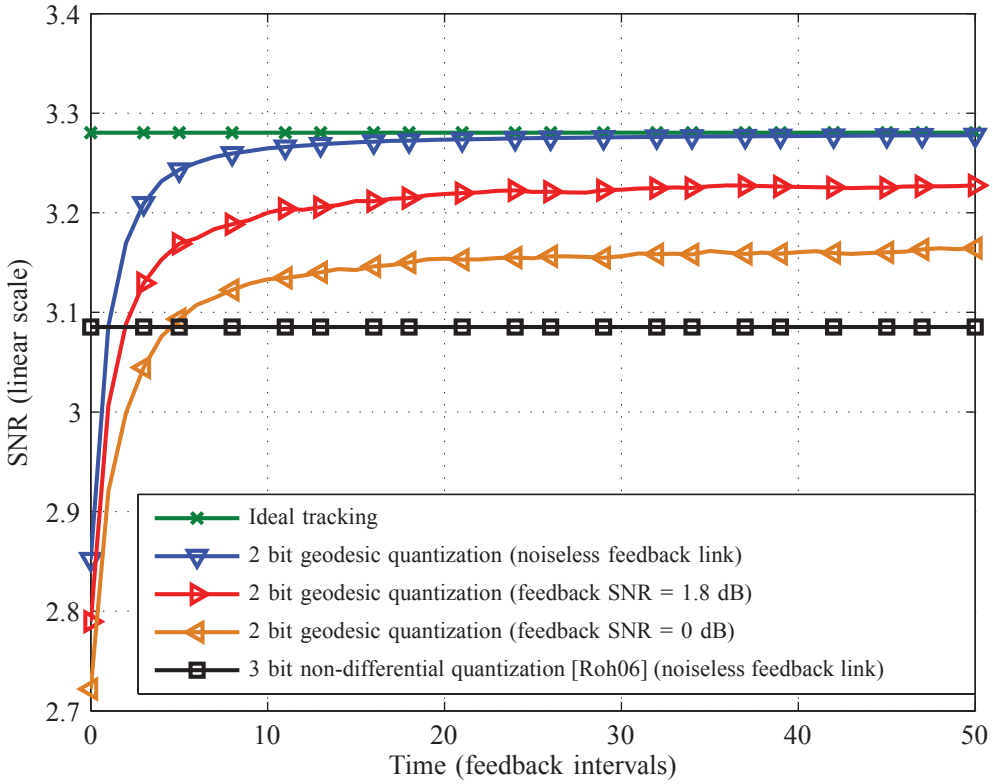

Figure 3.10: SNR in a 2x2 constant channel with a noisy feedback link.

BS used for the measurements is a workstation with four PLATON data acquisition cards and a Powerwave 3G broadband antenna (part no. 7760.00) composed of four elements which are arranged in two cross-polarized pairs. The User Equipment (UE) consists of a laptop computer with Eurecom's dual-RF CardBus/PCMCIA data acquisition card and two clip-on 3G Panorama Antennas (part no. TCLIP-DE3G). The platform is designed for a full software-radio implementation, in the sense that all protocol layers run on the host PCs under the control of a Linux real time operation system.

The EMOS uses an OFDM modulated sounding sequence with 256 subcarriers (out of which 160 are non-zero) and a cyclic prefix length of 64. One transmit frame is 64 OFDM symbols (2.667 ms) long and consists of a Synchronization Symbol (SCH), a Broadcast Data Channel (BCH) comprising 7 OFDM symbols, a guard interval

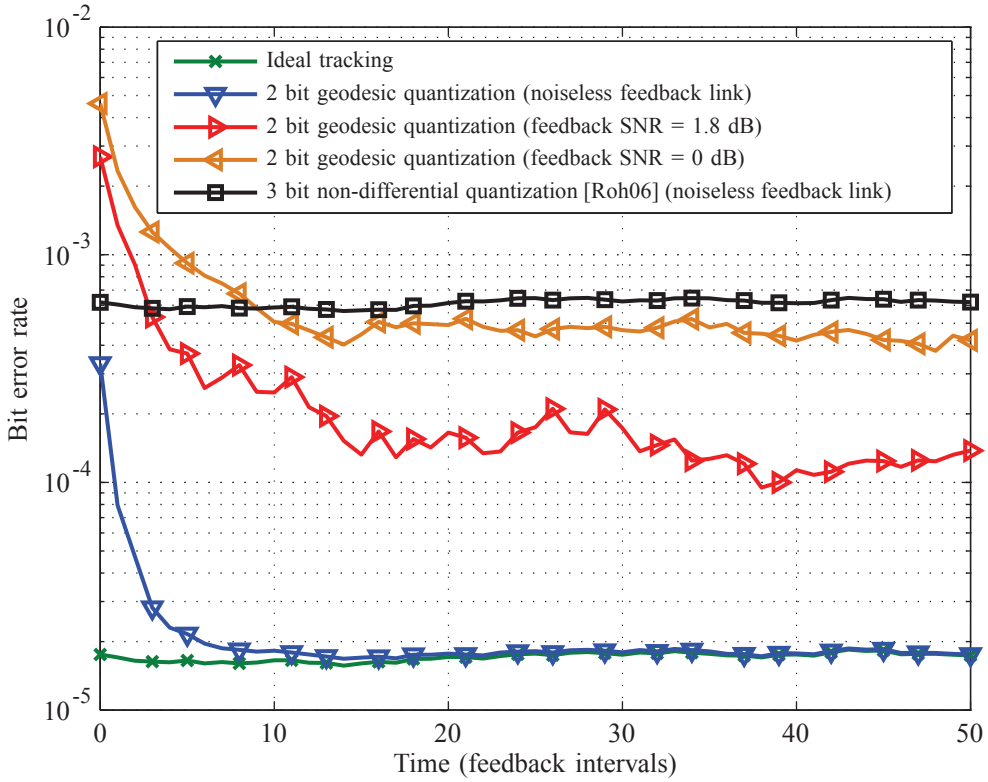

Figure 3.11: BER in a time variant 3x3 system with a noisy feedback link.

equivalent in length to 8 OFDM symbols, and 48 pilot symbols used for channel estimation. The pilot symbols are taken from a pseudo-random QPSK sequence defined in the frequency domain. The subcarriers of the pilot symbols are multiplexed over the transmit antennas to ensure orthogonality in the spatial domain. Therefore, one full MIMO channel estimate can be obtained for one group of a number of subcarriers equal to the number of transmit antennas. The BCH contains the frame number that is used for synchronization among the UEs.

The channel estimation procedure is described as follows. Each UE first synchronizes to the BS using the SCH. It then tries to decode the data in the BCH. If the BCH can be decoded successfully, i.e., the Cyclic Redundancy Check (CRC) is positive, then the channel estimation procedure is started. The channel estimation procedure consists of two steps. Firstly, the pilot symbols are derotated with respect to the first pilot

Parameter	**Value**
Center Frequency	1917.6 MHz
Bandwidth	4.8 MHz
BS Transmit Power	30 dBm
Number of Antennas at BS	4 (2 cross polarized)
Number of UE	1
Number of Antennas at UE	2

Table 3.1: EMOS parameters.

symbol to reduce the phase-shift noise generated by the dual-RF CardBus/PCMCIA card. Secondly, the pilot symbols are averaged to increase the measurement SNR. The estimated MIMO channel is finally stored to disk. For a more detailed description of the synchronization and channel estimation procedure see [Kal08a, Lac07].

The data used in the simulations of this section correspond to channel measurements conducted outdoors in the vicinity of Eurecom in Sophia Antipolis, France[15]. The scenario is characterized by a semi-urban hilly terrain, composed by short buildings and vegetation with a predominantly present Line of Sight (LOS). The BS is located at the roof of Eurecom's southmost building and the antenna is directed towards Garbejaire, a small nearby village. The measurement parameters are summarized in Table 3.1.

The simulations consider two different sets of measurements. In measurement 1, the UE is placed inside a standard passenger car which is being driven with an average speed of 50km/h. The channel conditions are changing between LOS and Non-Line of Sight (NLOS). In measurement 2, the UE is more or less stationary on the parking lot. This scenario is LOS.

[15]Eurecom has a frequency allocation for experimentation around its premises.

Simulations

In the simulations, the channel measurements performed with 4 transmit and 2 receive antennas are considered. Note that in order to mimic a narrowband system only the data from one subcarrier is used. Simulations show results for three cases: perfect CSI at the transmitter, non-differential Grassmannian packaging [Lov03], and differential quantization of the channel correlation matrices $\mathbf{R}_H(n)$ using the algorithm described in this chapter. In all the cases, simulations are performed using the optimum strategies to maximize the mutual information and the SNR, i.e., the strategy that maximizes the mutual information corresponds to a waterfilling distribution of power over the eigenmodes of the channel and the strategy that maximizes the SNR uses only the strongest eigenmode of the available channel response.

Two different scenarios are considered for the feedback model. In the first case the quantized CSI is transmitted instantaneously from the receiver to the transmitter. That is, the transmitter had knowledge of the quantized version of the current channel matrix. In a real situation, however, the transmission delay through the feedback channel is not zero and this affects the performance of the system. Therefore the case with delay in the feedback channel is also simulated.

The simulations corresponding to the instantaneous feedback scenario are shown in Figure 3.12. These simulations show that the differential strategy exploits the time-correlation of the channel and converges to perfect CSIT case, while the performance of the non-differential quantization scheme is lower, even when using more feedback bits. Also note that the differential quantization works better in more slow-varying channels and worse in the scenarios of high mobility where the channel is fast-fading. The impact of the feedback delay on the performance of the system is analyzed in the simulations corresponding to Figure 3.13. The plot shows the averaged SNR and MI for the high mobility and low mobility scenarios versus the delay measured in frames (e.g., a delay equal to 10 means that the delay is equal to 10 frames). For the

simulations a window containing frames from 500 to 520 was used to calculate the average SNR and mutual information. Three situations are compared: perfect CSI at the transmitter, differential feedback with no delay, and differential feedback with different values for the delay in the feedback link. The main conclusion is that the performance rapidly decreases when the delay exceeds a threshold.

3.6.6 Computational complexity comparison

This subsection presents a comparison in terms of computational complexity of the different simulated techniques. From section 3.4.2 we have that the complexity of the proposed algorithm grows as $O(n_T^3)$.

The non-differential strategies from [Lov03, Roh06] require the lowest complexity, as they only test each of the codewords and select the best one. The complexity of these techniques grows with $O(n_R^2 n_T)$ for the case of single beamforming. The complexity of the differential and the non-differential techniques from [Roh07] is determined by the SVD of the channel matrix, which is $\min\left(O(n_R n_T^2), O(n_R^2 n_T)\right)$. The complexity of the technique described in [Yan07] is given by the evaluation of the cost function, which is approximately $O(n_T^3)$. Finally, the algorithm from [Cha08] has a complexity determined by the computation of the channel Gram matrix, which is $O(n_R n_T^2)$.

The algorithm presented in this chapter has a similar complexity than other differential feedback algorithms, and a slightly higher complexity than the considered non-differential algorithms.

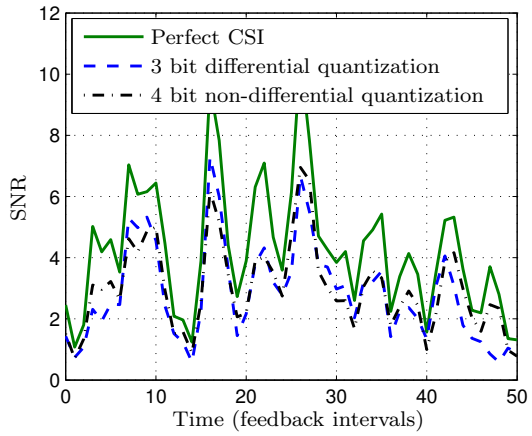

(a) SNR in a high mobility scenario (measurement 1)

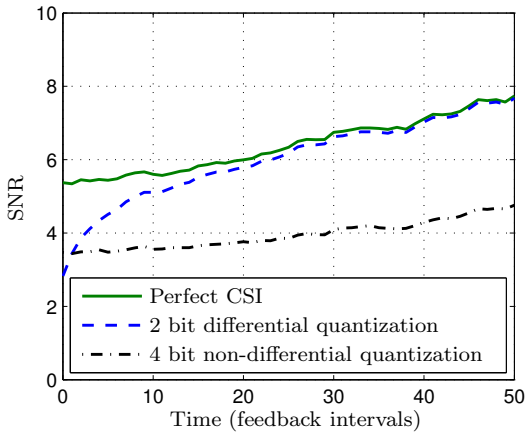

(b) SNR in a low mobility scenario (measurement 2)

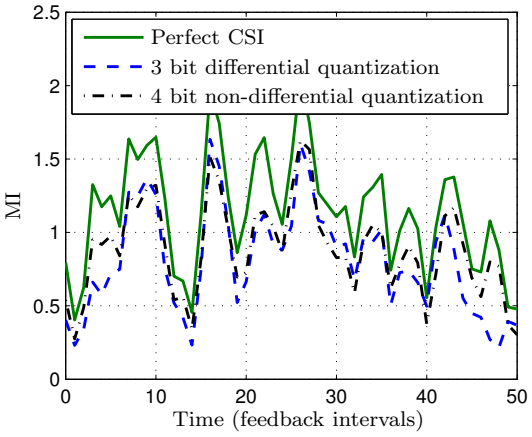

(c) MI in a high mobility scenario (measurement 1)

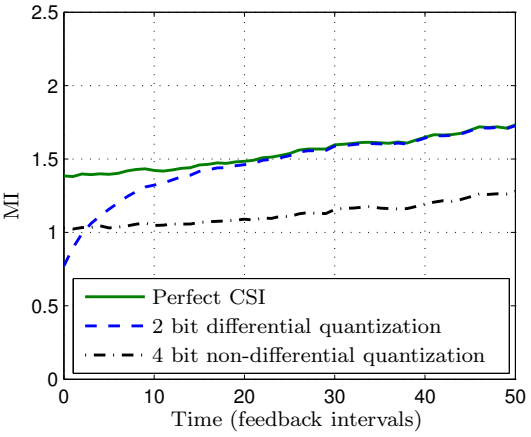

(d) MI in a low mobility scenario (measurement 2)

Figure 3.12: Performance in real channels.

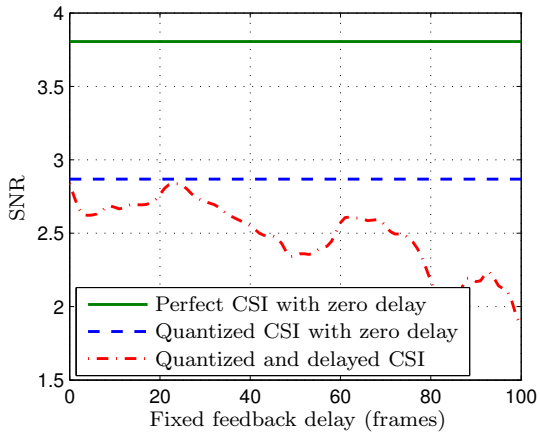

(a) SNR in a high mobility scenario (measurement 1)

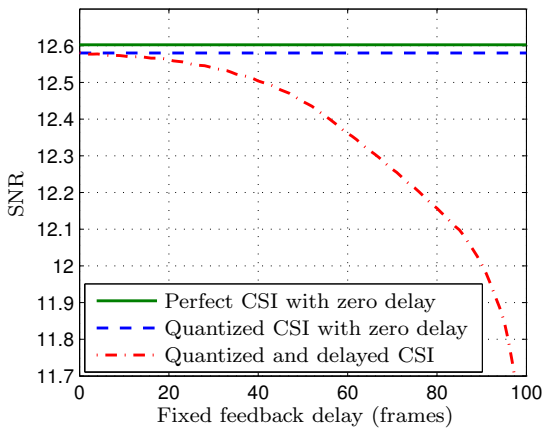

(b) SNR in a low mobility scenario (measurement 2)

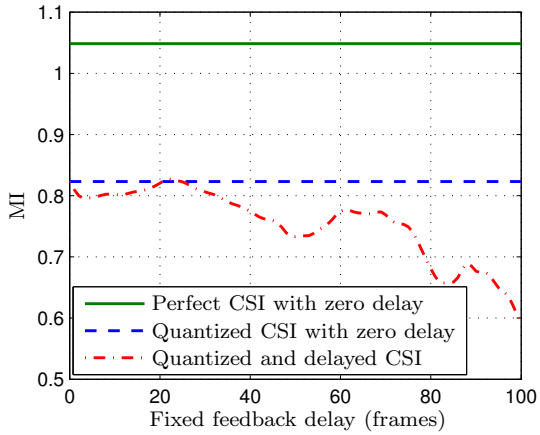

(c) MI in a high mobility scenario (measurement 1)

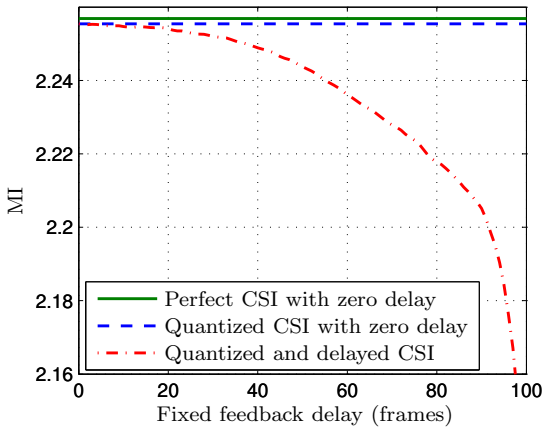

(d) MI in a low mobility scenario (measurement 2)

Figure 3.13: Performance in real channels: effect of delayed feedback.

3.7 Chapter summary and conclusions

This chapter has presented a feedback strategy proposed for MIMO communications, which is based on a differential quantization of the channel Gram matrix using geodesic routes and has several advantages over other existing feedback strategies. The proposed technique exploits the intrinsic geometry of channel Gram matrices (positive, definite, and Hermitian) versus channel response matrices in order to improve quantization performance. The use of orthogonal geodesic routes generates quantization candidates at each feedback interval that are better distributed within the set than in the case of channel response matrix quantization. Another fundamental advantage lies on the fact that the transmitter is not forced to apply uniform power allocation among the spatial transmission modes, which translates into a design gain with respect to designs based on the Grassmannian manifold. The differential scheme exploits the correlation in time to progressively refine the accuracy of the feedback.

Furthermore, it has been proved that the proposed strategy follows in average the direction of the gradient and a closed form expression for the covariance matrix of the directions selected in the quantization has been presented.

Simulations have shown that the proposed algorithm based on differential quantization using geodesic curves achieves better performance than other techniques based on the direct quantization of the channel response matrix or the quantization of the subspace spanned by the strongest eigenmodes of the MIMO channel, as well as non-differential strategies like Grassmannian packaging.

3.A Derivations in the Taylor approximation of (3.17)

Equation (3.17) considers a first order Taylor approximation of the cost function with respect to the first variable (the discrete time index is omitted for clarity in the notation):

$$g\big(\widehat{\mathbf{R}}_H^{(-1)},\mathbf{H}\big)-g\big(\widehat{\mathbf{R}}_H^{(+1)},\mathbf{H}\big)=\operatorname{tr}\mathfrak{Re}\left[g_B^T\big(\widehat{\mathbf{R}}_H^{(-1)}-\widehat{\mathbf{R}}_H^{(+1)}\big)\right]+O\left(\|\mathbf{C}\|^2\right), \tag{3.43}$$

where $[g_B]_{ij}=\frac{\partial g(\mathbf{B},\mathbf{H})}{\partial \mathbf{B}_{ij}}$, ^{T} is the transpose operator and $O\left(\|\mathbf{C}\|^2\right)$ denotes symbolically that the error in the Taylor approximation is bounded quadratically (error $\leq b\|\mathbf{C}\|^2$) for $\mathbf{C}$ small.

Then, according to the Taylor approximation it follows that:

$$\begin{aligned}
g\big(\widehat{\mathbf{R}}_H^{(-1)},\mathbf{H}\big)&=g\big(\mathbf{B}+\widehat{\mathbf{R}}_H^{(-1)}-\mathbf{B},\mathbf{H}\big)=g\big(\mathbf{B},\mathbf{H}\big)+g_B^T\big(\widehat{\mathbf{R}}_H^{(-1)}-\mathbf{B}\big)+O\left(\|\widehat{\mathbf{R}}_H^{(-1)}-\mathbf{B}\|^2\right),\\
g\big(\widehat{\mathbf{R}}_H^{(+1)},\mathbf{H}\big)&=g\big(\mathbf{B}+\widehat{\mathbf{R}}_H^{(+1)}-\mathbf{B},\mathbf{H}\big)=g\big(\mathbf{B},\mathbf{H}\big)+g_B^T\big(\widehat{\mathbf{R}}_H^{(+1)}-\mathbf{B}\big)+O\left(\|\widehat{\mathbf{R}}_H^{(+1)}-\mathbf{B}\|^2\right),
\end{aligned}$$

which means that:

$$\begin{aligned}
g\big(\widehat{\mathbf{R}}_H^{(-1)},\mathbf{H}\big)-g\big(\widehat{\mathbf{R}}_H^{(+1)},\mathbf{H}\big)&=g_B^T\big(\widehat{\mathbf{R}}_H^{(-1)}-\widehat{\mathbf{R}}_H^{(+1)}\big)+O\left(\|\widehat{\mathbf{R}}_H^{(+1)}-\mathbf{B}\|^2\right)+O\left(\|\widehat{\mathbf{R}}_H^{(-1)}-\mathbf{B}\|^2\right)\\
&=g_B^T\big(\widehat{\mathbf{R}}_H^{(-1)}-\widehat{\mathbf{R}}_H^{(+1)}\big)+O\left(\|\mathbf{C}\|^2\right),
\end{aligned} \tag{3.44}$$

since

$$\begin{aligned}
O\left(\|\widehat{\mathbf{R}}_H^{(-1)}-\mathbf{B}\|^2\right)&=O\left(\|\mathbf{B}^{1/2}\exp\left(-\mathbf{C}\right)\mathbf{B}^{1/2}-\mathbf{B}\|^2\right) &(3.45)\\
&=O\left(\|\mathbf{B}^{1/2}\left(\mathbf{I}-\mathbf{C}+O\left(\|\mathbf{C}\|^2\right)\right)\mathbf{B}^{1/2}-\mathbf{B}\|^2\right) &(3.46)\\
&=O\left(\|\mathbf{C}+O\left(\|\mathbf{C}\|^2\right)\|^2\right)=O\left(\|\mathbf{C}\|^2\right), &(3.47)
\end{aligned}$$

and following the same process with $\widehat{\mathbf{R}}_H^{(+1)}$ results in $O\left(\|\widehat{\mathbf{R}}_H^{(+1)}-\mathbf{B}\|^2\right)=O\left(\|\mathbf{C}\|^2\right)$.

3.B Gradient in the space of Hermitian positive definite matrices

The gradient of function f at $\mathbf{Y}$ is defined to be the tangent vector ∇f such that [Ede98]:

$$\mathrm{tr}\left\{f_{\mathbf{Y}}^{T}\Delta\right\} = \langle \nabla f, \Delta \rangle_{\mathbf{Y}} \triangleq \mathrm{tr}\left\{\mathbf{Y}^{-1}\nabla f \mathbf{Y}^{-1}\Delta\right\}, \tag{3.48}$$

where $f_{\mathbf{Y}}$ is the matrix of partial derivatives and Δ is any direction vector.

Derivation of the gradient expression: We have that, if $\mathbf{B}^{-}$ and $\mathbf{B}^{+}$ are close to $\mathbf{B}$,

$$g\left(\mathbf{B}^{-},\mathbf{H}\right) - g\left(\mathbf{B}^{+},\mathbf{H}\right) \simeq \mathrm{tr}\left\{g_{B}^{T}\left(\mathbf{B}^{-}-\mathbf{B}^{+}\right)\right\}. \tag{3.49}$$

Equation (3.48) can be expressed using the scalar product in the space of Hermitian positive definite matrices:

$$\langle \nabla g, \mathbf{B}^{-}-\mathbf{B}^{+}\rangle_{\mathbf{B}} = \mathrm{tr}\left\{\mathbf{B}^{-1}\nabla g \mathbf{B}^{-1}\left(\mathbf{B}^{-}-\mathbf{B}^{+}\right)\right\}. \tag{3.50}$$

If $\nabla g = \mathbf{B} g_{B}^{T} \mathbf{B}$, then

$$\langle \nabla g, \mathbf{B}^{-}-\mathbf{B}^{+}\rangle_{\mathbf{B}} = \mathrm{tr}\left\{\mathbf{B}^{-1}\nabla g \mathbf{B}^{-1}\left(\mathbf{B}^{-}-\mathbf{B}^{+}\right)\right\} = \mathrm{tr}\left\{g_{B}^{T}\left(\mathbf{B}^{-}-\mathbf{B}^{+}\right)\right\}). \tag{3.51}$$

From (3.51) it follows that $\nabla g = \mathbf{B} g_{B}^{T} \mathbf{B}$ and

$$g_{B}^{T} = \mathbf{B}^{-1}\nabla g \mathbf{B}^{-1}. \tag{3.52}$$

3.C Extension of the lemma from [Ban03a] for Hermitian matrices

Corollary of lemma [[Ban03a], appendix A]: let $\mathbf{G}$ be a nonrandom Hermitian matrix, and $\mathbf{P}$ be a random Hermitian matrix, such that $\mathbf{P} = \mathbf{A}^{H} + \mathbf{A}$, where $\mathbf{A}$ has i.i.d. components, each one following a Gaussian distribution $\mathcal{CN}(0,\sigma^{2})$. If

$$\mathbf{Z} \triangleq \left[\mathrm{sign}\left(\mathrm{tr}\,\mathfrak{Re}\big(\mathbf{GP}\big)\right)\right]\mathbf{P}, \tag{3.53}$$

then

$$\mathbb{E}\{\mathbf{Z}\} = \frac{2\sigma}{\sqrt{\pi}} \frac{\mathbf{G}}{\|\mathbf{G}\|_F}. \tag{3.54}$$

Proof: Since $\mathbf{P} = \mathbf{A}^H + \mathbf{A}$,

$$\mathbf{Z} \triangleq \left[\text{sign}\left(\text{tr}\,\mathfrak{Re}\left(\mathbf{G}(\mathbf{A}^H + \mathbf{A})\right)\right)\right] \mathbf{A}^H + \left[\text{sign}\left(\text{tr}\,\mathfrak{Re}\left(\mathbf{G}(\mathbf{A}^H + \mathbf{A})\right)\right)\right] \mathbf{A}. \tag{3.55}$$

Matrix $\mathbf{G}$ is Hermitian, so it can be written as $\mathbf{G} = \mathbf{G}^H = \mathbf{U} + \mathbf{U}^H$. Then

$$\begin{aligned} \mathbf{G}\left(\mathbf{A}^H + \mathbf{A}\right) &= \left(\mathbf{U}^H + \mathbf{U}\right)\left(\mathbf{A}^H + \mathbf{A}\right) \\ &= \mathbf{U}\mathbf{A}^H + \mathbf{U}^H\mathbf{A} + \mathbf{U}\mathbf{A} + \mathbf{U}^H\mathbf{A}^H. \end{aligned} \tag{3.56}$$

Substituting the expressions of (3.56) in (3.55) results in:

$$\mathbf{Z} = \left[\text{sign}\left(\text{tr}\,\mathfrak{Re}\left(\mathbf{G}\mathbf{A}^H\right)\right)\right] \mathbf{A}^H + \left[\text{sign}\left(\text{tr}\,\mathfrak{Re}\left(\mathbf{G}\mathbf{A}\right)\right)\right] \mathbf{A}. \tag{3.57}$$

Consequently, and applying directly [[Ban03a], appendix A], it follows that

$$\begin{aligned} \mathbb{E}\{\mathbf{Z}\} \triangleq\ & \mathbb{E}\left\{\left[\text{sign}\left(\text{tr}\,\mathfrak{Re}\left(\mathbf{G}\mathbf{A}^H\right)\right)\right] \mathbf{A}^H\right\} + \mathbb{E}\left\{\left[\text{sign}\left(\text{tr}\,\mathfrak{Re}\left(\mathbf{G}\mathbf{A}\right)\right)\right] \mathbf{A}\right\} \\ =\ & \frac{2\sigma}{\sqrt{\pi}} \frac{\mathbf{G}}{\|\mathbf{G}\|_F}. \end{aligned} \tag{3.58}$$

3.D Quadratic error behavior in the result of appendix 3.C

The problem considered in appendix 3.C can be expressed in vector form by adequately defining vectors $\widetilde{\mathbf{p}} \in \Re^N$, $\mathbf{g} \in \Re^N$, whose elements correspond to the real and imaginary parts of the components of matrices $\mathbf{P}$ and $\mathbf{G}$ (see [[Ban03b], appendix A] for an example of a similar procedure). In the following it is assumed that $\widetilde{\mathbf{p}}$ has i.i.d. elements which are Gaussian with zero mean and variance σ^2. Considering an error term which results from a previous Taylor approximation that is upper bounded by a quadratic expression in the neighborhood of $\widetilde{\mathbf{p}}$ (see (3.22)), it follows that:

$$\mathbb{E}\left\{\text{sign}\left(\mathbf{g}^T\widetilde{\mathbf{p}} + O\left(\|\widetilde{\mathbf{p}}\|^2\right)\right)\widetilde{\mathbf{p}}\right\} = \mathbb{E}\left\{\text{sign}\left(\frac{\mathbf{g}^T}{\|\mathbf{g}\|}\widetilde{\mathbf{p}} + O\left(\|\widetilde{\mathbf{p}}\|^2\right)\right)\widetilde{\mathbf{p}}\right\}. \tag{3.59}$$

The objective of this appendix is to find a bound on the magnitude of the error of (3.59). If we define $\widetilde{\mathbf{p}} = \mathbf{U}\mathbf{p}$, with $\mathbf{U}$ unitary[16] such that $\frac{\mathbf{g}^T}{\|\mathbf{g}\|}\mathbf{U} = [1\ 0\ 0\ ...\ 0]$, then (3.59) can be written as:

$$\mathbb{E}\{\text{sign}(\mathbf{g}^T\mathbf{U}\mathbf{p}+O(\|\mathbf{p}\|^2))\,\mathbf{U}\mathbf{p}\} = \mathbf{U}\mathbb{E}\{\mathbf{x}\}\,;\ \mathbf{x} = \text{sign}\left(p_1 + O\left(\|\mathbf{p}\|^2\right)\right)\mathbf{p}, \tag{3.60}$$

and if the error is denoted by $\widetilde{\mathbf{r}}$, then

$$\mathbb{E}\{\widetilde{\mathbf{r}}\} = \mathbf{U}\mathbb{E}\{\mathbf{r}\}, \tag{3.61}$$

with $\mathbf{r} = \text{sign}(p_1)\,\mathbf{p} - \mathbf{x} = (\text{sign}(p_1) - \text{sign}(p_1 + O(\|\mathbf{p}\|^2)))\,\mathbf{p}$.

In order to calculate $\mathbb{E}\{\mathbf{r}\}$, the space over $\mathbf{p}$ can be divided into 2 regions: the neighborhood[17] of $\mathbf{p} = \mathbf{0}$ (where the approximation that leads to the quadratic bound on the error term is valid), and the outside of the neighborhood of $\mathbf{p} = \mathbf{0}$ (where the approximation is not valid and we will assume that there is always error). An upper bound on $\mathbb{E}\{\mathbf{r}\}$ can be calculated therefore as the sum of the bounds on the neighborhood of 0 (denoted by $\check{\mathbf{r}}_\mathbf{i}$) and outside the neighborhood of 0 (denoted by $\check{\mathbf{r}}_\mathbf{o}$). It will be shown that the expectance of the total error can be upper bounded as $\mathbb{E}\{\mathbf{r}\} = \check{\mathbf{r}}_\mathbf{i} + \check{\mathbf{r}}_\mathbf{o} = O(\sigma^2)$, where $\check{\mathbf{r}}_\mathbf{i} = \int_{\mathbf{p}\in[-\varepsilon,\varepsilon]^N} \mathbf{r}(\mathbf{p}) f_\mathbf{p}(\mathbf{p}) d\mathbf{p}$, $\check{\mathbf{r}}_\mathbf{o} = \int_{\mathbf{p}\notin[-\varepsilon,\varepsilon]^N} \mathbf{r}(\mathbf{p}) f_\mathbf{p}(\mathbf{p}) d\mathbf{p}$ and $f_\mathbf{p}(\mathbf{p})$ denotes the probability density function of $\mathbf{p}$.

3.D.1 Calculation of $\check{\mathbf{r}}_\mathbf{i}$ ($\mathbf{p}$ in the neighborhood of 0)

The worst case error in the neighborhood of $\mathbf{p} = \mathbf{0}$ comes from the upper bound on $O(\|\mathbf{p}\|^2)$, which is: $a\sum_{n=1}^{N} p_n^2$. Assuming this worst case, the k-th component of $\mathbf{x}$ can be written as:

$$x_k = \begin{cases} p_k\,, & p_1 + a\sum_{n=1}^{N} p_n^2 \geq 0 \\ -p_k\,, & p_1 + a\sum_{n=1}^{N} p_n^2 < 0. \end{cases} \tag{3.62}$$

[16] This transformation by a unitary matrix does not alter the magnitude of the error.

[17] The neighborhood of 0 is defined as an N-dimensional cube of side 2ε centered at the origin, i.e., $[-\varepsilon,\varepsilon]^N$, where ε is such that the bounds defined by Landau's O are valid for all the Taylor approximations that appear in this appendix within such cube.

For the calculation of an upper bound on $\check{\mathbf{r}}_{\mathbf{i}}$, the case of x_1 is studied first. Then the cases of $x_k, \forall k = 2, ..., N$ will be analyzed.

First parameter, x_1

From the equation without quadratic error it follows that the threshold where the sign function changes corresponds to $\gamma_l = 0$. In the case with quadratic error (3.62), the threshold corresponds to $\gamma_q = \frac{-1}{2a} + \frac{1}{2a}\sqrt{1 - 4a^2 \sum_{n=2}^{N} p_n^2}$, which leads to the following Taylor approximations: $\gamma_q = -a \sum_{n=2}^{N} p_n^2 + O\left(\left(\sum_{n=2}^{N} p_n^2\right)^2\right)$ and $\gamma_q^2 = O\left(\left(\sum_{n=2}^{N} p_n^2\right)^2\right)$.

The first component of $\check{\mathbf{r}}_{\mathbf{i}}$ is upper bounded by the following expression:

$$\check{r}_{i_1} \leq \int_{p_N=-\varepsilon}^{\varepsilon} ... \int_{p_2=-\varepsilon}^{\varepsilon} \int_{p_1=\gamma_q}^{0} 2|p_1| \frac{1}{\sqrt{2\pi}\sigma} \exp\left(-\frac{p_1^2}{2\sigma^2}\right) dp_1 \prod_{n=2}^{N} \left(\frac{1}{\sqrt{2\pi}\sigma} \exp\left(-\frac{p_n^2}{2\sigma^2}\right) dp_n\right). \tag{3.63}$$

An upper bound of the integral over p_1 is computed first, as expressed in:

$$\int_{p_1=\gamma_q}^{0} 2|p_1| \frac{1}{\sqrt{2\pi}\sigma} \exp\left(-\frac{p_1^2}{2\sigma^2}\right) dp_1 \leq |\gamma_q| 2 |\gamma_q| \frac{1}{\sqrt{2\pi}\sigma} \leq c \left(\sum_{n=2}^{N} p_n^2\right)^2 \frac{1}{\sigma}. \tag{3.64}$$

Then, since $\left(\sum_{n=2}^{N} p_n^2\right)^2 = \sum_{i=2}^{N} \sum_{j=2}^{N} p_i^2 p_j^2$, the following bound results:

$$\check{r}_{i_1} \leq \frac{c}{\sigma} \sum_{i=2}^{N} \sum_{j=2}^{N} \int_{-\infty}^{\infty} ... \int_{-\infty}^{\infty} p_i^2 p_j^2 \prod_{n=2}^{N} \left(\frac{1}{\sqrt{2\pi}\sigma} \exp\left(-\frac{p_n^2}{2\sigma^2}\right) dp_n\right). \tag{3.65}$$

The integral $\int_{-\infty}^{\infty} ... \int_{-\infty}^{\infty} p_i^2 p_j^2 \prod_{n=2}^{N} \left(\frac{1}{\sqrt{2\pi}\sigma} \exp\left(-\frac{p_n^2}{2\sigma^2}\right) dp_n\right)$ is equal to $3\sigma^4$ for $i = j$ and equal to σ^4 for $i \neq j$:

- case $i = j$:

$$\int_{-\infty}^{\infty} ... \int_{-\infty}^{\infty} p_i^4 \prod_{n=2}^{N} \left(\frac{1}{\sqrt{2\pi}\sigma} \exp\left(-\frac{p_n^2}{2\sigma^2}\right) dp_n\right) = 3\sigma^4. \tag{3.66}$$

- case $i \neq j$:

$$\int_{-\infty}^{\infty} ... \int_{-\infty}^{\infty} p_i^2 p_j^2 \prod_{n=2}^{N} \left(\frac{1}{\sqrt{2\pi}\sigma} \exp\left(-\frac{p_n^2}{2\sigma^2} \right) dp_n \right) = \sigma^2 \sigma^2 = \sigma^4. \tag{3.67}$$

Consequently, and since there are $N-1$ cases where $i = j$ and $(N-1)(N-2)$ cases where $i \neq j$, from (3.65) it follows that:

$$\check{r}_{i_1} \leq \frac{c}{\sigma} \left((N-1)3\sigma^4 + (N-1)(N-2)\sigma^4 \right) = c(N-1)(N+1)\sigma^3, \tag{3.68}$$

that is, $\check{r}_{i_1} = O(\sigma^3)$.

Rest of the parameters, $x_k, k = 2, ..., N$

The k-th component of $\check{\mathbf{r}}_\mathbf{i}$ is upper bounded by the following expression:

$$\check{r}_{i_k} \leq \int_{p_N=-\varepsilon}^{\varepsilon} ... \int_{p_2=-\varepsilon}^{\varepsilon} \int_{p_1=\gamma_q}^{0} 2|p_k| \frac{1}{\sqrt{2\pi}\sigma} \exp\left(-\frac{p_1^2}{2\sigma^2} \right) dp_1 \prod_{n=2}^{N} \left(\frac{1}{\sqrt{2\pi}\sigma} \exp\left(-\frac{p_n^2}{2\sigma^2} \right) dp_n \right). \tag{3.69}$$

An upper bound of the integral over p_1 is derived first:

$$\int_{p_1=\gamma_q}^{0} 2|p_k| \frac{1}{\sqrt{2\pi}\sigma} \exp\left(-\frac{p_1^2}{2\sigma^2} \right) dp_1 \leq 2|p_k||\gamma_q| \frac{1}{\sqrt{2\pi}\sigma}. \tag{3.70}$$

Since $|\gamma_q| \leq a \sum_{n=2}^{N} p_n^2 + O\left((\sum_{n=2}^{N} p_n^2)^2 \right)$, it follows that $|\gamma_q| \leq a p_k^2 + a \sum_{\substack{n=2 \\ n \neq k}}^{N} p_n^2 + c \sum_{i=2}^{N} \sum_{j=2}^{N} p_i^2 p_j^2$, and $\check{r}_{i_k}$ can be bounded as:

$$\begin{aligned} \check{r}_{i_k} \leq & \int_{-\varepsilon}^{\varepsilon} ... \int_{-\varepsilon}^{\varepsilon} \frac{2}{\sqrt{2\pi}\sigma} |p_k| \left(a p_k^2 + a \sum_{\substack{s=2 \\ s \neq k}}^{N} p_s^2 + c \sum_{i=2}^{N} \sum_{j=2}^{N} p_i^2 p_j^2 \right) \\ & \prod_{n=2}^{N} \left(\frac{1}{\sqrt{2\pi}\sigma} \exp\left(-\frac{p_n^2}{2\sigma^2} \right) dp_n \right) \qquad (3.71) \\ \leq & \int_{-\infty}^{\infty} ... \int_{-\infty}^{\infty} \frac{2}{\sqrt{2\pi}\sigma} \left(a|p_k|^3 + a|p_k| \sum_{\substack{s=2 \\ s \neq k}}^{N} p_s^2 + c|p_k| \sum_{i=2}^{N} \sum_{j=2}^{N} p_i^2 p_j^2 \right) \\ & \prod_{n=2}^{N} \left(\frac{1}{\sqrt{2\pi}\sigma} \exp\left(-\frac{p_n^2}{2\sigma^2} \right) dp_n \right). \qquad (3.72) \end{aligned}$$

The integrals for the three terms in (3.72) can be computed independently ((3.72) =(3.73)+(3.74)+(3.75)):

$$\int_{-\infty}^{\infty}\overset{...}{}\int_{-\infty}^{\infty}\frac{2}{\sqrt{2\pi}\sigma}\left(a|p_k|^3\right)\prod_{n=2}^{N}\left(\frac{1}{\sqrt{2\pi}\sigma}\exp\left(-\frac{p_n^2}{2\sigma^2}\right)dp_n\right)=\frac{4a}{\sqrt{2\pi}\sigma}\sqrt{\frac{2}{\pi}}\sigma^3=\frac{4a}{\pi}\sigma^2. \tag{3.73}$$

$$\int_{-\infty}^{\infty}\overset{...}{}\int_{-\infty}^{\infty}\frac{2}{\sqrt{2\pi}\sigma}\left(a|p_k|\sum_{\substack{s=1\\s\neq k}}^{N}p_s^2\right)\prod_{n=2}^{N}\left(\frac{1}{\sqrt{2\pi}\sigma}\exp\left(-\frac{p_n^2}{2\sigma^2}\right)dp_n\right)$$
$$=\frac{2a}{\sqrt{2\pi}\sigma}\frac{\sigma}{\sqrt{2\pi}}(N-2)2\sigma^2=\frac{2a}{\pi}(N-2)\sigma^2. \tag{3.74}$$

$$\int_{-\infty}^{\infty}\overset{...}{}\int_{-\infty}^{\infty}\frac{2}{\sqrt{2\pi}\sigma}\left(c|p_k|\sum_{\substack{i=1\\i\neq k}}^{N}\sum_{\substack{j=1\\j\neq k}}^{N}p_i^2p_j^2\right)\prod_{n=2}^{N}\left(\frac{1}{\sqrt{2\pi}\sigma}\exp\left(-\frac{p_n^2}{2\sigma^2}\right)dp_n\right)=\frac{a}{\pi}(N-1)^2\sigma^4. \tag{3.75}$$

Finally, from ((3.72) =(3.73)+(3.74)+(3.75)) it follows that:

$$\check{r}_{i_k}\leq\frac{4a}{\pi}\sigma^2+\frac{2a}{\pi}(N-2)\sigma^2+\frac{a}{\pi}(N-1)^2\sigma^4=\sigma^2\frac{a}{\pi}\left(4+2(N-2)+(N-1)^2\sigma^2\right). \tag{3.76}$$

From (3.76) it follows that $\check{r}_{i_k}=O(\sigma^2)$.

3.D.2 Calculation of $\check{\mathbf{r}}_\mathbf{o}$ (p outside the neighborhood of 0)

In the calculation of $\check{\mathbf{r}}_\mathbf{o}$ a worst case situation will be considered, where there is always error in the sign function, i.e., the error is upper bounded at each point and component by $2|p_k|$ It is computed as the integral over the complete domain space minus the

integral on the neighborhood of 0. For the k-th element, $\check{r}_{o_k}$ the expression is given by

$$\begin{aligned}\check{r}_{o_k} &= \int_{-\infty}^{\infty}\ldots\int_{-\infty}^{\infty} 2|p_k| \prod_{n=1}^{N}\left(\frac{1}{\sqrt{2\pi\sigma^2}}\exp\left(-\frac{p_n^2}{2\sigma^2}\right)dp_n\right) \\ &\quad - \int_{-\varepsilon}^{\varepsilon}\ldots\int_{-\varepsilon}^{\varepsilon} 2|p_k| \prod_{n=1}^{N}\left(\frac{1}{\sqrt{2\pi\sigma^2}}\exp\left(-\frac{p_n^2}{2\sigma^2}\right)dp_n\right) \qquad (3.77)\\ &= 4\frac{\sigma}{\sqrt{2\pi}} - 4\left[\operatorname{erf}\left(\frac{\varepsilon}{\sigma\sqrt{2}}\right)\right]^{N-1}\left(\frac{\sigma}{\sqrt{2\pi}} - \frac{\sigma}{\sqrt{2\pi}}\exp\left(-\frac{\varepsilon^2}{2\sigma^2}\right)\right) \qquad (3.78)\\ &= 4\frac{\sigma}{2\sqrt{\pi}}\left(1 - \left(\operatorname{erf}\left(\frac{\varepsilon}{\sigma\sqrt{2}}\right)\right)^{N-1}\left(1-\exp\left(-\frac{\varepsilon^2}{2\sigma^2}\right)\right)\right). \qquad (3.79)\end{aligned}$$

By applying L'Hôpital's rule it follows that:

$$\begin{aligned}&\lim_{\sigma\to 0}\frac{1-\left(\operatorname{erf}\left(\frac{\varepsilon}{\sigma\sqrt{2}}\right)\right)^{N-1}\left(1-\exp\left(-\frac{\varepsilon^2}{2\sigma^2}\right)\right)}{\sigma} \\ &\quad= \lim_{\sigma\to 0}\left((N-1)\left[\operatorname{erf}\left(\frac{\varepsilon}{\sigma\sqrt{2}}\right)\right]^{N-2}\frac{2}{\sqrt{\pi}}\exp\left(\frac{-\varepsilon^2}{2\sigma^2}\right)\left(\frac{-\varepsilon}{\sqrt{2}\sigma^2}\right)\left[1-\exp\left(\frac{-\varepsilon^2}{2\sigma^2}\right)\right]\right. \\ &\qquad\left. + \left[\operatorname{erf}\left(\frac{\varepsilon}{\sigma\sqrt{2}}\right)\right]^{N-1}\left[-\exp\left(\frac{-\varepsilon^2}{2\sigma^2}\right)\frac{\varepsilon^2}{\sigma^3}\right]\right) = 0. \qquad (3.80)\end{aligned}$$

The last comes from the fact that: $\lim_{\sigma\to 0}\frac{\exp\left(-\frac{m}{\sigma^2}\right)}{\sigma^k} = 0,\ \forall m,k>0$. This implies that:

$$\check{r}_{o_k} = \sigma O(\sigma) = O(\sigma^2). \qquad (3.81)$$

3.E Covariance of the direction of the selected geodesic curves

Lemma: Let $\mathbf{G}$ be nonrandom Hermitian and $\mathbf{P}$ random Hermitian, such that $\mathbf{P} = \mathbf{A}^H + \mathbf{A}$, where $\mathbf{A}$ has i.i.d. components, each one following a Gaussian distribution $\mathcal{CN}(0,\sigma^2)$. If

$$\begin{aligned}\mathbf{Z} &\triangleq \left[\operatorname{sign}\left(\operatorname{tr}\mathfrak{Re}\left(\mathbf{GP}\right) + O\left(\|\mathbf{P}\|^2\right)\right)\right]\mathbf{P}, \qquad (3.82)\\ \mathbf{z} &\triangleq \operatorname{vec}\left(\mathbf{Z}\right),\quad \mathbf{e} \triangleq \mathbf{z} - \mathbb{E}\{\mathbf{z}\},\end{aligned}$$

then

$$\mathbb{E}\{\mathbf{e}\mathbf{e}^H\} = \left(2\mathbf{I} - \frac{4}{\pi}\frac{\mathbf{g}^*\mathbf{g}^T}{\|\mathbf{g}\|^2}\right)\sigma^2 + O(\sigma^3), \tag{3.83}$$

where $\mathbf{g}$ is the result of stacking the columns of matrix $\mathbf{G}^T$.

Proof: (3.82) can be written as

$$\mathbf{Z} = \left[\text{sign}\left(\text{tr}\,\mathfrak{Re}\left(\mathbf{G}\mathbf{A}^H\right) + f(\mathbf{A})\right)\right]\mathbf{A}^H + \left[\text{sign}\left(\text{tr}\,\mathfrak{Re}\left(\mathbf{G}\mathbf{A}\right) + f(\mathbf{A})\right)\right]\mathbf{A}, \tag{3.84}$$

(see (3.55)-(3.57)), where $f(\mathbf{A}) = O\left(\|\mathbf{A}\|^2\right)$, and its vectorized form $\mathbf{z}$ is given by:

$$\mathbf{z} \triangleq \text{vec}\,(\mathbf{Z}) = \left[\text{sign}\left(\mathfrak{Re}\left(\widetilde{\mathbf{a}}^H\mathbf{g}^*\right) + f(\mathbf{A})\right)\right]\widetilde{\mathbf{a}} + \left[\text{sign}\left(\mathfrak{Re}\left(\mathbf{a}^H\mathbf{g}^*\right) + f(\mathbf{A})\right)\right]\mathbf{a}, \tag{3.85}$$

where $\mathbf{g}$ is the result of stacking the columns of $\mathbf{G}^T$, $\mathbf{a}$ is the result of stacking the columns of $\mathbf{A}$, and $\widetilde{\mathbf{a}}$ is the result of stacking the columns of $\mathbf{A}^H$. The covariance of $\mathbf{z}$ is:

$$\mathbf{C}_{\mathbf{zz}} = \mathbf{C}_{\mathbf{cc}} + \mathbf{C}_{\mathbf{dd}} + \mathbf{C}_{\mathbf{cd}} + \mathbf{C}_{\mathbf{dc}}, \tag{3.86}$$

where $\mathbf{C}_{\mathbf{uv}} = \mathbb{E}\left\{\mathbf{u}\mathbf{v}^H\right\} - \mathbb{E}\left\{\mathbf{u}\right\}\mathbb{E}\left\{\mathbf{v}^H\right\}$, $\mathbf{c} = \left[\text{sign}\left(\mathfrak{Re}\left(\widetilde{\mathbf{a}}^H\mathbf{g}^*\right) + f(\mathbf{A})\right)\right]\widetilde{\mathbf{a}}$, and $\mathbf{d} = \left[\text{sign}\left(\mathfrak{Re}\left(\mathbf{a}^H\mathbf{g}^*\right) + f(\mathbf{A})\right)\right]\mathbf{a}$.

The following theorem (which is an extended version of [[Ban03b], appendix A]) is used next.

Theorem: For a nonrandom $\mathbf{g}$ and a zero mean complex Gaussian vector $\mathbf{s}$ with autocorrelation $\sigma^2\mathbf{I}$, define the decision vector $\mathbf{x}$ and error vector $\mathbf{e}$ as follows:

$$\mathbf{x} \triangleq \text{sign}\left(\mathfrak{Re}\left(\mathbf{s}^H\mathbf{g}\right)\right)\mathbf{s}, \qquad \mathbf{e} \triangleq \mathbf{x} - \mathbb{E}\left\{\mathbf{x}\right\}. \tag{3.87}$$

Then, the first and second moments are given by:

$$\mathbb{E}\left\{\mathbf{x}\right\} = \frac{\sigma}{\sqrt{\pi}}\frac{\mathbf{g}}{\|\mathbf{g}\|}; \tag{3.88}$$

$$\mathbb{E}\left\{\mathbf{e}\mathbf{e}^H\right\} = \mathbb{E}\left\{\left(\mathbf{x} - \frac{\sigma}{\sqrt{\pi}}\frac{\mathbf{g}}{\|\mathbf{g}\|}\right)\left(\mathbf{x} - \frac{\sigma}{\sqrt{\pi}}\frac{\mathbf{g}}{\|\mathbf{g}\|}\right)^H\right\} = \sigma^2\mathbf{I} - \frac{\sigma^2}{\pi}\frac{\mathbf{g}\mathbf{g}^H}{\|\mathbf{g}\|^2}. \tag{3.89}$$

For the case where there is an error term $O(\|\mathbf{s}\|^2)$ inside the sign function, then:

$$\widetilde{\mathbf{x}} \triangleq \text{sign}\left(\mathfrak{Re}\left(\mathbf{s}^H\mathbf{g}\right) + O\left(\|\mathbf{s}\|^2\right)\right)\mathbf{s}, \qquad \widetilde{\mathbf{e}} \triangleq \widetilde{\mathbf{x}} - \mathbb{E}\left\{\widetilde{\mathbf{x}}\right\}. \tag{3.90}$$

Then, the first and second order moments can be calculated straightforwardly and are given by the following expressions (See appendix 3.D):

$$\mathbb{E}\left\{\widetilde{\mathbf{x}}\right\} = \frac{\sigma}{\sqrt{\pi}}\frac{\mathbf{g}}{\|\mathbf{g}\|} + O\left(\sigma^2\right), \tag{3.91}$$

$$\begin{aligned}\mathbb{E}\left\{\widetilde{\mathbf{e}}\widetilde{\mathbf{e}}^H\right\} &= \mathbb{E}\left\{\left(\widetilde{\mathbf{x}} - \frac{\sigma}{\sqrt{\pi}}\frac{\mathbf{g}}{\|\mathbf{g}\|} + O\left(\sigma^2\right)\right)\left(\widetilde{\mathbf{x}} - \frac{\sigma}{\sqrt{\pi}}\frac{\mathbf{g}}{\|\mathbf{g}\|} + O\left(\sigma^2\right)\right)^H\right\} \\ &= \sigma^2\mathbf{I} - \frac{\sigma^2}{\pi}\frac{\mathbf{g}\mathbf{g}^H}{\|\mathbf{g}\|^2} + O\left(\sigma^3\right).\end{aligned} \tag{3.92}$$

which follow from $\mathbb{E}\left\{\widetilde{\mathbf{x}}\widetilde{\mathbf{x}}^H\right\} = \sigma^2\mathbf{I}$, $\mathbb{E}\left\{\widetilde{\mathbf{x}}\frac{\sigma}{\sqrt{\pi}}\frac{\mathbf{g}}{\|\mathbf{g}\|}\right\} = \frac{\sigma^2}{\pi}\frac{\mathbf{g}\mathbf{g}^H}{\|\mathbf{g}\|^2} + O(\sigma^3)$, and $\mathbb{E}\left\{\widetilde{\mathbf{x}}O(\sigma^2)\right\} = O(\sigma^3)$.

This theorem can be applied directly to the first two terms of (3.86), while for the cross-terms of the covariance we have:

$$\mathbf{C}_{\mathbf{cd}} = \mathbb{E}\left\{\left(\mathbf{c} - \mathbb{E}\left\{\mathbf{c}\right\}\right)\left(\mathbf{d} - \mathbb{E}\left\{\mathbf{d}\right\}\right)^H\right\} = \mathbb{E}\left\{\mathbf{c}\mathbf{d}^H\right\} - \mathbb{E}\left\{\mathbf{c}\right\}\mathbb{E}\left\{\mathbf{d}^H\right\}. \tag{3.93}$$

The first term is zero as shown in (3.94) (we have used the fact that $\mathfrak{Re}\left(\widetilde{\mathbf{a}}^H\mathbf{g}^*\right) = \mathfrak{Re}\left(\mathbf{a}^H\mathbf{g}^*\right)$), and, for the second term, the results of the theorem can be applied directly.

$$\mathbb{E}\left\{\mathbf{c}\mathbf{d}^H\right\} = \mathbb{E}\left\{\left[\text{sign}\left(\mathfrak{Re}\left(\widetilde{\mathbf{a}}^H\mathbf{g}^*\right) + f(\mathbf{A})\right)\right]\left[\text{sign}\left(\mathfrak{Re}\left(\mathbf{a}^H\mathbf{g}^*\right) + f(\mathbf{A})\right)\right]\widetilde{\mathbf{a}}\mathbf{a}^H\right\} \tag{3.94}$$

$$= \mathbb{E}\left\{\widetilde{\mathbf{a}}\mathbf{a}^H\right\} = 0. \tag{3.95}$$

The same procedure can be applied to $\mathbb{E}\left\{\left(\mathbf{d} - \mathbb{E}\left\{\mathbf{d}\right\}\right)\left(\mathbf{c} - \mathbb{E}\left\{\mathbf{c}\right\}\right)^H\right\}$. Finally, (3.86) can be written as:

$$\begin{aligned}\mathbf{C}_{\mathbf{zz}} &= 2\left(\sigma^2\mathbf{I} - \frac{\sigma^2}{\pi}\frac{\mathbf{g}^*\mathbf{g}^{*H}}{\|\mathbf{g}\|^2} + O(\sigma^3)\right) - 2\left(\frac{\sigma^2}{\pi}\frac{\mathbf{g}^*\mathbf{g}^{*H}}{\|\mathbf{g}\|^2} + O(\sigma^3)\right) \\ &= \sigma^2\left(2\mathbf{I} - \frac{4}{\pi}\frac{\mathbf{g}^*\mathbf{g}^T}{\|\mathbf{g}\|^2}\right) + O(\sigma^3).\end{aligned} \tag{3.96}$$

Chapter 4

Feedback in the multiuser MIMO broadcast channel with block diagonalization

4.1 Introduction

The previous chapter showed a quantization and feedback scheme for linear transceiver designs which is valid for all the usual quality criteria (SNR, MI, MSE, etc.) in point-to-point MIMO communication systems. In the case of MIMO BC (downlink) channels, the optimum transmission strategy is Dirty Paper Coding (DPC) [Cos83], which is a non-linear processing technique that has been proved to achieve the capacity region [Wei06]. However, DPC is not implemented in practice due to its high computational complexity. Instead, much simpler linear transceiver designs, such as the ones considered in this chapter, have been shown to achieve almost the same capacity using much lower computational resources [Lee06]. This chapter is focused on the direct application of the feedback algorithm presented in the previous chapter to some specific multiuser linear precoding techniques which are of high relevance and are based

on block diagonalization. Chapter 5 will then present a generalization of the feedback scheme for any multiuser linear design which involves an additional operation at both transmitter and receivers.

As mentioned before, the techniques presented in this chapter are based on BD [Spe04] and are interesting and widely implemented in practice because they provide the same multiplexing gain as DPC, while incurring only in an absolute loss in terms of throughput [She07, Lee07, Hun09] but requiring extremely less computational power.

BD decomposes the overall MIMO BC of the different users into a set of virtual parallel single-user MIMO channels without inter-user interference. In order to do this, accurate CSI is required at the transmitter. In scenarios where channel reciprocity does not hold, a feedback channel with limited capacity is used to send the CSI from the receiver to the transmitter. Because of the limited capacity of the feedback links and the impact that accurate CSI has on the design of the transmitter, proper quantization procedures to be applied to the channel estimates are of great importance.

This chapter is structured as follows. First, the BC system model and a brief introduction on BD is presented in section 4.2. The minimum CSI for the implementation of BD is then shown to be the channel Gram matrix from the transmitter to each receiver, which can be estimated at each receiver and fed back to the transmitter using the technique presented in Chapter 3. Numerical simulations and an analysis of this implementation follow. It is shown through simulations that the proposed scheme outperforms other feedback designs proposed recently in [Cha08, Xia09] and [Rav08]. In section 4.3, a practical scenario of a MIMO backhaul link in the presence of interference is considered and a variation of the BD design with channel Gram matrix feedback is presented. Simulations of the performance and a summary and conclusions section wrap up the chapter.

4.2 Block diagonalized multiuser MIMO systems

This section presents an application of the channel Gram matrix quantization and feedback algorithm presented in chapter 3 to multiuser BD, which is a system architecture framework widely implemented in practice. First, in section 4.2.1 the system and signal models for the BC are introduced. Secondly, a detailed description of BD is presented in section 4.2.2, along with the CSI required at the transmitter for the precoder design based on BD. Then, the feedback algorithm based on differential feedback of each user's channel Gram matrix is presented in section 4.2.3 and simulations of the performance are shown in section 4.2.4.

4.2.1 System and signal models

A MIMO BC system with a single transmitter and K receivers or users is considered, as depicted in Figure 4.1. The transmitter has n_T antennas and the k-th receiver has $n_R^{(k)}$ antennas. The channel matrix from the transmitter to the k-th receiver is denoted by $\mathbf{H}^{(k)} \in \mathbb{C}^{n_R^{(k)} \times n_T}$ and its associated precoding matrix is denoted by $\mathbf{B}^{(k)} \in \mathbb{C}^{n_T \times n_S^{(k)}}$, where $n_S^{(k)}$ is the number of streams to be transmitted to user k. $\mathbf{x}^{(k)} \in \mathbb{C}^{n_S^{(k)}}$ represents the $n_S^{(k)}$ streams of signals to be transmitted with $\mathbb{E}\left\{\mathbf{x}^{(k)}\mathbf{x}^{(k)^H}\right\} = \mathbf{I}$. According to the linear model, the signal at the k-th receiver is, thus:

$$\mathbf{y}^{(k)} = \sum_{i=1}^{K} \mathbf{H}^{(k)}\mathbf{B}^{(i)}\mathbf{x}^{(i)} + \mathbf{w}^{(k)} \in \mathbb{C}^{n_R^{(k)}} \tag{4.1}$$

$$= \mathbf{H}^{(k)}\mathbf{B}^{(k)}\mathbf{x}^{(k)} + \mathbf{H}^{(k)}\tilde{\mathbf{B}}^{(k)}\tilde{\mathbf{x}}^{(k)} + \mathbf{w}^{(k)}, \tag{4.2}$$

where $\mathbf{w}^{(k)} \in \mathbb{C}^{n_R^{(k)}}$ is the AWGN at the receiver with $\mathbb{E}\left\{\mathbf{w}^{(k)}\mathbf{w}^{(k)^H}\right\} = \sigma_w^2\mathbf{I}$. $\tilde{\mathbf{B}}^{(k)}$ and $\tilde{\mathbf{x}}^{(k)}$ result, respectively, from the stack of the the precoding matrices and the transmit vectors for all users other than receiver k:

$$\tilde{\mathbf{B}}^{(k)} = \left[\mathbf{B}^{(1)} \ ... \ \mathbf{B}^{(k-1)} \ \mathbf{B}^{(k+1)} \ ... \ \mathbf{B}^{(K)}\right] \in \mathbb{C}^{n_T \times \sum_{i=1, i\neq k}^{K} n_S^{(i)}}, \tag{4.3}$$

$$\tilde{\mathbf{x}}^{(k)^T} = \left[\mathbf{x}^{(1)^T} \ ... \ \mathbf{x}^{(k-1)^T} \ \mathbf{x}^{(k+1)^T} \ ... \ \mathbf{x}^{(K)^T}\right] \in \mathbb{C}^{\sum_{i=1, i\neq k}^{K} n_S^{(i)}}. \tag{4.4}$$

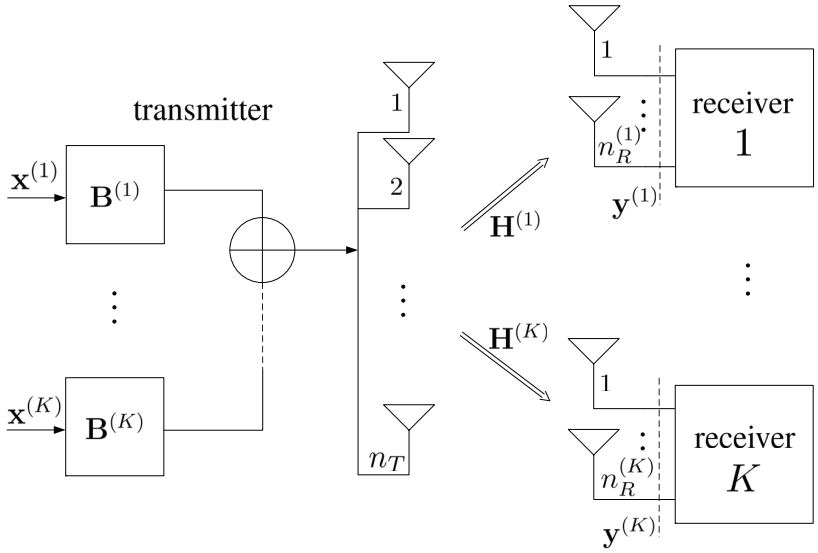

Figure 4.1: MIMO BC system model.

The technique of BD [Spe04] exploits the CSI in order to eliminate interference between users, i.e., the precoding matrices $\mathbf{B}^{(k)}$ are designed so that $\mathbf{H}^{(i)}\mathbf{B}^{(j)} = \mathbf{0}$ for $i \neq j$. The process is explained in detail in section 4.2.2. Consequently, the multiuser channel is divided into parallel single-user MIMO channels, and (4.2) simplifies to:

$$\mathbf{y}^{(k)} = \mathbf{H}^{(k)}\mathbf{B}^{(k)}\mathbf{x}^{(k)} + \mathbf{w}^{(k)}, \quad k = 1, ..., K. \tag{4.5}$$

Appropriate single-user precoding techniques can then be used on top of the BD (for example, waterfilling over the channel eigenmodes to achieve capacity).

Single user MIMO techniques depend on accurate CSI in order to fully exploit the channel characteristics. In multiuser schemes the need for accurate CSI is even higher because, apart from a loss in each user performance, imperfect CSI produces inter-user interference (since in that case BD can not eliminate interference completely). This is more critical in the high SNR regime, precisely where multiuser MIMO shines most.

For this design it is assumed that each receiver estimates perfectly its current channel matrix $\mathbf{H}^{(k)}$, and that the transmitter designs $\mathbf{B}^{(k)}$ assuming that the available CSI at its side is also perfect, i.e., as if quantization or feedback errors were not

present. As will be shown in section 4.2.2, the CSI required at the transmitter for BD corresponds to the Gram matrix of the individual MIMO channels (i.e., $\mathbf{H}^{(k)^H}\mathbf{H}^{(k)}, k = 1, ..., K$).

4.2.2 Introduction to block diagonalization

In the general MIMO BC the signals sent from the transmitter to each receiver are picked up by all the other receivers, causing interference with the signals actually intended for them. The technique BD aims at avoiding interference between signals sent to different users while allowing that all the antennas of each user receive the signals transmitted to such user. That is, the precoder forces transmission nulls in the direction of the non-intended receivers but not in the direction of the antennas of the intended receiver (which is the case in the techniques based on complete zero forcing [Joh05, Wie08]) as depicted in Figure 4.2.

In order to remove all inter-user interference in the system, the precoding matrices $\mathbf{B}^{(k)}$ are designed so that $\mathbf{H}^{(i)}\mathbf{B}^{(j)} = \mathbf{0}$ for $i \neq j$ [Spe04]. This constraint forces $\mathbf{B}^{(k)}$ to lie in the right null space of $\tilde{\mathbf{H}}^{(k)}$, with $\tilde{\mathbf{H}}^{(k)}$ defined as:

$$\tilde{\mathbf{H}}^{(k)} = \left[\mathbf{H}^{(1)^T} \ ... \ \mathbf{H}^{(k-1)^T} \ \mathbf{H}^{(k+1)^T} \ ... \ \mathbf{H}^{(K)^T}\right]^T. \tag{4.6}$$

Note that the system dimension constraint is obtained from this definition. BD as presented here is possible only if $n_T > \max\left\{\text{rank}\left(\tilde{\mathbf{H}}^{(1)}\right), ..., \text{rank}\left(\tilde{\mathbf{H}}^{(K)}\right)\right\}$.

An orthogonal basis for the null space of $\tilde{\mathbf{H}}^{(k)}$ can be obtained as the right singular vectors of $\tilde{\mathbf{H}}^{(k)}$ corresponding to its zero singular values. Then, a matrix $\tilde{\mathbf{V}}_0^{(k)} \in \mathbb{C}^{n_T \times (n_T - \text{rank}\{\tilde{\mathbf{H}}^{(k)}\})}$ can be defined containing as columns such singular vectors of $\tilde{\mathbf{H}}^{(k)}$. These are equal to the eigenvectors corresponding to the zero eigenvalues of $\tilde{\mathbf{H}}^{(k)^H}\tilde{\mathbf{H}}^{(k)}$, which is obtained from the feedback. From (4.6), it follows directly that $\tilde{\mathbf{H}}^{(k)^H}\tilde{\mathbf{H}}^{(k)}$ can be computed at the transmitter as the sum of the individual channel Gram matrices

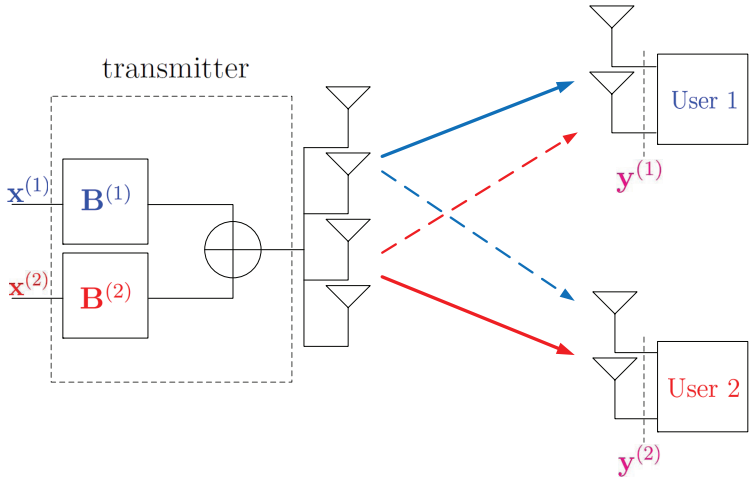

(a)

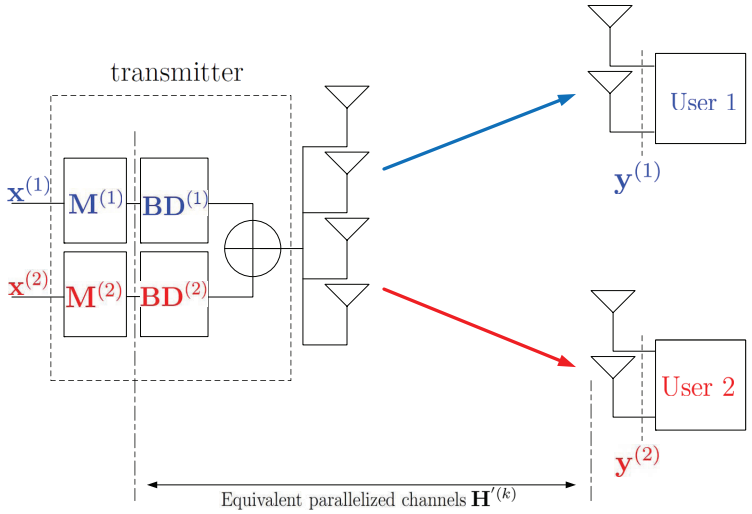

(b)

Figure 4.2: In the general BC scenario (a) the signal sent to each user is received by the other users and this is a source of interference. In a BC scenario with BD design (b) the transmission is constrained through the nullspace of the non-desired users in order not to interfere with other users.

corresponding to users different from k:

$$\tilde{\mathbf{H}}^{(k)^H}\tilde{\mathbf{H}}^{(k)} = \sum_{i=1, i\neq k}^{K} \mathbf{R}_H^{(i)}, \tag{4.7}$$

where $\mathbf{R}_H^{(i)} = \mathbf{H}^{(i)^H}\mathbf{H}^{(i)}$, i.e., by means of the feedback of individual matrices $\mathbf{R}_H^{(i)}$, matrix $\tilde{\mathbf{H}}^{(k)^H}\tilde{\mathbf{H}}^{(k)}$ can be computed. This allows to apply the quantization and feedback algorithm presented in chapter 3 in a per-user basis.

The interference elimination is achieved through multiplying at the transmitter by the corresponding $\tilde{\mathbf{V}}_0^{(k)}$, i.e., the channel is transformed to $\mathbf{H}^{(k)'} = \mathbf{H}^{(k)}\tilde{\mathbf{V}}_0^{(k)}$. This scheme divides the multiuser channel into parallel single-user MIMO channels with no interference between them. The transmitter then has to send a second sounding sequence through the parallelized channels so that the receivers can estimate the "new" equivalent channels $\mathbf{H}^{(k)'}$. On top of such parallelized channels, any single-user MIMO scheme can be implemented[1] through a precoder $\mathbf{M}^{(k)}$. One possible example could consist in applying waterfilling over the parallelized channel eigenmodes to achieve capacity. For this particular design criterion the eigenvalues $\mathbf{\Sigma}^{(k)}$ and their associated eigenvectors $\mathbf{V}_1^{(k)}$ are computed for each of the channel Gram matrices $\mathbf{H}^{(k)'^H}\mathbf{H}^{(k)'}$. The optimal power allocation coefficients $\mathbf{\Lambda}^{(k)}$ are then found using water-filling on $\mathbf{\Sigma}^{(k)}$, assuming a total power constraint $P^{(k)}$ for user k [Cov06]. Finally the precoding matrix $\mathbf{B}^{(k)}$ is set as:

$$\mathbf{B}^{(k)} = \tilde{\mathbf{V}}_0^{(k)}\mathbf{M}^{(k)}, \quad \mathbf{M}^{(k)} = \mathbf{V}_1^{(k)}\mathbf{\Lambda}^{(k)^{1/2}}. \tag{4.8}$$

The term $\tilde{\mathbf{V}}_0^{(k)}$ ensures that there is no multiuser interference and $\mathbf{V}_1^{(k)}\mathbf{\Lambda}^{(k)^{1/2}}$ is the optimum design satisfying the previous constraint. This example considered the design that achieves capacity but other design criteria can also be used to design $\mathbf{M}^{(k)}$ [Pal03b].

[1]Note that the power constraint in the design of the precoder $\mathbf{M}^{(k)}$ does not change since $\tilde{\mathbf{V}}_0^{(k)}$ is a unitary transformation (i.e., if $\mathbf{B}^{(k)} = \tilde{\mathbf{V}}_0^{(k)}\mathbf{M}^{(k)}$ then $\|\mathbf{B}^{(k)}\|_F^2 = \|\mathbf{M}^{(k)}\|_F^2$).

4.2.3 Extension of the channel Gram matrix feedback algorithm to multiuser MIMO with block diagonalization

As shown in the previous section, the transmitter can eliminate multiuser interference with knowledge of the channel Gram matrices of the individual receivers, i.e., it is not necessary to have knowledge of the whole channel matrices; only the channel Gram matrices are required. Furthermore, once the interference has been removed, single-user MIMO precoder designs can be applied. The optimum transmitter design for most interesting criteria such as the maximization of the mutual information or the SNR, or the minimization of the BER or the MSE, has been shown to depend also on the channel Gram matrix rather than on the complete channel matrix [Pal03b], as commented in the previous chapter.

Consequently, by implementing the feedback of the channel Gram matrix described in chapter 3 it is possible to first eliminate multiuser interference through BD and then compute the precoder designs. A summary of the BD design with geodesic feedback of the channel Gram matrices is given in Table 4.1.

4.2.4 Simulations

In the simulations, a random multiuser MIMO channel is considered, with 4 antennas at the transmitter and 2 receivers with 2 antennas each. The time correlation of the channel is generated following a first order auto-regressive time-variation model according to the expression:

$$\mathbf{H}(n) = \rho\mathbf{H}(n-1) + \sqrt{1-\rho^2}\mathbf{N}(n), \tag{4.9}$$

where matrices $\mathbf{H}(n-1)$ and $\mathbf{N}(n)$ are assumed to be independent and composed of i.i.d. zero-mean complex Gaussian entries with unit variance. The time correlation factor ρ models the variability of the channel and depends on the Doppler frequency of the terminal f_D through the expression $\rho = J_0\big(2\pi f_D \tau\big)$ [Ste99], where J_0 is the zeroth-

Table 4.1: Block diagonalization with Gram matrix feedback

1) Receiver k estimates $\mathbf{H}^{(k)}$ and sends $\mathbf{R}_H^{(k)}$ through the feedback link.

2) At the transmitter, compute $\tilde{\mathbf{H}}^{(k)^H}\tilde{\mathbf{H}}^{(k)} = \sum_{i=1,i\neq k}^{K} \mathbf{R}_H^{(i)}$.

3) At the transmitter, compute $\tilde{\mathbf{V}}_0^{(k)}$, the right null space of $\tilde{\mathbf{H}}^{(k)^H}\tilde{\mathbf{H}}^{(k)}$.

The parallelized channels are then $\mathbf{H}^{(k)'} = \mathbf{H}^{(k)}\tilde{\mathbf{V}}_0^{(k)}$, and the transmitter knows $\mathbf{H}^{(k)'^H}\mathbf{H}^{(k)'} = \tilde{\mathbf{V}}_0^{(k)^H}\mathbf{R}_H^{(k)}\tilde{\mathbf{V}}_0^{(k)}$.

4) Send a second sounding signal so that the receiver can estimate $\mathbf{H}^{(k)'}$.

5) At the transmitter, design a precoder $\mathbf{M}^{(k)}$ for each of the parallel channels $\mathbf{H}^{(k)'}$ with the given design criterion using $\mathbf{H}^{(k)'^H}\mathbf{H}^{(k)'}$.

6) Set the precoding matrices as: $\mathbf{B}^{(k)} = \tilde{\mathbf{V}}_0^{(k)}\mathbf{M}^{(k)}$.

order Bessel function of the first kind and τ is the time difference between consecutive feedback instants. The case of a constant channel corresponds to $\rho = 1$.

The first 2 simulations (Figure 4.3 and Figure 4.4) show the achievable sum-rate of different feedback strategies versus the elapsed time, for a constant and a time variant channel ($\rho = 0.999$), respectively. It can be seen how the proposed algorithm exploits the temporal correlation of the channel to improve progressively the accuracy of the feedback. For these simulations the transmitted power is fixed to 20 dB more than the channel noise. The presented algorithm based on geodesic curves is compared to a system with full cooperation between receivers (which is an upper bound to the performance, as it is equivalent to the single-user system with 4 receive antennas), to the case of BD with perfect CSI, a differential strategy based on the DPCM quantization used in [Xia09], and a strategy based on non-differential uniform quantization of the channel Gram matrix coefficients presented in [Cha08]. The plot shows how the proposed algorithm using only 4 bits of feedback performs similar to [Xia09] with 16 bits

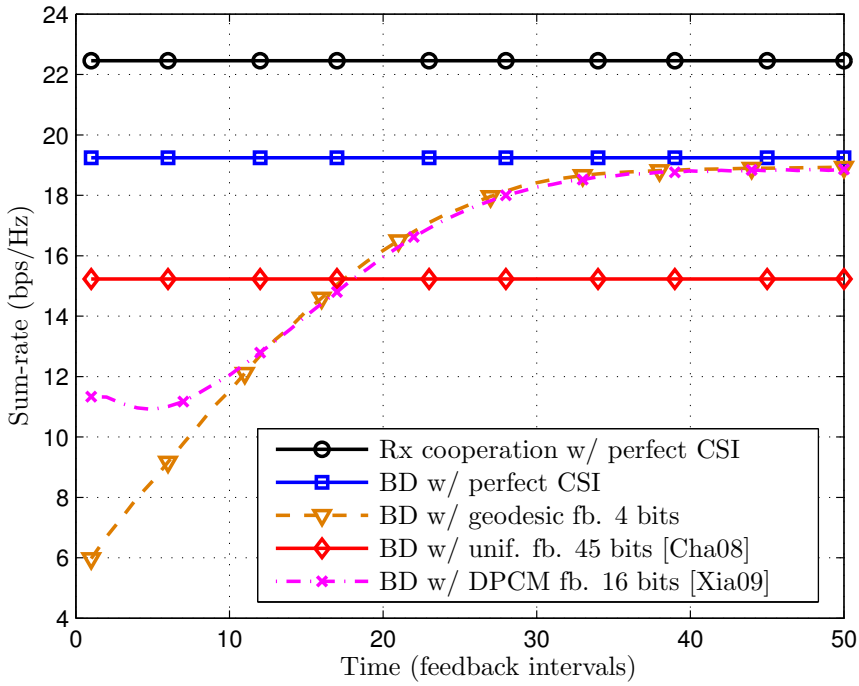

Figure 4.3: Achievable sum-rate in a constant {2,2}x4 system.

of feedback. The differential algorithms clearly outperform the non-differential ones after few time instants, even when using 45 bits in the non-differential scheme (this applies also to other non-differential algorithms such as the one presented in [Rav08]).

Figure 4.5 shows the achievable sum-rate as a function of the SNR, defined as the ratio between the transmitted power and the noise power. Special interest should be paid to the mid and high SNR regime, because it is where multiuser MIMO provides the largest performance gain. In order to take into account the fact that the algorithm exploits the correlation in time of the channel, the performance is compared after 30 time intervals. The case of full cooperation between the receivers is an upper bound to the performance and is depicted for comparison reasons. The simulations show how BD with perfect CSI achieves the maximum multiplexing gain, although an absolute difference in terms of throughput exists when compared to full receive

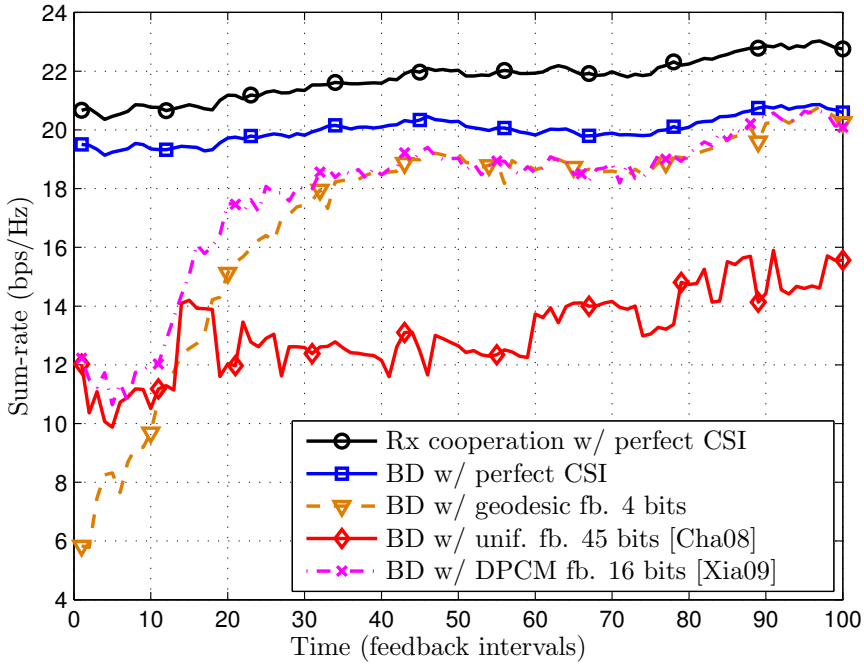

Figure 4.4: Achievable sum-rate in a time variant {2,2}x4 system.

cooperation. The algorithm presented here clearly provides a better sum-rate than the non-differential algorithm from [Cha08]. As the transmission power increases, the accuracy of the CSI is more important, since the system is interference-limited and small inaccuracies in the channel estimate at the transmitter introduce a fixed amount of interference that produces a ceiling in the throughput of the system.

Regarding the Signal to Interference Plus Noise Ratio (SINR) at the receivers, Figure 4.6 shows the result of a simulation using different techniques. Note that the interference is due to the CSI quantization for the feedback. Due to the CSI quantization error, the BD precoder does not pre-cancel the interference completely. For this simulation the transmitted power is distributed evenly among the users, $\sigma_w^2 = 1$, and the results are averaged over 3000 channel realizations. The performance of the geodesic feedback algorithm corresponds to the instant after 30 feedback intervals in a constant channel. This simulation shows that the algorithm presented in this chapter

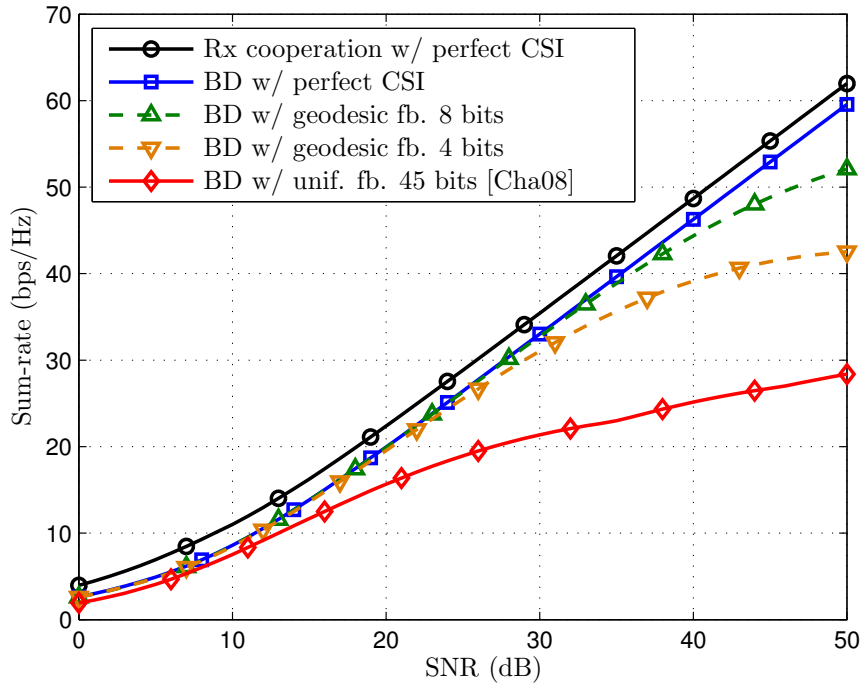

Figure 4.5: Achievable sum-rate vs. SNR in a {2,2}x4 system.

performs better than the other feedback strategies, even with fewer bits of feedback.

Finally, the BER using a Binary Phase Shift Keying (BPSK) modulation is simulated and the results after 30 time intervals are shown in Figure 4.7. The transmission power is distributed evenly among the users, and the results are averaged over 3000 channel realizations. The figure shows that the proposed algorithm achieves a lower BER than the feedback strategies from [Cha08] while requiring fewer feedback bits.

4.3 Precoding and feedback schemes for a MIMO backhaul link in the presence of interference

This section presents a novel scenario, which emerges from the planing of interference-aware all-wireless networks that feature aggressive frequency reuse. We consider a

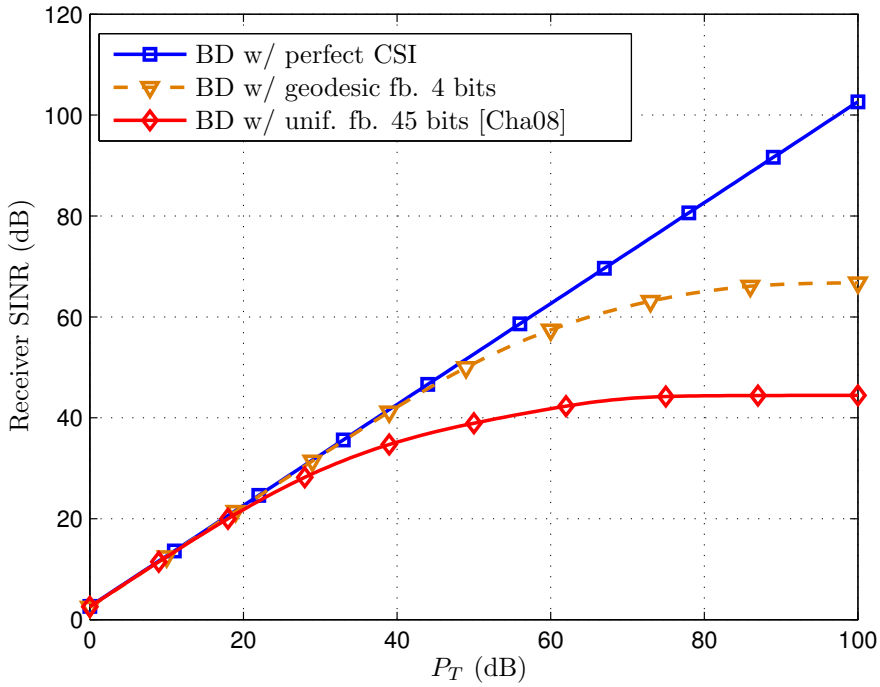

Figure 4.6: Receiver SINR vs. P_T in a {2,2}x4 system.

network topology composed of access and backhaul links which are both wireless. Having a wireless backhaul link greatly reduces the cost in time and resources of the deployment of the network. In the access network, multiple Access Base Stations (ABSs), which are fixed in space, communicate over the wireless channel with different Mobile Stations (MSs) which have a given mobility. In the backhaul links the Hub Base Stations (HBSs), which are connected directly to the fixed operator's network, communicate with the ABSs through what is called the backhaul links (each HBS handles the aggregated traffic of multiple ABSs). Traditional communication networks feature a wired backhaul link, which translates into large deployment times and costs. Recently there is a trend to evolve the backhaul link to be wireless, as for example in the WiMAX standard [iee04,And07]. The novelty of this scenario resides in the fact that an array of omnidirectional antennas is considered at both ends of the radio backhaul link and that the links can be adapted dynamically to mitigate incoming interference. This

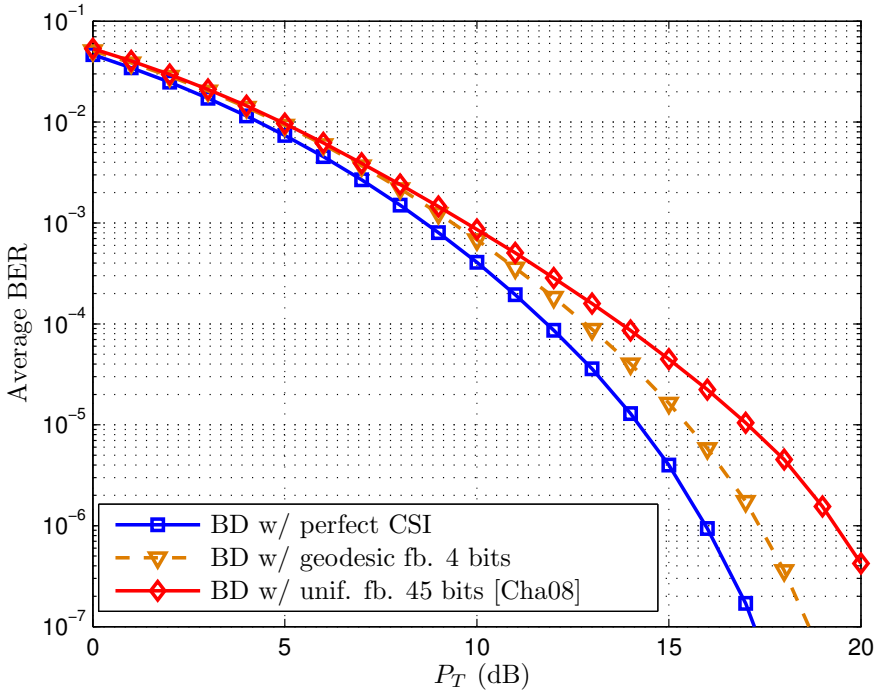

Figure 4.7: BER vs. P_T in a {2,2}x4 system.

also removes the planning needed when using very directive antennas in the wireless backhaul link. Besides, in order to increase the spectral efficiency of the system, the same frequencies are used for the backhaul and the access networks, which means that cross-segment (or cross-system) interference has to be taken care of. This is also a novel deployment.

This section considers a cross-segment (or cross-system) design of the transmit precoding matrix of the ABS for the communication towards the HBS under the following design considerations: first, the backhaul link should be completely transparent to the access network, i.e., the signals sent to the HBS should not cause interference to the MSs; and second, the design should also minimize the effect of interference at the HBS created by the MSs. Since the MSs have a certain mobility, the interference varies in time and therefore this design should be adaptive.

Section 4.3.1 describes in detail the considered system and signal models, for the

different channels and feedback links. The proposed precoding and feedback algorithm is described in section 4.3.2, and simulations of the performance are presented in section 4.3.3.

4.3.1 System and signal models

We consider a wireless network with one ABS, one HBS, K MSs, and backhauling and access links as depicted in Figure 4.8. The ABS has n_A transmit antennas, while the HBS has n_H, and the i-th MS has $n_M^{(i)}$ receive antennas, with $\sum_{i=1}^{K} n_M^{(i)} < n_A$. The channel matrix from the ABS to the HBS at time instant t is denoted by $\mathbf{H}_{AH}(t) \in \mathbb{C}^{n_H \times n_A}$, and the channel matrices of the links between ABS and the MSs, and between MSs and HBS are represented by $\mathbf{H}_{AM}^{(i)}(t) \in \mathbb{C}^{n_M^{(i)} \times n_A}$ and $\mathbf{H}_{MH}^{(i)}(t) \in \mathbb{C}^{n_H \times n_M^{(i)}}$, respectively. $\mathbf{B} \in \mathbb{C}^{n_A \times n_S}$ is the precoding matrix of the backhaul link to be used at the ABS to transmit n_S streams to the HBS. $\mathbf{x} \in \mathbb{C}^{n_S}$ represents the n_S streams of signals to be transmitted from the ABS to the HBS with $\mathbb{E}\left\{\mathbf{x}\mathbf{x}^H\right\} = \mathbf{I}$. The AWGN at the HBS is $\mathbf{w} \in \mathbb{C}^{n_H}$ with $\mathbb{E}\left\{\mathbf{w}\mathbf{w}^H\right\} = \sigma_w^2\mathbf{I}$. The received signal at the HBS is, therefore (we drop the dependency with respect to the time index t for the sake of clarity in the notation):

$$\mathbf{y} = \mathbf{H}_{AH}\mathbf{B}\mathbf{x} + \sum_{i=1}^{K} \mathbf{H}_{MH}^{(i)}\mathbf{x}_M^{(i)} + \mathbf{w} \in \mathbb{C}^{n_H}, \tag{4.10}$$

where $\mathbf{H}_{MH}^{(i)}\mathbf{x}_M^{(i)}$ is the interference caused by the signal $\mathbf{x}_M^{(i)}$ transmitted from the i-th MS with power $P^{(i)}$. We assume $\mathbb{E}\left\{\mathbf{x}_M^{(i)}\mathbf{x}_M^{(i)^H}\right\} = P^{(i)}\mathbf{I},\ \forall i$ for simplicity reasons, although the extension to a generic transmit correlation matrix is straightforward.

Channel model

The scenario described in Figure 4.8 contains three different types of propagation channels:

- Channel from the ABS to the HBS: This channel is static, or very slow varying,

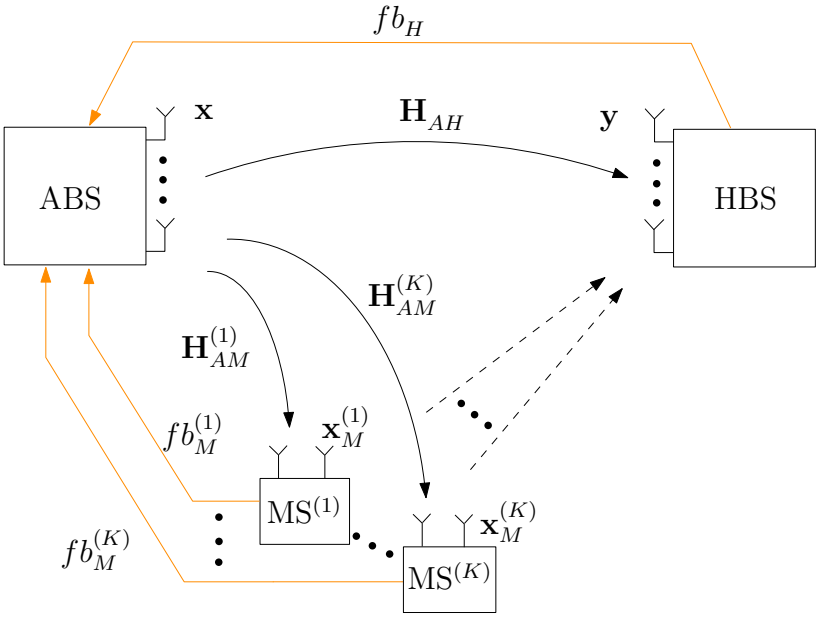

Figure 4.8: System model of the wireless backhaul link in the presence of interference from MSs.

since both ABS and HBS have no mobility. Therefore the channel response matrix $\mathbf{H}_{AH}$ can be assumed to be known at both ends.

- Channels from the ABS to the MSs: The MSs have a given mobility, which translates into a Doppler-shift. These channels $\mathbf{H}_{AM}^{(i)}$ are considered to be time varying, and the MSs are assumed to be able to estimate them with the help of pilot symbols.

- Channels from the MSs to the HBS: It is a system design decision that there is no communication between the HBS and the MSs, therefore these channels $\mathbf{H}_{MH}^{(i)}$ are unknown. The interference plus noise at the HBS, $\sum_{i=1}^{K} \mathbf{H}_{MH}^{(i)} \mathbf{x}_M^{(i)} + \mathbf{w}$, has a covariance matrix expressed as:

$$\mathbf{R}_n = \sigma_w^2 \mathbf{I} + \sum_{i=1}^{K} P^{(i)} \mathbf{H}_{MH}^{(i)} \mathbf{H}_{MH}^{(i)H} \in \mathbb{C}^{n_H \times n_H}, \tag{4.11}$$

which can be estimated at the HBS.

Feedback links

The scenario presented in this section considers the following feedback links, which are depicted in Figure 4.8:

- Link from HBS to ABS (fb_H): The HBS estimates the interference plus noise correlation matrix $\mathbf{R}_n$ and sends it to the ABS through the limited feedback link fb_H. The ABS then uses this knowledge to minimize the effect of $\mathbf{R}_n$ on the performance of the backhaul link by a proper design of the transmit matrix $\mathbf{B}$, as will be explained in section 4.3.2.

- Links from the MSs to the ABS ($fb_M^{(i)}$): The i-th MS estimates the propagation channel $\mathbf{H}_{AM}^{(i)}$ and sends its Gram matrix $\mathbf{H}_{AM}^{(i)^H}\mathbf{H}_{AM}^{(i)}$ through $fb_M^{(i)}$ to the ABS. This CSI is used at the ABS to reduce the interference caused by the backhaul link over the MSs by a proper design of the precoding matrix $\mathbf{B}$.

The information to be fed back through the feedback links corresponds in all cases to positive definite Hermitian matrices, and therefore, the differential feedback technique presented in section 3.4 could be applied.

4.3.2 Precoding matrix design

The optimization of the precoding matrix $\mathbf{B}$ in the backhaul link can be done according to several quality criteria, such as maximization of the mutual information, SINR, or minimization of the BER. Given a constraint on the maximum transmit power P_T and the constraint of zero-interference to the MSs (the backhaul link should be completely transparent to the access network) and taking into account interfering signals at the HBS, the design of $\mathbf{B}$ according to a general design criterion $f(\mathbf{B}, \mathbf{H}_{AH}, \mathbf{R}_n)$, can be formulated as the following maximization problem:

$$\max_{\mathbf{B}} \quad f\left(\mathbf{B}, \mathbf{H}_{AH}, \mathbf{R}_n\right) \tag{4.12}$$

$$\text{s.t.} \quad \text{tr}\left\{\mathbf{B}\mathbf{B}^H\right\} \leq P_T, \tag{4.13}$$

$$\mathbf{H}_{AM}^{(i)}\mathbf{B} = \mathbf{0}, \ \ \forall i \ (i = 1...K), \tag{4.14}$$

where the effect of $\mathbf{R}_n$ is considered in the cost function in (4.12), the constraint on the total power available for the transmission is expressed in (4.13), and (4.14) represents the zero-interference constraints to the MSs links. This last constraint can also be written as:

$$\widetilde{\mathbf{H}}_{AM}\mathbf{B} = \mathbf{0}, \tag{4.15}$$

where $\widetilde{\mathbf{H}}_{AM}$ is defined as:

$$\widetilde{\mathbf{H}}_{AM} = \left[\mathbf{H}_{AM}^{(1)^T} ... \ \mathbf{H}_{AM}^{(K)^T}\right]^T. \tag{4.16}$$

From (4.15), $\mathbf{B}$ is forced to have the following structure:

$$\mathbf{B} = \mathbf{V}_0\widetilde{\mathbf{B}}, \tag{4.17}$$

where $\widetilde{\mathbf{B}} \in \mathbb{C}^{(n_A - \sum_{i=1}^{K} n_M^{(i)}) \times n_S}$ and the columns of $\mathbf{V}_0 \in \mathbb{C}^{n_A \times (n_A - \sum_{i=1}^{K} n_M^{(i)})}$ are orthonormal and span the right-nullspace of $\widetilde{\mathbf{H}}_{AM}$ (as in [Spe04]). Since the nullspace of $\widetilde{\mathbf{H}}_{AM}$ is equal to the nullspace of $\widetilde{\mathbf{H}}_{AM}^H\widetilde{\mathbf{H}}_{AM}$, and $\widetilde{\mathbf{H}}_{AM}^H\widetilde{\mathbf{H}}_{AM}$ can be written as (see (4.16)):

$$\widetilde{\mathbf{H}}_{AM}^H\widetilde{\mathbf{H}}_{AM} = \sum_{i=1}^{K} \mathbf{H}_{AM}^{(i)^H}\mathbf{H}_{AM}^{(i)}, \tag{4.18}$$

then matrix $\mathbf{V}_0$ can be computed containing as columns the eigenvectors associated to the null eigenvalues of $\sum_{i=1}^{K} \mathbf{H}_{AM}^{(i)^H}\mathbf{H}_{AM}^{(i)}$. Note that from each MS, only the channel Gram matrix $\mathbf{H}_{AM}^{(i)^H}\mathbf{H}_{AM}^{(i)}$ is needed, and also that the zero forcing applied to each additional MS reduces the degrees of freedom available at the ABS for the communication with the HBS, reducing the performance of the backhaul link.

The total power in (4.13) can be written as a function of $\widetilde{\mathbf{B}}$: since $\mathbf{V}_0^H\mathbf{V}_0 = \mathbf{I}$, then $\mathrm{tr}\left\{\mathbf{B}\mathbf{B}^H\right\} = \mathrm{tr}\left\{\widetilde{\mathbf{B}}\widetilde{\mathbf{B}}^H\right\}$. Taking this into account, the optimization problem can be rewritten as:

$$\max_{\widetilde{\mathbf{B}}} \quad f\left(\mathbf{V}_0\widetilde{\mathbf{B}}, \mathbf{H}_{AH}, \mathbf{R}_n\right) \tag{4.19}$$

$$\text{s.t.} \qquad \mathrm{tr}\left\{\widetilde{\mathbf{B}}\widetilde{\mathbf{B}}^H\right\} \leq P_T. \tag{4.20}$$

This optimization problem can be easily solved now for the different design criteria, such as maximization of the mutual information, SINR, minimization of the BER, etc. A couple of examples of design criterion f are commented next; however, the same procedure can be applied to other criteria following the same steps [Pal03b].

Example 1: Maximization of the mutual information

In this case the cost function is defined as

$$\begin{aligned} f &= \log_2\left|\mathbf{I} + \mathbf{B}^H\mathbf{H}_{AH}^H\mathbf{R}_n^{-1}\mathbf{H}_{AH}\mathbf{B}\right| = \\ &= \log_2\left|\mathbf{I} + \widetilde{\mathbf{B}}^H\mathbf{V}_0^H\mathbf{H}_{AH}^H\mathbf{R}_n^{-1}\mathbf{H}_{AH}\mathbf{V}_0\widetilde{\mathbf{B}}\right| = \\ &= \log_2\left|\mathbf{I} + \widetilde{\mathbf{B}}^H\overline{\mathbf{R}}_H\widetilde{\mathbf{B}}\right|, \end{aligned} \tag{4.21}$$

where $\overline{\mathbf{R}}_H = \mathbf{V}_0^H\mathbf{H}_{AH}^H\mathbf{R}_n^{-1}\mathbf{H}_{AH}\mathbf{V}_0$.

The solution to the maximization problem (4.19) for this cost function is known to be [Cov06]:

$$\widetilde{\mathbf{B}} = \mathbf{V}\mathbf{P}^{1/2}, \quad \mathbf{P} = \mathrm{diag}(p_1, \ldots, p_{n_S}), \tag{4.22}$$

where $\mathbf{V}$ consists of n_S columns that are the n_S eigenvectors of $\overline{\mathbf{R}}_H$ associated to its n_S maximum eigenvalues $\{\lambda_i\}_{i=1}^{n_S}$. The power $\mathbf{P}$ is allocated according to the waterfilling solution ($p_i = \max\{0, \mu - 1/\lambda_i\}$, where μ is a constant such that $\sum_{i=1}^{n_S} p_i = P_T$).

Example 2: Maximization of the SINR with single beamforming

In this case the beamforming matrix $\widetilde{\mathbf{B}}$ has only 1 column (therefore the notation $\widetilde{\mathbf{b}}$ will be used), and the cost function is defined as:

$$f = \widetilde{\mathbf{b}}^H \mathbf{V}_0^H \mathbf{H}_{AH}^H \mathbf{R}_n^{-1} \mathbf{H}_{AH} \mathbf{V}_0 \widetilde{\mathbf{b}} = \widetilde{\mathbf{b}}^H \overline{\mathbf{R}}_H \widetilde{\mathbf{b}}, \tag{4.23}$$

and the solution to (4.19) using this criterion as cost function is:

$$\widetilde{\mathbf{b}} = \sqrt{P_T} \mathbf{u}_{\max}\left(\overline{\mathbf{R}}_H\right) \in \mathbb{C}^{n_A}, \tag{4.24}$$

where $\mathbf{u}_{\max}(\cdot)$ stands for the unit-norm eigenvector of maximum associated eigenvalue.

4.3.3 Simulations

There are several factors that have a direct effect on the performance of the communication in the backhaul link of the proposed scenario. This section first presents the performance loss in the link between ABS and HBS when the constraint of zero interference at the MSs is enforced. Then, the gain obtained when using different feedback techniques to send information of the second order statistics of the interference from the HBS to the ABS is analyzed, as a function of the transmission rate of the feedback link. Finally, the degradation in performance is simulated for different values of the interfering power and different number of MSs.

For all the simulations, the time correlated propagation channels are generated as described in section 4.2.4, see (4.9).

It is important to note that the CSI sent from the MSs to the ABS through the feedback link is quantized and may contain errors, but this does not affect the average performance of the backhaul link ABS-HBS. Imperfect CSI received through the links $fb_M^{(i)}$ degrades the performance of the communication between the ABS and the MSs (which is not considered in this scenario), and only the rank of the transmitted $\mathbf{H}_{AM}^{(i)^H} \mathbf{H}_{AM}^{(i)}$ reduces the average performance of the backhaul link because some degrees

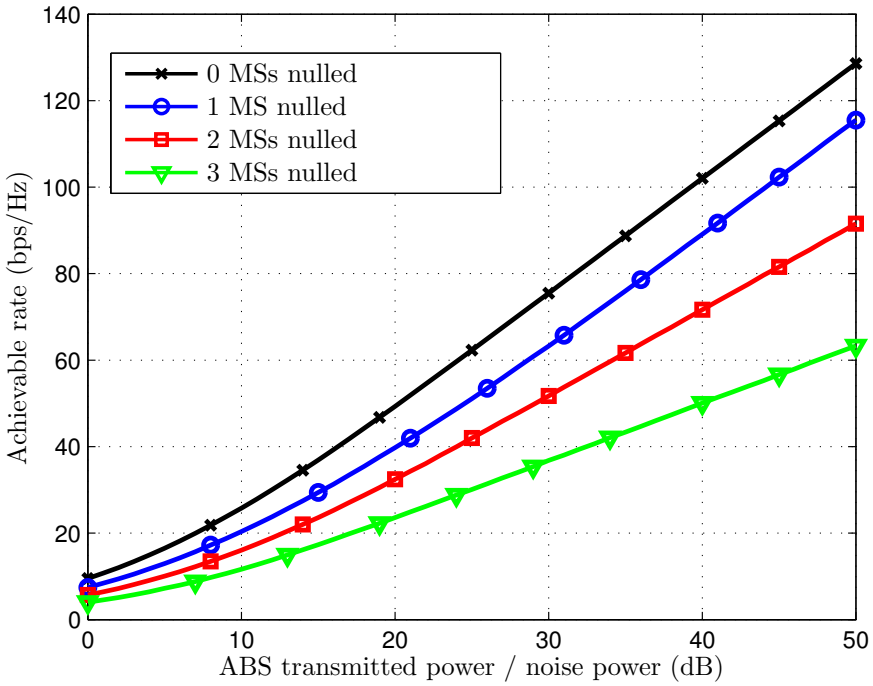

Figure 4.9: Effect of interference nulling at the MSs.

of freedom in the design of the precoder $\mathbf{B}$ are lost. For this reason, the accuracy of the feedback links $fb_M^{(i)}$ is not relevant for the simulations and will not be commented explicitly.

First, a scenario where $n_A = 10$, $n_H = 8$, and there are up to 3 MSs with $n_M = 2$ is considered. Each MS transmits with a power 10 dB higher than the AWGN. Figure 4.9 shows the achievable rate of the ABS-HBS link as a function of the transmit power and averaged over 1000 realizations of the propagation channel, for the cases where the precoding matrix is constrained to create nulls in the directions of the MSs. As expected, the simulation shows that the highest rate is achieved when there are no interfering MSs. The slope of the curve is reduced when the number of degrees of freedom of the system decreases, i.e., when the number of interfering MSs increases. It is interesting to observe that, with this setup, in the presence of 1 interfering MS with 2 antennas, the ABS can do interference nulling towards the MS without losing

degrees of freedom in the link with the HBS (the curves have the same slope for 0 and 1 MSs). There is some performance loss due to the fact that system resources are used in the interference nulling but it is a constant loss that does not scale with the transmitted power. The presence of a second MS with 2 antennas reduces the degrees of freedom, and a third MS decreases it further, as shown by the slope of the curves. The maximum degrees of freedom of the ABS-HBS link with interference nulling at all K MSs is $\min\left(n_A - \sum_{i=1}^{K} n_M^{(i)}, n_H\right)$.

The covariance matrix of the interference plus noise (4.11) can be estimated at the HBS and sent to the ABS through fb_H. Figure 4.10 shows the gains that can be achieved by the use of such feedback link averaged over 3000 channel realizations as a function of the power of the interfering signal from the MSs and after 30 feedback intervals for a system with $n_A = 6$, $n_H = 5$, and 1 interfering MS with $n_M = 2$. In the case of [Cha08] the x-axis represents the number of feedback bits for each of the 25 parameters to be quantized. The simulation shows that the differential algorithm outperforms the one based on non-differential quantization [Cha08], which features a uniform quantization of the real and imaginary parts of the elements of $\mathbf{R}_n$ (i.e., there are 25 scalar parameters to quantize in this case since $\mathbf{R}_n$ has dimensions 5×5), because it is capable of exploiting the fact that $\mathbf{R}_n$ is slowly variant in time. Also note that having a very inaccurate CSI is worse than having no CSI at all, as shown in the curve corresponding the non-differential scheme.

The performance in terms of SINR and BER using a QPSK modulation is evaluated as a function of the interfering power in the simulations corresponding to Figure 4.11 and Figure 4.12. For these simulations the following setup was used: $n_A = 8$, $n_H = 6$, $n_M = 2$, and the ABS transmits at a power 10 dB higher than the AWGN. The curves show how the performance of the backhaul link is degraded by increasing the power of the interfering MS, and part of this loss can be compensated by using a feedback link with limited capacity to convey the second order statistics of the interfering signal from the HBS to the ABS. The quantization and feedback strategy considered is the

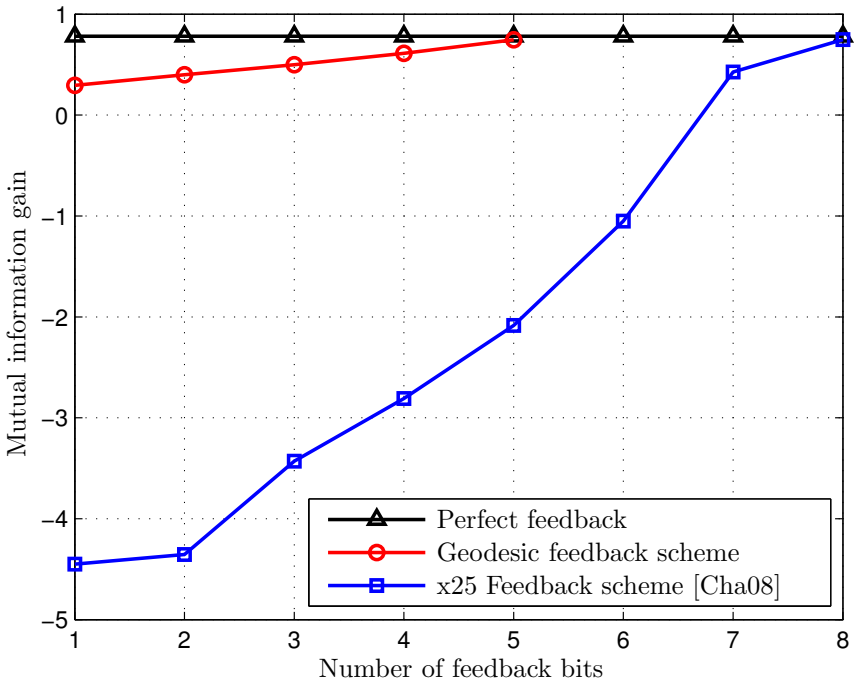

Figure 4.10: Mutual information gain vs. number of feedback bits.

one described in section 4.3.2, and the results are plotted after 30 feedback intervals and averaged over 6000 channel realizations. These simulations also show that the performance loss due to additional interfering MSs is higher than the loss due to an increase in interfering power of each MS.

4.4 Chapter summary and conclusions

This chapter has shown that the channel Gram matrix quantization and feedback technique presented in chapter 3 can be applied directly to the multiuser BC scenario within the framework of BD, and it has several advantages over other existing feedback techniques.

First, it considers exclusively the CSI that is absolutely required for optimum BD and precoding designs. Techniques based on quantization of the whole channel matrix

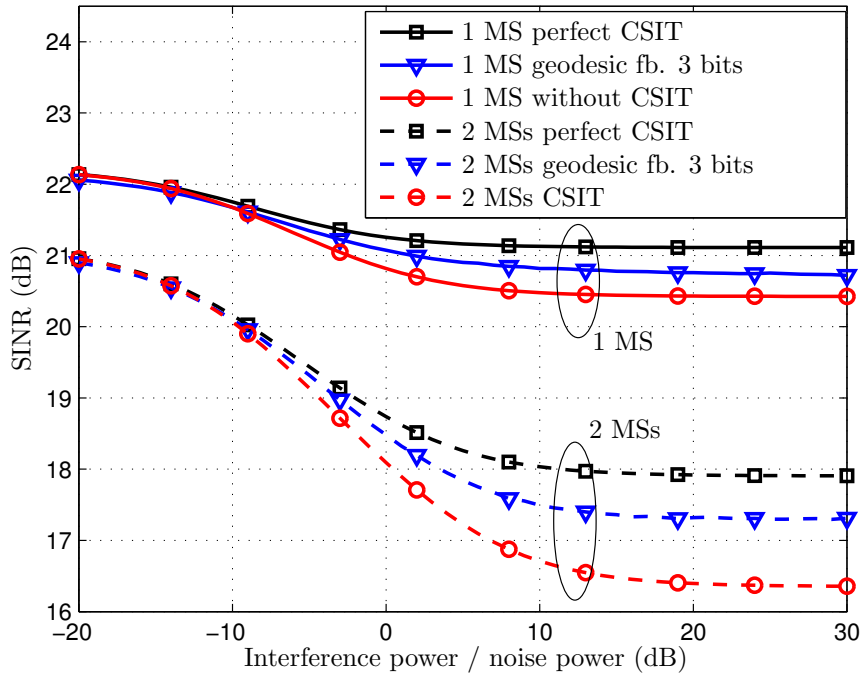

Figure 4.11: SINR vs. interference power.

are suboptimum because, as has been proved, only the Gram of the channel matrix is required at the transmitter. Furthermore, the quantization is performed over the cone of positive Hermitian matrices, exploiting the geometry of the domain space using geodesic curves.

Secondly, the differential nature of the algorithm exploits the correlation in time present in most channels to progressively refine the accuracy of the feedback.

Simulations have shown that this strategy achieves better performance than other techniques based on direct quantization of the coefficients of the Gram matrix.

This chapter has also considered a novel scenario for the backhaul link in an all-wireless network. The communication between a static ABS and a static HBS has been considered in the presence of interfering MSs. The scenario features two types of limited feedback links, one from the HBS to the ABS which is used to transmit information on the second order statistics of the interference plus noise at the HBS,

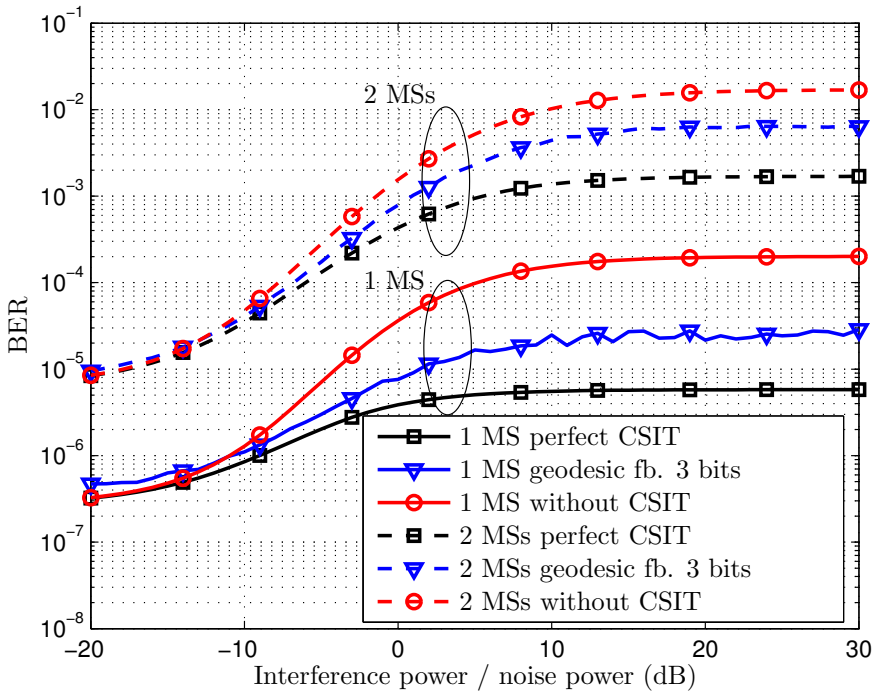

Figure 4.12: BER vs. interference power.

and another feedback link from each MS to the ABS which sends information of the current channel Gram matrix.

It is a design decision that the link between ABS and HBS does not interfere with the access network and also that the effect of the interference caused by the MSs at the HBS is taken into account for the design of the precoding matrix at the ABS. The solution presented in this section is the optimum precoding matrix given these considerations.

Simulations have shown the performance of the precoder and the gain achieved by using a differential quantization algorithm in the feedback links.

Chapter 5

Transceiver design framework for multiuser MIMO-OFDM broadcast systems with channel Gram matrix feedback

5.1 Introduction

Orthogonal Frequency-Division Multiplexing (OFDM) is an effective and extensively implemented strategy that converts a frequency selective channel into a set of parallel flat fading channels. This is done by dividing the available channel bandwidth into F subchannels. When the subchannel bandwidth is sufficiently narrow, the frequency response across each subchannel can be considered approximately flat, which avoids the need of complex equalization procedures [Gol05, Wan00].

Following the OFDM principle, it is possible to transform a MIMO frequency selective channel into a collection of F parallel flat fading MIMO channels. In such a system, the maximum achievable diversity order is the product of the number of

transmit antennas, the number of receive antennas, and the number of propagation paths represented by the channel impulse response length [B$\ddot{0}$0, Lu00]. In order to achieve this full diversity the information symbols should be allowed to be spread not only over the transmitting antennas, but also over the carriers. Note, however, that conventional linear space codes are designed to exploit the spatial diversity of flat fading MIMO channels, and do not take into account the frequency diversity of an OFDM scheme.

This chapter introduces a framework for the transceiver design in multiuser MIMO-OFDM BC systems which, instead of the feedback of the MIMO channel response matrix $\mathbf{H}$ for each user, considers the feedback of the channel Gram matrices (i.e., $\mathbf{H}^H\mathbf{H}$). This idea is based on the feedback scheme presented in chapter 3, where it was shown that, for point-to-point single-user MIMO systems, the minimum amount of CSI required at the transmitter in order to perform the optimum linear precoding corresponds to such channel Gram matrix. Chapter 4 presented a method to apply directly the channel Gram matrix feedback to the MIMO BC systems that are based on BD, while this chapter goes one step further and extends the proposed feedback scheme to the generalized multiuser BC scenario and also to robust designs. Note that using the framework described in this chapter the restrictions of BD regarding the relation between the number of antennas in transmitter and receivers and the zero-forcing constraint are no longer mandatory. The framework presented in this chapter is based on a unique decomposition of the channel Gram matrix of each user, which results in a triangular equivalent propagation channel response matrix. Additionally, a feedback based on the temporal channel impulse response is proposed, as opposed to the usual quantization and feedback based on the frequency response per carrier. This enables to exploit the frequency correlation of the CSI in order to further improve the efficiency of the quantization and feedback. The propagation of the CSI quantization error through the computation of the equivalent channel is also studied analytically and this result is later used, as an example, in the design of a robust precoding scheme.

The proposed framework is valid for any precoder design criterion and in this chapter it is considered, as an illustrative example, the robust minimization of the sum of the MSE of all the symbol streams for all the users, with fixed decoders. This design maps information symbols to antennas and carriers in order to exploit both spatial and frequency diversity, and requires estimates of the multiuser channel responses at the transmitter. It is a robust design in the sense that it takes explicitly into account the errors in the quantization for the feedback transmission to optimize the performance. Note that there is a wide range of designs based on MSE in the literature, such as [Wan10, Sun09] which also consider fixed decoders, or [Ten04, Shi07, Vuc09], which present iterative designs. The scheme presented in this chapter can be applied on its own and also as part of iterative designs such as the ones in [Ten04, Shi07, Vuc09], at the step where the transmitter is computed at each iteration. Other works such as [Cai10, Cha07] assume single-antenna receivers, in which case the decoder design is not an issue.

Summarizing, the main contributions of this chapter can be listed as follows:

1. An extension of the feedback based on Gram matrices to the case of BC multiuser MIMO-OFDM.

2. The computation of the equivalent triangular channels from the channel Gram matrices.

3. The analysis of the propagation of the quantization errors through the computation of the equivalent MIMO triangular channels.

4. An example of robust design implementation within the proposed framework.

The first three points are what constitute the general framework. On top of this framework, any design criteron or architecture can be implemented (even non-linear designs). The fourth topic is an example of application to a particular scenario and design criterion.

The remainder of this chapter is organized as follows. The system and signal models are described in section 5.2. Section 5.3 describes the proposed per user feedback scheme and presents the linear transformation applied to uniquely obtain the equivalent triangular channels. The model considered for the CSI quantization error and its propagation through the processing at the transmitter are presented in section 5.4, while section 5.5 presents an example of application consisting in a robust precoder that takes into account the errors in the CSI. Finally, section 5.6 provides numerical simulations to evaluate the performance of the proposed strategies in a MIMO-OFDM BC system, and section 5.7 presents a summary of the main results contained in the chapter.

5.2 System and signal models

A multiuser MIMO-OFDM BC system is considered, with F carriers and K users, denoted by the indices $f = 0, ..., F-1$ and $k = 1, ..., K$, respectively. The transmitter features n_T antennas and the k-th receiver has $n_R^{(k)}$ antennas. The propagation channel of user k is characterized by its temporal impulse response, which consists of a maximum of L taps[1] and is denoted by $\bar{\mathbf{H}}_l^{(k)} \in \mathbb{C}^{n_R^{(k)} \times n_T}$, $l = 0, ..., L-1$ (the horizontal overline is used to denote that the variable is defined in the time domain). Accordingly, the frequency channel response at carrier f and user k is given by:

$$\mathbf{H}_f^{(k)} = \sum_{l=0}^{L-1} \bar{\mathbf{H}}_l^{(k)} e^{-j\frac{2\pi}{F}fl} \in \mathbb{C}^{n_R^{(k)} \times n_T}. \tag{5.1}$$

Classically, parallel linear precoding per carrier at the transmitter is considered, which is denoted by a precoding matrix $\mathbf{P}_f^{(k)} \in \mathbb{C}^{n_T \times n_{S_f}^{(k)}}$, for user k and carrier f, where $n_{S_f}^{(k)}$ is the number of streams transmitted to the k-th receiver through the f-th carrier. The corresponding linear processing at the k-th receiver for carrier f is represented by

[1]For the case where the channel impulse responses of the different users have different number of taps, L is defined as the maximum among the number of taps for all users.

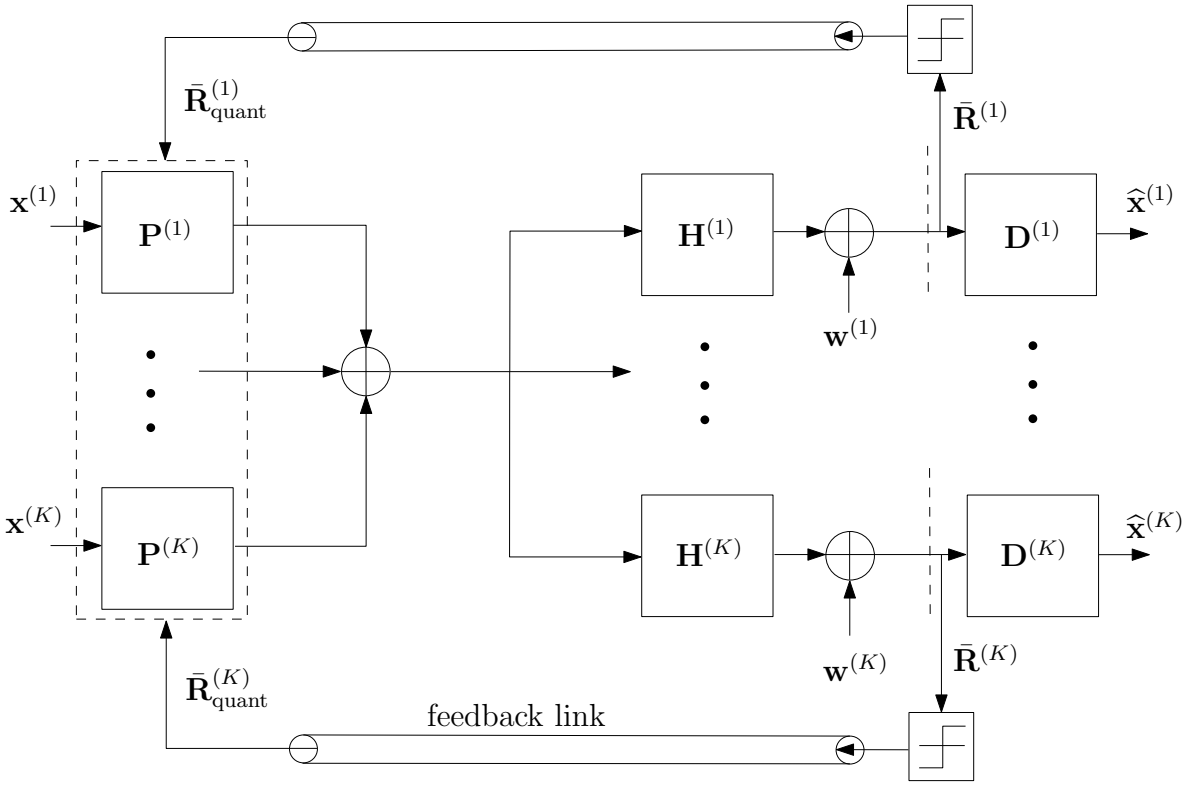

Figure 5.1: MIMO-OFDM broadcast system model with feedback.

the decoding matrix $\mathbf{D}_f^{(k)} \in \mathbb{C}^{n_{S_f}^{(k)} \times n_R^{(k)}}$. Following this model, the estimated symbols $\widehat{\mathbf{x}}_f^{(k)} \in \mathbb{C}^{n_{S_f}^{(k)}}$ corresponding to the f-th carrier at the k-th receiver are given by:

$$\widehat{\mathbf{x}}_f^{(k)} = \mathbf{D}_f^{(k)} \mathbf{H}_f^{(k)} \sum_{i=1}^{K} \mathbf{P}_f^{(i)} \mathbf{x}_f^{(i)} + \mathbf{D}_f^{(k)} \mathbf{w}_f^{(k)} \in \mathbb{C}^{n_{S_f}^{(k)}}, \quad \forall f, k, \tag{5.2}$$

where $\mathbf{x}_f^{(k)} \in \mathbb{C}^{n_{S_f}^{(k)}}$ is the vector containing the streams of symbols transmitted to user k through carrier f and $\mathbf{w}_f^{(k)} \in \mathbb{C}^{n_R^{(k)}}$ is the AWGN at receiver k.

Using a notation with block diagonal matrices to group the symbols transmitted through all carriers corresponding to each receiver, the estimated symbols at the k-th receiver are given by:

$$\widehat{\mathbf{x}}^{(k)} = \mathbf{D}^{(k)} \mathbf{H}^{(k)} \sum_{i=1}^{K} \mathbf{P}^{(i)} \mathbf{x}^{(i)} + \mathbf{D}^{(k)} \mathbf{w}^{(k)} \in \mathbb{C}^{\sum_{f=0}^{F-1} n_{S_f}^{(k)}}, \quad \forall k, \tag{5.3}$$

where

$\mathbf{D}^{(k)} = \text{blockdiag}\left(\mathbf{D}_0^{(k)}, ..., \mathbf{D}_{F-1}^{(k)}\right) \in \mathbb{C}^{\sum_{f=0}^{F-1} n_{S_f}^{(k)} \times F n_R^{(k)}}$,
$\widehat{\mathbf{x}}^{(k)} = \left[\widehat{\mathbf{x}}_0^{(k)^T}, ..., \widehat{\mathbf{x}}_{F-1}^{(k)^T}\right]^T \in \mathbb{C}^{\sum_{f=0}^{F-1} n_{S_f}^{(k)}}$,
$\mathbf{x}^{(k)} = \left[\mathbf{x}_0^{(k)^T}, ..., \mathbf{x}_{F-1}^{(k)^T}\right]^T \in \mathbb{C}^{\sum_{f=0}^{F-1} n_{S_f}^{(k)}}$,
$\mathbf{H}^{(k)} = \text{blockdiag}\left(\mathbf{H}_0^{(k)}, ..., \mathbf{H}_{F-1}^{(k)}\right) \in \mathbb{C}^{F n_R^{(k)} \times F n_T}$,
$\mathbf{w}^{(k)} = \left[\mathbf{w}_0^{(k)^T}, ..., \mathbf{w}_{F-1}^{(k)^T}\right]^T \in \mathbb{C}^{F n_R^{(k)}}$,
and $\mathbf{P}^{(k)} = \text{blockdiag}\left(\mathbf{P}_0^{(k)}, ..., \mathbf{P}_{F-1}^{(k)}\right) \in \mathbb{C}^{F n_T \times \sum_{f=0}^{F-1} n_{S_f}^{(k)}}$ (see Figure 5.1 for a complete diagram of the BC system).

Note that in expressions (5.2) and (5.3) each symbol is constrained to be transmitted through one single carrier as shown by the fact that the precoding and decoding matrices, $\mathbf{P}^{(k)}$ and $\mathbf{D}^{(k)}$, are block-diagonal. It is possible to achieve higher diversity by not forcing a block-diagonal structure at the precoding $\mathbf{P}^{(k)}$ and decoding $\mathbf{D}^{(k)}$ stages. Following this idea, a space-frequency precoder is designed in this chapter, as a mean to extract both spatial and frequency diversity and, consequently, the precoding and decoding matrices are not constrained to be block-diagonal. Since the symbols are now spread among the carriers, it does not make sense to use the notation $n_{S_f}^{(k)}$ corresponding to the number of symbols per carrier. Instead, a total number of streams $n_S^{(k)}$ is considered for transmission to receiver k through all carriers, which results in a global precoder $\mathbf{P}^{(k)} \in \mathbb{C}^{F n_T \times n_S^{(k)}}$ for receiver k and a global decoder $\mathbf{D}^{(k)} \in \mathbb{C}^{n_S^{(k)} \times F n_R^{(k)}}$ for receiver k. Note that equation (5.3) is still correct in this setup (with $\mathbf{P}^{(k)}$ and $\mathbf{D}^{(k)}$ no longer being forced to be block diagonal), by simply substituting $\sum_{f=0}^{F-1} n_{S_f}^{(k)}$ by $n_S^{(k)}$. Observe that, as will be shown in section 5.5.3, for some particular cases the precoder and decoder matrices do turn out to be block-diagonal as a result of the optimization and without being imposed from the beginning.

For the sake of compactness in the notation, it is convenient to further group the symbols estimated at all receivers in a single vector $\widehat{\mathbf{x}}$, which can be expressed as:

$$\widehat{\mathbf{x}} = \mathbf{DHPx} + \mathbf{Dw} \in \mathbb{C}^{\sum_{k=1}^{K} n_S^{(k)}}, \tag{5.4}$$

where

$\mathbf{x} = \left[\mathbf{x}^{(1)^T}, ..., \mathbf{x}^{(K)^T}\right]^T \in \mathbb{C}^{\sum_{k=1}^{K} n_S^{(k)}}$,
$\widehat{\mathbf{x}} = \left[\widehat{\mathbf{x}}^{(1)^T}, ..., \widehat{\mathbf{x}}^{(K)^T}\right]^T \in \mathbb{C}^{\sum_{k=1}^{K} n_S^{(k)}}$,
$\mathbf{H} = \left[\mathbf{H}^{(1)^T}, ..., \mathbf{H}^{(K)^T}\right]^T \in \mathbb{C}^{F\sum_{k=1}^{K} n_R^{(k)} \times F n_T}$,
$\mathbf{P} = \left[\mathbf{P}^{(1)}, ..., \mathbf{P}^{(K)}\right] \in \mathbb{C}^{F n_T \times \sum_{k=1}^{K} n_S^{(k)}}$,
$\mathbf{D} = \text{blockdiag}\left(\mathbf{D}^{(1)}, ..., \mathbf{D}^{(K)}\right) \in \mathbb{C}^{\sum_{k=1}^{K} n_S^{(k)} \times F\sum_{k=1}^{K} n_R^{(k)}}$,
and $\mathbf{w} = \left[\mathbf{w}^{(1)^T}, ..., \mathbf{w}^{(K)^T}\right]^T \in \mathbb{C}^{F\sum_{k=1}^{K} n_R^{(k)}}$. Then we define $\mathbf{R}_x^{(k)} = \mathbb{E}\left\{\mathbf{x}^{(k)}\mathbf{x}^{(k)^H}\right\}$ and $\mathbf{R}_w^{(k)} = \mathbb{E}\left\{\mathbf{w}^{(k)}\mathbf{w}^{(k)^H}\right\}$. Therefore, $\mathbf{R}_x = \mathbb{E}\left\{\mathbf{x}\mathbf{x}^H\right\} = \text{blockdiag}\left(\mathbf{R}_x^{(1)}, ..., \mathbf{R}_x^{(K)}\right)$ and $\mathbf{R}_w = \mathbb{E}\left\{\mathbf{w}\mathbf{w}^H\right\} = \text{blockdiag}\left(\mathbf{R}_w^{(1)}, ..., \mathbf{R}_w^{(K)}\right)$.

5.3 Feedback and equivalent channels

As is shown in section 5.5, in general, in order to optimally design the precoding matrix $\mathbf{P}$ at the transmitter under a generic optimization criterion, the CSI needed from each user corresponds to the channel propagation matrices for all F carriers. That is, knowledge of $\mathbf{H}_f^{(k)} \in \mathbb{C}^{n_R^{(k)} \times n_T}$, $\forall f, k$ (or, equivalently, $\mathbf{H}^{(k)}$ as defined just after (5.3)) is used to build the optimum precoder. In [Bog12, Pay09b], however, the authors proved that, for the single-user point-to-point MIMO scenario, the optimum linear precoding design can be calculated with just the channel Gram matrix (which is defined as $\mathbf{R}_f^{(k)} = \mathbf{H}_f^{(k)^H}\mathbf{H}_f^{(k)}$), for all the usual criteria. The motivation for using Gram matrix feedback is that it contains less information than the channel matrix feedback, but this information is sufficient for the precoder designs. Since less information has to be quantized and sent through the feedback link, the feedback can be performed more efficiently and the achieved system performance can improve. In some specific multiuser systems, such as in the BC with BD [Spe04], the transmitter design also depends only on the channel Gram matrix of each user and, therefore, the CSI quantization and feedback technique presented in chapter 3 can be applied directly, as shown in chapter 4. Note, however, that in the general multiuser scenario

(i.e., without constraining a BD transmission and/or for a general quality criterion for the design), as well as in robust precoder designs, complete knowledge of each $\mathbf{H}_f^{(k)}$ has been assumed so far by the research community. This chapter presents a linear transformation technique that still enables the use of channel Gram matrix feedback per user even in the general multiuser scenario by adding a unitary pre-transformation at the decoder to identify uniquely an equivalent triangular MIMO channel for each receiver. That is, knowledge of $\mathbf{R}_f^{(k)} \triangleq \mathbf{H}_f^{(k)H}\mathbf{H}_f^{(k)} \in \mathbb{C}^{n_T \times n_T}$ of each carrier and user is sufficient to design the optimum precoder.

At this point the possibility of performing feedback of the temporal CSI instead of the frequency CSI in a per carrier basis, as is usually done in OFDM systems, is also considered. Following from (5.1), the F channel Gram matrices $\mathbf{R}_f^{(k)}$ of size $n_T \times n_T$ for each user can also be computed as:

$$\mathbf{R}_f^{(k)} \triangleq \mathbf{H}_f^{(k)H}\mathbf{H}_f^{(k)} = \sum_{n=0}^{L-1}\sum_{m=0}^{L-1} \bar{\mathbf{H}}_n^{(k)H}\bar{\mathbf{H}}_m^{(k)} e^{-j\frac{2\pi}{F}f(m-n)} \in \mathbb{C}^{n_T \times n_T}, \quad f = 0, ..., F-1. \tag{5.5}$$

Following from (5.5) the necessary CSI corresponding to the k-th user at the transmitter can be computed with knowledge of the L matrices $\bar{\mathbf{H}}_l^{(k)} \in \mathbb{C}^{n_R^{(k)} \times n_T}$ or, alternatively, using one temporal Gram matrix $\bar{\mathbf{R}}^{(k)} \in \mathbb{C}^{Ln_T \times Ln_T}$ defined as (note that the sub-blocks of the following matrix are used directly within the sum in (5.5)):

$$\bar{\mathbf{R}}^{(k)} \triangleq \begin{bmatrix} \bar{\mathbf{H}}_0^{(k)H} \\ \bar{\mathbf{H}}_1^{(k)H} \\ \vdots \\ \bar{\mathbf{H}}_{L-1}^{(k)\ H} \end{bmatrix} \begin{bmatrix} \bar{\mathbf{H}}_0^{(k)} & \bar{\mathbf{H}}_1^{(k)} & \dots & \bar{\mathbf{H}}_{L-1}^{(k)} \end{bmatrix} \tag{5.6}$$

$$= \begin{bmatrix} \bar{\mathbf{H}}_0^{(k)H}\bar{\mathbf{H}}_0^{(k)} & \bar{\mathbf{H}}_0^{(k)H}\bar{\mathbf{H}}_1^{(k)} & \dots & \bar{\mathbf{H}}_0^{(k)H}\bar{\mathbf{H}}_{L-1}^{(k)} \\ \bar{\mathbf{H}}_1^{(k)H}\bar{\mathbf{H}}_0^{(k)} & \bar{\mathbf{H}}_1^{(k)H}\bar{\mathbf{H}}_1^{(k)} & \dots & \vdots \\ \vdots & \vdots & \ddots & \vdots \\ \bar{\mathbf{H}}_{L-1}^{(k)\ H}\bar{\mathbf{H}}_0^{(k)} & \bar{\mathbf{H}}_{L-1}^{(k)\ H}\bar{\mathbf{H}}_1^{(k)} & \dots & \bar{\mathbf{H}}_{L-1}^{(k)\ H}\bar{\mathbf{H}}_{L-1}^{(k)} \end{bmatrix} \in \mathbb{C}^{Ln_T \times Ln_T}. \tag{5.7}$$

Observe that matrices $\mathbf{R}_f^{(k)}$ and $\bar{\mathbf{R}}^{(k)}$ are positive semidefinite and Hermitian by construction. Since, as will be seen in the following subsections, the precoder design depends on the propagation channel of each user through $\mathbf{R}_f^{(k)}$, the most straightforward approach would be to quantize and feed back $\mathbf{R}_f^{(k)}$ individually for each carrier and user. However, this is suboptimal because: (i) it does not exploit the correlation in frequency of the propagation channel, and (ii) in systems with many carriers the feedback overhead would be too large. Therefore, in order to improve the performance of the CSI quantization, the scheme proposed in this chapter considers the possibility of feeding back the temporal channel Gram matrix $\bar{\mathbf{R}}^{(k)}$ of each user. This allows to exploit the correlation in frequency of the channel and also the fact that the size of the matrix to be quantized grows with the number of channel impulse response taps L instead of the number of carriers F. This can help to greatly improve the performance of the CSI quantization in some situations, as will be shown in section 5.6.

From the knowledge of the temporal channel Gram matrix $\bar{\mathbf{R}}^{(k)}$ (and therefore, of the individual Gram matrix $\mathbf{R}_f^{(k)}$ associated to each carrier), it is possible to compute (as is described in the next section), for each user and carrier, a unique equivalent channel response triangular matrix which can be used to apply any type of multiuser design on top of it (without the restrictions of BD, which spends degrees of freedom to completely avoid inter-user interference), for any quality criterion in the same way as if knowledge of the actual channel response matrix $\mathbf{H}_f^{(k)}$ was available.

5.3.1 Equivalent channel transformation

Following the feedback model presented in the previous section, knowledge of an estimate of the channel Gram matrix of each user is assumed at the transmitter. Note that there are multiple possible channel matrices $\mathbf{H}^{(k)}$ that generate the same Gram matrix $\mathbf{R}^{(k)} \triangleq \mathbf{H}^{(k)H}\mathbf{H}^{(k)}$ (for example $\mathbf{H}^{(k)}$ and $\mathbf{U}\mathbf{H}^{(k)}$, with $\mathbf{U}$ being a unitary matrix, generate the same Gram matrix). Since the transmitter has knowledge only of

the fed back Gram matrix, it cannot know which of the multiple channel matrices that generate such Gram matrix is the actual channel matrix. However, there is only one of the possible matrices that can generate the Gram matrix that is upper triangular and with real positive elements in the diagonal, and this matrix can be computed at the transmitter, as will be shown in this subsection. At the same time, note also that, by applying a properly calculated unitary linear transformation $\mathbf{Q}^{(k)H}$, with $\mathbf{Q}^{(k)} \in \mathbb{C}^{Fn_R^{(k)} \times Fn_R^{(k)}}$ at each receiver k, it is possible to generate an equivalent channel response matrix $\mathbf{T}^{(k)} \in \mathbb{C}^{Fn_R^{(k)} \times Fn_T}$ from the transmitter to the output of such unitary transformation at each receiver (as shown in Figure 5.2), which is upper triangular and with real elements in the diagonal. Since there is only one possible upper triangular matrix with real elements in the diagonal associated to the Gram matrix, and the unitary transformation does not change the Gram matrix, the equivalent channel matrix computed at the transmitter and the equivalent channel generated by the application of such unitary transformation $\mathbf{Q}^{(k)}$ at the receiver are the same ones. This scheme is depicted in Figure 5.2 (note that in Figure 5.2, $\widetilde{\mathbf{D}}^{(k)}$ is defined as $\widetilde{\mathbf{D}}^{(k)} = \mathbf{D}^{(k)}\mathbf{Q}^{(k)} \in \mathbb{C}^{n_S^{(k)} \times Fn_R^{(k)}}$, so that $\mathbf{D}^{(k)} = \widetilde{\mathbf{D}}^{(k)}\mathbf{Q}^{(k)H}$).

Finally, it is important to note that this matrix $\mathbf{Q}^{(k)}$ does not introduce a penalty in the performance of the system since it is a unitary linear transformation that could be reversed at the receiver by a proper processing after such unitary transformation. This transformation allows any arbitrary multiuser transmission design to be applied on top of the basis of these new equivalent channel matrices $\left\{\mathbf{T}^{(k)}\right\}_{k=1}^{K}$, where now the transmitter is required to know only the channel Gram matrices $\mathbf{R}_f^{(k)}$ or $\bar{\mathbf{R}}^{(k)}$.

According to the previous definitions, the equivalent triangular channel $\mathbf{T}^{(k)}$ is such that satisfies:

$$\mathbf{H}^{(k)} = \mathbf{Q}^{(k)}\mathbf{T}^{(k)}, \quad k = 1, ..., K. \tag{5.8}$$

The computation of the equivalent channel response matrix $\mathbf{T}^{(k)}$ at the transmitter as a function of the matrix $\mathbf{R}^{(k)}$, and the computation of matrices $\mathbf{Q}^{(k)}$ and $\mathbf{T}^{(k)}$ from $\mathbf{H}^{(k)}$ at the receiver are described next.

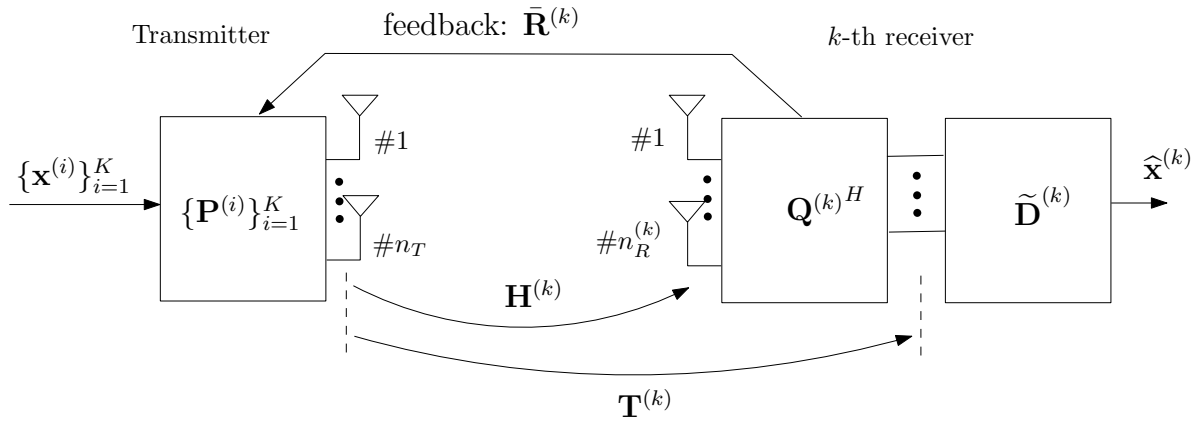

Figure 5.2: Equivalent channel model.

Observe that, since $\mathbf{H}^{(k)}$ is a block diagonal matrix as defined in section 5.2, the resulting $\mathbf{Q}^{(k)}$ and $\mathbf{T}^{(k)}$ are also block diagonal. In fact, the computation can be performed in parallel for each block of $\mathbf{H}^{(k)}$, which corresponds to the channel response matrix for each carrier, $\mathbf{H}_f^{(k)}$, $f = 0, ..., F-1$. This greatly reduces the required computational complexity, and, for this reason, the transformation will be presented next for each individual matrix $\mathbf{H}_f^{(k)}, \mathbf{R}_f^{(k)}$.

The channel response matrix for the f-th carrier and the k-th receiver $\mathbf{H}_f^{(k)}$ can be written as:

$$\mathbf{H}_f^{(k)} = \mathbf{Q}_f^{(k)} \mathbf{T}_f^{(k)}, \quad f = 0, ..., F-1, \tag{5.9}$$

where $\mathbf{Q}_f^{(k)} \in \mathbb{C}^{n_R^{(k)} \times n_R^{(k)}}$ is unitary and $\mathbf{T}_f^{(k)} \in \mathbb{C}^{n_R^{(k)} \times n_T}$ is upper triangular [Hor85] (consequently, the channel Gram matrix $\mathbf{R}_f^{(k)}$ can also be written as $\mathbf{R}_f^{(k)} = \mathbf{H}_f^{(k)H} \mathbf{H}_f^{(k)} = \mathbf{T}_f^{(k)H} \mathbf{T}_f^{(k)}$). The decomposition that allows to calculate $\mathbf{T}_f^{(k)}$ from $\mathbf{R}_f^{(k)}$ is unique if $\mathbf{T}_f^{(k)}$ is required to be upper triangular and with the elements $t_{i,i}$ on the main diagonal being positive and real, as will be shown next.

Calculation of $\mathbf{T}_f^{(k)}$ at the transmitter

Matrix $\mathbf{R}_f^{(k)}$ is obtained at the transmitter from $\bar{\mathbf{R}}^{(k)}$ received through the feedback link using (5.5) and (5.7). From $\mathbf{R}_f^{(k)}$, the transmitter can uniquely compute $\mathbf{T}_f^{(k)}$ as

described next. Observe that there is only one possible $\mathbf{T}_f^{(k)} \in \mathbb{C}^{n_R^{(k)} \times n_T}$ satisfying that the elements $t_{i,i}$ are real and positive and $t_{i,j} = 0,\ \forall i > j$.

From $\mathbf{R}_f^{(k)} = {\mathbf{T}_f^{(k)}}^H \mathbf{T}_f^{(k)}$, matrix $\mathbf{T}_f^{(k)}$ is computed as $(j \geq i)$:[2]

$$t_{i,j} = \begin{cases} \sqrt{r_{1,1}}\,, & i = j = 1, \\ \frac{r_{1,j}}{t_{1,1}}\,, & i = 1, \forall\, j > 1, \\ \frac{r_{i,j} - \sum_{k=1}^{i-1} t_{k,i}^* t_{k,j}}{t_{i,i}}\,, & \forall\, i,j;\ 1 < i < j, \\ \sqrt{r_{i,i} - \sum_{k=1}^{i-1} |t_{k,i}|^2}\,, & \forall\, i,j;\ i = j > 1, \end{cases} \tag{5.10}$$

where $r_{i,j}$ and $t_{i,j}$ are the elements i,j of $\mathbf{R}_f^{(k)}$ and $\mathbf{T}_f^{(k)}$, respectively, and where, for the sake of clarity in the notation, we have dropped the dependence of $r_{i,j}$ and $t_{i,j}$ on f.

Calculation of $\mathbf{T}_f^{(k)}$ and $\mathbf{Q}_f^{(k)}$ at the receiver

At the receiver there is knowledge of $\mathbf{H}_f^{(k)}$ and, therefore, it is possible to obtain $\mathbf{T}_f^{(k)} = {\mathbf{Q}_f^{(k)}}^H \mathbf{H}_f^{(k)}$, which is the same equivalent channel calculated at the transmitter, as is described in the following algorithm based on the QR decomposition [Gol96]. From (5.9) it follows that matrices $\mathbf{T}_f^{(k)}$ and $\mathbf{Q}_f^{(k)}$ can be computed as:[3]

$$\mathbf{q}_i = \begin{cases} \frac{\mathbf{h}_1}{\|\mathbf{h}_1\|}, & i = 1, \\ \frac{\left(\mathbf{I} - \sum_{k=1}^{i-1} \mathbf{q}_k \mathbf{q}_k^H\right)\mathbf{h}_i}{\left\|\left(\mathbf{I} - \sum_{k=1}^{i-1} \mathbf{q}_k \mathbf{q}_k^H\right)\mathbf{h}_i\right\|}\,, & \forall i;\ 1 < i \leq n_T, \end{cases} \tag{5.11}$$

$$t_{i,j} = \begin{cases} \mathbf{q}_i^H \mathbf{h}_j\,, & \forall\, i < j, \\ \|\mathbf{h}_1\|\,, & i = j = 1, \\ \left\|\left(\mathbf{I} - \sum_{k=1}^{i-1} \mathbf{q}_k \mathbf{q}_k^H\right)\mathbf{h}_i\right\|\,, & \forall\, i,j;\ i = j > 1, \end{cases} \tag{5.12}$$

[2]Note that the decomposition presented in (5.10) is not exactly the Cholesky factorization [Hou06] because the resulting matrix $\mathbf{T}_f^{(k)} \in \mathbb{C}^{n_R^{(k)} \times n_T}$ is not forced to be square (the equivalent channel propagation matrix $\mathbf{T}_f^{(k)}$ must have the same dimensions as the actual channel propagation matrix $\mathbf{H}_f^{(k)}$).

[3]Note that, since at the receiver there is knowledge of $\mathbf{H}_f^{(k)}$, it would also be possible to calculate $\mathbf{R}_f^{(k)} = {\mathbf{H}_f^{(k)}}^H \mathbf{H}_f^{(k)}$ and compute $\mathbf{T}_f^{(k)}$ locally as explained in the decomposition to be calculated at the transmitter.

where $\mathbf{q}_i$ and $\mathbf{h}_i$ correspond to the i-th column of matrices $\mathbf{Q}_f^{(k)}$ and $\mathbf{H}_f^{(k)}$, respectively, and, again, the dependence on f is omitted for clarity in the notation.

In the case where $n_R^{(k)} > n_T$, the last $n_R^{(k)} - n_T$ columns of $\mathbf{Q}_f^{(k)}$ are chosen such that ${\mathbf{Q}_f^{(k)}}^H \mathbf{Q}_f^{(k)} = \mathbf{I}$, i.e., they just have to be orthogonal with each other and with the previous columns and have a norm equal to 1 and they can be calculated following the Gram-Schmidt procedure [Gol96]. In this case, it is assumed that the rank of the matrix $\mathbf{R}_f^{(k)}$ is given by n_T. It is important to note that the equivalent channel $\mathbf{T}_f^{(k)}$ is a tall matrix with the last $n_R^{(k)} - n_T$ rows equal to zero. This means that, at the receiver, after the application of the transformation represented by ${\mathbf{Q}_f^{(k)}}^H$, the last $n_R^{(k)} - n_T$ outputs contain only noise, which is uncorrelated with the data. Observe that, in the case of spatially white noise, i.e., if $\mathbf{R}_{w_f}^{(k)} = \sigma_{w_f}^2 \mathbf{I}$, the last $n_R^{(k)} - n_T$ outputs contain no useful information. Consequently, for the computation of the estimates of the transmitted symbols at the receiver, the last $n_R^{(k)} - n_T$ columns of $\mathbf{Q}_f^{(k)}$ could be ignored, reducing the complexity of computing $\mathbf{Q}_f^{(k)}$. In the case where $n_R^{(k)} \leq n_T$ it is assumed that the rank of the matrix $\mathbf{R}_f^{(k)}$ is given by $n_R^{(k)}$ and the transformation is performed as already described in this subsection.

5.4 Error analysis

In general, robust transceiver designs require the characterization of the CSI error in order to minimize its effect. In the presented framework, this characterization has been performed in terms of the second-order statistics of the resulting error at the equivalent triangular channel matrix, as will be shown in this section. This will exploited in the robust design presented in section 5.5 as an illustrative example of application.

The error in the equivalent triangular channel is the result of the propagation of the initial error generated in the CSI quantization. In general, only the second-order statistics of the initial quantization error are known. This section presents the analytic study of the linear relation, for small errors, between the initial quantization error and

the final error in the equivalent triangular channel matrix. From this derivation it will be possible to compute the second order statistics of the error in the equivalent triangular channel.

5.4.1 Error model

There are three different sources of inaccuracies in the CSI sent through the feedback link from the receiver to the transmitter: estimation errors at the receiver, quantization errors which are inherent to the feedback process, and errors due to noise in the feedback link. In practical situations, where the part of the transmission dedicated to feedback is greatly constrained, the quantization error is the dominant factor of the error. Consequently, in the following derivations only the errors resulting from the quantization process are considered. The CSI at the transmitter $\bar{\mathbf{R}}^{(k)}_{\text{quant}} \triangleq \text{quantiz}\left(\bar{\mathbf{R}}^{(k)}\right)$ is modeled through the error matrix $\bar{\mathbf{R}}^{(k)}_{\text{err}}$:

$$\bar{\mathbf{R}}^{(k)} = \bar{\mathbf{R}}^{(k)}_{\text{quant}} + \bar{\mathbf{R}}^{(k)}_{\text{err}} \in \mathbb{C}^{Ln_T \times Ln_T}. \tag{5.13}$$

Note that, although the rank of matrix $\bar{\mathbf{R}}^{(k)} \in \mathbb{C}^{Ln_T \times Ln_T}$ before the quantization is $\min\left(n_R^{(k)}, Ln_T\right)$, depending on the quantization strategy that is applied and if $n_R^{(k)} < Ln_T$, it is possible that after the quantization the rank of the resulting matrix is increased up to Ln_T. Consequently, if $n_R^{(k)} < Ln_T$, then matrix $\bar{\mathbf{R}}^{(k)}_{\text{quant}}$ should be projected on the space of the matrices with a rank equal to $n_R^{(k)}$ at the transmitter in order to maintain the rank.[4] The error after the projection is then propagated at the transmitter through the Fourier transformation used to compute the channel Gram matrix associated to carrier f and user k and through the computation of the equivalent triangular channel $\mathbf{T}_f^{(k)}$ (see section 5.3). The final error in the resulting knowledge of $\mathbf{T}_f^{(k)}$ is denoted in the following by $\mathbf{T}^{(k)}_{\text{err}_f}$:

$$\mathbf{T}_f^{(k)} = \mathbf{T}^{(k)}_{\text{quant}_f} + \mathbf{T}^{(k)}_{\text{err}_f}, \tag{5.14}$$

[4] In the case where $n_R^{(k)} \geq Ln_T$ the quantization process maintains the rank of the matrix, but in the case that $n_R^{(k)} < Ln_T$ the projection presented here is required in order to keep the same rank.

where $\mathbf{T}^{(k)}_{\text{quant}_f}$ is the estimated value of the actual equivalent triangular channel $\mathbf{T}^{(k)}_f$ calculated using the quantized and projected channel Gram matrix sent through the feedback link. The expression of $\mathbf{T}^{(k)}_{\text{err}_f}$ as a result of the error propagation is derived in subsection 5.4.2.

Following this notation, (5.4) can be rewritten reflecting the errors in the CSI at the transmitter and incorporating the notation corresponding to the equivalent channels as:

$$\widehat{\mathbf{x}} = \widetilde{\mathbf{D}}\mathbf{T}_{\text{quant}}\mathbf{P}\mathbf{x} + \widetilde{\mathbf{D}}\mathbf{T}_{\text{err}}\mathbf{P}\mathbf{x} + \widetilde{\mathbf{D}}\mathbf{Q}^H\mathbf{w} \in \mathbb{C}^{\sum_{k=1}^{K} n_S^{(k)}}, \tag{5.15}$$

where

$$\begin{aligned}
\mathbf{T}^{(k)}_{\text{quant}} &= \text{blockdiag}\left(\mathbf{T}^{(k)}_{\text{quant}\,0}, ..., \mathbf{T}^{(k)}_{\text{quant}\,F-1}\right) \in \mathbb{C}^{Fn_R^{(k)} \times Fn_T},\\
\mathbf{T}^{(k)}_{\text{err}} &= \text{blockdiag}\left(\mathbf{T}^{(k)}_{\text{err}\,0}, ..., \mathbf{T}^{(k)}_{\text{err}\,F-1}\right) \in \mathbb{C}^{Fn_R^{(k)} \times Fn_T},\\
\widetilde{\mathbf{D}} &= \text{blockdiag}\left(\widetilde{\mathbf{D}}^{(1)}, ..., \widetilde{\mathbf{D}}^{(K)}\right) \in \mathbb{C}^{\sum_{k=1}^{K} n_S^{(k)} \times F\sum_{k=1}^{K} n_R^{(k)}},\\
\mathbf{Q} &= \text{blockdiag}\left(\mathbf{Q}^{(1)}, ..., \mathbf{Q}^{(K)}\right) \in \mathbb{C}^{F\sum_{k=1}^{K} n_R^{(k)} \times F\sum_{k=1}^{K} n_R^{(k)}},\\
\mathbf{T}_{\text{quant}} &= \left[\mathbf{T}^{(1)^T}_{\text{quant}}, ..., \mathbf{T}^{(K)^T}_{\text{quant}}\right]^T \in \mathbb{C}^{F\sum_{k=1}^{K} n_R^{(k)} \times Fn_T},\\
\mathbf{T}_{\text{err}} &= \left[\mathbf{T}^{(1)^T}_{\text{err}}, ..., \mathbf{T}^{(K)^T}_{\text{err}}\right]^T \in \mathbb{C}^{F\sum_{k=1}^{K} n_R^{(k)} \times Fn_T}.
\end{aligned}$$

5.4.2 Error propagation

As shown in the previous subsection, the CSI inaccuracies are defined in the matrix $\bar{\mathbf{R}}^{(k)}$, which is quantized and then sent through the feedback link. At the transmitter, the received matrix $\bar{\mathbf{R}}^{(k)}_{\text{quant}}$ is projected, if needed, to guarantee that its rank is $\min(n_R^{(k)}, Ln_T)$, and an estimate of the channel Gram matrix $\mathbf{R}^{(k)}_{\text{quant}_f}$ is computed using the projected matrix $\bar{\mathbf{R}}^{(k)}_{\text{quant,p}}$, following (5.5). In a third step, the estimated equivalent channel $\mathbf{T}^{(k)}_{\text{quant}}$ is computed from $\mathbf{R}^{(k)}_{\text{quant}_f}$ following (5.10).

First, the propagation of the error through the semidefinite projection is presented. Next, the transformation of the resulting error through the computation of $\mathbf{R}^{(k)}_f$ at the transmitter is studied. Finally, the result is further propagated through the equivalent

channel computation, in order to obtain an expression of $\mathbf{T}_{\text{err}}^{(k)}$. This result will then be used for the design of the robust precoder in section 5.5.

Propagation through the semidefinite projection

As it has been pointed out above, the first step where the quantization error propagates through is the positive semidefinite projection. Note that if $n_R^{(k)} \geq Ln_T$ this step is not necessary, since $\bar{\mathbf{R}}_{\text{quant}}^{(k)}$ already maintains the same rank as $\bar{\mathbf{R}}^{(k)}$; so, in the following in this subsection it is assumed that $n_R^{(k)} < Ln_T$. The positive semidefinite projection operator, $\mathcal{P}$, is defined as:

$$\mathcal{P}(\mathbf{X}, N) = \sum_{i=1}^{N} \lambda_i(\mathbf{X})\mathbf{u}_i(\mathbf{X})\mathbf{u}_i(\mathbf{X})^H, \tag{5.16}$$

where $\mathbf{X}$ represents any Hermitian matrix, $\lambda_i(\mathbf{X})$ is the i-th eigenvalue of $\mathbf{X}$ (sorted in decreasing order), and $\mathbf{u}_i(\mathbf{X})$ is its associated unitary eigenvector.

Consequently, this first step can be written as $\bar{\mathbf{R}}_{\text{quant,p}}^{(k)} = \mathcal{P}(\bar{\mathbf{R}}_{\text{quant}}^{(k)}, n_R^{(k)})$ and, from (5.13), we have that $\bar{\mathbf{R}}_{\text{quant,p}}^{(k)} = \mathcal{P}(\bar{\mathbf{R}}^{(k)} - \bar{\mathbf{R}}_{\text{err}}^{(k)}, n_R^{(k)})$. This can also be written as:

$$\bar{\mathbf{R}}_{\text{quant,p}}^{(k)} = \mathcal{P}(\bar{\mathbf{R}}^{(k)} - \bar{\mathbf{R}}_{\text{err}}^{(k)}, n_R^{(k)}) = \mathcal{P}(\bar{\mathbf{R}}^{(k)}, n_R^{(k)}) - \bar{\mathbf{R}}_{\text{err,p}}^{(k)} = \bar{\mathbf{R}}^{(k)} - \bar{\mathbf{R}}_{\text{err,p}}^{(k)}, \tag{5.17}$$

where the error after the projection is defined as $\bar{\mathbf{R}}_{\text{err,p}}^{(k)} \triangleq \mathcal{P}(\bar{\mathbf{R}}^{(k)}, n_R^{(k)}) - \mathcal{P}(\bar{\mathbf{R}}^{(k)} - \bar{\mathbf{R}}_{\text{err}}^{(k)}, n_R^{(k)}) = \bar{\mathbf{R}}^{(k)} - \mathcal{P}(\bar{\mathbf{R}}^{(k)} - \bar{\mathbf{R}}_{\text{err}}^{(k)}, n_R^{(k)})$. Now, it remains to linearly relate the real and imaginary parts of the elements in $\bar{\mathbf{R}}_{\text{err,p}}^{(k)}$ with those in $\bar{\mathbf{R}}_{\text{err}}^{(k)}$, which can be done using a first order approximation and the results in [Mag02] as:

$$\widetilde{\mathsf{vec}}\left(\bar{\mathbf{R}}_{\text{err,p}}^{(k)}\right) \approx \left(\mathsf{D}_{\bar{\mathbf{r}}^{(k)}}\mathcal{P}(\bar{\mathbf{R}}^{(k)}, n_R^{(k)})\right)\widetilde{\mathsf{vec}}\left(\bar{\mathbf{R}}_{\text{err}}^{(k)}\right), \tag{5.18}$$

where the operator $\widetilde{\mathsf{vec}}\,(\cdot) = \left[\mathsf{vech}(\Re\mathrm{e}(\cdot))^T\mathsf{veci}(\Im\mathrm{m}(\cdot))^T\right]^T$ [5] has been used and $\bar{\mathbf{r}}^{(k)} = \widetilde{\mathsf{vec}}\left(\bar{\mathbf{R}}^{(k)}\right)$. Finally, with a modicum of algebra and using the results in [Pay09a,

[5] The operators $\mathsf{vec}(\cdot)$, $\mathsf{vech}(\cdot)$ and $\mathsf{veci}(\cdot)$ act upon matrices and transform them into column vectors as described next. First, $\mathsf{vec}(\cdot)$ represents the vector obtained by stacking the columns from left to right. Next $\mathsf{vech}(\cdot)$ transforms its matrix argument into a vector, by stacking only the elements of each column that lie on or below the main diagonal. Similarly, $\mathsf{veci}(\cdot)$ represents the result of stacking only the elements of each column that lie strictly below the main diagonal.

Lemmas A.4 and B.7], the expression of the Jacobian matrix $\mathsf{D}_{\bar{\mathbf{r}}^{(k)}}\mathcal{P}(\bar{\mathbf{R}}^{(k)}, n_R^{(k)})$ can be computed as:

$$\begin{aligned}\mathsf{D}_{\bar{\mathbf{r}}^{(k)}}\mathcal{P}(\bar{\mathbf{R}}^{(k)}, n_R^{(k)}) = &\sum_{i=1}^{n_R^{(k)}} \mathsf{vec}\big(\mathbf{u}_i(\bar{\mathbf{R}}^{(k)})\mathbf{u}_i(\bar{\mathbf{R}}^{(k)})^H\big)\left(\mathsf{D}_{\bar{\mathbf{r}}^{(k)}}\lambda_i(\bar{\mathbf{R}}^{(k)})\right) \\ &+ \sum_{i=1}^{n_R^{(k)}} \lambda_i(\bar{\mathbf{R}}^{(k)})(\mathbf{u}_i(\bar{\mathbf{R}}^{(k)})^* \otimes \mathbf{I}_{n_T})(\mathsf{D}_{\bar{\mathbf{r}}^{(k)}}\mathbf{u}_i(\bar{\mathbf{R}}^{(k)})) \\ &+ \sum_{i=1}^{n_R^{(k)}} \lambda_i(\bar{\mathbf{R}}^{(k)})(\mathbf{I}_{n_T} \otimes \mathbf{u}_i(\bar{\mathbf{R}}^{(k)}))(\mathsf{D}_{\bar{\mathbf{r}}^{(k)}}\mathbf{u}_i(\bar{\mathbf{R}}^{(k)}))^*, \end{aligned} \tag{5.19}$$

where the explicit expressions for $\mathsf{D}_{\bar{\mathbf{r}}^{(k)}}\lambda_i(\bar{\mathbf{R}}^{(k)})$ and $\mathsf{D}_{\bar{\mathbf{r}}^{(k)}}\mathbf{u}_i(\bar{\mathbf{R}}^{(k)})$ can be straightforwardly found from the results in [Mag02, Chapter 9].

Propagation through the Fourier transformation

Equation (5.5) describes the computation of $\mathbf{R}_f^{(k)}$ from $\bar{\mathbf{R}}^{(k)}$, which corresponds to the Fourier transformation of the projected time domain Gram matrix. The error propagation through the computation of $\mathbf{R}_f^{(k)}$ is studied next. From (5.5) and (5.17) it follows that:

$$\mathbf{R}_f^{(k)} = {\mathbf{F}_f}^H \bar{\mathbf{R}}^{(k)} \mathbf{F}_f = {\mathbf{F}_f}^H \left(\bar{\mathbf{R}}^{(k)}_{\text{quant,p}} + \bar{\mathbf{R}}^{(k)}_{\text{err,p}}\right) \mathbf{F}_f, \tag{5.20}$$

where $\mathbf{F}_f$ is the extended Fourier matrix defined as
$\mathbf{F}_f = \left[e^{-j\frac{2\pi}{F}(f-0)},\, e^{-j\frac{2\pi}{F}(f-1)},\, ...,\, e^{-j\frac{2\pi}{F}(f-(L-1))}\right]^T \otimes \mathbf{I}_{n_T} \in \mathbb{C}^{Ln_T \times n_T}$.

Following from (5.20), the error in the computation of $\mathbf{R}_f^{(k)}$ at the transmitter is given by

$$\mathbf{R}^{(k)}_{\text{err}_f} \triangleq {\mathbf{F}_f}^H \bar{\mathbf{R}}^{(k)}_{\text{err,p}} \mathbf{F}_f, \tag{5.21}$$

where $\mathbf{R}_f^{(k)} = \mathbf{R}^{(k)}_{\text{quant}_f} + \mathbf{R}^{(k)}_{\text{err}_f}$ and $\mathbf{R}^{(k)}_{\text{quant}_f}$ is the estimated Gram matrix associated to receiver k and carrier f, i.e., $\mathbf{R}^{(k)}_{\text{quant}_f} = {\mathbf{F}_f}^H \bar{\mathbf{R}}^{(k)}_{\text{quant,p}} \mathbf{F}_f$. Following the structure used in the previous subsection, the propagation of the error through the Fourier transformation, (5.21), can be expressed as:

$$\widetilde{\mathsf{vec}}\left(\mathbf{R}^{(k)}_{\text{err}_f}\right) = \widetilde{\mathbf{F}}_f \widetilde{\mathsf{vec}}\left(\bar{\mathbf{R}}^{(k)}_{\text{err,p}}\right), \tag{5.22}$$

where

$$\widetilde{\mathbf{F}} = \begin{bmatrix} \mathbf{D}_{n_T}^{+}\left(\mathbf{F}_{f_r}^{T}\otimes\mathbf{F}_{f_r}^{T}+\mathbf{F}_{f_i}^{T}\otimes\mathbf{F}_{f_i}^{T}\right)\mathbf{D}_{Ln_T} & \mathbf{D}_{n_T}^{+}\left(\mathbf{F}_{f_r}^{T}\otimes\mathbf{F}_{f_i}^{T}-\mathbf{F}_{f_i}^{T}\otimes\mathbf{F}_{f_r}^{T}\right)\mathbf{D}_{Ln_T} \\ \mathbf{C}_{n_T}^{+}\left(\mathbf{F}_{f_i}^{T}\otimes\mathbf{F}_{f_r}^{T}-\mathbf{F}_{f_r}^{T}\otimes\mathbf{F}_{f_i}^{T}\right)\mathbf{C}_{Ln_T} & \mathbf{C}_{n_T}^{+}\left(\mathbf{F}_{f_r}^{T}\otimes\mathbf{F}_{f_r}^{T}+\mathbf{F}_{f_i}^{T}\otimes\mathbf{F}_{f_i}^{T}\right)\mathbf{C}_{Ln_T} \end{bmatrix}, \tag{5.23}$$

and the following notation was used: $\mathbf{F}_{f_r} = \Re\mathrm{e}(\mathbf{F}_f)$ and $\mathbf{F}_{f_i} = \Im\mathrm{m}(\mathbf{F}_f)$. Also, $(\cdot)^+$ stands for the pseudo-inverse operation and $\mathbf{D}_n$ corresponds to the duplication matrix, whose definition is given in [Mag02]. Similarly, the antiduplication matrix $\mathbf{C}_n$ is defined as the unique matrix such that, for all $\mathbf{X} \in \mathbb{R}^{n\times n}$, $\mathsf{vec}(\mathbf{X}-\mathbf{X}^T) = \mathbf{C}_n\mathsf{veci}(\mathbf{X}-\mathbf{X}^T)$.

Propagation through the equivalent channel computation

After the computation of $\mathbf{R}^{(k)}_{\mathrm{quant}_f}$, the error $\mathbf{R}^{(k)}_{\mathrm{err}_f}$ is propagated through the matrix factorization at the transmitter described in section 5.3.1. The objective now is to obtain the expression of the error in the equivalent triangular channel response matrix $\mathbf{T}^{(k)}_{\mathrm{err}_f}$ as a function of $\mathbf{R}^{(k)}_{\mathrm{err}_f}$. A first order approximation of the error propagation is considered, which is valid for small errors. From (5.20) it follows that

$$\mathbf{R}_f^{(k)} = \mathbf{T}_f^{(k)H}\mathbf{T}_f^{(k)}, \tag{5.24}$$

$$\mathbf{R}^{(k)}_{\mathrm{quant}_f} + \mathbf{R}^{(k)}_{\mathrm{err}_f} = \left(\mathbf{T}^{(k)}_{\mathrm{quant}_f} + \mathbf{T}^{(k)}_{\mathrm{err}_f}\right)^H\left(\mathbf{T}^{(k)}_{\mathrm{quant}_f} + \mathbf{T}^{(k)}_{\mathrm{err}_f}\right). \tag{5.25}$$

After some manipulations described in appendix 5.A, the error in the equivalent channel response matrix $\mathbf{T}^{(k)}_{\mathrm{err}_f}$ can be expressed as a function of $\mathbf{R}^{(k)}_{\mathrm{err}_f}$ as:

$$\widetilde{\mathsf{vec}}\left(\mathbf{T}^{(k)\,T}_{\mathrm{err}_f}\right) \simeq \left(\mathsf{D}_{\mathbf{r}_f^{(k)}}\mathbf{t}_f^{(k)}\right)\widetilde{\mathsf{vec}}\left(\mathbf{R}^{(k)}_{\mathrm{err}_f}\right), \tag{5.26}$$

where $\mathsf{D}_{\mathbf{r}_f^{(k)}}\mathbf{t}_f^{(k)}$ is the Jacobian matrix of $\mathbf{t}_f^{(k)}$ as defined in (5.51), and whose expression is derived in appendix 5.A.

Summary

The complete CSI error propagation process described in the previous 3 steps is summarized in the diagram in Figure 5.3, which reflects also the notation used through the

derivations. Mathematically, the complete error propagation process can be expressed from (5.18), (5.22), and (5.26) as:

$$\widetilde{\mathsf{vec}}\left(\mathbf{T}_{\mathrm{err}_f}^{(k)\ T}\right) \simeq \mathbf{X}_f^{(k)} \bar{\mathbf{r}}_{err}^{(k)}, \tag{5.27}$$

where $\bar{\mathbf{r}}_{err}^{(k)} = \widetilde{\mathsf{vec}}\left(\bar{\mathbf{R}}_{\mathrm{err}}^{(k)}\right) \in \mathbb{R}^{L^2 n_T^2 \times 1}$ and $\mathbf{X}_f^{(k)}$ is the linear transformation that results from the error propagation through all the steps:

$$\mathbf{X}_f^{(k)} = \begin{cases} \left(\mathsf{D}_{\mathbf{r}_f^{(k)}} \mathbf{t}_f^{(k)}\right) \widetilde{\mathbf{F}}_f \left(\mathsf{D}_{\bar{\mathbf{r}}^{(k)}} \mathcal{P}(\bar{\mathbf{R}}^{(k)}, n_R^{(k)})\right), & \text{if } n_R^{(k)} < L n_T, \\ \left(\mathsf{D}_{\mathbf{r}_f^{(k)}} \mathbf{t}_f^{(k)}\right) \widetilde{\mathbf{F}}_f, & \text{if } n_R^{(k)} \geq L n_T. \end{cases} \tag{5.28}$$

Finally, appendix 5.A.1 presents a notation that relates the subindices of the error in the triangular matrix $\mathbf{T}_{\mathrm{err}_f}^{(k)}$ with the corresponding row index of matrix $\mathbf{X}_f^{(k)}$. This notation will be used in the following section.

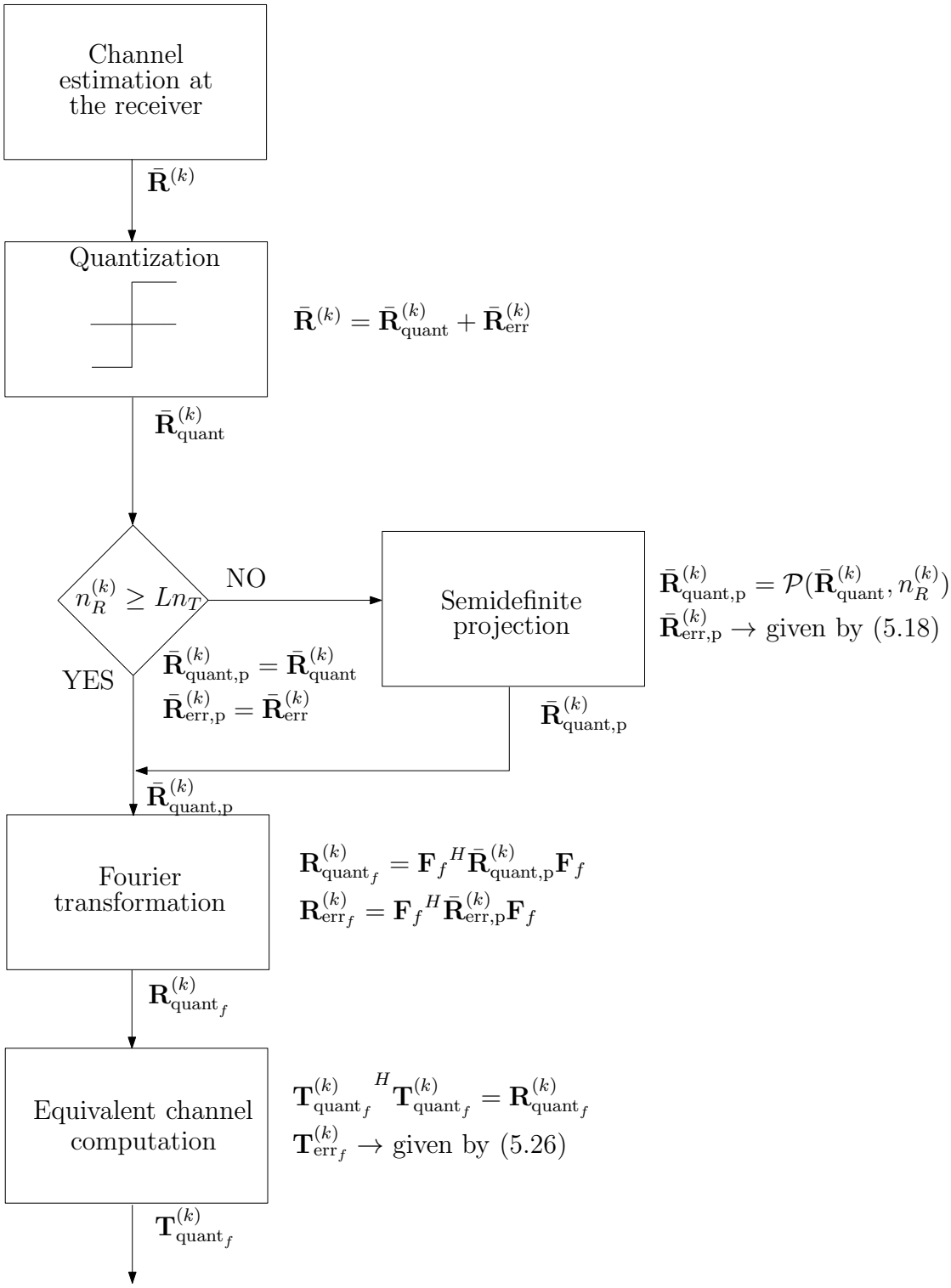

Figure 5.3: Diagram of the complete CSI processing and the error propagation through the stages of such processing.

5.5 Application to robust precoder design

This section presents an example of a robust design of the precoder matrix taking into account the error in the available CSI due to the quantization applied for the feedback transmission. As explained before, with the help of the transformation described in section 5.3.1, the transmitter is able to compute equivalent propagation channels using the channel Gram matrices sent through the feedback links. This will allow to apply a robust MSE precoding strategy, which takes into account explicitly the statistics of the inaccuracies in the CSI at the transmitter defined by $\bar{\mathbf{R}}_{\text{err}}^{(k)}$ in (5.13). The advantage of the robust design is that it is less sensitive to such errors.

5.5.1 Optimization of the MSE

It is important to emphasize that the equivalent channel transformation from section 5.3.1 can be used to apply any arbitrary design criterion and system architecture (also for joint precoder and decoder design) on top of it. In this section, and for illustrative purposes, the specific design criterion of minimization of the MSE with fixed decoders[6] is considered as an example of application and because it is analytically tractable. First, the expression of the MSE is presented and then the robust precoder design is derived.

In order to adjust the dynamic range of $\widehat{\mathbf{x}}$ before computing the MSE, the factor β is included, as in [Joh02, Cho02c], which could be understood as a gain control at

[6]The assumption of fixed decoders for the precoder design is common in the literature, and is considered in works such as [Wan10, Sun09, Ten04, Shi07, Vuc09].

the receivers. The MSE is then given by:

$$\begin{aligned}\mathrm{MSE}(\mathbf{P},\beta) &= \sum_{k=1}^{K}\mathbb{E}_{\mathbf{T}_{\mathrm{err}}^{(k)},\mathbf{x}^{(k)},\mathbf{w}^{(k)}}\left\{\|\mathbf{x}^{(k)}-\beta^{-1}\widehat{\mathbf{x}}^{(k)}\|_2^2\right\} = \mathbb{E}_{\mathbf{T}_{\mathrm{err}},\mathbf{x},\mathbf{w}}\left\{\|\mathbf{x}-\beta^{-1}\widehat{\mathbf{x}}\|_2^2\right\} \\ &= \frac{1}{\beta^2}\mathrm{tr}\Big(\widetilde{\mathbf{D}}\mathbf{T}_{\mathrm{quant}}\mathbf{P}\mathbf{R}_x\mathbf{P}^H\mathbf{T}_{\mathrm{quant}}^H\widetilde{\mathbf{D}}^H \\ &\quad -\beta\widetilde{\mathbf{D}}\mathbf{T}_{\mathrm{quant}}\mathbf{P}\mathbf{R}_x - \beta\mathbf{R}_x\mathbf{P}^H\mathbf{T}_{\mathrm{quant}}^H\widetilde{\mathbf{D}}^H + \beta^2\mathbf{R}_x\Big) \\ &\quad +\frac{1}{\beta^2}\mathrm{tr}\left(\mathbf{P}\mathbf{R}_x\mathbf{P}^H\boldsymbol{\Delta}\right) + \frac{1}{\beta^2}\mathrm{tr}\left(\widetilde{\mathbf{D}}\mathbf{Q}^H\mathbf{R}_w\mathbf{Q}\widetilde{\mathbf{D}}^H\right), \end{aligned} \tag{5.29}$$

with $\boldsymbol{\Delta} = \mathbb{E}_{\mathbf{T}_{\mathrm{err}}}\left\{\mathbf{T}_{\mathrm{err}}^H\widetilde{\mathbf{D}}^H\widetilde{\mathbf{D}}\mathbf{T}_{\mathrm{err}}\right\} = \sum_{k=1}^{K}\mathbb{E}_{\mathbf{T}_{\mathrm{err}}^{(k)}}\left\{\mathbf{T}_{\mathrm{err}}^{(k)H}\widetilde{\mathbf{D}}^{(k)H}\widetilde{\mathbf{D}}^{(k)}\mathbf{T}_{\mathrm{err}}^{(k)}\right\}$. Note that matrix $\boldsymbol{\Delta}$ depends on the second-order statistics of the error in the equivalent channel matrix $\mathbf{T}_{\mathrm{err}}$. Such statistics can be computed assuming that the second-order statistics of the original quantization error $\bar{\mathbf{R}}_{\mathrm{err}}^{(k)}$ are known and using the analytic study of the error propagation presented in section 5.4. Appendix 5.B describes the procedure to compute matrix $\boldsymbol{\Delta}$ for the particular case where the error matrix $\bar{\mathbf{R}}_{\mathrm{err}}^{(k)}$ is composed of i.i.d. elements and using explicitly the derivation presented in section 5.4. Note that the extension for any correlation of the elements in $\bar{\mathbf{R}}_{\mathrm{err}}^{(k)}$ could be addressed following similar steps as those presented in appendix 5.B.

5.5.2 Robust precoder design

The robust system design can be expressed as the following optimization problem based on the MSE criterion (5.29) and including a constraint on the maximum power P_t available at the transmitter:

$$[\mathbf{P}_{rob}^{\star},\beta_{rob}^{\star}] = \arg\min_{\{\mathbf{P},\beta\}} \quad \mathrm{MSE}(\mathbf{P},\beta) \tag{5.30}$$

$$\text{s.t.:} \quad \mathbb{E}\left\{\|\mathbf{P}\mathbf{x}\|_2^2\right\} = P_t. \tag{5.31}$$

Note that the MSE is not jointly convex in $\mathbf{P}$ and β. However, two necessary conditions arise from the fact that the optimum solution must fulfill that the optimum $\mathbf{P}$ minimizes the MSE for the optimum β subject to the power constraint and at the

same time, the optimum value of β must minimize the MSE for $\mathbf{P}$ equal to its optimum value:

$$\mathbf{P}_{rob}^{\star} = \arg\min_{\mathbf{P}} \quad \mathrm{MSE}(\mathbf{P}, \beta_{rob}^{\star}) \tag{5.32}$$

$$\text{s.t.:} \quad \mathbb{E}\left\{\|\mathbf{P}\mathbf{x}\|_2^2\right\} = P_t. \tag{5.33}$$

and

$$\beta_{rob}^{\star} = \arg\min_{\beta} \quad \mathrm{MSE}(\mathbf{P}_{rob}^{\star}, \beta). \tag{5.34}$$

The problem (5.32)-(5.33) is convex and therefore the optimum solution must satisfy the expression obtained by constructing the Lagrangian function $L(\mathbf{P};\lambda)$ with Lagrange multiplier $\lambda \in \mathbb{R}^+$ and setting its derivatives equal to zero [Boy04]:

$$L(\mathbf{P};\lambda) = \mathbb{E}\left\{\|\mathbf{x} - \beta_{rob}^{\star^{-1}}\widehat{\mathbf{x}}\|_2^2\right\} + \lambda\left(\mathrm{tr}(\mathbf{P}\mathbf{R}_x\mathbf{P}^H) - P_t\right). \tag{5.35}$$

$$\begin{aligned}\nabla_{\mathbf{P}^H} L = &\frac{1}{\beta_{rob}^{\star 2}}\mathbf{T}_{\text{quant}}^H\widetilde{\mathbf{D}}^H\widetilde{\mathbf{D}}\mathbf{T}_{\text{quant}}\mathbf{P}\mathbf{R}_x - \frac{1}{\beta_{rob}^{\star}}\mathbf{T}_{\text{quant}}^H\widetilde{\mathbf{D}}^H\mathbf{R}_x \\ &+\frac{1}{\beta_{rob}^{\star 2}}\mathbf{\Delta}\mathbf{P}\mathbf{R}_x + \lambda\mathbf{P}\mathbf{R}_x = 0.\end{aligned} \tag{5.36}$$

Similarly, the condition (5.34) is convex in β and deriving the MSE with respect to β results in:

$$\begin{aligned}\frac{\partial \mathrm{MSE}(\mathbf{P}_{rob}^{\star},\beta)}{\partial\beta} = &-\frac{2}{\beta^3}\mathrm{tr}\left(\widetilde{\mathbf{D}}\mathbf{T}_{\text{quant}}\mathbf{P}_{rob}^{\star}\mathbf{R}_x\mathbf{P}_{rob}^{\star H}\mathbf{T}_{\text{quant}}^H\widetilde{\mathbf{D}}^H\right) - \frac{2}{\beta^3}\mathrm{tr}\left(\mathbf{P}_{rob}^{\star}\mathbf{R}_x\mathbf{P}_{rob}^{\star H}\mathbf{\Delta}\right) \\ &-\frac{2}{\beta^3}\mathrm{tr}\left(\widetilde{\mathbf{D}}\mathbf{Q}^H\mathbf{R}_w\mathbf{Q}\widetilde{\mathbf{D}}^H\right) + \frac{1}{\beta^2}\mathrm{tr}\left(\widetilde{\mathbf{D}}\mathbf{T}_{\text{quant}}\mathbf{P}_{rob}^{\star}\mathbf{R}_x\right) \\ &+\frac{1}{\beta^2}\mathrm{tr}\left(\mathbf{R}_x\mathbf{P}_{rob}^{\star H}\mathbf{T}_{\text{quant}}^H\widetilde{\mathbf{D}}^H\right) = 0,\end{aligned} \tag{5.37}$$

which, using the fact that $\mathrm{tr}\left(\widetilde{\mathbf{D}}\mathbf{T}_{\text{quant}}\mathbf{P}_{rob}^{\star}\mathbf{R}_x\right) = \mathrm{tr}\left(\mathbf{R}_x\mathbf{P}_{rob}^{\star H}\mathbf{T}_{\text{quant}}^H\widetilde{\mathbf{D}}^H\right)$, results in:

$$\begin{aligned}&-\mathrm{tr}\left(\widetilde{\mathbf{D}}\mathbf{T}_{\text{quant}}\mathbf{P}_{rob}^{\star}\mathbf{R}_x\mathbf{P}_{rob}^{\star H}\mathbf{T}_{\text{quant}}^H\widetilde{\mathbf{D}}^H\right) - \mathrm{tr}\left(\mathbf{P}_{rob}^{\star}\mathbf{R}_x\mathbf{P}_{rob}^{\star H}\mathbf{\Delta}\right) \\ &\qquad - \mathrm{tr}\left(\widetilde{\mathbf{D}}\mathbf{Q}^H\mathbf{R}_w\mathbf{Q}\widetilde{\mathbf{D}}^H\right) + \beta\mathrm{tr}\left(\widetilde{\mathbf{D}}\mathbf{T}_{\text{quant}}\mathbf{P}_{rob}^{\star}\mathbf{R}_x\right) = 0.\end{aligned} \tag{5.38}$$

The following change of variables in now introduced: $\xi = \lambda\beta^2$ and $\mathbf{P} = \beta\widetilde{\mathbf{P}}$. Then (5.38) results in[7]:

$$\xi\beta^2 \mathrm{tr}\left(\widetilde{\mathbf{P}}^{\star}_{rob}\mathbf{R}_x\widetilde{\mathbf{P}}^{\star H}_{rob}\right) - \mathrm{tr}\left(\widetilde{\mathbf{D}}\mathbf{Q}^H\mathbf{R}_w\mathbf{Q}\widetilde{\mathbf{D}}^H\right) = 0 \tag{5.39}$$

$$\Rightarrow \xi^{\star}_{rob} = \frac{\mathrm{tr}\left(\widetilde{\mathbf{D}}\mathbf{Q}^H\mathbf{R}_w\mathbf{Q}\widetilde{\mathbf{D}}^H\right)}{P_t}. \tag{5.40}$$

From (5.36) it follows that:

$$\mathbf{P}^{\star}_{rob} = \beta^{\star}_{rob}\left(\mathbf{T}^H_{\mathrm{quant}}\widetilde{\mathbf{D}}^H\widetilde{\mathbf{D}}\mathbf{T}_{\mathrm{quant}} + \mathbf{\Delta} + \xi^{\star}_{rob}\mathbf{I}\right)^{-1}\mathbf{T}^H_{\mathrm{quant}}\widetilde{\mathbf{D}}^H, \tag{5.41}$$

and from the power constraint $\mathrm{tr}\left(\mathbf{P}\mathbf{R}_x\mathbf{P}^H\right) = P_t$ and (5.41), it follows directly that:

$$\beta^{\star}_{rob} = \sqrt{\frac{P_t}{\mathrm{tr}\left[\left(\mathbf{T}^H_{\mathrm{quant}}\widetilde{\mathbf{D}}^H\widetilde{\mathbf{D}}\mathbf{T}_{\mathrm{quant}} + \mathbf{\Delta} + \xi^{\star}_{rob}\mathbf{I}\right)^{-2}\mathbf{T}^H_{\mathrm{quant}}\widetilde{\mathbf{D}}^H\mathbf{R}_x\widetilde{\mathbf{D}}\mathbf{T}_{\mathrm{quant}}\right]}}. \tag{5.42}$$

Since there is only one solution (up to a phase change) that satisfies the two necessary conditions, (5.32)-(5.33) and (5.34), this solution is the optimum one.

Note that, for the computation of (5.40), an additional parameter associated to the noise power of each user, $\xi^{(k)} = \mathrm{tr}\left(\widetilde{\mathbf{D}}^{(k)}\mathbf{Q}^{(k)H}\mathbf{R}^{(k)}_w\mathbf{Q}^{(k)}\widetilde{\mathbf{D}}^{(k)H}\right)$, has to be fed back to the transmitter. However, this scalar parameter varies very slowly over time and does not imply a relevant increase in the feedback load. From (5.40), it follows that $\xi^{\star}_{rob} = \frac{\sum_{k=1}^{K}\xi^{(k)}}{P_t}$. Observe that, in the case that there is no knowledge of the CSI error at the transmitter, a naive design would assume $\mathbf{\Delta} = 0$, and in this case (5.41)-(5.42) results in a non-robust design which coincides with the optimum non-robust design derived in [Joh02].

5.5.3 Particular case: independent processing per carrier

In the particular case where the decoder matrix of each user $\mathbf{D}^{(k)}$ is constrained to be block diagonal, which is the case for example when joint-processing of the signals

[7] The fact that $\mathrm{tr}\left(\widetilde{\mathbf{D}}\mathbf{T}_{\mathrm{quant}}\widetilde{\mathbf{P}}\mathbf{R}_x\right) = \mathrm{tr}\left(\left(\mathbf{T}^H_{\mathrm{quant}}\widetilde{\mathbf{D}}^H\widetilde{\mathbf{D}}\mathbf{T}_{\mathrm{quant}} + \xi\mathbf{I}\right)\widetilde{\mathbf{P}}\mathbf{R}_x\widetilde{\mathbf{P}}^H\right)$ was used in the derivations.

from different carriers is not possible at the receiver, the optimum solution given by (5.40)-(5.42) is also block diagonal. This means that if the decoder is not capable of processing the signals of different carriers jointly, the optimum precoder does not spread the information symbols across carriers. Consequently, in this particular case, the solution from (5.40)-(5.42) is also valid for the MIMO-OFDM scheme as described in expression (5.2).

5.6 Simulations

This section evaluates numerically the performance of the proposed example of use of the design framework detailed in this chapter. For the simulations, a scenario is considered featuring a transmitter with $n_T = 4$ antennas and $K = 2$ receivers with $n_R^{(k)} = 2, k = 1, 2$, antennas each. The l-th tap of the channel impulse response is generated as $\bar{\mathbf{H}}_l^{(k)} = \sigma_l \mathbf{N}_l^{(k)}$, where σ_l characterizes the power delay profile and $\mathbf{N}_l^{(k)}$ is composed of i.i.d. zero-mean circularly symmetric complex Gaussian entries with unit variance. For the simulations, an exponential decaying power delay profile given by $\sigma_l^2 = ae^{\frac{-l}{\tau}}$ is considered, (where $a = (\sum_{n=0}^{L-1} e^{\frac{-n}{\tau}})^{-1}$) with a normalized delay spread of $\tau = 3$. The simulations are averaged over a sufficiently large number of realizations to obtain stabilized averages. Since the joint optimal design of $\mathbf{P}$ and $\mathbf{D}$ is still an open problem, a decoder matrix $\mathbf{D}$ has to be fixed for the simulations. A simple choice is to set $\mathbf{D}^{(k)} = \mathbf{I}$, as in [Sun09]. Note that this implies that the number of streams is chosen as $n_S^{(k)} = Fn_R^{(k)}$.

5.6.1 Evaluation of the robust precoder

In this subsection the performance of the proposed robust scheme, implemented within the presented feedback framework, is compared numerically with that of the optimum non-robust design from [Joh02]. To show the applicability of the presented framework, both the naive (i.e., non-robust) and the robust versions of BD [Spe04] are also im-

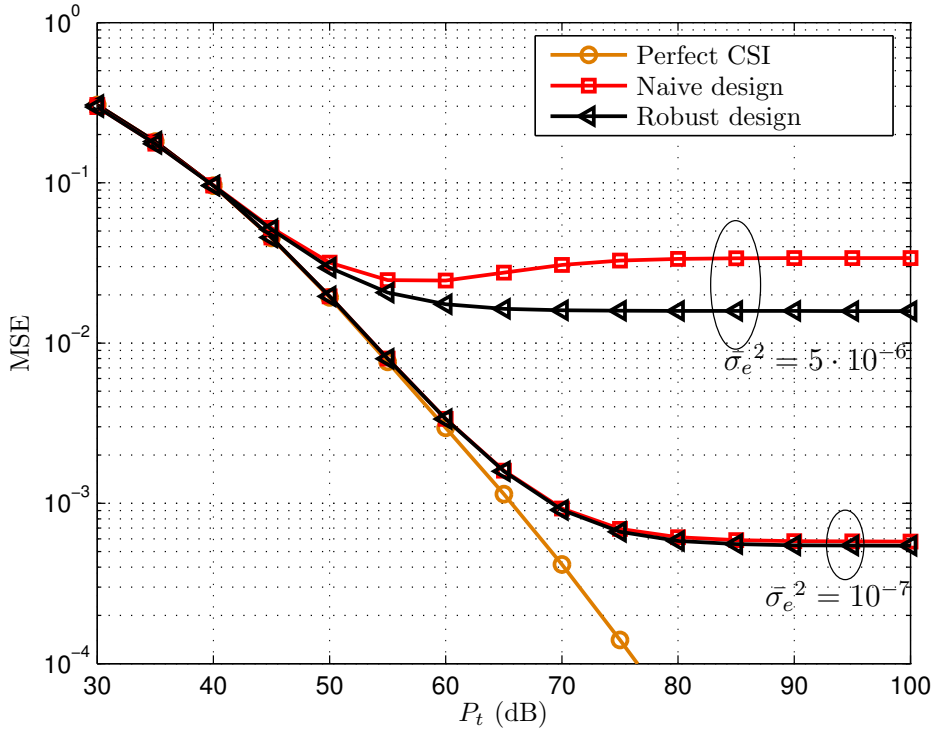

Figure 5.4: MSE vs. total transmission power allocated among all the 128 carriers in a {2,2}x4 system.

plemented and compared, in a setup with $L = 16$ taps and $F = 128$ carriers. For these simulations, the error matrix $\bar{\mathbf{R}}_{\text{err}}^{(k)}$ is assumed to be composed of i.i.d. elements following a Gaussian distribution with zero mean and variance $\bar{\sigma_e}^2$.

Using this setup, Figure 5.4 shows the MSE versus the transmit power P_t for different values of the variance of each element of the error matrix $\bar{\mathbf{R}}_{\text{err}}^{(k)}$. These simulations show that the improvement in terms of MSE of the robust design with respect to the non-robust solution is higher as the error in the quantization and feedback increases. The same conclusion applies to the case when a Symbol Error Rate (SER) cost function is used, as shown in Figure 5.5 for a scenario featuring a QPSK constellation and with 512 symbols transmitted simultaneously.

The framework allows also other design implementations and, as an example, a

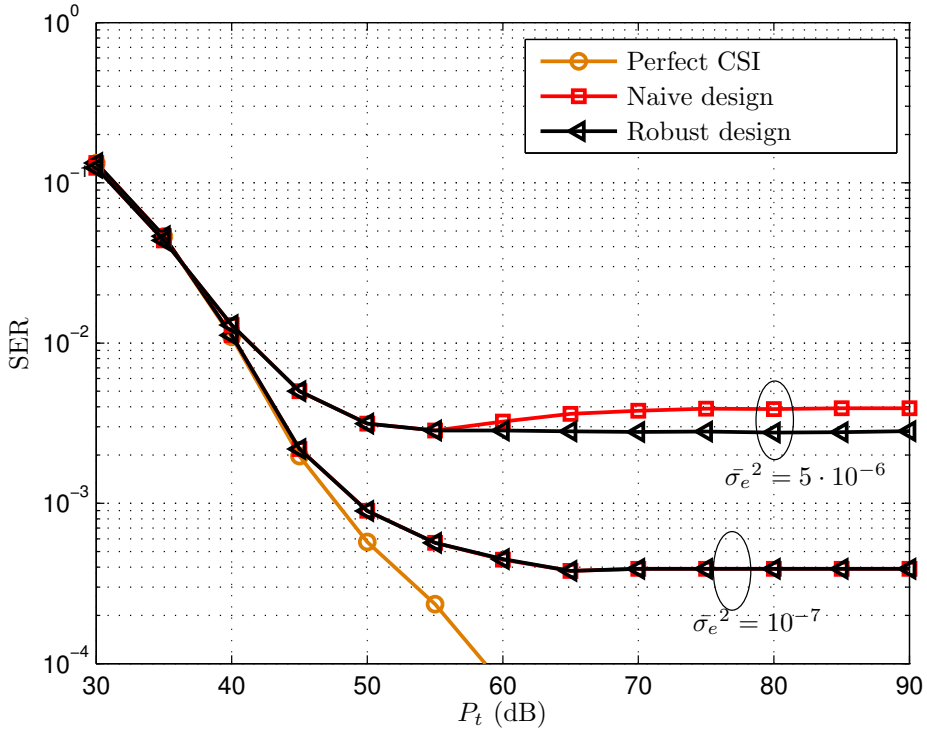

Figure 5.5: SER vs. total transmission power allocated among all the 128 carriers in a {2,2}x4 system.

design based on BD [Spe04] is now considered.[8] Using the feedback and equivalent channel framework, the robust and non-robust BD designs are applied, and the results in the considered scenario are shown in Figure 5.6. Note that this is shown as an example of the applicability of the framework but, if the designs based on BD were to be compared to the non-BD designs, the performance in terms of MSE would be worse for the BD schemes since they spend degrees of freedom to force interference nulling among users.

The performance as a function of the amount of error in the CSI is considered next. Figure 5.7 shows the achievable MSE versus the SNR in the estimation of $\bar{\mathbf{R}}^{(k)}$, defined

[8]The transceiver design is implemented within the proposed framework by applying the BD scheme on top of the equivalent triangular channels presented in section 5.3.

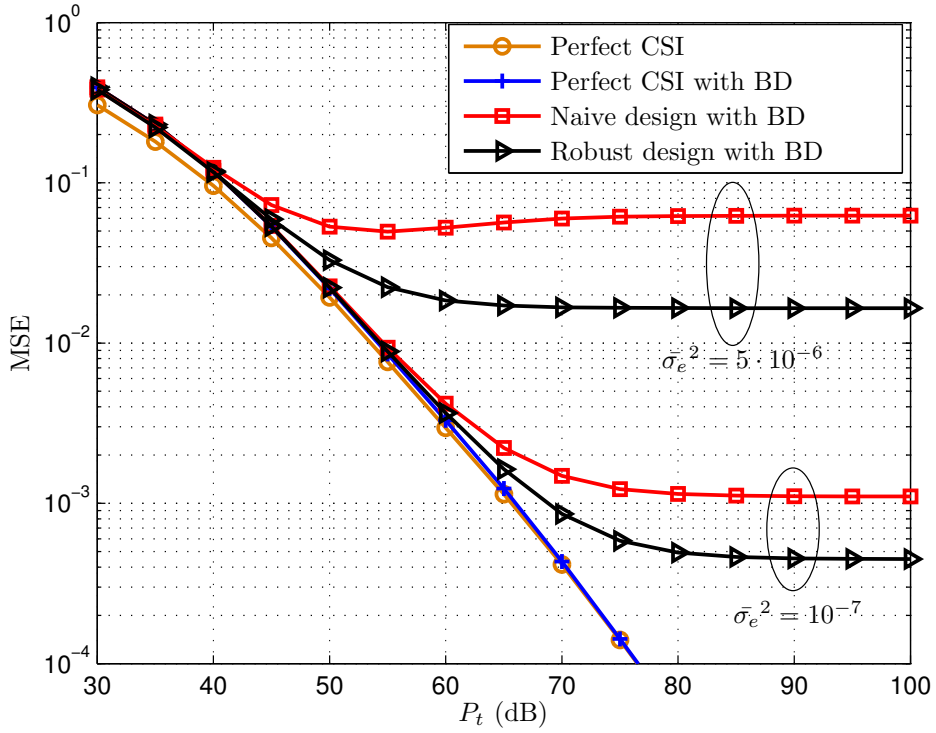

Figure 5.6: MSE vs. total transmission power allocated among all the 128 carriers in a {2,2}x4 system with an implementation of a BD design.

as $\text{SNR}_e = \frac{1}{\bar{\sigma_e}^2}$, for a fixed value of the transmit power $P_t = 60$ dB. The curves show that the robust designs outperform the other precoding techniques when the estimation of $\bar{\mathbf{R}}^{(k)}$ is not very good, i.e., when the SNR_e is low and consequently the error is high, while at high SNR_e the error in the CSI is very small and the curves corresponding to the non-robust techniques converge to the curves corresponding to the robust designs, as expected. The designs based on BD show a small performance loss due to the fact that some degrees of freedom are used to guarantee an interference-free transmission.

5.6.2 Comparison of feedback strategies

A numerical analysis of the performance of the feedback scheme based on the quantization and feedback of one temporal channel Gram matrix $\bar{\mathbf{R}}^{(k)}$ per user (as described

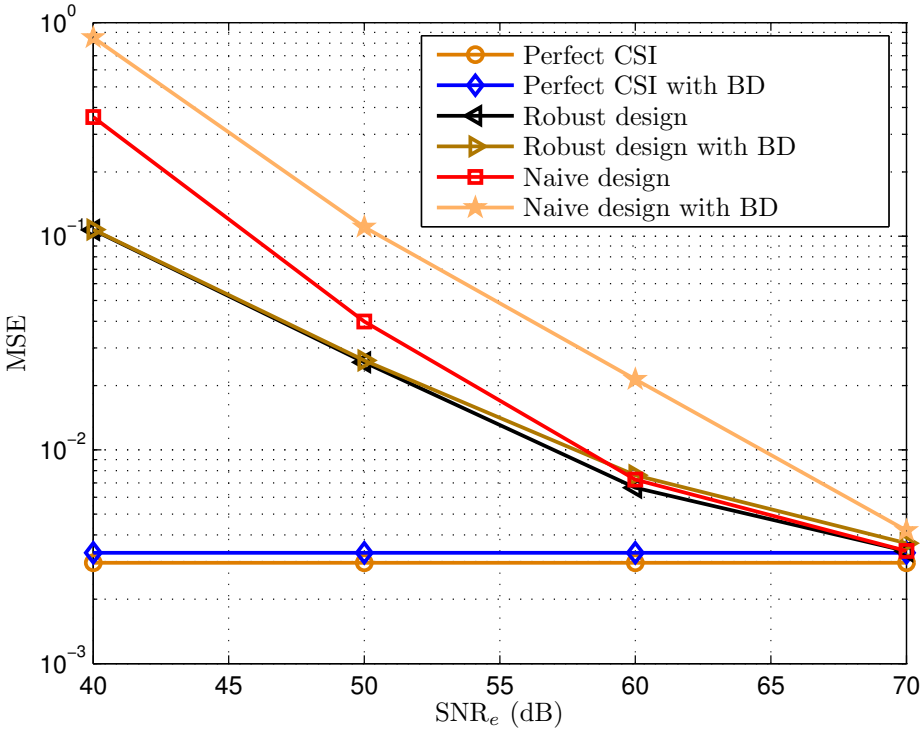

Figure 5.7: MSE vs. SNR$_e$ in a {2,2}x4 system with a total transmission power allocated among all the 128 carriers.

in section 5.3), instead of the usual feedback per carrier per user and the traditional feedback of the complete channel propagation matrix is presented in this subsection. This performance comparison is characterized numerically by constraining the same number of quantization bits for the different approaches in order to obtain a fair evaluation. There are multiple quantization and feedback algorithms that can be used to quantize either $\bar{\mathbf{R}}^{(k)} \in \mathbb{C}^{Ln_T \times Ln_T}$ or the F matrices $\mathbf{R}_f^{(k)} \in \mathbb{C}^{n_T \times n_T}$. Since the focus of this comparison is on the objective of the quantization and not on the algorithm itself, the algorithm from [Cha08] will be taken as a reference[9] for the comparison due to its

[9]The algorithm from [Cha08] used as a reference is based on an individual quantization of the real and imaginary non-repeated elements of the matrix, i.e., in the scheme based on quantization of temporal CSI, $L^2 n_T^2$ real scalar elements have to be quantized, while in the scheme based on quantization of frequency CSI, $F n_T^2$ real scalar elements have to be quantized.

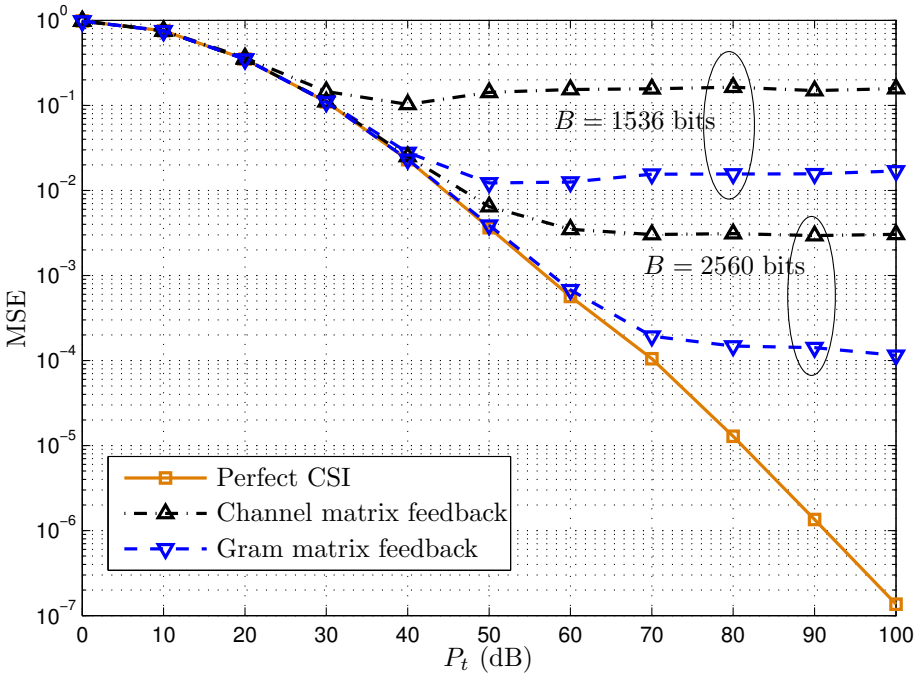

Figure 5.8: Feedback based on the channel Gram matrix vs. feedback based on the complete channel response matrix, for different values of the feedback overhead in number of bits.

simplicity. The performance of a system using both the quantization of $\bar{\mathbf{R}}^{(k)}$ and the quantization of the F matrices $\mathbf{R}_f^{(k)}$ and featuring the same number of feedback bits for both cases will be shown next.

First, a comparison of the feedback based on the channel Gram matrix versus the feedback of the complete channel response matrix is presented in Figure 5.8. A scenario with $L = 16$ taps and $F = 16$ carriers is considered, and the results are shown for different values of the feedback overhead in number of bits. It can be observed that the feedback of the Gram matrix provides a lower MSE than the technique based on direct quantization of the channel response matrix, for the cases of $B = 1536$ and $B = 2560$ total feedback bits.

Next, Figure 5.9 shows a comparison of the performance using feedback of the

time domain CSI versus feedback of the frequency domain CSI in a scenario with $L = 8$ taps and $F = 128$ carriers, for different values of the feedback load in terms of number of bits. The transmit power P_t is spread over all 128 carriers and all 4 antennas, and 512 QPSK symbols are transmitted simultaneously. First, the scenario with $B = 12288$ bits of feedback is considered. This means that each of the 1024 real and scalar parameters that have to be fed back in the time domain CSI feedback is quantized using 12 bits, while each of the 2048 parameters corresponding to the frequency domain CSI feedback case is quantized using 6 bits. The figure also shows the results of simulations featuring 14336 bits per feedback update (which corresponds to 14 bits for the quantization of each element in the scheme based on time domain CSI and 7 bits for each element in the scheme based on frequency domain CSI). These curves show that, for this specific setup, the quantization and feedback of matrix $\bar{\mathbf{R}}^{(k)}$ (which is based on the time domain CSI) provides a lower SER than the quantization and feedback of $\mathbf{R}_f^{(k)}$ (which is based on frequency domain CSI) when using the same feedback algorithm. This is due to the fact that, in the case of time domain CSI feedback, the number of parameters to be quantized is half the number of parameters to be quantized using the same number of bits in the case of frequency domain CSI feedback. A different scenario with $L = 8$ taps and $F = 64$ carriers is considered next, and the simulations are shown in Figure 5.10. In such scenario, with $F = 64$ carriers instead of the 128 carriers considered in Figure 5.9, the number of elements to be quantized is higher in the time domain CSI feedback than in the frequency domain CSI feedback and the later shows better performance.

From this it can be concluded that the choice of the most adequate feedback scheme (either feedback of the time domain CSI or feedback of the frequency domain CSI) depends on the number of taps of the temporal channel response and the number of carriers, and this should be taken into consideration at the system design stage. Note that the trend in wireless communication systems is to increase the number of carriers (WiMAX for example supports up to 1728 usable carriers [iee05]), which implies that

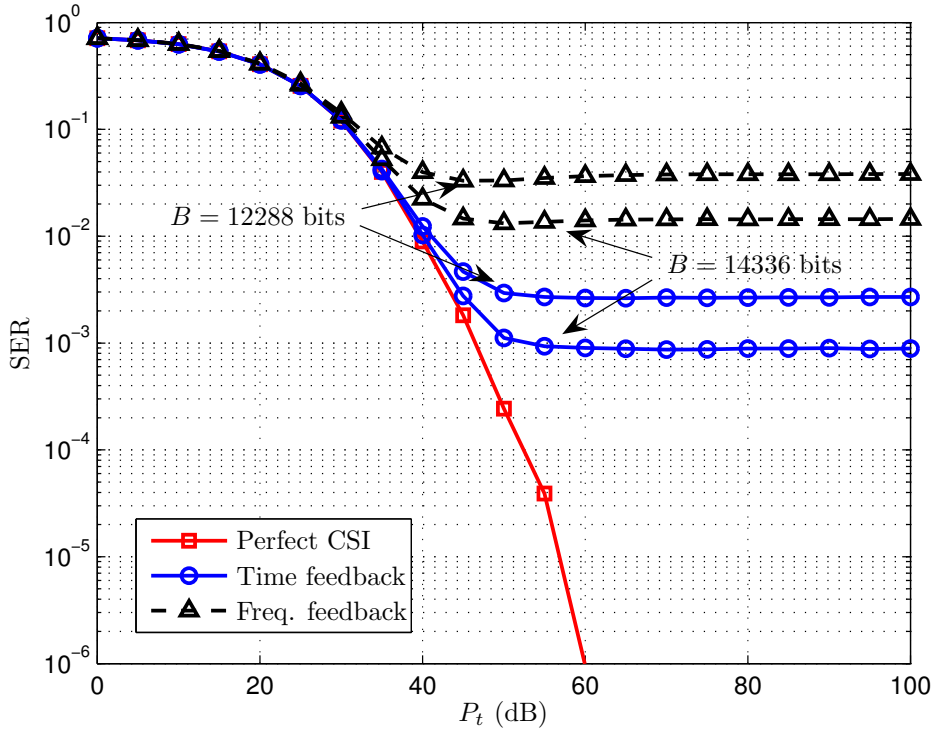

Figure 5.9: Feedback of the frequency domain CSI vs. feedback of the time domain CSI in a system with 128 carriers.

for such standard the feedback of the time domain CSI provides better performance.

5.7 Chapter summary and conclusions

This chapter has presented a framework for the design of multiuser MIMO-OFDM BC systems with CSI feedback. The proposed framework is based on the computation of an equivalent triangular channel response matrix, and enables the use of efficient CSI feedback techniques based on the quantization of the Gram matrix of the temporal response of the channels. This scheme is valid for and can be applied to any given design quality criterion. An analytical study of the propagation of CSI quantization error through the channel Gram matrix computation and the posterior equivalent channel

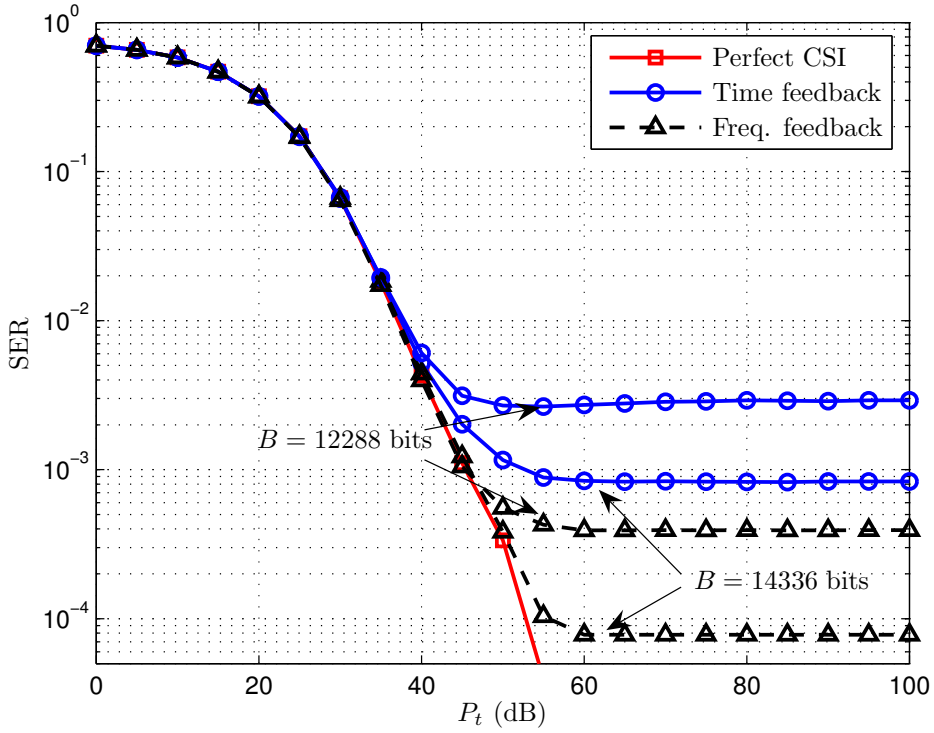

Figure 5.10: Feedback of the frequency domain CSI vs. feedback of the time domain CSI in a system with 64 carriers.

response matrix computation has also been presented. As an illustrative example of the potential of this framework for transceiver designs, the case of MSE minimization has been considered and a closed form expression for a robust space-frequency linear precoding design has been derived. Numerical simulations have revealed the advantages of the proposed feedback scheme and also of the MSE minimization precoding technique compared to other feedback techniques and to the non-robust counterpart precoding designs for different scenarios.

5.A CSI error propagation through the computation of the equivalent channel

In the neighborhood of $\mathbf{R}_f^{(k)}$ the errors $\mathbf{R}_{\mathrm{err}_f}^{(k)}$ and $\mathbf{T}_{\mathrm{err}_f}^{(k)}$ can be approximated by the differentials, $\mathrm{d}\mathbf{R}_f^{(k)}$ and $\mathrm{d}\mathbf{T}_f^{(k)}$, respectively. From (5.24), it readily follows:

$$\mathrm{d}\mathbf{R}_f^{(k)} = \mathrm{d}\mathbf{T}_f^{(k)H}\mathbf{T}_f^{(k)} + \mathbf{T}_f^{(k)H}\,\mathrm{d}\mathbf{T}_f^{(k)}. \tag{5.43}$$

By separating the real and imaginary parts of the individual matrices, $\mathbf{R}_{f_r}^{(k)} = \Re\mathrm{e}(\mathbf{R}_f^{(k)})$, $\mathbf{R}_{f_i}^{(k)} = \Im\mathrm{m}(\mathbf{R}_f^{(k)})$, $\mathbf{T}_{f_r}^{(k)} = \Re\mathrm{e}(\mathbf{T}_f^{(k)})$, $\mathbf{T}_{f_i}^{(k)} = \Im\mathrm{m}(\mathbf{T}_f^{(k)})$, and defining $\mathrm{d}\mathbf{R}_f^{(k)} = \mathrm{d}\mathbf{R}_{f_r}^{(k)} + j\,\mathrm{d}\mathbf{R}_{f_i}^{(k)}$ and $\mathrm{d}\mathbf{T}_f^{(k)} = \mathrm{d}\mathbf{T}_{f_r}^{(k)} + j\,\mathrm{d}\mathbf{T}_{f_i}^{(k)}$, it follows:

$$\mathrm{d}\mathbf{R}_{f_r}^{(k)} = \mathrm{d}\mathbf{T}_{f_r}^{(k)T}\mathbf{T}_{f_r}^{(k)} + \mathrm{d}\mathbf{T}_{f_i}^{(k)T}\mathbf{T}_{f_i}^{(k)} + \mathbf{T}_{f_r}^{(k)T}\,\mathrm{d}\mathbf{T}_{f_r}^{(k)} + \mathbf{T}_{f_i}^{(k)T}\,\mathrm{d}\mathbf{T}_{f_i}^{(k)}, \tag{5.44}$$

$$\mathrm{d}\mathbf{R}_{f_i}^{(k)} = \mathrm{d}\mathbf{T}_{f_r}^{(k)T}\mathbf{T}_{f_i}^{(k)} - \mathrm{d}\mathbf{T}_{f_i}^{(k)T}\mathbf{T}_{f_r}^{(k)} + \mathbf{T}_{f_r}^{(k)T}\,\mathrm{d}\mathbf{T}_{f_i}^{(k)} - \mathbf{T}_{f_i}^{(k)T}\,\mathrm{d}\mathbf{T}_{f_r}^{(k)}. \tag{5.45}$$

The following facts are considered in the derivations:

1. From the fact that $\mathbf{T}_f^{(k)}$ is upper triangular with real and positive elements in the main diagonal, it follows that $\mathrm{d}\mathbf{T}_{f_i}^{(k)}$ is strictly upper triangular. Thus, the only non-zero elements of $\mathrm{d}\mathbf{T}_{f_r}^{(k)}$ and $\mathrm{d}\mathbf{T}_{f_i}^{(k)}$ are contained in the vectors $\mathsf{vech}(\mathrm{d}\mathbf{T}_{f_r}^{(k)^T})$ and $\mathsf{veci}(\mathrm{d}\mathbf{T}_{f_i}^{(k)^T})$.

2. From (5.44), it follows that $\mathrm{d}\mathbf{R}_{f_r}^{(k)}$ is symmetric. Thus, its non-repeated elements are contained in the vector $\mathsf{vech}(\mathrm{d}\mathbf{R}_{f_r}^{(k)})$.

3. From (5.45), it follows that $\mathrm{d}\mathbf{R}_{f_i}^{(k)}$ is anti-symmetric. Thus, it has zeros in the main diagonal and all its non-repeated elements (up to a change of sign) are contained in the vector $\mathsf{veci}(\mathrm{d}\mathbf{R}_{f_i}^{(k)})$.

Consequently, from all what has been mentioned above, in order to compute the derivative of $\mathbf{T}_f^{(k)}$ with respect to $\mathbf{R}_f^{(k)}$, the objective is to linearly relate the elements of $\mathsf{vech}(\mathrm{d}\mathbf{T}_{f_r}^{(k)^T})$ and $\mathsf{veci}(\mathrm{d}\mathbf{T}_{f_i}^{(k)^T})$ to those of $\mathsf{vech}(\mathrm{d}\mathbf{R}_{f_r}^{(k)})$ and $\mathsf{veci}(\mathrm{d}\mathbf{R}_{f_i}^{(k)})$ and apply the first identification theorem [Mag02].

By applying vech at both sides in (5.44), it follows that[10]:

$$\mathsf{vech}(\mathrm{d}\mathbf{R}_{f_r}^{(k)}) = \mathsf{vech}\left(\mathrm{d}\mathbf{T}_{f_r}^{(k)^T}\mathbf{T}_{f_r}^{(k)} + \mathrm{d}\mathbf{T}_{f_i}^{(k)^T}\mathbf{T}_{f_i}^{(k)} + \mathbf{T}_{f_r}^{(k)^T}\mathrm{d}\mathbf{T}_{f_r}^{(k)} + \mathbf{T}_{f_i}^{(k)^T}\mathrm{d}\mathbf{T}_{f_i}^{(k)}\right) \tag{5.46}$$

$$= \mathbf{D}_{n_T}^{+}\mathsf{vec}\left(\mathrm{d}\mathbf{T}_{f_r}^{(k)^T}\mathbf{T}_{f_r}^{(k)} + \mathrm{d}\mathbf{T}_{f_i}^{(k)^T}\mathbf{T}_{f_i}^{(k)} + \mathbf{T}_{f_r}^{(k)^T}\mathrm{d}\mathbf{T}_{f_r}^{(k)} + \mathbf{T}_{f_i}^{(k)^T}\mathrm{d}\mathbf{T}_{f_i}^{(k)}\right) \tag{5.47}$$

$$\begin{aligned} = 2\mathbf{D}_{n_T}^{+}\Big(&\left(\mathbf{T}_{f_r}^{(k)^T}\otimes\mathbf{I}_{n_T}\right)\mathbf{V}_{n_T,n_R^{(k)}}\mathsf{vech}\left(\mathrm{d}\mathbf{T}_{f_r}^{(k)^T}\right) \\ &+\left(\mathbf{T}_{f_i}^{(k)^T}\otimes\mathbf{I}_{n_T}\right)\mathbf{V}^{S}_{n_T,n_R^{(k)}}\mathsf{veci}\left(\mathrm{d}\mathbf{T}_{f_i}^{(k)^T}\right)\Big). \end{aligned} \tag{5.48}$$

Now, applying veci at both sides in (5.45), and operating similarly as before, it follows that:

$$\mathsf{veci}(\mathrm{d}\mathbf{R}_{f_i}^{(k)}) = \mathsf{veci}\left(\mathrm{d}\mathbf{T}_{f_r}^{(k)^T}\mathbf{T}_{f_i}^{(k)} + \mathrm{d}\mathbf{T}_{f_i}^{(k)^T}\mathbf{T}_{f_r}^{(k)} + \mathbf{T}_{f_r}^{(k)^T}\mathrm{d}\mathbf{T}_{f_i}^{(k)} + \mathbf{T}_{f_i}^{(k)^T}\mathrm{d}\mathbf{T}_{f_r}^{(k)}\right) \tag{5.49}$$

$$\begin{aligned} = 2\mathbf{C}_{n_T}^{+}\Big(&\left(\mathbf{T}_{f_i}^{(k)^T}\otimes\mathbf{I}_{n_T}\right)\mathbf{V}_{n_T,n_R^{(k)}}\mathsf{vech}\left(\mathrm{d}\mathbf{T}_{f_r}^{(k)^T}\right) \\ &-\left(\mathbf{T}_{f_r}^{(k)^T}\otimes\mathbf{I}_{n_T}\right)\mathbf{V}^{S}_{n_T,n_R^{(k)}}\mathsf{veci}\left(\mathrm{d}\mathbf{T}_{f_i}^{(k)^T}\right)\Big). \end{aligned} \tag{5.50}$$

Now, defining

$$\mathbf{t}_f^{(k)} \triangleq \widetilde{\mathsf{vec}}\left(\mathbf{T}_f^{(k)^T}\right), \quad \mathrm{d}\mathbf{t}_f^{(k)} \triangleq \widetilde{\mathsf{vec}}\left(\mathrm{d}\mathbf{T}_f^{(k)^T}\right), \tag{5.51}$$

$$\mathbf{r}_f^{(k)} \triangleq \widetilde{\mathsf{vec}}\left(\mathbf{R}_f^{(k)}\right), \quad \mathrm{d}\mathbf{r}_f^{(k)} \triangleq \widetilde{\mathsf{vec}}\left(\mathrm{d}\mathbf{R}_f^{(k)}\right), \tag{5.52}$$

from (5.48) and (5.50), it follows that

$$\mathrm{d}\mathbf{r}_f^{(k)} = 2\begin{bmatrix} \mathbf{D}_{n_T}^{+}\left(\mathbf{T}_{f_r}^{(k)^T}\otimes\mathbf{I}_{n_T}\right)\mathbf{V}_{n_T,n_R^{(k)}} & \mathbf{D}_{n_T}^{+}\left(\mathbf{T}_{f_i}^{(k)^T}\otimes\mathbf{I}_{n_T}\right)\mathbf{V}^{S}_{n_T,n_R^{(k)}} \\ \mathbf{C}_{n_T}^{+}\left(\mathbf{T}_{f_i}^{(k)^T}\otimes\mathbf{I}_{n_T}\right)\mathbf{V}_{n_T,n_R^{(k)}} & -\mathbf{C}_{n_T}^{+}\left(\mathbf{T}_{f_r}^{(k)^T}\otimes\mathbf{I}_{n_T}\right)\mathbf{V}^{S}_{n_T,n_R^{(k)}} \end{bmatrix}\mathrm{d}\mathbf{t}_f^{(k)}. \tag{5.53}$$

It only remains to take the pseudo-inverse in the last equation to obtain the desired

[10]The following matrices are used in the developments: the triangularization matrix $\mathbf{V}_{n,m}$, which is the unique matrix of the appropriate dimensions such that, for all lower triangular $\mathbf{X} \in \mathbb{R}^{n\times m}$, satisfies that $\mathsf{vec}(\mathbf{X}) = \mathbf{V}_{n,m}\mathsf{vech}(\mathbf{X})$, and the strict triangularization matrix $\mathbf{V}^S_{n,m}$, which is the unique matrix of the appropriate dimensions such that, for all strictly lower triangular $\mathbf{X} \in \mathbb{R}^{n\times m}$, satisfies that $\mathsf{vec}(\mathbf{X}) = \mathbf{V}^S_{n,m}\mathsf{vech}(\mathbf{X})$.

Jacobian matrix:

$$\mathsf{D}_{\mathbf{r}_f^{(k)}}\mathbf{t}_f^{(k)} = \frac{1}{2}\begin{bmatrix} \mathbf{D}_{n_T}^{+}\left(\mathbf{T}_{f_r}^{(k)^T}\otimes\mathbf{I}_{n_T}\right)\mathbf{V}_{n_T,n_R^{(k)}} & \mathbf{D}_{n_T}^{+}\left(\mathbf{T}_{f_i}^{(k)^T}\otimes\mathbf{I}_{n_T}\right)\mathbf{V}^S_{n_T,n_R^{(k)}} \\ \mathbf{C}_{n_T}^{+}\left(\mathbf{T}_{f_i}^{(k)^T}\otimes\mathbf{I}_{n_T}\right)\mathbf{V}_{n_T,n_R^{(k)}} & -\mathbf{C}_{n_T}^{+}\left(\mathbf{T}_{f_r}^{(k)^T}\otimes\mathbf{I}_{n_T}\right)\mathbf{V}^S_{n_T,n_R^{(k)}} \end{bmatrix}^{+}. \tag{5.54}$$

Consequently, matrix $\mathbf{T}_{\mathrm{err}_f}^{(k)}$ can be computed as a function of $\mathbf{R}_{\mathrm{err}_f}^{(k)}$ as:

$$\widetilde{\mathsf{vec}}\left(\mathbf{T}_{\mathrm{err}_f}^{(k)^T}\right) \simeq \mathsf{D}_{\mathbf{r}_f^{(k)}}\mathbf{t}_f^{(k)}\widetilde{\mathsf{vec}}\left(\mathbf{R}_{\mathrm{err}_f}^{(k)}\right). \tag{5.55}$$

5.A.1 Element-wise propagation error vector

This subsection presents an expression of the total error propagation following (5.27) using element-wise notation. The i-th row of matrix $\mathbf{X}_f^{(k)}$ is denoted as $\mathbf{x}_{f_{(i)}}^{(k)}$. The element n, r of the error matrix $\mathbf{T}_{\mathrm{err}\,f}^{(k)} \in \mathbb{C}^{n_R^{(k)}\times n_T}$ is denoted by $t_{\mathrm{err}\,f_{(n,r)}}^{(k)}$ and can be computed as:

$$\Re\mathrm{e}(t_{\mathrm{err}\,f_{(n,r)}}^{(k)}) \approx \begin{cases} \mathbf{a}_{f_{(n,r)}}^{(k)}\bar{\mathbf{r}}_{err}^{(k)}, & \forall n \le r, \\ 0 & \forall n > r, \end{cases} \tag{5.56}$$

$$\Im\mathrm{m}(t_{\mathrm{err}\,f_{(n,r)}}^{(k)}) \approx \begin{cases} \mathbf{b}_{f_{(n,r)}}^{(k)}\bar{\mathbf{r}}_{err}^{(k)}, & \forall n < r, \\ 0 & \forall n \ge r, \end{cases} \tag{5.57}$$

where vectors $\mathbf{a}_{f_{(n,r)}}^{(k)}$ and $\mathbf{b}_{f_{(n,r)}}^{(k)}$ are defined as follows considering 2 cases based on the antenna topology:

a) $n_R^{(k)} \ge n_T$

In this case, $\widetilde{\mathsf{vec}}\left(\mathbf{T}_{\mathrm{err}_f}^{(k)^T}\right) \in \mathbb{R}^{n_T^2\times 1}$ and $\mathbf{X}_f^{(k)} \in \mathbb{C}^{n_T^2\times L^2 n_T^2}$. Because of this matrix structure, the following expressions result:

$$\mathbf{a}_{f_{(n,r)}}^{(k)} = \mathbf{x}_{f_{\left(\substack{r+n_T(n-1)-\sum^n{}_{x=1}^{x\neq n\,x\neq n-1}\ x}\right)}}^{(k)} \tag{5.58}$$

and

$$\mathbf{b}_{f_{(n,r)}}^{(k)} = \mathbf{x}_{f_{\left(\frac{n_T(n_T+1)}{2}+n_T(n-1)-\frac{n(n-1)}{2}+r\right)}}^{(k)}. \tag{5.59}$$

b) $n_R^{(k)} < n_T$

In this case, $\widetilde{\mathsf{vec}}\left(\mathbf{T}_{\mathrm{err}_f}^{(k)\,T}\right) \in \mathbb{R}^{n_R^{(k)}\left(2n_T-n_R^{(k)}\right)\times 1}$ and $\mathbf{X}_f^{(k)} \in \mathbb{C}^{n_R^{(k)}\left(2n_T-n_R^{(k)}\right)\times L^2 n_T^2}$. This results in

$$\mathbf{a}_{f_{(n,r)}}^{(k)} = \mathbf{x}_f^{(k)\left(\begin{smallmatrix} r+n_T(n-1)-\sum_{x=1}^{n} x \\ x\neq n \\ x\neq n-1 \end{smallmatrix}\right)} \tag{5.60}$$

and

$$\mathbf{b}_{f_{(n,r)}}^{(k)} = \mathbf{x}_f^{(k)\left(\frac{n_R^{(k)}(n_R^{(k)}+1)}{2}+(n_T-n_R^{(k)})n_R^{(k)}+n_T(n-1)-\frac{n(n-1)}{2}+r\right)}. \tag{5.61}$$

5.B Computation of matrix $\mathbf{\Delta}$

From (5.29), the element i,j of matrix $\mathbf{\Delta} \in \mathbb{C}^{Fn_T\times Fn_T}$ can be computed as:

$$\begin{aligned}\mathbf{\Delta}_{(i,j)} &= \sum_{k=1}^{K} \mathbb{E}_{\mathbf{T}_{\mathrm{err}}^{(k)}}\left\{\mathbf{t}_{\mathrm{err}_i}^{(k)\,H}\widetilde{\mathbf{D}}^{(k)H}\widetilde{\mathbf{D}}^{(k)}\mathbf{t}_{\mathrm{err}_j}^{(k)}\right\} = \sum_{k=1}^{K} \mathbb{E}_{\mathbf{T}_{\mathrm{err}}^{(k)}}\left\{\mathrm{tr}\left(\mathbf{t}_{\mathrm{err}_i}^{(k)\,H}\widetilde{\mathbf{D}}^{(k)H}\widetilde{\mathbf{D}}^{(k)}\mathbf{t}_{\mathrm{err}_j}^{(k)}\right)\right\} \\ &= \sum_{k=1}^{K} \mathrm{tr}\left(\widetilde{\mathbf{D}}^{(k)H}\widetilde{\mathbf{D}}^{(k)}\mathbb{E}_{\mathbf{T}_{\mathrm{err}}^{(k)}}\left\{\mathbf{t}_{\mathrm{err}_j}^{(k)}\mathbf{t}_{\mathrm{err}_i}^{(k)\,H}\right\}\right),\end{aligned} \tag{5.62}$$

where $\mathbf{t}_{\mathrm{err}_j}^{(k)}$ is the j-th column of matrix $\mathbf{T}_{\mathrm{err}}^{(k)}$.

For simplicity with the notation, the elements of $\mathbf{\Delta} \in \mathbb{C}^{Fn_T\times Fn_T}$ will be denoted as $\mathbf{\Delta}_{(n_Tf+n,n_Tg+m)}$, where $f,g \in \{0,...,F-1\}$ and $n,m \in \{1,...,n_T\}$. Using this notation, (5.62) can be expressed as:

$$\mathbf{\Delta}_{(n_Tf+n,n_Tg+m)} = \sum_{k=1}^{K} \mathrm{tr}\left(\widetilde{\mathbf{D}}^{(k)H}\widetilde{\mathbf{D}}^{(k)}\mathbb{E}\left\{\mathbf{t}_{\mathrm{err}_{n_Tg+m}}^{(k)}\mathbf{t}_{\mathrm{err}_{n_Tf+n}}^{(k)\,H}\right\}\right) \tag{5.63}$$

$$= \sum_{k=1}^{K}\sum_{x=1}^{n_R^{(k)}}\sum_{r=1}^{n_R^{(k)}} \bar{d}_{(n_R^{(k)}f+x,n_R^{(k)}g+r)}^{(k)}\mathbb{E}\left\{t_{\mathrm{err}_{g(r,m)}}^{(k)}t_{\mathrm{err}_{f(x,n)}}^{(k)*}\right\}, \tag{5.64}$$

where $t_{\mathrm{err}_{f_{(i,j)}}}^{(k)}$ is the element i,j of matrix $\mathbf{T}_{\mathrm{err}\,f}^{(k)}$ (see appendix 5.A.1 for the expression of $t_{\mathrm{err}_{f_{(i,j)}}}^{(k)}$ in the cases of $n_R^{(k)} \geq n_T$ and $n_R^{(k)} < n_T$, respectively) and $\bar{d}_{(i,j)}^{(k)}$ is the element i,j of matrix $\widetilde{\mathbf{D}}^{(k)H}\widetilde{\mathbf{D}}^{(k)}$. Note that some of the elements of the summation in (5.64)

are zero due to the fact that matrix $\mathbf{T}_{\mathrm{err}_f}^{(k)}$ is upper triangular. Expression (5.64) can be manipulated further to write it as a function of $\mathbb{E}\left\{\bar{\mathbf{r}}_{err}^{(k)}\bar{\mathbf{r}}_{err}^{(k)^T}\right\}$, the variance of the error introduced in the quantization of the temporal Gram matrix:

$$\begin{aligned}\boldsymbol{\Delta}_{(n_T f+n,n_T g+m)} \simeq \sum_{k=1}^{K}\sum_{x=1}^{n_R^{(k)}}\sum_{r=1}^{n_R^{(k)}} \bar{d}^{(k)}_{\left(n_R^{(k)}f+x,n_R^{(k)}g+r\right)}\left(\mathbf{a}^{(k)}_{g_{(r,m)}}+j\mathbf{b}^{(k)}_{g_{(r,m)}}\right)\\ \cdot\mathbb{E}\left\{\bar{\mathbf{r}}_{err}^{(k)}\bar{\mathbf{r}}_{err}^{(k)^T}\right\}\left(\mathbf{a}^{(k)^T}_{f_{(x,n)}}-j\mathbf{b}^{(k)^T}_{f_{(x,n)}}\right).\end{aligned} \tag{5.65}$$

In the particular case when the error in the CSI at the transmitter, $\bar{\mathbf{R}}_{\mathrm{err}}^{(k)}$, is composed of i.i.d. elements with zero mean and variance $\bar{\sigma}^{(k)^2}$, it follows that

$$\mathbb{E}\left\{\bar{\mathbf{r}}_{err}^{(k)}\bar{\mathbf{r}}_{err}^{(k)^T}\right\} = \bar{\sigma}^{(k)^2}\mathbf{I} \tag{5.66}$$

and (5.65) results in:

$$\begin{aligned}\boldsymbol{\Delta}_{(n_T f+n,n_T g+m)} \simeq \sum_{k=1}^{K}\sum_{x=1}^{n_R^{(k)}}\sum_{r=1}^{n_R^{(k)}} \bar{\sigma}^{(k)^2}\bar{d}^{(k)}_{\left(n_R^{(k)}f+x,n_R^{(k)}g+r\right)}\left(\mathbf{a}^{(k)}_{g_{(r,m)}}+j\mathbf{b}^{(k)}_{g_{(r,m)}}\right)\\ \cdot\left(\mathbf{a}^{(k)^T}_{f_{(x,n)}}-j\mathbf{b}^{(k)^T}_{f_{(x,n)}}\right).\end{aligned} \tag{5.67}$$

Chapter 6

Resource allocation between feedback and forward links: analysis and optimization

6.1 Introduction

The performance analysis in MIMO wireless systems with feedback is usually evaluated without taking into account the cost of using such feedback. If this cost is taken into account explicitly it turns out that, while using a large amount of feedback improves the quality of the CSI available at the transmitter, it is not optimum from a perspective of system performance since the remaining radio resources available for the data link are lower. This is because the differential gain obtained by each additional feedback bit is a decreasing function and, eventually, it becomes lower than the cost of dedicating an additional bit to feedback. In this chapter this tradeoff is presented for Time Division Duplex (TDD) and Frequency Division Duplex (FDD) MIMO systems and it is shown that using low feedback rate is better than not using feedback at all and also better than using large amounts of feedback.

The topic of feedback sizing is introduced in [Kob08], which studies the resource allocation tradeoff for the case of the BC with zero-forcing beamforming and assuming a block fading channel model and analog feedback, where each receiver sends through the feedback link a scaled version of its channel Minimum Mean Square Error (MMSE) estimate using unquantized amplitude modulation. A similar analysis is conducted in [AY09] for the case of FDD, however, only a full duplex communication scheme is considered and a block fading model is assumed instead of the time variant model considered in this dissertation. Furthermore, in [AY09] CSI symmetry is necessary, while in the work presented in this thesis it is not required.

The chapter presents a detailed analysis of the tradeoff in a scenario that features a data transmission phase, a feedback transmission phase, and a training phase, which relates to the accuracy of the CSI at the receiver prior to its quantization and feedback. Additionally, the effect produced by a delay in the acquisition of the CSI at the transmitter is also taken into account.

Summarizing, the main contributions of this chapter can be listed as follows:

1. This chapter presents a general formulation of the mentioned tradeoff taking into account all the parameters associated to the radio resource allocation, which are training and CSI estimation, CSI quantization, feedback transmission, CSI delay, and data transmission.

2. An optimization problem is presented in order to determine the optimum radio resource allocation in terms of power and duration associated to the training, feedback, and data transmission phases.

3. The general optimization problem is solved for a number of particular cases.

The remainder of this chapter is organized as follows. First, the simplified performance expression of the duplexing schemes are introduced in 6.2 under the assumption of perfect CSI at the receiver. A more complex scenario that includes a training phase,

channel estimation errors, and CSI delay is then introduced in section 6.3, and the corresponding system model is described in section 6.4. The resource allocation problem is expressed analytically in section 6.5, and numerical simulations are shown in section 6.7. Finally, section 6.8 summarizes the results and concludes the chapter.

6.2 TDD and FDD systems

In systems where different information streams share the same physical communications link, the available link resources have to be distributed. This means that the data and feedback information share the same pool of radio resources. From this point of view, two duplexing schemes can be considered: dividing the time axis in different time slots and assigning each slot to the transmission of either data or feedback information (TDD), and dividing the frequency axis in different frequency bands, corresponding to feedback or data transmission (FDD). For the equations describing these schemes the following notation is used:

- W_t: total available bandwidth.
- W_d: bandwidth dedicated to transmission of data.
- $W_f = W_t - W_d$: bandwidth dedicated to transmission of feedback.
- T_t: total duration of a time frame.
- T_d: time dedicated to transmission of data.
- $T_f = T_t - T_d$: time dedicated to transmission of feedback.
- E_t: total available energy for the transmission of data.
- N_0: noise power spectral density (AWGN).
- R_d: rate at which data can be transmitted.

- $\mathbf{H} \in \mathbb{C}^{n_R \times n_T}$: flat fading MIMO channel with n_T and n_R transmit and receive antennas, respectively.

- $\mathbf{B}(n) \in \mathbb{C}^{n_T \times n_S}$: linear transmitter matrix that satisfies $\|\mathbf{B}(n)\|_F^2 \leq 1$.

Frequency-division duplex (FDD):

The FDD scheme features continuous transmission of data and feedback simultaneously, by dividing the total bandwidth available W_t between the data and the feedback links, as depicted in Figure 6.1.

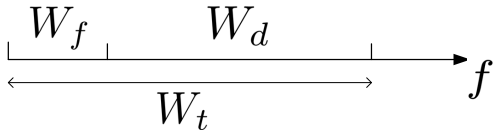

Figure 6.1: FDD system model.

In such a system, the maximum achievable data rate is given by the following expression:

$$R_d = W_d \mathsf{log}_2 \mathsf{det}\left(\mathbf{I} + \frac{\frac{E_t}{T_t}}{W_d N_0}\mathbf{H}^H\mathbf{H}\mathbf{B}\mathbf{B}^H\right) \quad \text{(bits/s)}. \tag{6.1}$$

Time-division duplex (TDD):

On the other hand, the TDD scheme makes use of the complete bandwidth to transmit either data or feedback information. The scheduling is performed in the time domain, i.e., there are time slots where all the bandwidth is devoted to sending data and in the other time slots all the bandwidth is dedicated to the feedback link, as depicted in Figure 6.2.

Note that in the literature it is sometimes assumed that in TDD systems there is channel reciprocity and, therefore, feedback is not required. In practical systems, however, the Radio Frequency (RF) chains (with the high power amplifiers and the mixers), have a different response for transmission and for reception which makes the

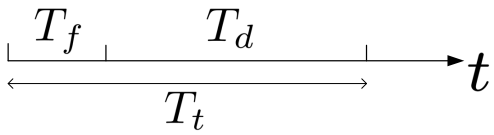

Figure 6.2: TDD system model.

global channel response be non-reciprocal. There are two solutions to this issue: one option is to do feedback of the CSI (which includes obviously the effect of the RF chain) and the other option is to perform a calibration of the RF chains for transmission and for reception. The calibration of the RF chains is an expensive and technologically complex process that includes additional hardware at both transmitter and receivers and high quality RF chains, which increases the cost of the terminals significantly. Currently, such calibration is not implemented in conventional terminals and, thus, is not considered in this dissertation.

In a TDD system, the maximum achievable data rate is given by the following expression:

$$R_d = \frac{T_d}{T_t} W_t \mathsf{log_2det}\left(\mathbf{I} + \frac{\frac{E_t}{T_d}}{W_t N_0}\mathbf{H}^H\mathbf{H}\mathbf{B}\mathbf{B}^H\right) \quad \text{(bits/s)}. \tag{6.2}$$

General expression:

As observed in (6.1) and (6.2), the expressions of the data rate for both TDD and FDD are dual, and they behave exactly the same as a function of variables T_d and W_d, respectively. It is possible to jointly formulate this dependance (based on (6.1) and (6.2)) as:

$$R_d = \frac{T_d}{T_t}\frac{W_d}{W_t} W_t \mathsf{log_2det}\left(\mathbf{I} + \frac{E_t}{T_t W_t N_0}\frac{1}{\frac{T_d}{T_t}\frac{W_d}{W_t}}\mathbf{H}^H\mathbf{H}\mathbf{B}\mathbf{B}^H\right) \quad \text{(bits/s)} \tag{6.3}$$

The case where $T_d = T_t$ corresponds to FDD, and $W_d = W_t$ corresponds to TDD.

Expression (6.3), normalized to the bandwidth, can also be written as:

$$\frac{R_d}{W_t} = \alpha \mathsf{log_2det}\left(\mathbf{I} + \frac{snr}{\alpha}\mathbf{H}^H\mathbf{H}\mathbf{B}\mathbf{B}^H\right) \quad \text{(bits/s/Hz)}, \tag{6.4}$$

where $\alpha = \frac{T_d}{T_t}\frac{W_d}{W_t}$ $(0 \leq \alpha \leq 1)$ and $snr = \frac{E_t}{T_t W_t N_0}$.

6.3 Tradeoff between CSI estimation, feedback, and data transmission

This section presents a more detailed description and provides further insight into the problem of radio resource allocation in MIMO wireless systems with feedback. A two-way MIMO communication link with feedback is considered, where two users communicate following a TDD scheme[1] with given transceiver and feedback design criteria. Under these conditions, the accuracy of the CSI at the transmitter depends on: (i) the power and duration of the training phase devoted to channel estimation at the receiver, (ii) the power and duration of the feedback phase related to the quantization of such channel estimate, (iii) the errors produced in the feedback communication, and (iv) the delays associated to the CSI estimation and feedback transmission. The communication performance depends not only on the accuracy of the CSI at the transmitter, but also on the resources allocated to the data transmission phase. In this sense, a tradeoff exists, since if more resources are allocated to training and feedback, then the accuracy of the CSI increases, but less resources are available for transmission of data. This chapter presents a general formulation of such tradeoff taking into account all the parameters associated to the radio resource allocation.

An optimization problem is presented in terms of power and duration associated to the training, feedback, and data transmission phases. Furthermore, the effect of the tradeoff on the base band energy consumption [Ros10] is also modeled and analyzed in terms of its variation with respect to the resource allocation.

[1]For clarity in the notation only the case of TDD is presented analytically in this chapter. Note, however, that an equivalent derivation for FDD can be followed straightforwardly. Only the case of TDD is considered here for clarity in the notation.

6.4 System and signal models

For the rest of the chapter a flat fading MIMO channel with 2 half duplex users that communicate with each other using a TDD scheme will be considered. The propagation channels of user 1 and user 2 are denoted by $\mathbf{H}_1 \in \mathbb{C}^{N_2 \times N_1}$ and $\mathbf{H}_2 \in \mathbb{C}^{N_1 \times N_2}$, respectively, where $N_i, i = \{1, 2\}$, denotes the number of antennas of user i, as depicted in Figure 6.3. The correlation in time of the channel is modeled as a first-order Gauss-Markov process such that at time instant $n+1$ the channel response matrix associated to user i is given by:

$$\mathbf{H}_i(n+1) = \rho \mathbf{H}_i(n) + \sqrt{1-\rho^2}\, \mathbf{N}_i(n), \tag{6.5}$$

where matrices $\mathbf{H}_i(0)$ and $\mathbf{N}_i(n)$, $\forall n$ are assumed to be independent and composed of i.i.d. zero-mean complex and circularly symmetric Gaussian entries with unit variance. Consequently, also the components of $\mathbf{H}_i(n)$ follow the same distribution. The time correlation factor ρ models the variability of the channel and depends on the Doppler frequency f_D caused by the movement of the users according to Jakes' model, $\rho = J_0\big(2\pi f_D \tau\big)$ [Ste99], where $J_0(\cdot)$ is the zeroth-order Bessel function of the first kind, f_D denotes the maximum Doppler frequency, and τ corresponds to the channel instantiation interval. Following from (6.5), we have that at instant $n+k$,

$$\mathbf{H}_i(n+k) = \rho^k \mathbf{H}_i(n) + \sqrt{1-\rho^{2k}}\, \widetilde{\mathbf{N}}_i(n+k),\ \forall k > 0, \tag{6.6}$$

where $\widetilde{\mathbf{N}}_i(n+k)$ is composed of i.i.d. zero-mean complex Gaussian entries with unit variance that are independent from $\mathbf{H}_i(n)$.

The communication in each direction over a block of frame length T channel uses is modeled as having three phases: a training phase, where each user sends a training sequence of pilot symbols which are used by the other user to estimate the propagation channel; a feedback phase, where the estimated CSI is fed back to each user; and the data transmission phase, where the CSI is used to design the precoder to transmit the

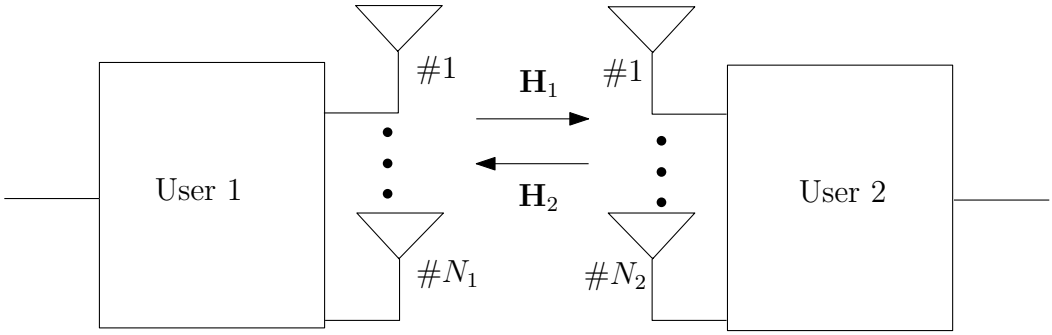

Figure 6.3: System model with 2 users.

communication data.[2] The allocation of power and number of channel uses among these phases and for each user is the objective of this section. The power used by user i to transmit the training symbols and the number of channel uses dedicated to its training phase are denoted by P_{t_i} and T_{t_i}, respectively. In a similar way, the power used by user i to transmit the CSI feedback to the other user and the number of channel uses used in this feedback phase are expressed by P_{f_i} and T_{f_i}, respectively. Finally, the power used by user i for data transmission and the number of channel uses dedicated to this data transmission phase are denoted by P_{d_i} and T_{d_i}, respectively. The structure of the communication scheme described here is depicted in Figure 6.4 for one frame consisting of T channel uses. Note that the depicted phase ordering will be assumed in the rest of the chapter because it minimizes the CSI delays at each side of the communication. However, other phase orderings could be considered without loss of generalization. Also, the proposed notation could be adapted to the case of full-duplex FDD transmission just by changing the duration of the phases by their bandwidths.

[2]The CSI available at the transmitter for the precoding design contains errors derived from the channel estimation process, from the quantization required for the feedback, and errors due to the time delay that these procedures require. Furthermore, the possibility of transmission errors in the feedback link, which translates into incorrect CSI at the transmitter, is also taken into account.

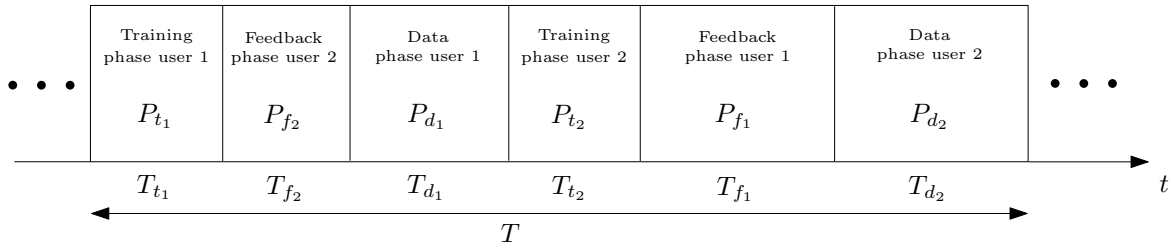

Figure 6.4: Structure of the TDD communication phases for one frame of T channel uses.

6.4.1 Training phase and channel estimation

As previously stated, the propagation channel associated to the transmission from user i, denoted as $\mathbf{H}_i$, is modeled to have independent complex symmetric Gaussian distributed elements with zero mean and unit variance. The channel estimation process results in a channel estimate given by:

$$\mathbf{H}_{\mathbf{e}i} = \mathbf{H}_i - \mathbf{\Delta}_{\mathbf{e}i}; \qquad \mathbf{H}_i = \mathbf{H}_{\mathbf{e}i} + \mathbf{\Delta}_{\mathbf{e}i}, \tag{6.7}$$

where $\mathbf{\Delta}_{\mathbf{e}i}$ is the channel estimation error and $\mathbf{H}_{\mathbf{e}i}$ and $\mathbf{\Delta}_{\mathbf{e}i}$ are independent of each other. Using a MMSE estimator and an orthogonal training sequence, the channel estimation error $\mathbf{\Delta}_{\mathbf{e}i}$ corresponding to user i is known to be also Gaussian distributed (when at least N_i channel uses are employed for the training phase) [Has03], where each element is i.i.d. with zero mean and variance $\sigma_{e_i}^2$. The variance of such estimation noise $\sigma_{e_i}^2$ can be expressed in terms of the SNR of the channel during the estimation process for a unit transmission power, denoted as $\mathrm{SNR}_{h_i} = \frac{1}{\sigma_{n_i}^2}$, where $\sigma_{n_i}^2$ is the Gaussian noise power at the receiver when transmitting from side i to the other side. This leads to a variance of the estimation error given by [Has03]:

$$\sigma_{e_i}^2 = \frac{\mathrm{SNR}_{h_i}^{-1}}{1 + \frac{P_{t_i} T_{t_i}}{N_i}}. \tag{6.8}$$

6.4.2 Feedback phase

There are three factors that degrade the accuracy of the CSI when it is sent through the feedback link. First, the transmission time of the feedback introduces a delay in the CSI availability at the transmitter. Besides, in order to transmit the CSI from the receiver to the transmitter through the limited feedback link, the CSI has to be quantized previously. This introduces a quantization error in the CSI available at the transmitter, and this error depends on the specific quantization scheme employed. Finally, there may be transmission errors during the feedback phase which further degrade the CSI available at the transmitter. In the following, the three sources of error associated to the feedback transmission are modeled in detail.

Error due to delay

Since in the system model considered in this chapter the channel is slowly time varying, there is an additional source of uncertainty in the channel estimation available for the transmitter design. This is due to the delay between the transmission of the training symbols and the use of such CSI at the transmitter. The delay error $\mathbf{\Delta}_{d_i}$ for a given delay μ is described by the following equation:

$$\mathbf{H}_i(n) = \mathbf{H}_i(n-\mu) + \mathbf{\Delta}_{d_i}(\mu). \tag{6.9}$$

The estimated channel of user i, denoted by $\mathbf{H}_{\mathbf{e}i}$, is modeled as corresponding to the instant in the middle of the training phase and we model the actual channel $\mathbf{H}_i$ during the data transmission phase as the channel in the middle of such phase. Consequently, the delay between each acquisition of the channel estimate and the posterior use of this channel estimate in the data transmission phase is $\mu_{d1} = \frac{T_{t_1}}{2} + T_{f_2} + \frac{T_{d_1}}{2}$ for user 1 and $\mu_{d2} = \frac{T_{t_2}}{2} + T_{f_1} + \frac{T_{d_2}}{2}$ for user 2. Considering the same model for the delay in the CSI used during the feedback phase, it follows that the delay between each acquisition of the channel estimate and the posterior use of this channel estimate for the design

of the precoder in the feedback transmission is $\mu_{f1} = \frac{T_{t_1}}{2} + T_{f_2} + T_{d_1} + T_{t_2} + \frac{T_{f_1}}{2}$ for user 1 and $\mu_{f2} = \frac{T_{t_2}}{2} + T_{f_1} + T_{d_2} + T_{t_1} + \frac{T_{f_2}}{2}$ for user 2.[3]

Quantization error

It has been shown in [Pay09b, Pal03b] that the minimum necessary information for the design of the optimum linear precoder for the usual design criteria is contained in the channel Gram matrix defined as $\mathbf{R}_i = \mathbf{H}_i^H \mathbf{H}_i$ for user i; therefore, in the following, quantization and feedback of the Gram matrix will be assumed, as done in [Mon10, Cha08, SM10b, SM10a, SM12]. This means that only a quantized version of the estimated channel Gram matrix $\mathbf{R}_{\mathbf{e}i}$, denoted by $\mathbf{R}_{\mathbf{eq}_i}$, is available at user i. The quantization introduces a quantization error $\mathbf{\Delta}_{\mathbf{q}_i}$ to the estimated CSI, as modeled by the following equation:

$$\mathbf{R}_{\mathbf{eq}_i} = \mathbf{R}_{\mathbf{e}i} + \mathbf{\Delta}_{\mathbf{q}_i}, \tag{6.10}$$

with $\mathbf{R}_{\mathbf{e}i} = \mathbf{H}_{\mathbf{e}_i}^H \mathbf{H}_{\mathbf{e}i}$.

The quantization error depends on the specific quantization scheme used. Since comparing different quantization schemes is not the focus of this chapter, and in order not to add unnecessary complexity to the analysis of the resource allocation, we assume that the quantization is performed using a uniform quantization of the real and imaginary parts of each element independently as is done for example in [Cha08]. Since the matrix $\mathbf{R}_{\mathbf{e}i}$ is Hermitian and, for user i, it has size $N_i \times N_i$, there are N_i^2 different real elements to be quantized (the real and imaginary parts of the m, n-th element of the matrix, $\forall m < n$ and the real part of the N_i elements of the diagonal). A uniform quantization is then applied to the real and imaginary parts using a quantization step ϵ_{q_i}, where $\epsilon_{q_i} = \frac{\gamma_i}{2^{q_i}}$, q_i is the number of bits, and γ_i is the dynamic range of the quantizer, that is fixed so that overflows in the quantization occur with a

[3] In the feedback phase the CSI is sent using a precoder designed with the CSI available at that moment, and therefore the CSI accuracy during the feedback phase has to be taken into account because it has an effect on the precoder used for the feedback transmission.

probability lower than 0.99. Since there are N_i^2 real elements to be quantized by the receiver, the total number of required quantization bits is given by $n_{b2} = q_1 N_1^2$ at user 2 and $n_{b1} = q_2 N_2^2$ at user 1.

Transmission errors in the feedback link

The transmission errors in the feedback link can be modeled as an outage probability p_{o_i} for the feedback link from user i. In the event of feedback error, the fed back CSI is incorrect and the achievable performance cannot be guaranteed and, therefore, since this section is focused on the evaluation of a lower bound of the worst-case performance in the forward link, it will be assumed to be zero.

During the feedback phase the design of the precoder for feedback transmission is carried out according to the imperfect CSI available at the user performing such feedback, which corresponds to the estimated, quantized, and delayed channel Gram matrix. This means that, if single beamforming is considered for the feedback transmission,[4] the precoding vector for the feedback transmission phase of user i, $\mathbf{b}_{fi}$, is chosen as the eigenvector associated to the largest eigenvalue of the CSI available at the feedback transmitter (the estimated, quantized, and delayed channel Gram matrix), which is denoted by $\mathbf{R}^{(\mathbf{f})}_{\mathbf{edq}_i}$ and formulated in what follows in this subsection. The estimated and delayed propagation matrix $\mathbf{H}^{(\mathbf{f})}_{\mathbf{ed}\,i}(n)$ for the feedback communication can be computed as follows:

$$\mathbf{H}_i(n-\mu_{fi}) \triangleq \mathbf{H}_{\mathbf{e}i}(n-\mu_{fi}) + \mathbf{\Delta}_{\mathbf{e}i}(n-\mu_{fi}); \tag{6.11}$$

$$\mathbf{H}^{(\mathbf{f})}_{\mathbf{ed}\,i}(n) \triangleq \mathbf{H}_{\mathbf{e}i}(n-\mu_{fi}) \tag{6.12}$$

$$= \rho^{-\mu_{fi}}\mathbf{H}_i(n) - \left(\mathbf{\Delta}_{\mathbf{e}i}(n-\mu_{fi}) + \rho^{-\mu_{fi}}\sqrt{1-\rho^{2\mu_{fi}}}\widetilde{\mathbf{N}}_i(n)\right) \tag{6.13}$$

$$= \rho^{-\mu_{fi}}\mathbf{H}_i(n) + \rho^{-\mu_{fi}}\mathbf{\Delta}^{(\mathbf{f})}_{\mathbf{ed}\,i}(n), \tag{6.14}$$

[4]Note that the single beamforming precoding strategy is considered here for simplicity, but any other precoding strategy could also have been used within the proposed model for the feedback transmission.

where $\mathbf{\Delta}^{(\mathbf{f})}_{\mathbf{ed}\,i}(n) = -\left(\rho^{\mu_{fi}}\mathbf{\Delta}_{\mathbf{e}i}(n-\mu_{fi}) + \sqrt{1-\rho^{2\mu_{fi}}}\widetilde{\mathbf{N}}_i(n)\right)$, which is a matrix with i.i.d. elements that are Gaussian distributed with zero mean and variance $\sigma^2_{ed_i} = 1 + \rho^{2\mu_{fi}}(\sigma^2_{e_i} - 1)$.

The estimated and delayed channel Gram matrix, prior to the quantization, is given by:

$$\mathbf{R}^{(\mathbf{f})}_{\mathbf{ed}\,i}(n) \triangleq \mathbf{H}^{(\mathbf{f})\,H}_{\mathbf{ed}\,i}(n)\mathbf{H}^{(\mathbf{f})}_{\mathbf{ed}\,i}(n) \tag{6.15}$$

$$= \rho^{-2\mu_{fi}}\mathbf{H}^H_i(n)\mathbf{H}_i(n) + \rho^{-2\mu_{fi}}\mathbf{H}^H_i(n)\mathbf{\Delta}^{(\mathbf{f})}_{\mathbf{ed}\,i}(n) + \rho^{-2\mu_{fi}}\mathbf{\Delta}^{(\mathbf{f})\,H}_{\mathbf{ed}\,i}(n)\mathbf{H}_i(n) + \rho^{-2\mu_{fi}}\mathbf{\Delta}^{(\mathbf{f})\,H}_{\mathbf{ed}\,i}(n)\mathbf{\Delta}^{(\mathbf{f})}_{\mathbf{ed}\,i}(n), \tag{6.16}$$

and, finally, the CSI available at user i for feedback transmission, which is the estimated, delayed, and quantized channel Gram matrix, is given by:

$$\mathbf{R}^{(\mathbf{f})}_{\mathbf{edq}_i}(n) \triangleq \mathbf{R}^{(\mathbf{f})}_{\mathbf{ed}\,i}(n) + \mathbf{\Delta}_{\mathbf{q}_i}(n) \tag{6.17}$$

$$= \rho^{-2\mu_{fi}}\mathbf{R}_i(n) + \rho^{-2\mu_{fi}}\mathbf{H}^H_i(n)\mathbf{\Delta}^{(\mathbf{f})}_{\mathbf{ed}\,i}(n) + \rho^{-2\mu_{fi}}\mathbf{\Delta}^{(\mathbf{f})\,H}_{\mathbf{ed}\,i}(n)\mathbf{H}_i(n) + \rho^{-2\mu_{fi}}\mathbf{\Delta}^{(\mathbf{f})\,H}_{\mathbf{ed}\,i}(n)\mathbf{\Delta}^{(\mathbf{f})}_{\mathbf{ed}\,i}(n) + \mathbf{\Delta}_{\mathbf{q}_i}(n), \tag{6.18}$$

where $\mathbf{R}_i(n) = \mathbf{H}^H_i(n)\mathbf{H}_i(n)$. Directly from (6.18) follows that:

$$\mathbf{R}_i(n) = \rho^{2\mu_{fi}}\mathbf{R}^{(\mathbf{f})}_{\mathbf{edq}_i}(n) - \mathbf{H}^H_i(n)\mathbf{\Delta}^{(\mathbf{f})}_{\mathbf{ed}\,i}(n) - \mathbf{\Delta}^{(\mathbf{f})\,H}_{\mathbf{ed}\,i}(n)\mathbf{H}_i(n) - \mathbf{\Delta}^{(\mathbf{f})\,H}_{\mathbf{ed}\,i}(n)\mathbf{\Delta}^{(\mathbf{f})}_{\mathbf{ed}\,i}(n) - \rho^{2\mu_{fi}}\mathbf{\Delta}_{\mathbf{q}_i}(n). \tag{6.19}$$

The following scalar is defined: $\mathrm{SNR}_{fi}(n) \triangleq P_{f_i}\mathrm{SNR}_{h_i}\mathbf{b}^H_{fi}\mathbf{R}_i(n)\mathbf{b}_{fi}$. The temporal index n and the user index i will be omitted from now on for clarity reasons. Consequently, SNR_f can be expressed as:

$$\mathrm{SNR}_f \triangleq P_f\mathrm{SNR}_h\mathbf{b}^H_f\mathbf{R}\mathbf{b}_f \tag{6.20}$$

$$= P_f\mathrm{SNR}_h\rho^{2\mu_f}\mathbf{b}^H_f\left(\mathbf{R}^{(\mathbf{f})}_{\mathbf{edq}} - \rho^{-2\mu_f}\mathbf{H}^H\mathbf{\Delta}^{(\mathbf{f})}_{\mathbf{ed}} - \rho^{-2\mu_f}\mathbf{\Delta}^{(\mathbf{f})\,H}_{\mathbf{ed}}\mathbf{H} - \rho^{-2\mu_f}\mathbf{\Delta}^{(\mathbf{f})\,H}_{\mathbf{ed}}\mathbf{\Delta}^{(\mathbf{f})}_{\mathbf{ed}} - \mathbf{\Delta}_{\mathbf{q}}\right)\mathbf{b}_f \tag{6.21}$$

$$= P_f\mathrm{SNR}_f\left(\rho^{2\mu_f}\lambda_{max}\{\mathbf{R}^{(\mathbf{f})}_{\mathbf{edq}}\} - \mathbf{b}^H_f\left(\mathbf{H}^H\mathbf{\Delta}^{(\mathbf{f})}_{\mathbf{ed}} + \mathbf{\Delta}^{(\mathbf{f})\,H}_{\mathbf{ed}}\mathbf{H}\right)\mathbf{b}_f - \mathbf{b}^H_f\left(\mathbf{\Delta}^{(\mathbf{f})\,H}_{\mathbf{ed}}\mathbf{\Delta}^{(\mathbf{f})}_{\mathbf{ed}}\right)\mathbf{b}_f - \rho^{2\mu_f}\mathbf{b}^H_f\mathbf{\Delta}_{\mathbf{q}}\mathbf{b}_f\right). \tag{6.22}$$

The SNR_{f_i} can be written as $\mathrm{SNR}_{f_i} = P_{f_i}\mathrm{SNR}_{h_i}\left(A_{f_i} + B_{f_i} + C_{f_i} + D_{f_i}\right)$ and lower bounded by bounding each of its terms as shown next for user 1:

$$A_{f_1} \triangleq \rho^{2\mu_{f1}}\lambda_{max}\{\mathbf{R}^{(\mathbf{f})}_{\mathbf{edq_1}}\}, \tag{6.23}$$

$$B_{f_1} \triangleq -\mathbf{b}_{f1}^H\left(\mathbf{H}_1^H\mathbf{\Delta}^{(\mathbf{f})}_{\mathbf{ed}\,1} + \mathbf{\Delta}^{(\mathbf{f})H}_{\mathbf{ed}\,1}\mathbf{H}_1\right)\mathbf{b}_{f1} \geq -2\sqrt{\epsilon_{ed_1}\lambda_{max}\{\mathbf{R}_1\}}, \tag{6.24}$$

$$C_{f_1} \triangleq -\mathbf{b}_{f1}^H\left(\mathbf{\Delta}^{(\mathbf{f})H}_{\mathbf{ed}\,1}\mathbf{\Delta}^{(\mathbf{f})}_{\mathbf{ed}\,1}\right)\mathbf{b}_{f1} \geq -N_2\epsilon^2_{ed_1}\left(1+\sqrt{N_1\left(N_1-1\right)}\right), \tag{6.25}$$

$$D_{f_1} \triangleq -\rho^{2\mu_{f1}}\mathbf{b}_{f1}^H\mathbf{\Delta}_{\mathbf{q_1}}\mathbf{b}_{f1} \geq -\rho^{2\mu_{f1}}\epsilon_{q_1}\left(\frac{N_1-1}{N_1}+\sqrt{\frac{N_1\left(N_1-1\right)}{2}}\right), \tag{6.26}$$

where the Gaussian distributed error $\mathbf{\Delta}^{(\mathbf{f})}_{\mathbf{ed}\,i}$ is within the sphere of radius $\|\mathbf{\Delta}^{(\mathbf{f})}_{\mathbf{ed}\,i}\|_F \leq \sqrt{\epsilon_{ed_i}}$ with a probability of p_{g_i}, which has an analytical expression that is derived in appendix 6.A. Since the focus is on the evaluation of a lower bound of the worst-case performance, it will be assumed that when the error is out of this bound the system is in outage and the performance in the data forward link is zero.

Note that by considering a lower bound for B_{f_i} and C_{f_i} independently we are dealing with a bound of the worst-case. The computations that result in the lower bound expressions for B_{f_i}, C_{f_i}, and D_{f_i} are contained in appendix 6.B.

The system is considered to be in feedback outage when the achievable throughput cannot guarantee a successful transmission of the number of bits through the feedback link. Consequently, the outage probability associated to the feedback sent by user i using a bandwidth W_t is given by

$$p_{o_i} = p\left(T_{f_i}W_t\mathsf{log}_2\left(1+P_{f_i}\mathrm{SNR}_{h_i}\mathbf{b}_{fi}^H\mathbf{R}_i\mathbf{b}_{fi}\right) < n_{b_i}\right), \tag{6.27}$$

where $\mathbf{b}_{fi}$ is the beamforming vector used during the feedback transmission from user i (which has a delay of μ_{fi}) and is chosen as the eigenvector associated to the largest eigenvalue[5] of the Gram matrix estimate available at the transmitter, i.e., user i.

[5]The case of single beamforming for the transmission of feedback is considered for the analysis. Note, however, that other transmission schemes could also be assumed following the same process and adapting the presented notation properly.

This means that, with the phase ordering considered in this chapter and depicted in Figure 6.4, $\mathbf{b}_{fi}$ is equal to the precoder used for data transmission in the previous data transmission phase of the corresponding user.

6.4.3 Data transmission phase

In this phase the design of the precoder is carried out according to the imperfect CSI available at the transmitter, which corresponds to the estimated, quantized, and delayed channel Gram matrix. This means that the single beamforming precoding vector for the data transmission phase of user i, $\mathbf{b}_{di}$, is chosen[6] as the eigenvector associated to the largest eigenvalue of the CSI available at the transmitter (the estimated, quantized, and delayed channel Gram matrix), which is denoted by $\mathbf{R}^{(\mathbf{d})}_{\mathbf{edq}_i}$ and formulated in what follows in this subsection. We compute the estimated and delayed propagation matrix for the data transmission phase, $\mathbf{H}^{(\mathbf{d})}_{\mathbf{ed}\,i}(n)$, as follows:

$$\mathbf{H}_i(n-\mu_{di}) \triangleq \mathbf{H}_{\mathbf{e}i}(n-\mu_{di}) + \mathbf{\Delta}_{\mathbf{e}i}(n-\mu_{di}); \tag{6.28}$$

$$\mathbf{H}^{(\mathbf{d})}_{\mathbf{ed}\,i}(n) \triangleq \mathbf{H}_{\mathbf{e}i}(n-\mu_{di}) \tag{6.29}$$

$$= \rho^{-\mu_{di}}\mathbf{H}_i(n) - \left(\mathbf{\Delta}_{\mathbf{e}i}(n-\mu_{di}) + \rho^{-\mu_{di}}\sqrt{1-\rho^{2\mu_{di}}}\widetilde{\mathbf{N}}_i(n)\right) \tag{6.30}$$

$$= \rho^{-\mu_{di}}\mathbf{H}_i(n) + \rho^{-\mu_{di}}\mathbf{\Delta}^{(\mathbf{d})}_{\mathbf{ed}\,i}(n), \tag{6.31}$$

where $\mathbf{\Delta}^{(\mathbf{d})}_{\mathbf{ed}\,i}(n) = -\left(\rho^{\mu_{di}}\mathbf{\Delta}_{\mathbf{e}i}(n-\mu_{di}) + \sqrt{1-\rho^{2\mu_{di}}}\widetilde{\mathbf{N}}_i(n)\right)$, which is a matrix with i.i.d. elements that are Gaussian distributed with zero mean and variance $\sigma^2_{ed_i} = 1+\rho^{2\mu_{di}}(\sigma^2_{e_i}-1)$.

The estimated and delayed channel Gram matrix, prior to the quantization, in the

[6]Note that the single beamforming precoding strategy is considered here for simplicity, but any other precoding strategy could also be considered within the proposed model.

data transmission phase, is given by:

$$\mathbf{R}^{(\mathbf{d})}_{\mathbf{ed}\,i}(n) \triangleq \mathbf{H}^{(\mathbf{d})\,H}_{\mathbf{ed}\,i}(n)\mathbf{H}^{(\mathbf{d})}_{\mathbf{ed}\,i}(n) \tag{6.32}$$

$$= \rho^{-2\mu_{di}}\mathbf{H}_i^H(n)\mathbf{H}_i(n) + \rho^{-2\mu_{di}}\mathbf{H}_i^H(n)\mathbf{\Delta}^{(\mathbf{d})}_{\mathbf{ed}\,i}(n) + \rho^{-2\mu_{di}}\mathbf{\Delta}^{(\mathbf{d})\,H}_{\mathbf{ed}\,i}(n)\mathbf{H}_i(n)$$
$$+\rho^{-2\mu_{di}}\mathbf{\Delta}^{(\mathbf{d})\,H}_{\mathbf{ed}\,i}(n)\mathbf{\Delta}^{(\mathbf{d})}_{\mathbf{ed}\,i}(n), \tag{6.33}$$

and, finally, the CSI available at user i for data transmission, which is the estimated, delayed, and quantized channel Gram matrix, is given by:

$$\mathbf{R}^{(\mathbf{d})}_{\mathbf{edq}_i}(n) \triangleq \mathbf{R}^{(\mathbf{d})}_{\mathbf{ed}\,i}(n) + \mathbf{\Delta}_{\mathbf{q}_i}(n) \tag{6.34}$$

$$= \rho^{-2\mu_{di}}\mathbf{R}_i(n) + \rho^{-2\mu_{di}}\mathbf{H}_i^H(n)\mathbf{\Delta}^{(\mathbf{d})}_{\mathbf{ed}\,i}(n) + \rho^{-2\mu_{di}}\mathbf{\Delta}^{(\mathbf{d})\,H}_{\mathbf{ed}\,i}(n)\mathbf{H}_i(n)$$
$$+\rho^{-2\mu_{di}}\mathbf{\Delta}^{(\mathbf{d})\,H}_{\mathbf{ed}\,i}(n)\mathbf{\Delta}^{(\mathbf{d})}_{\mathbf{ed}\,i}(n) + \mathbf{\Delta}_{\mathbf{q}_i}(n), \tag{6.35}$$

where $\mathbf{R}_i(n) = \mathbf{H}_i^H(n)\mathbf{H}_i(n)$. Directly from (6.35) follows that:

$$\mathbf{R}_i(n) = \rho^{2\mu_{di}}\mathbf{R}^{(\mathbf{d})}_{\mathbf{edq}_i}(n) - \mathbf{H}_i^H(n)\mathbf{\Delta}^{(\mathbf{d})}_{\mathbf{ed}\,i}(n) - \mathbf{\Delta}^{(\mathbf{d})\,H}_{\mathbf{ed}\,i}(n)\mathbf{H}_i(n) - \mathbf{\Delta}^{(\mathbf{d})\,H}_{\mathbf{ed}\,i}(n)\mathbf{\Delta}^{(\mathbf{d})}_{\mathbf{ed}\,i}(n)$$
$$-\rho^{2\mu_{di}}\mathbf{\Delta}_{\mathbf{q}_i}(n). \tag{6.36}$$

We define the following scalar $\mathrm{SNR}_{di}(n) \triangleq P_{d_i}\mathrm{SNR}_{h_i}\mathbf{b}_{di}^H\mathbf{R}_i(n)\mathbf{b}_{di}$, (as commented previously, the beamforming vector $\mathbf{b}_{di}$ is chosen as the normalized eigenvector associated to the largest eigenvalue of $\mathbf{R}_{\mathbf{edq}_i}(n)$ and, consequently, $\|\mathbf{b}_{di}\| = 1$). The temporal index n and the user index i will be omitted from now on for clarity reasons. Consequently, SNR_d can be expressed as:

$$\mathrm{SNR}_d \triangleq P_d\mathrm{SNR}_h\mathbf{b}_d^H\mathbf{R}\mathbf{b}_d \tag{6.37}$$

$$= P_d\mathrm{SNR}_h\rho^{2\mu_d}\mathbf{b}_d^H\left(\mathbf{R}^{(\mathbf{d})}_{\mathbf{edq}} - \rho^{-2\mu_d}\mathbf{H}^H\mathbf{\Delta}^{(\mathbf{d})}_{\mathbf{ed}} - \rho^{-2\mu_d}\mathbf{\Delta}^{(\mathbf{d})\,H}_{\mathbf{ed}}\mathbf{H} - \rho^{-2\mu_d}\mathbf{\Delta}^{(\mathbf{d})\,H}_{\mathbf{ed}}\mathbf{\Delta}^{(\mathbf{d})}_{\mathbf{ed}}\right.$$
$$\left.-\mathbf{\Delta}_{\mathbf{q}}\right)\mathbf{b}_d \tag{6.38}$$

$$= P_d\mathrm{SNR}_h\left(\rho^{2\mu_d}\lambda_{max}\{\mathbf{R}^{(\mathbf{d})}_{\mathbf{edq}}\} - \mathbf{b}_d^H\left(\mathbf{H}^H\mathbf{\Delta}^{(\mathbf{d})}_{\mathbf{ed}} + \mathbf{\Delta}_{\mathbf{ed}}{}^H\mathbf{H}\right)\mathbf{b}_d\right.$$
$$\left.-\mathbf{b}_d^H\left(\mathbf{\Delta}^{(\mathbf{d})\,H}_{\mathbf{ed}}\mathbf{\Delta}^{(\mathbf{d})}_{\mathbf{ed}}\right)\mathbf{b}_d - \rho^{2\mu_d}\mathbf{b}_d^H\mathbf{\Delta}_{\mathbf{q}}\mathbf{b}_d\right). \tag{6.39}$$

The previous expression can be written as $\mathrm{SNR}_{d_i} = P_{d_i}\mathrm{SNR}_{h_i}\left(A_{d_i}+B_{d_i}+C_{d_i}+D_{d_i}\right)$ and lower bounded by bounding each of its terms as shown next for user 1:

$$A_{d_1} \triangleq \rho^{2\mu_{d1}}\lambda_{max}\{\mathbf{R}^{(\mathbf{d})}_{\mathbf{edq}_1}\}, \tag{6.40}$$

$$B_{d_1} \triangleq -\mathbf{b}_{d1}^H\left(\mathbf{H}_1^H\boldsymbol{\Delta}^{(\mathbf{d})}_{\mathbf{ed}\ 1}+\boldsymbol{\Delta}^{(\mathbf{d})H}_{\mathbf{ed}\ 1}\mathbf{H}_1\right)\mathbf{b}_{d1} \geq -2\sqrt{\epsilon_{ed_1}\lambda_{max}\{\mathbf{R}_1\}}, \tag{6.41}$$

$$C_{d_1} \triangleq -\mathbf{b}_{d1}^H\left(\boldsymbol{\Delta}^{(\mathbf{d})H}_{\mathbf{ed}\ 1}\boldsymbol{\Delta}^{(\mathbf{d})}_{\mathbf{ed}\ 1}\right)\mathbf{b}_{d1} \geq -N_2\epsilon^2_{ed_1}\left(1+\sqrt{N_1\left(N_1-1\right)}\right), \tag{6.42}$$

$$D_{d_1} \triangleq -\rho^{2\mu_{d1}}\mathbf{b}_{d1}^H\boldsymbol{\Delta}_{\mathbf{q}_1}\mathbf{b}_{d1} \geq -\rho^{2\mu_{d1}}\epsilon_{q_1}\left(\frac{N_1-1}{N_1}+\sqrt{\frac{N_1\left(N_1-1\right)}{2}}\right), \tag{6.43}$$

where the Gaussian distributed error $\boldsymbol{\Delta}^{(\mathbf{d})}_{\mathbf{ed}\ i}$ is within the sphere of radius $\|\boldsymbol{\Delta}^{(\mathbf{d})}_{\mathbf{ed}\ i}\|_F \leq \sqrt{\epsilon_{ed_i}}$ with a probability p_{g_i}, which has an analytical expression that is derived in appendix 6.A. Since this section is focused on the evaluation of a lower bound of the worst-case performance, it will be assumed that when the error is out of this bound the system is in outage and the performance corresponding to the data transmission phase is zero.

Note that by considering a lower bound for B_{d_i} and C_{d_i} independently we are dealing with a bound of the worst-case. The computations that result in the expressions for B_{d_i}, C_{d_i} and D_{d_i} are contained in appendix 6.B.

6.5 Problem statement

The objective is to optimize a generic cost function g that measures the system performance given a total frame length T and a total energy constraint per user, E_1 and E_2, respectively. The optimization variables are the time duration and power associated to each phase of each user.

$$\max_{\left\{T_{t_i},T_{f_i},T_{d_i},P_{t_i},P_{f_i},P_{d_i},\epsilon_{ed_i},q_i\right\}_{i=\{1,2\}}} \quad g\left(\left\{T_{t_i},T_{f_i},T_{d_i},P_{t_i},P_{f_i},P_{d_i},\epsilon_{ed_i},q_i\right\}_{i=\{1,2\}}\right) \tag{6.44}$$

$$\text{s.t.:} \quad T_{t_1}+T_{f_1}+T_{d_1}+T_{t_2}+T_{f_2}+T_{d_2}=T \tag{6.45}$$

$$T_{t_i}P_{t_i}+T_{f_i}P_{f_i}+T_{d_i}P_{d_i}=E_i=TP_i;\ \ i=\{1,2\}$$

$$\epsilon_{ed_i}>0;\ \ i=\{1,2\} \tag{6.46}$$

$$q_i\in\mathcal{N};\ \ i=\{1,2\} \tag{6.47}$$

Note that the parameter q_i is related directly to n_{b_i} and ϵ_{q_i} as described in section 6.4.2. The case in which the cost function is the worst-case average two-way achievable communication rate with single beamforming is studied next.[7] In the following, a lower bound of such rate is presented. Note that the precoding design of single beamforming is chosen for simplicity reasons, since the focus of this chapter is on the resource allocation scheme itself and not on a particular transceiver design. Other transceiver designs such as multiple-streams with waterfilling-like power allocation to maximize capacity could also be studied following the same procedure.

Therefore, considering a block length of T time slots (denoted as $n=1,...,T$) as depicted in Figure 6.4 and a bandwidth W_t, the mean data throughput for user 1 is given by:

$$\widetilde{g_1}=\frac{T_{d_1}}{T}W_t\mathbb{E}_{\mathbf{H}_1,\mathbf{H}_2}\left\{(1-p_{o_2})\log_2\left(1+P_{d_1}\mathrm{SNR}_{h_1}\mathbf{b}_{d1}^H\mathbf{R}_1^{(d)}\mathbf{b}_{d1}\right)\right\}, \tag{6.48}$$

where $\mathbf{R}_1^{(d)}$ is the channel Gram matrix of the channel from user 1 during the data transmission phase, i.e., $\mathbf{R}_1$ at time instant $n=T_{t_1}+T_{f_2}+\frac{T_{d_1}}{2}$, and p_{o_2} is the probability of outage in the feedback from user 2 given by

$$p_{o_2}=p\left(T_{f_2}W_t\log_2\left(1+P_{f_2}\mathrm{SNR}_{h_2}\mathbf{b}_{f2}^H\mathbf{R}_2^{(f)}\mathbf{b}_{f2}\right)<n_{b_2}\right), \tag{6.49}$$

[7]The worst-case average achievable communication rate is chosen as an example of cost function since it is frequently used to measure system performance. However, other cost functions such as packet error rate or SNR could also be considered following the same procedure described in this chapter.

with $n_{b_2} = q_1 N_1^2$ and $\mathbf{R}_2^{(f)}$ corresponding to the channel from user 2 during the feedback transmission phase, i.e., $\mathbf{R}_2$ at time instant $n = T_{t_1} + \frac{T_{f_2}}{2}$. Expression (6.48) can be lower bounded following the derivations in (6.39)-(6.43) as:

$$\widetilde{g_1} \geq \frac{T_{d_1}}{T} W_t p_{g_1} \mathbb{E}_{\mathbf{H}_1,\mathbf{H}_2} \left\{ (1-p_{o_2}) \log_2 \left(1 + P_{d_1} \mathrm{SNR}_{h_1} \left(\rho^{2\mu_{d1}} \lambda_{max}\{\mathbf{R}_{\mathbf{edq}_1}^{(\mathbf{d})}\} \right.\right.\right.$$
$$-2\sqrt{\epsilon_{ed_1} \lambda_{max}\{\mathbf{R}_1^{(d)}\}} - N_2 \epsilon_{ed_1}^2 \left(1 + \sqrt{N_1 (N_1 - 1)}\right)$$
$$\left.\left.\left. -\rho^{2\mu_{d1}} \epsilon_{q_1} \left(\frac{N_1 - 1}{N_1} + \sqrt{\frac{N_1 (N_1 - 1)}{2}} \right) \right) \right) \right\} = g_1, \tag{6.50}$$

and, in an equivalent manner, expression (6.49) can be upper bounded as:

$$p_{o_2} \leq p \left(T_{f_2} W_t p_{g_2} \log_2 \left(1 + P_{f_2} \mathrm{SNR}_{h_2} \left(\rho^{2\mu_{f2}} \lambda_{max}\{\mathbf{R}_{\mathbf{edq}_2}^{(\mathbf{f})}\} - 2\sqrt{\epsilon_{ed_2} \lambda_{max}\{\mathbf{R}_2^{(f)}\}} \right.\right.\right. \tag{6.51}$$
$$\left.\left.\left. -N_1 \epsilon_{ed_2}^2 \left(1 + \sqrt{N_2 (N_2 - 1)}\right) - \rho^{2\mu_{f2}} \epsilon_{q_2} \left(\frac{N_2 - 1}{N_2} + \sqrt{\frac{N_2 (N_2 - 1)}{2}} \right) \right) \right) < n_{b_2} \right).$$

Following an equivalent development for user 2 results in a throughput given by

$$\widetilde{g_2} = \frac{T_{d_2}}{T} W_t \mathbb{E}_{\mathbf{H}_1,\mathbf{H}_2} \left\{ (1-p_{o_1}) \log_2 \left(1 + P_{d_2} \mathrm{SNR}_{h_2} \mathbf{b}_{d2}^H \mathbf{R}_2^{(d)} \mathbf{b}_{d2} \right) \right\}, \tag{6.52}$$

where $\mathbf{R}_2^{(d)}$ is the channel Gram matrix of the channel from user 2 during the data transmission phase, i.e., $\mathbf{R}_2$ at time instant $n = T - \frac{T_{d_2}}{2}$, and p_{o_1} is the probability of outage in the feedback from user 1 given by

$$p_{o_1} = p \left(T_{f_1} W_t \log_2 \left(1 + P_{f_1} \mathrm{SNR}_{h_1} \mathbf{b}_{f1}^H \mathbf{R}_1^{(f)} \mathbf{b}_{f1} \right) < n_{b_1} \right), \tag{6.53}$$

with $n_{b_1} = q_2 N_2^2$ and $\mathbf{R}_1^{(f)}$ corresponding to the channel from user 1 during the feedback transmission phase, i.e., $\mathbf{R}_1$ at time instant $n = T - T_{d_2} - \frac{T_{f_1}}{2}$. Expression (6.52) can be lower bounded following a similar procedure as in (6.50) as:

$$\widetilde{g_2} \geq \frac{T_{d_2}}{T} W_t p_{g_2} \mathbb{E}_{\mathbf{H}_1,\mathbf{H}_2} \left\{ (1-p_{o_1}) \log_2 \left(1 + P_{d_2} \mathrm{SNR}_{h_2} \left(\rho^{2\mu_{d2}} \lambda_{max}\{\mathbf{R}_{\mathbf{edq}_2}^{(\mathbf{d})}\} \right.\right.\right.$$
$$-2\sqrt{\epsilon_{ed_2} \lambda_{max}\{\mathbf{R}_2^{(d)}\}} - N_1 \epsilon_{ed_2}^2 \left(1 + \sqrt{N_2 (N_2 - 1)}\right)$$
$$\left.\left.\left. -\rho^{2\mu_{d2}} \epsilon_{q_2} \left(\frac{N_2 - 1}{N_2} + \sqrt{\frac{N_2 (N_2 - 1)}{2}} \right) \right) \right) \right\} = g_2, \tag{6.54}$$

and, in an equivalent manner, expression (6.53) can be upper bounded as:

$$p_{o_1} \leq p\left(T_{f_1} W p_{g_1} \mathsf{log}_2\left(1+P_{f_1}\mathrm{SNR}_{h_1}\left(\rho^{2\mu_{f1}}\lambda_{max}\{\mathbf{R}^{(\mathbf{f})}_{\mathbf{edq}_1}\}-2\sqrt{\epsilon_{ed_1}\lambda_{max}\{\mathbf{R}^{(f)}_1\}}\right.\right.\right. \quad (6.55)$$
$$\left.\left.\left.-N_2\epsilon^2_{ed_1}\left(1+\sqrt{N_1\left(N_1-1\right)}\right)-\rho^{2\mu_{f1}}\epsilon_{q_1}\left(\frac{N_1-1}{N_1}+\sqrt{\frac{N_1\left(N_1-1\right)}{2}}\right)\right)\right)<n_{b_1}\right).$$

Observe that, in the transmission model described in Figure 6.4, the design of the transceiver for the data transmission phase of each user is performed with the same available CSI as the design of the transceiver for the following feedback transmission phase of the same user. This means that, if the same transceiver architecture/design criterion is considered for both the transmission of data and feedback information, then the resulting transceiver for the data transmission phase and the following feedback transmission phase of each user is the same, i.e., $\mathbf{b}_{f1} = \mathbf{b}_{d1}$ and $\mathbf{b}_{f2} = \mathbf{b}_{d2}$. Note that if a different phase ordering is considered, this can be adapted accordingly.

This chapter presents an optimization of a lower bound of the total two-way communication rate defined as

$$g = g_1 + g_2. \quad (6.56)$$

6.6 Energy consumption in the base band

The signal processing and decoding required at the receiver to process the received signals also requires a relevant amount of energy [Ros10], which has not been included in the formulation of (6.44)-(6.47). At the transmitter this effect is not so important because the computational complexity is lower and the energy consumption can be assumed negligible [Ros10]. The consumption at the receiver depends greatly on the specific hardware used and is usually modeled in other works such as [Ros10] as an exponential function of the communication rate (other consumption models that are currently being investigated could also be used).

In this section the energy required for the base band signal processing is considered, given the optimization problem presented in section 6.5. For this purpose the energy

consumed in the base band of user i is modeled as:

$$E_{bb_i} = T_{d_j} c_1 c_3^{c_2 R_j}, \tag{6.57}$$

where the constants c_1, c_2, and c_3 are decoder specific, and R_j is the instantaneous transmission rate during user's j data transmission phase lower bounded by $R_j = g_j \frac{T}{T_{d_j}}$.

6.7 Simulations

The performance of the resource allocation is analyzed numerically for different scenarios in this section. The following parameters are considered in the simulations: $\rho = 0.9999$, $N_1 = 3$ antennas, $N_2 = 3$ antennas, a normalized bandwidth ($W_t = 1$), ϵ_{ed_i} such that estimation plus delay error for the data transmission phase is within the sphere of radius $\sqrt{\epsilon_{ed_i}}$ with probability $p_{g_i} = 0.7$, ϵ_{q_i} such that there is no quantization overflow in 99% of the cases, $T = 60$, $E_1 = 400$, and $E_2 = 400$.

6.7.1 Computation of ϵ_{q_i} and the dynamic range of the quantizer for an overflow of 1%

For the computation of ϵ_{q_i}, a system with $T_{t_1} = T_{t_2} = 2$, $P_{t_1} = P_{t_2} = 25$, $\text{SNR}_{h_1} = \text{SNR}_{h_2} = 10$, and $q_1 = q_2 = 4$ quantization bits per element (i.e., $n_{b_1} = n_{b_2} = 32$ bits) is considered.

The numerical simulations averaged over 80000 channel realizations show that, in order to satisfy the constraint, the dynamic range of the quantizer is $\gamma_1 = \gamma_2 = 13.827$, which corresponds to $\epsilon_{q_1} = \epsilon_{q_2} = 0.8642$.

6.7.2 Computation of ϵ_{ed_i} for $p_{g_i} = 0.7$

For the computation of ϵ_{ed_i} a system with $T_{t_1} = T_{t_2} = 2$, $T_{f_1} = T_{f_2} = 10$, $T_{d_1} = T_{d_2} = 18$, $P_{t_1} = P_{t_2} = 25$, $\text{SNR}_{h_1} = \text{SNR}_{h_2} = 10$, and $p_{g_1} = p_{g_2} = 0.7$ is considered. The

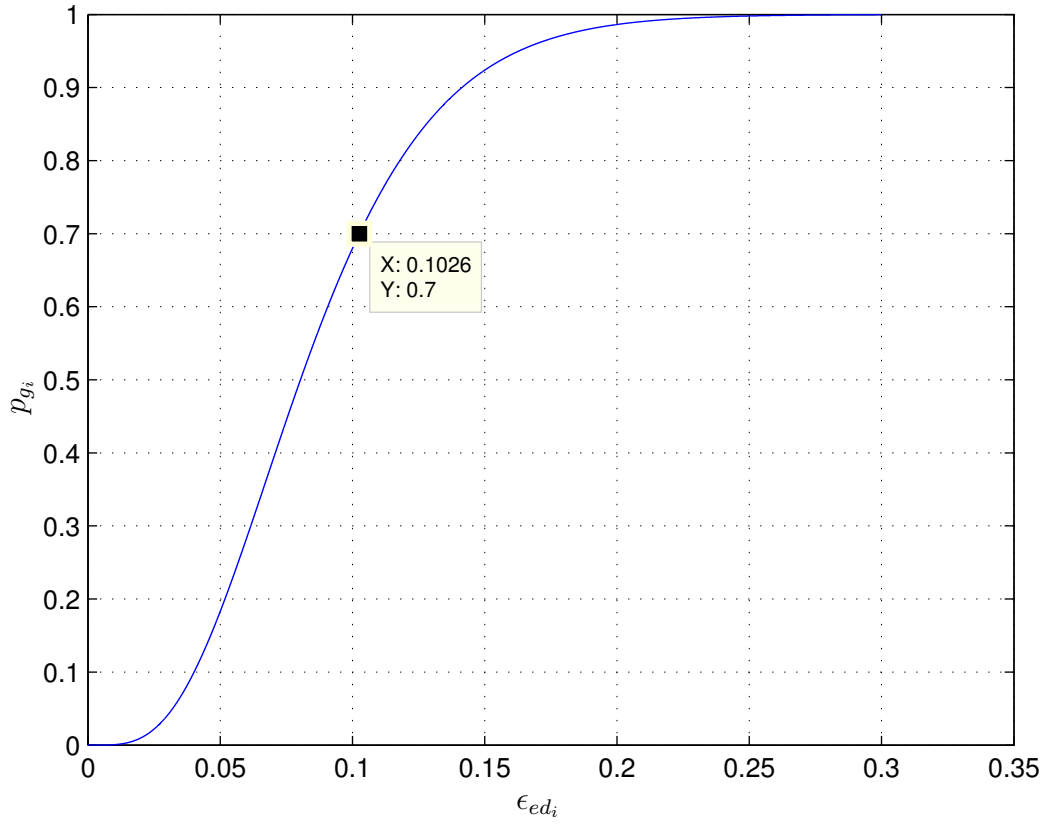

Figure 6.5: Computation of ϵ_{ed_i} for a given probability p_{g_i}.

result of the simulations is represented in Figure 6.5, and shows that the value of ϵ_{ed_i} that corresponds with $p_{g_i} = 0.7$ is $\epsilon_{ed_i} = 0.1026$.

6.7.3 Tradeoff between feedback and data transmission energy

In this subsection the allocation of energy between the feedback and data transmission phases is studied in the scenario considered in the previous simulations and with a fixed training phase power $P_{t_1} = P_{t_2} = 25$. Figure 6.6 shows the system performance g as a function of the power dedicated to the data transmission. Note that if no power is

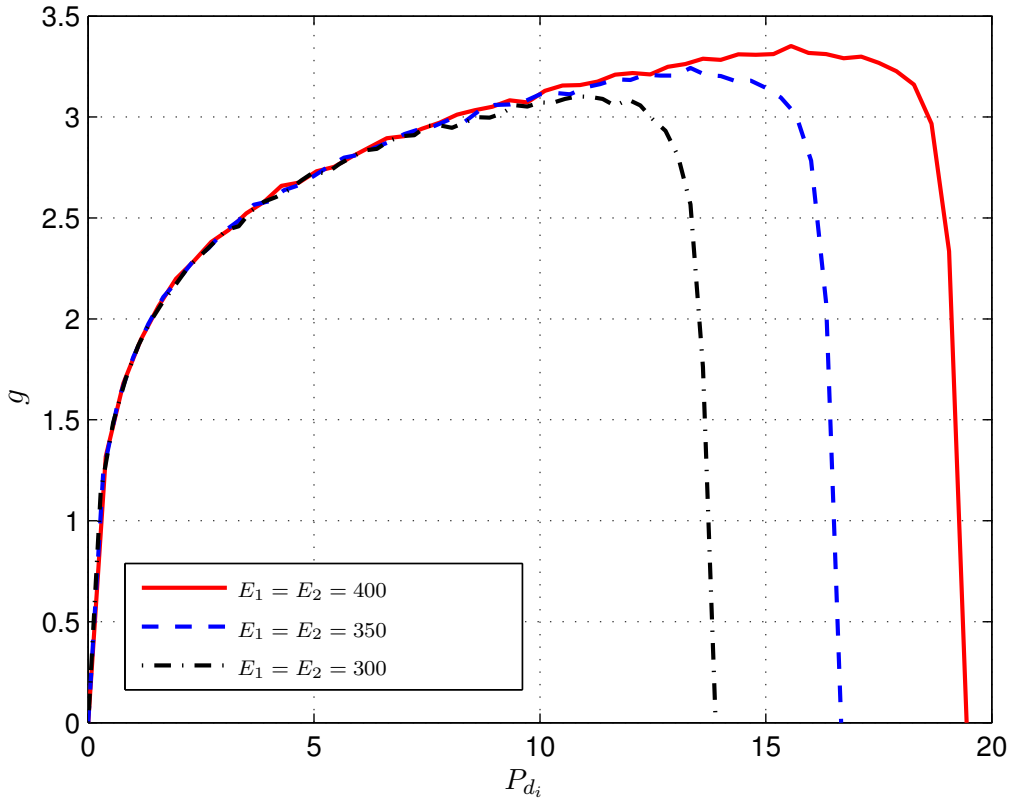

Figure 6.6: Power allocation between training and data transmission phases.

dedicated to data transmission then the performance is zero, and also if all the power is dedicated to data transmission and nothing is used for the transmission of feedback then there is feedback outage and the performance is also zero.

As shown in Figure 6.6, for the case of $E_1 = E_2 = 400$, the optimum allocation is achieved with $P_{d_1} = P_{d_2} = 14.78$, which corresponds to $P_{f_1} = P_{f_2} = 8.396$. This results in a total energy used in the feedback phase of each user equal to $P_{f_i}T_{f_i} = 83.96$, and a total energy used in the data transmission phase of each user equal to $P_{d_i}T_{d_i} = 266.04$.

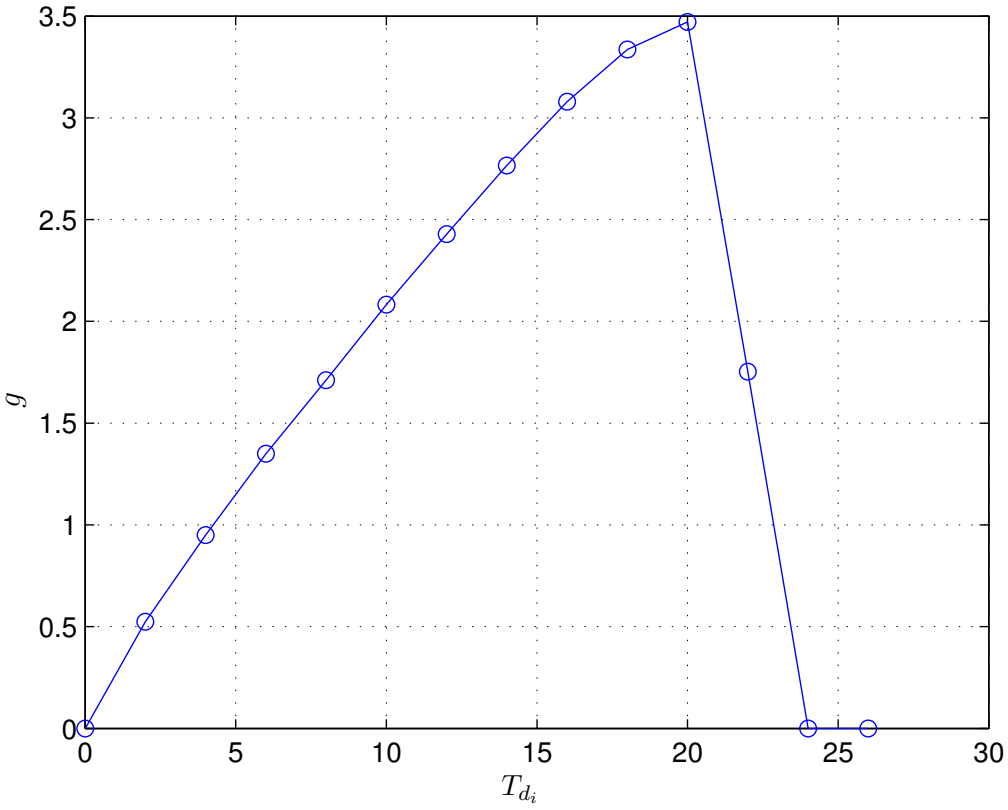

Figure 6.7: Time allocation between training and data transmission phases.

6.7.4 Tradeoff between feedback and data transmission duration

In this subsection the energy allocation between phases is fixed: $P_{t_i}T_{t_i} = 50$, $P_{f_i}T_{f_i} = 83.96$, and $P_{d_i}T_{d_i} = 266.04$. Furthermore, the duration of the training phase is set to $T_{t_1} = T_{t_2} = 2$. In this setup the allocation of time between feedback and training phases is considered, with the additional constraint that $T_{f_1} = T_{f_2}$ and $T_{d_1} = T_{d_2}$. Numerical simulations were conducted and the result is represented in Figure 6.7. The result of the simulations shows that the best performance is achieved when $T_{d_1} = T_{d_2} = 20$.

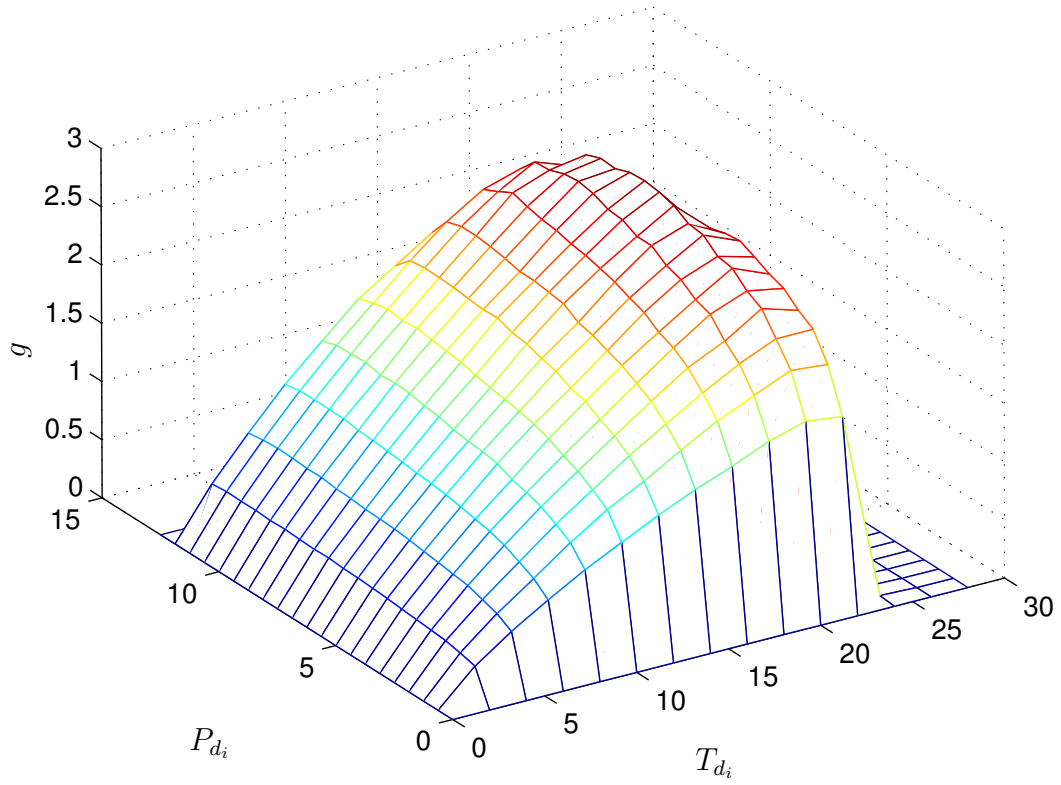

Figure 6.8: Joint time and power allocation between training and data transmission phases.

6.7.5 Joint optimization of feedback and data transmission

In this subsection only the training phase is fixed in advance, with $T_{t_1} = T_{t_2} = 2$ and $P_{t_1} = P_{t_2} = 25$, while both the power and duration of the feedback and data transmission phase are optimized. The result of the simulations is represented in Figure 6.8. The result of the simulations shows that, in the considered scenario, the best performance is achieved when $T_{d_1} = T_{d_2} = 20$ and $P_{d_1} = P_{d_2} = 7.5$.

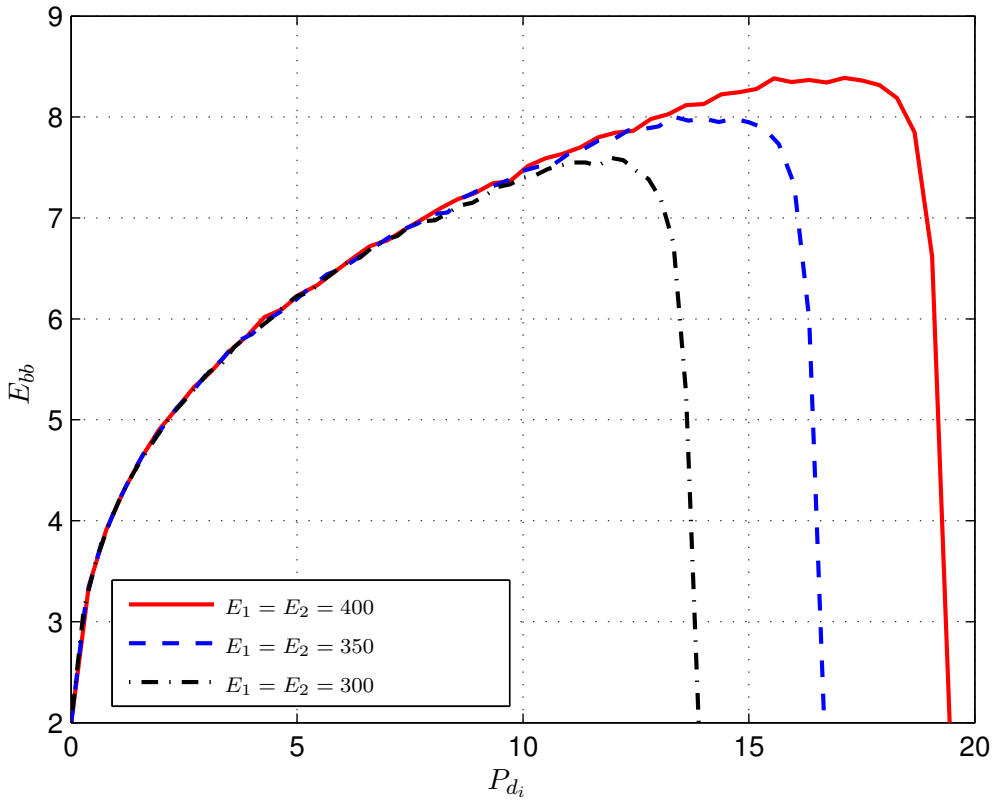

Figure 6.9: Energy consumed in base band as a function of power allocated to the data transmission phase.

6.7.6 Energy consumed in the base band

This subsection evaluates the energy consumed in base band, $E_{bb} = E_{bb_1} + E_{bb_2}$, versus the power allocated to the data transmission phase in the considered scenario following the model presented in section 6.6. For the sake of simplicity, the decoder specific constants considered are $c_1 = c_2 = 1$ and $c_3 = 2$. Note that, since the simulations consider normalized values, the shape of the resulting curve is more relevant than the particular absolute values obtained. The result of the numerical simulations performed is represented in Figure 6.9. It can be observed that the resource allocation that maximizes the performance is also very demanding in terms of E_{bb}.

6.8 Chapter summary and conclusions

This chapter has presented the resource allocation tradeoff between training, feedback, and data transmission phases in a MIMO wireless system with feedback. The system characterization that has been analyzed includes CSI inaccuracies originated in the channel estimation process (training phase), the quantization and feedback transmission process (feedback phase), and also the inaccuracies derived from delay of the CSI available at the transmitter for the precoder design (data transmission phase), and the associated base band energy consumption. It has been shown that, since resources for the feedback transmission come at a cost of resources for the data transmission, there is an optimum resource allocation strategy that maximizes system throughput.

6.A Computation of p_{g_i}

For the performance analysis in this section we considered the case where $\mathbf{\Delta_{ed}}_i$ is within a sphere of radius $\sqrt{\epsilon_{ed_i}}$, i.e., when $\|\mathbf{\Delta_{ed}}_i\|_F^2 \leq \epsilon_{ed_i}$. The probability of this event, denoted as p_{g_i} is derived next.

This probability is expressed as:

$$p_{g_i} \triangleq p\left(\|\mathbf{\Delta_{ed}}_i\|_F^2 \leq \epsilon_{ed_i}\right) = p\left(\sum_{n=1}^{N_1}\sum_{m=1}^{N_2} |[\mathbf{\Delta_{ed}}_i]_{nm}|^2 \leq \epsilon_{ed_i}\right), \tag{6.58}$$

where $[\mathbf{\Delta_{ed}}_i]_{nm}$ is the element n, m of matrix $\mathbf{\Delta_{ed}}_i$. The term $\sum_{n=1}^{N_1}\sum_{m=1}^{N_2} |\,[\mathbf{\Delta_{ed}}_i]_{nm}\,|^2$ follows a chi-square distribution with N_1N_2 degrees of freedom. Consequently p_{g_i} can be determined by the cumulative density function cdf of such term, which is computed as:

$$p_{g_i} = \text{cdf}\left(\frac{\epsilon_{ed_i}}{\sigma_{ed_i}^2}\right) = \frac{\gamma\left(\frac{\epsilon_{ed_i}}{2\sigma_{ed_i}^2}, \frac{N_1N_2}{2}\right)}{\Gamma\left(\frac{N_1N_2}{2}\right)}, \tag{6.59}$$

where the Gamma function is defined as $\Gamma(x) \triangleq \int_0^\infty t^{x-1}e^{-t}\mathrm{d}t$ and the lower incomplete Gamma function is defined as $\gamma(s,x) \triangleq \int_0^s t^{x-1}e^{-t}\mathrm{d}t$.

This can also be written as $p_{g_i} = P\left(\frac{N_1N_2}{2}, \frac{\epsilon_{ed_i}}{2\sigma_{ed_i}^2}\right)$, where $P(x,s) = \frac{\gamma(s,x)}{\Gamma(x)}$ is the cumulative distribution function for Gamma random variables with shape parameter s and scale parameter 1.

6.B Computation of lower bounds for B, C, and D

A lower bound on the term B with a constraint on the error $\mathbf{\Delta_{ed}}$ is computed next. The constraint is that $\|\mathbf{\Delta_{ed}}\|_F \leq \sqrt{\epsilon_{ed}}$, i.e. $\mathbf{\Delta_{ed}}$ is within a sphere of radius $\sqrt{\epsilon_{ed}}$.

$$B \triangleq -\mathbf{b}^H\left(\mathbf{H}^H\mathbf{\Delta_{ed}} + \mathbf{\Delta_{ed}}^H\mathbf{H}\right)\mathbf{b} \tag{6.60}$$

$$= -\text{Tr}\left(\mathbf{b}^H\mathbf{H}^H\mathbf{\Delta_{ed}}\mathbf{b}\right) - \text{Tr}\left(\mathbf{b}^H\mathbf{\Delta_{ed}}^H\mathbf{H}\mathbf{b}\right). \tag{6.61}$$

Using the equality $\mathrm{Tr}\left(\mathbf{ABCD}\right) = \mathrm{vec}\left(\mathbf{D}^H\right)^H \left(\mathbf{C}^T \otimes \mathbf{A}\right) \mathrm{vec}\left(\mathbf{B}\right)$ [Mag02] it follows that

$$-\mathrm{Tr}\left(\mathbf{b}^H\mathbf{H}^H\boldsymbol{\Delta}_{\mathbf{ed}}\mathbf{b}\right) = -\mathbf{b}^H\left(\mathbf{b}^T \otimes \mathbf{H}^H\right)\mathrm{vec}\left(\boldsymbol{\Delta}_{\mathbf{ed}}\right), \tag{6.62}$$

and, since $\mathrm{Tr}\left(\mathbf{b}^H{\boldsymbol{\Delta}_{\mathbf{ed}}}^H\mathbf{Hb}\right) = \mathrm{Tr}\left(\mathbf{b}^H\mathbf{H}^H\boldsymbol{\Delta}_{\mathbf{ed}}\mathbf{b}\right)^H$, it follows that

$$B = -\mathbf{b}^H\mathbf{X}^H\boldsymbol{\delta} - \boldsymbol{\delta}^H\mathbf{Xb}, \tag{6.63}$$

where $\mathbf{X} = \left(\mathbf{b}^T \otimes \mathbf{H}^H\right)^H = \mathbf{b}^* \otimes \mathbf{H}$, and $\boldsymbol{\delta} = \mathrm{vec}\left(\boldsymbol{\Delta}_{\mathbf{ed}}\right)$.

Since B depends linearly on $-\boldsymbol{\delta}$, it is straightforward that the minimization is achieved when $\|\boldsymbol{\delta}\|^2 = \epsilon_{ed}$ (remember the constraint is $\|\boldsymbol{\Delta}_{\mathbf{ed}}\|_F = \|\boldsymbol{\delta}\| \leq \sqrt{\epsilon_{ed}}$).

Then, the vector that minimizes B subject to then norm constraint is $\boldsymbol{\delta}_{\mathbf{wc}} = \sqrt{\epsilon_{ed}}\frac{\mathbf{Xb}}{\|\mathbf{Xb}\|}$, which results in[8]

$$B \geq -2\sqrt{\epsilon_{ed}}\|\mathbf{Xb}\| = -2\sqrt{\epsilon_{ed}}\|\mathrm{vec}\left(\mathbf{Hbb}^H\right)\| = -2\sqrt{\epsilon_{ed}}\|\mathbf{Hbb}^H\| \tag{6.64}$$

$$= -2\sqrt{\epsilon_{ed}}\sqrt{\mathbf{b}^H\mathbf{H}^H\mathbf{Hb}} \geq -2\sqrt{\epsilon_{ed}\lambda_{max}\{\mathbf{H}^H\mathbf{H}\}}. \tag{6.65}$$

A lower bound for C with a constraint on the error $\boldsymbol{\Delta}_{\mathbf{ed}}$ is computed next. The constraint is that $\|\boldsymbol{\Delta}_{\mathbf{ed}}\|_F \leq \sqrt{\epsilon_{ed}}$, i.e. its norm is in a sphere or radius $\sqrt{\epsilon_{ed}}$.

$$C \triangleq -\mathbf{b}^H\left({\boldsymbol{\Delta}_{\mathbf{ed}}}^H\boldsymbol{\Delta}_{\mathbf{ed}}\right)\mathbf{b} \geq -N_2\epsilon_{ed}^2\left(1 + \sqrt{N_1\left(N_1 - 1\right)}\right) \tag{6.66}$$

A lower bound for D with a constraint over the maximum norm of the elements of the quantization error matrix $\boldsymbol{\Delta}_{\mathbf{q}}$ is computed in what follows. The constraint assumes that the quantization is performed using a uniform quantization of the real and imaginary parts of each element independently, as is done for example in [Cha08] (in that work, a multiuser scenario is considered, but the feedback scheme can be applied also to the single-user case). Since the matrix is Hermitian and of size $N_1 \times N_1$, there are N_1^2 different real elements to be quantized (the real and imaginary parts of

[8]Note that in the last step we used the equality $\mathrm{vec}\left(\mathbf{ABC}\right) = \left(\mathbf{C}^T \otimes \mathbf{A}\right)\mathrm{vec}\left(\mathbf{B}\right)$ [Mag02].

the i,j-th element $\forall i < j$ and the real part of the N_1 elements of the diagonal). Consequently, the quantization error is bounded as:

$$-\frac{\epsilon_q}{2} \leq \Im\left\{\delta_{q_{ij}}\right\} \leq \frac{\epsilon_q}{2}, -\frac{\epsilon_q}{2} \leq \Re\left\{\delta_{q_{ij}}\right\} \leq \frac{\epsilon_q}{2}; \forall i \neq j \text{ and } -\frac{\epsilon_q}{2} \leq \delta_{q_{ii}} \leq \frac{\epsilon_q}{2}, \quad (6.67)$$

where $\delta_{q_{ij}}$ is the element i,j of $\mathbf{\Delta_q}$, ϵ_q is the quantization step given by $\epsilon_q = \frac{\gamma}{2^{n_b}}$, γ is the dynamic range taken from the quantization, and n_b is the number of bits used to quantize each element.

$$\begin{aligned}
D &\triangleq -\rho^{2\mu}\mathbf{b}^H\mathbf{\Delta_q}\mathbf{b} \\
&= -\rho^{2\mu}\mathbf{b}^H\mathbf{\Delta_q}\mathbf{b} \\
&= -\rho^{2\mu}\left(-\frac{1}{N_1}\sum_{i=1}^{N_1}\delta_{q_{ii}} + \sum_{i=1}^{N_1}\sum_{j=1}^{N_1} b_i^*\delta_{q_{ij}}b_j\right) \\
&= -\rho^{2\mu}\left(-\sum_{i=1}^{N_1}\Delta_{ii}\left(\frac{1}{N_1} - b_i^*b_i\right) + \sum_{i=1}^{N_1}\sum_{j\neq i}^{N_1} b_i^*\delta_{q_{ij}}b_j\right) \\
&\geq -\rho^{2\mu}\left(\frac{\epsilon_q}{2}\sum_{i=1}^{N_1}\left|\frac{1}{N_1} - |b_i|^2\right| + \left|\sum_{i=1}^{N_1}\sum_{j\neq i}^{N_1} b_i^*\delta_{q_{ij}}b_j\right|\right) \\
&\geq -\rho^{2\mu}\left(\epsilon_q\frac{N_1-1}{N_1} + \sum_{i=1}^{N_1}|b_i|\sum_{j\neq i}^{N_1}\left|\delta_{q_{ij}}b_j\right|\right) \\
&\geq -\rho^{2\mu}\left(\epsilon_q\frac{N_1-1}{N_1} + \sum_{i=1}^{N_1}|b_i|\sqrt{\sum_{j\neq i}^{N_1}\left|\delta_{q_{ij}}\right|^2}\sqrt{\sum_{j\neq i}^{N_1}|b_j|^2}\right) \\
&\geq -\rho^{2\mu}\left(\epsilon_q\frac{N_1-1}{N_1} + \sum_{i=1}^{N_1}|b_i|\,\epsilon_q\sqrt{\frac{N_1-1}{2}}\right) \\
&\geq -\rho_{\text{wc}}^{2\mu}\left(\epsilon_q\frac{N_1-1}{N_1} + \epsilon_q\sqrt{\frac{N_1-1}{2}}\sqrt{\sum_{i=1}^{N_1}|b_i|^2}\sqrt{\sum_{i=1}^{N_1}1}\right) \\
&= -\rho^{2\mu}\epsilon_q\left(\frac{N_1-1}{N_1} + \sqrt{\frac{N_1(N_1-1)}{2}}\right),
\end{aligned}$$

where b_i is the i-th element of vector $\mathbf{b}$, and the Cauchy-Schwarz inequality was used.

Chapter 7

Conclusions and future work

7.1 Conclusions

This dissertation has dealt with the design and optimization of the feedback link in wireless MIMO communications. The CSI required at the transmitter in order to implement an optimum linear precoder has been identified and an appropriate quantization algorithm that exploits the differential geometry of the domain space and the temporal correlation of the propagation channel has been developed. The implementation of a feedback link based on this quantization algorithm has been compared, in terms of overall system performance, with other existing feedback schemes proposed in the literature. This has been done first for the single-user MIMO link, then for two particular multiuser BC setups, and finally the feedback algorithm has been extended to the general multiuser BC scenario through a linear transformation at the receivers. An increase in system performance resulting from the use of the proposed algorithm has been shown by means of numerical simulations, both in point-to-point MIMO scenario and also in the multiuser MIMO BC case. Additionally, and for a given quantization and feedback strategy, the fundamental tradeoff regarding the radio resource allocation between feedback and forward links, and the feedback link sizing have been studied.

Chapter 1 has presented the motivation for this research and the outline of the dissertation and chapter 2 has shown a review of the existing state of the art regarding CSI feedback in MIMO communication systems.

Chapter 3 has focused on the quantization of the MIMO channel Gram matrix for the feedback in the single-user scenario. The quantization algorithm that has been developed exploits the differential geometry of the set of positive definite and Hermitian matrices and also the temporal correlation present in the propagation channel. It has been shown through numerical simulations, in both computer generated and real channels obtained from channel measurements, that a MIMO system featuring the proposed CSI feedback algorithm outperforms other MIMO communication schemes in the literature. Simulations have also revealed that the proposed technique is similarly resilient to feedback delay and feedback transmission errors as other feedback schemes.

Chapter 4 has introduced the multiuser BC scenario for linear transceiver designs based on BD, which is an architecture that presents several advantages specially in environments with heavy interference and reliable CSI. This chapter has presented the application of the channel Gram matrix quantization and feedback scheme to such designs involving BD. It has been shown, by means of numerical simulations, that the performance is better than that of other feedback algorithms. This has been analyzed for the general BD architecture and also for a modified scenario corresponding to a network design in an all-wireless environment in which backhauling and access links coexist using the same frequencies.

Chapter 5 has derived the generalization of the channel Gram matrix feedback scheme for its application in any MIMO BC architecture. This has been achieved through an equivalent channel computation that introduces an additional linear transformation at each receiver and enables the use of the efficient channel Gram matrix feedback per user. Additionally, the propagation of the CSI error inherent to the quantization process has been studied analytically, and this error propagation has been taken into account for the design of a robust precoder. Numerical simulations

have shown that the proposed CSI feedback architecture for the BC also outperforms other feedback techniques.

Finally, chapter 6 has studied the issue of feedback link sizing. The allocation of transmission time, bandwidth, and power among the training, CSI feedback, and data transmission presents a tradeoff in terms of overall system performance. This tradeoff results in a very complex optimization problem that has been analyzed, and the optimum resource allocation has been obtained numerically for a number of particular scenarios. Simulations have revealed the importance of correct feedback link sizing and its effect on the overall system performance.

7.2 Future work

This work opens several issues for future investigation. First, regarding the differential quantization algorithm, the following topics could be extended:

- The analysis of the average and covariance of the geodesic routes could be extended to the case of more than 1 bit of feedback.
- The performance loss introduced by delay and transmission errors in the feedback link could be studied analytically.
- The performance analysis could also be extended for more complex channel models.
- It would be interesting to combine feedback quantization with the design of robust MIMO precoding schemes (i.e., incorporate cost functions that take into account imperfections in the available CSI).
- The optimization of the quantization step could be done analytically for different channel models, or even make the quantization step variable.

Regarding the field of application of CSI feedback, the following future lines of work could be considered:

- The CSI quantization and feedback algorithm could be optimized for cooperative communication schemes, in the modality of virtual MIMO, relaying communications, and network MIMO. The amount of CSI feedback in these type of architectures can be very high and efficient feedback strategies are vital to help to reduce feedback overhead and the size of the control plane.

- A performance evaluation of the behavior of the feedback algorithm in the multiuser MAC could also be carried out.

The topic of feedback link sizing introduced in chapter 6 offers also several interesting possibilities for future work:

- The radio resource allocation could be optimized analytically, taking into account the training and CSI estimation, quantization and feedback, and data transmission phases.

- The tradeoff analysis could be extended using different channel models and the performance evaluation could be implemented using actual channel measurement data.

- The energy consumed in the base band circuits and the energy consumption of different feedback algorithms, which can be related to their complexity, could be taken into account explicitly in the tradeoff analysis and optimization.

- The analysis of the radio resource allocation tradeoff could be extended to more complex system architectures, such as multiuser scenarios, network MIMO, and cooperative MIMO communications, in which the size of the feedback overhead is usually higher and can be a very important factor in the overall system performance.

Bibliography

[Abe07] T. Abe, and G. Bauch, "Differential codebook MIMO precoding technique", *Proc. IEEE Global Communications Conference*, nov. 2007.

[Ala98] S. M. Alamouti, "A simple transmit diversity technique for wireless communications", *IEEE Journal on Selected Areas in Communications*, vol. 16, no. 8, pp. 1451–1458, oct. 1998.

[And07] J. G. Andrews, A. Ghosh, and R. Muhamed, *Fundamentals of WiMAX: Understanding Broadband Wireless Networking*, Prentice Hall, 2007.

[AY09] C. K. Au-Yeung, and D. J. Love, "Optimization and tradeoff analysis of two-way limited feedback beamforming systems", *IEEE Trans. on Wireless Communications*, vol. 8, no. 5, pp. 2570–2579, may 2009.

[BÖ0] H. Bölcskei, and A. J. Paulraj, "Space-frequency coded broadband OFDM systems", *Proc. IEEE Wireless Communications and Networking Conference (WCNC) 2000*, vol. 1, pp. 1–6, set. 2000.

[Ban03a] B. C. Banister, and J. R. Zeidler, "Feedback assisted transmission subspace tracking for MIMO systems", *IEEE Journal on Selected Areas in Communications*, vol. 21, no. 3, pp. 452–463, apr. 2003.

[Ban03b] B. C. Banister, and J. R. Zeidler, "A simple gradient sign algorithm for transmit antenna weight adaptation with feedback", *IEEE Trans. on Signal Processing*, vol. 51, no. 5, pp. 1156–1171, may 2003.

[Bas12] U. Basher, A. Shirazi, and H. Permuter, "Capacity region of finite state multiple-access channel with delayed state information at the transmitters", *IEEE Trans. on Information Theory*, in print 2012.

[Bel05] J. C. Belfiore, G. Rekaya, and E. Viterbo, "The golden code: a 2x2 full-rate space-time code with nonvanishing determinants", *IEEE Trans. on Information Theory*, vol. 51, no. 4, pp. 1432–1436, apr. 2005.

[Ber08] S. Bergman, and B. Ottersten, "Lattice-based linear precoding for MIMO channels with transmitter CSI", *IEEE Trans. on Signal Processing*, vol. 56, no. 7, pp. 2902–2914, jul. 2008.

[Bha02] S. Bhashyam, A. Sabharwal, and B. Aazhang, "Feedback gain in multiple antenna systems", *IEEE Trans. on Communications*, vol. 50, no. 5, pp. 785–798, may 2002.

[Bog11] T. E. Bogale, B. K. Chalise, and L. Vandendorpe, "Robust transceiver optimization for downlink multiuser MIMO systems", *IEEE Trans. on Signal Processing*, vol. 59, no. 1, pp. 446–453, jan. 2011.

[Bog12] T. E. Bogale, and L. Vandendorpe, "Robust sum MSE optimization for downlink multiuser MIMO systems with arbitrary power constraint: generalized duality approach", *IEEE Trans. on Signal Processing*, vol. 6, no. 4, pp. 1862–1875, apr. 2012.

[Bou06] J. J. Boutros, F. Kharrat-Kammoun, and H. Randriambololona, "A classification of multiple antenna channels", *Proc. IEEE International Zurich Seminar on Communications*, feb. 2006.

[Boy04] S. Boyd, and L. Vandenberghe, *Convex Optimization*, Cambridge University Press, 2004.

[Cai10] G. Caire, N. Jindal, M. Kobayashi, and N. Ravindran, "Multiuser MIMO achievable rates with downlink training and channel state feedback", *IEEE Trans. on Information Theory*, vol. 56, no. 6, pp. 2845–2866, jun. 2010.

[Cha07] B. K. Chalise, S. Shahbazpanahi, A. Czylwik, and A. B. Gershman, "Robust downlink beamforming based on outage probability spacifications", *IEEE Trans. on Wireless Communications*, vol. 6, no. 10, pp. 3498–3503, oct. 2007.

[Cha08] Chan-Byoung Chae, D. Mazzarese, N. Jindal, and R. W. Heath, "Coordinated beamforming with limited feedback in the MIMO broadcast channel", *IEEE Journal on Selected Areas in Communications*, vol. 26, no. 8, pp. 1505–1515, oct. 2008.

[Cho02a] J. Choi, "Performance analysis for transmit antenna diversity with/without channel information", *IEEE Trans. on Vehicular Technology*, vol. 51, no. 1, pp. 101–113, jan. 2002.

[Cho02b] J. Choi, "Performance limitation of closed-loop transmit antenna diversity over fast rayleigh fading channels", *IEEE Trans. on Vehicular Technology*, vol. 51, no. 4, pp. 771–775, jul. 2002.

[Cho02c] R. L. Choi, and R. D. Murch, "Transmit MMSE pre-rake pre-processing with simplified receivers for the downlink of MISO TDD-CDMA systems", *Proc. IEEE Global Communications Conference*, pp. 429–433, nov. 2002.

[Cos83] M. Costa, "Writing on dirty paper", *IEEE Trans. on Information Theory*, vol. 29, no. 3, pp. 439–441, may 1983.

[Cov06] T. M. Cover, and J. A. Thomas, *Elements of Information Theory*, Wiley-Interscience, 2006.

[Dab06] A. D. Dabbagh, and D. J. Love, "Feedback rate-capacity loss tradeoff for limited feedback MIMO systems", *IEEE Trans. on Information Theory*, vol. 52, no. 5, pp. 2190–2202, may 2006.

[Ede98] A. Edelman, T. A. Arias, and S. T. Smith, "The geometry of algorithms with orthogonality constraints", *SIAM Journal on Matrix Analysis and Applications*, vol. 20, no. 2, pp. 303–353, oct. 1998.

[Fos96] G. J. Foschini, "Layered space-time architecture for wireless communication in a fading environment when using multi-element antennas", *Bell Labs Technical Journal*, vol. 1, no. 2, pp. 41–59, 1996.

[Fos98] G. J. Foschini, and M. J. Gans, "On limits of wireless communications in a fading environment when using multiple antennas", *Wireless Personal Communications*, vol. 6, no. 3, pp. 311–335, mar. 1998.

[Gan01] G. Ganesan, and P. Stoica, "Space-time block codes: A maximum snr approach", *IEEE Trans. on Information Theory*, vol. 47, no. 4, pp. 1650–1656, may 2001.

[Gan02] G. Ganesan, *Designing space-time codes using orthogonal designs*, PhD Thesis, Uppsala University, Uppsala, Sweden, 2002.

[Gol96] G. H. Golub, and C. F. Van Loan, *Matrix Computations*, The Johns Hopkins University Press, 3rd ed., 1996.

[Gol03] A. Goldsmith, S. A. Jafar, N. Jindal, and S. Vishwanath, "Capacity limits of MIMO channels", *IEEE Journal on Selected Areas in Communications*, vol. 21, no. 5, pp. 684–702, jun. 2003.

[Gol05] A. Goldsmith, *Wireless Communications*, Cambridge University Press, 2005.

[Gol06] A. Goldsmith, *MIMO Wireless Communications*, Cambridge University Press, 2006.

[Has03] B. Hassibi, and B. M. Hochwald, "How much training is needed in multiple antenna wireless links?", *IEEE Trans. on Information Theory*, vol. 49, no. 4, pp. 951–963, apr. 2003.

[Hea09] R. W. Heath, T. Wu, and A. C. K. Soong, "Progressive refinement of beamforming vectors for high-resolution limited feedback", *EURASIP Journal on Advances in Signal Processing*, pp. 1–13, 2009.

[Hor85] R. A. Horn, and C. R. Johnson (eds.), *Matrix Analysis*, Cambridge University Press, 1985.

[Hou06] A. S. Householder, *The Theory of Matrices in Numerical Analysis*, Dover Publications, 2006.

[Hua06a] K. Huang, B. Mondal, R. W. Heath, and J. G. Andrews, "Effect of feedback delay on multi-antenna limited feedback for temporally-correlated channels", *Proc. IEEE Global Communications Conference*, nov. 2006.

[Hua06b] K. Huang, B. Mondal, R. W. Heath, and J. G. Andrews, "Multi-antenna limited feedback for temporally correlated channels: feedback compression", *Proc. IEEE Global Communications Conference*, nov. 2006.

[Hun09] R. Hunger, and M. Johan, "On the asymptotic optimality of block-diagonalization for the MIMO BC under linear filtering", *Proc. International ITG Workshop on Smart Antennas*, feb. 2009.

[iee04] "IEEE 802.16-2004 standard for local and metropolitan area networks part 16: Air interface for fixed broadband wireless access systems", oct. 2004.

[iee05] "IEEE standard for local and metropolitan area networks part 16: Air interface for broadband wireless access systems", 2005.

[Ino09] T. Inoue, and R. W. Heath, "Geodesic prediction for limited feedback multiuser MIMO systems in temporally correlated channels", *Proc. IEEE Radio and Wireless Symposium*, jan. 2009.

[Jae09] S. Jaewoo, and J. M. Cioffi, "Multiuser diversity in a MIMO system with opportunistic feedback", *IEEE Trans. on Vehicular Technology*, vol. 58, no. 7, pp. 4909–4918, nov. 2009.

[Jaf01] S. A. Jafar, S. Vishwanath, and A. Goldsmith, "Channel capacity and beamforming for multiple transmit and receive antennas with covariance feedback", *Proc. IEEE Intl. Conf. on Communications*, jun. 2001.

[Jaf03] H. Jafarkhani, and N. Seshadri, "Super-orthogonal space-time trellis codes", *IEEE Trans. on Information Theory*, vol. 49, no. 4, pp. 937–950, apr. 2003.

[Joh02] M. Joham, K. Kusume, M. H. Gzara, W. Utschick, and J. A. Nossek, "Transmit Wiener filter for the downlink of TDDDS-CDMA systems", *Proc. IEEE International Symposium on Spread-Spectrum Tech. & Appl.*, set. 2002.

[Joh05] M. Joham, W. Utschick, and J. A. Nossek, "Linear transmit processing in MIMO communication systems", *IEEE Trans. on Signal Processing*, vol. 53, no. 8, pp. 2700–2712, aug. 2005.

[Jor03] E. Jorswieck, and H. Boche, "Transmission strategies for the MIMO MAC with MMSE receiver: average MSE optimization and achievable individual

MSE region", *IEEE Trans. on Signal Processing*, vol. 51, no. 11, pp. 2872––2881, nov. 2003.

[Kal08a] F. Kaltenberger, L. Bernardo, and T. Zemen, "Characterization of measured multi-user mimo channels using the spectral divergence measure", Tech. Rep. TD(08) 640, COST 2100, Lille, France, nov. 2008.

[Kal08b] F. Kaltenberger, M. Kountouris, D. Gesbert, and R. Knopp, "Correlation and Capacity of Measured Multi-user MIMO Channels", *Proc. IEEE Intl. Symp. on Personal, Indoor and Mobile Radio Comm. (PIMRC)*, Cannes, France, set. 2008.

[Kal08c] F. Kaltenberger, M. Kountouris, D. Gesbert, and R. Knopp, "Performance of Multi-user MIMO Precoding with Limited Feedback over Measured Channels", *Proc. IEEE Global Communications Conference (IEEE GLOBECOM 2008)*, New Orleans, USA, Nov.–Dec. 2008.

[Kay93] S. M. Kay, *Fundamentals of Statistical Signal Processing: Estimation Theory*, Prentice Hall International, 1993.

[Kim08a] I. H. Kim, and D. J. Love, "On the capacity and design of limited feedback multiuser MIMO uplinks", *IEEE Trans. on Information Theory*, vol. 54, no. 10, pp. 1451–1458, oct. 2008.

[Kim08b] T. Kim, D. J. Love, B. Clerckx, and S. J. Kim, "Differential rotation feedback MIMO system for temporally correlated channels", *Proc. IEEE Global Communications Conference*, pp. 1–6, dec. 2008.

[Kim11] T. Kim, D. J. Love, and B. Clerckx, "MIMO systems with limited rate differential feedback in slowly varying channels", *IEEE Trans. on Communications*, vol. 59, no. 4, pp. 1175–1189, apr. 2011.

[Kob08] M. Kobayashi, G. Caire, and N. Jindal, "How much training and feedback are needed in MIMO broadcast channels?", *Proc. IEEE International Symposium on Information Theory (ISIT'08)*, pp. 2663–2667, jul. 2008.

[Lac07] R. de Lacerda, L. S. Cardoso, R. Knopp, M. Debbah, and D. Gesbert, "EMOS platform: real-time capacity estimation of MIMO channels in the UMTS-TDD band", *Proc. International Symposium on Wireless Communication Systems (IWCS)*, Trondheim, Norway, oct. 2007.

[Lau05] A. J. Laub, *Matrix Analysis for Scientists and Engineers*, SIAM Publications, 2005.

[Lee06] J. Lee, and N. Jindal, "Dirty paper coding vs. linear precoding for MIMO broadcast channels", *Fortieth Asilomar Conference on Signals, Systems and Computers*, pp. 779–783, oct. 2006.

[Lee07] J. Lee, and N. Jindal, "High SNR analysis for MIMO broadcast channels: dirty paper coding versus linear precoding", *IEEE Trans. on Information Theory*, vol. 52, no. 12, pp. 4787–4792, dec. 2007.

[Lo99] T. K. Y. Lo, "Maximum ratio transmission", *IEEE Trans. on Communications*, vol. 47, no. 10, pp. 1458–1461, oct. 1999.

[Lov03] D. J. Love, R. W. Heath, and T. Strohmer, "Grassmannian beamforming for multiple-input multiple-output wireless systems", *IEEE Trans. on Information Theory*, vol. 49, no. 10, pp. 2735–2747, oct. 2003.

[Lov05a] D. J. Love, and R. W. Heath, "Limited feedback unitary precoding for orthogonal space-time block codes", *IEEE Trans. on Signal Processing*, vol. 53, no. 1, pp. 64–73, jan. 2005.

[Lov05b] D. J. Love, R. W. Heath, and T. Strohmer, "Multimode precoding for MIMO wireless systems", *IEEE Trans. on Signal Processing*, vol. 53, no. 10, pp. 3674–3687, oct. 2005.

[Loz02] A. Lozano, and C. B. Papadias, "Layered space-time receivers for frequency-selective wireless channels", *IEEE Trans. on Wireless Communications*, vol. 50, no. 1, pp. 65–73, jan. 2002.

[Lu00] B. Lu, and X. Wang, "Space-time code design in OFDM systems", *Proc. IEEE Global Communications Conference*, vol. 2, pp. 1000–1004, 2000.

[Mag02] J. R. Magnus, and H. Neudecker, *Matrix Differential Calculus with Applications in Statistics and Econometrics*, Wiley, 3$\underline{\text{rd}}$ ed., 2002.

[Mar79] A. W. Marshall, and I. Olkin, *Inequalities: Theory of Majorization and Its Applications*, Academic Press, 1979.

[MN08] E. Martos-Naya, J. F. Paris, U. Fernandez-Plazaola, and A. Goldsmith, "Exact BER analysis for M-QAM modulation with transmit beamforming under channel prediction errors", *IEEE Trans. on Wireless Communications*, vol. 7, no. 10, pp. 3674–3678, oct. 2008.

[Mol11] A. Molisch, *Wireless Communications*, Wiley-IEEE Press, 2011.

[Mon06a] B. Mondal, and R. W. Heath, "Channel adaptive quantization for limited feedback MIMO beamforming systems", *IEEE Trans. on Signal Processing*, vol. 54, no. 12, pp. 4717–4729, dec. 2006.

[Mon06b] B. Mondal, and R. W. Heath, "Performance analysis of quantized beamforming MIMO systems", *IEEE Trans. on Signal Processing*, vol. 54, no. 12, pp. 4753–4766, dec. 2006.

[Mon10] F. A. Monteiro, and I. J. Wassell, "Recovery of a lattice generator matrix from its gram matrix for feedback and precoding in MIMO", *Proc. 4th International Symposium on Communications, Control and Signal Processing (ISCCSP)*, mar. 2010.

[Muk12] A. Mukherjee, and A. L. Swindlehurst, "Modified waterfilling algorithms for MIMO spatial multiplexing with asymmetric CSI", *IEEE Communications Letters*, vol. 1, no. 2, pp. 89–92, apr. 2012.

[NM11] B. Nosrat-Makouei, J. G. Andrews, and R. W. Heath, "MIMO interference alignment over correlated channels with imperfect CSI", *IEEE Trans. on Signal Processing*, vol. 59, no. 6, pp. 2783–2794, jun. 2011.

[Pal03a] D. P. Palomar, *A unified framework for communications through MIMO channels*, PhD Thesis, Universitat Politècnica de Catalunya, Barcelona, Spain, 2003.

[Pal03b] D. P. Palomar, J. M. Cioffi, and M. A. Lagunas, "Joint Tx-Rx beamforming design for multicarrier MIMO channels: a unified framework for convex optimization", *IEEE Trans. on Signal Processing*, vol. 51, no. 9, pp. 2381–2401, set. 2003.

[Pan07] T. Pande, D. J. Love, and J. V. Krogmeier, "Reduced feedback MIMO-OFDM precoding and antenna selection", *IEEE Trans. on Signal Processing*, vol. 55, no. 5, pp. 2284–2293, may 2007.

[Par08] J. M. Paredes, A. B. Gershman, and M. Gharavi-Alkhansari, "A new full-rate full-diversity space-time block code with nonvanishing determinants and simplified maximum-likelihood decoding", *IEEE Trans. on Signal Processing*, vol. 56, no. 6, pp. 2461–2469, jun. 2008.

[Pay07] M. Payaró, A. Pascual-Iserte, and M. Lagunas, "Robust power allocation designs for multiuser and multiantenna downlink communication systems through convex optimization", *IEEE Journal on Selected Areas in Communications*, vol. 25, no. 7, pp. 1390–1401, set. 2007.

[Pay09a] M. Payaró, and D. P. Palomar, "Hessian and concavity of mutual information, differential entropy, and entropy power in linear vector Gaussian channels", *IEEE Trans. on Information Theory*, vol. 55, no. 8, pp. 3613–3628, aug. 2009.

[Pay09b] M. Payaró, and D. P. Palomar, "On optimal precoding in linear vector Gaussian channels with arbitrary input distribution", *Proc. IEEE International Symposium on Information Theory (ISIT'09)*, pp. 1085 – 1089, jul. 2009.

[Pen06a] X. Pennec, "Intrinsic statistics on Riemannian manifolds: basic tools for geometric measurements", *Journal of Mathematical Imaging and Vision*, vol. 25, no. 1, pp. 127–154, jul. 2006.

[Pen06b] X. Pennec, P. Fillard, and N. Ayache, "A Riemannian framework for tensor computing", *International Journal of Computer Vision*, vol. 66, no. 1, pp. 41–66, jan. 2006.

[PI04] A. Pascual-Iserte, A. I. Pérez-Neira, and M. A. Lagunas, "On power allocation strategies for maximum signal to noise and interference ratio in an OFDM-MIMO system", *IEEE Trans. on Wireless Communications*, vol. 3, no. 3, pp. 808–820, may 2004.

[PI05] A. Pascual-Iserte, *Channel state information and joint transmitter-receiver design in multi-antenna systems*, PhD Thesis, Universitat Politècnica de Catalunya, Barcelona, Spain, feb. 2005.

[PI06] A. Pascual-Iserte, D. P. Palomar, A. Pérez-Neira, and M. Lagunas, "A robust maximin approach for MIMO communications with imperfect channel state information based on convex optimization", *IEEE Trans. on Signal Processing*, vol. 54, no. 1, pp. 346–360, jan. 2006.

[Rag07] V. Raghavan, R. W. Heath, and A. M. Sayeed, "Systematic codebook designs for quantized beamforming in correlated MIMO channels", *IEEE Journal on Selected Areas in Communications*, vol. 25, no. 7, pp. 1298 –1310, set. 2007.

[Ral98] G. G. Raleigh, and J. M. Cioffi, "Spatio-temporal coding for wireless communication", *IEEE Trans. on Communications*, vol. 46, no. 3, pp. 357–366, mar. 1998.

[Rav08] N. Ravindran, and N. Jindal, "Limited feedback-based block diagonalization for the MIMO broadcast channel", *IEEE Journal on Selected Areas in Communications*, vol. 26, no. 8, pp. 1473–1482, oct. 2008.

[Roh06] J. C. Roh, and B. D. Rao, "Design and analysis of MIMO spatial multiplexing systems with quantized feedback", *IEEE Trans. on Signal Processing*, vol. 54, no. 8, pp. 2874–2886, aug. 2006.

[Roh07] J. C. Roh, and B. D. Rao, "Efficient feedback methods for MIMO channels based on parameterization", *IEEE Trans. on Wireless Communications*, vol. 6, no. 1, pp. 282–292, jan. 2007.

[Ron05] Y. Rong, S. Shahbazpanahi, and A. Gershman, "Robust linear receivers for space-time block coded multiaccess MIMO systems with imperfect channel state information", *IEEE Trans. on Signal Processing*, vol. 53, no. 8, pp. 3081–3090, aug. 2005.

[Ron06] Y. Rong, S. A. Vorobyov, and A. Gershman, "Robust linear receivers for multiaccess space-time block-coded MIMO systems: a probabilistically constrained approach", *IEEE Journal on Selected Areas in Communications*, vol. 24, no. 8, pp. 1560–1570, aug. 2006.

[Ros10] P. Rost, and G. Fettweis, "On the transmission-computation-energy tradeoff in wireless and fixed networks", *Proc. IEEE Globecom'10*, pp. 1394–1399, dec. 2010.

[Rud86] W. Rudin, *Real and Complex Analysis*, McGraw-Hill Book Company, 1986.

[Sad06] M. A. Sadrabadi, A. K. Khandani, and F. Lahouti, "Channel feedback quantization for high data rate MIMO systems", *IEEE Trans. on Wireless Communications*, vol. 5, no. 12, pp. 3335–3338, dec. 2006.

[Saf04] Z. Safar, and K. J. R. Liu, "Systematic space-time trellis code construction for correlated rayleigh-fading channels", *IEEE Trans. on Information Theory*, vol. 50, no. 11, pp. 2855–2865, nov. 2004.

[Sca02] A. Scaglione, P. Stoica, S. Barbarossa, G. B. Giannakis, and H. Sampath, "Optimal designs for space-time linear precoders and decoders", *IEEE Trans. on Signal Processing*, vol. 50, no. 5, pp. 1051–1064, may 2002.

[She07] Z. Shen, R. Chen, J. G. Andrews, R. W. Heath, and B. L. Evans, "Sum capacity of multiuser MIMO broadcast channels with block diagonalization", *IEEE Trans. on Wireless Communications*, vol. 6, no. 6, pp. 2040–2045, jun. 2007.

[Shi07] S. Shi, M. Schubert, and H. Boche, "Downlink MMSE transceiver optimization for multiuser MIMO systems: duality and sum-MSE minimization", *IEEE Trans. on Signal Processing*, vol. 55, no. 11, pp. 5436–5446, nov. 2007.

[Shi08] S. Shi, M. Schubert, and H. Boche, "Rate optimization for multiuser MIMO systems with linear processing", *IEEE Trans. on Signal Processing*, vol. 56, no. 8, pp. 4020–4030, aug. 2008.

[SM10a] D. Sacristán-Murga, and A. Pascual-Iserte, "Differential feedback of channel Gram matrices for block diagonalized multiuser MIMO systems", *Proc. IEEE Intl. Conf. on Communications*, pp. 1–5, may 2010.

[SM10b] D. Sacristán-Murga, and A. Pascual-Iserte, "Differential feedback of MIMO channel Gram matrices based on geodesic curves", *IEEE Trans. on Wireless Communications*, vol. 9, no. 12, pp. 3714–3727, dec. 2010.

[SM12] D. Sacristán-Murga, M. Payaró, and A. Pascual-Iserte, "Transceiver design framework for multiuser MIMO-OFDM broadcast systems with channel gram matrix feedback", *accepted for publication in IEEE Trans. on Wireless Communications*, 2012.

[Soy09] A. Soysal, and S. Ulukus, "Optimality of beamforming in fading MIMO multiple access channels", *IEEE Trans. on Communications*, vol. 57, no. 4, pp. 1171–1183, apr. 2009.

[Spe04] Q. H. Spencer, A. L. Swindlehurst, and M. Haardt, "Zero-forcing methods for downlink spatial multiplexing in multiuser MIMO channels", *IEEE Trans. on Signal Processing*, vol. 52, no. 2, pp. 461–471, feb. 2004.

[Ste99] R. Steele, and L. Hanzo (eds.), *Mobile Radio Communications*, John Wiley & Sons, 2nd ed., 1999.

[Sto02] P. Stoica, and G. Ganesan, "Maximum-SNR spatial-temporal formatting designs for MIMO channels", *IEEE Trans. on Signal Processing*, vol. 50, no. 12, pp. 3036—-3042, dec. 2002.

[Sun09] H. Sung, S. Lee, and I. Lee, "Generalized channel inversion methods for multiuser MIMO systems", *IEEE Trans. on Communications*, vol. 57, no. 11, pp. 3489–3499, nov. 2009.

[Tal07] M. Talih, "Geodesic Markov chains on covariance matrices", Tech. rep., Statistical and Applied Mathematical Sciences Institute, mar. 2007.

[Tan07] T. Tang, R. W. Heath, S. Cho, and S. Yun, "Opportunistic feedback for multiuser MIMO systems with linear receivers", *IEEE Trans. on Communications*, vol. 55, no. 5, pp. 1020–1032, may 2007.

[Tar98] V. Tarokh, N. Seshadri, and A. R. Calderbank, "Space-time codes for high data rate wireless communication: performance criterion and code construction", *IEEE Trans. on Information Theory*, vol. 44, no. 2, pp. 744–765, mar. 1998.

[Tar99a] V. Tarokh, H. Jafharkani, and A. R. Calderbank, "Space-time block codes from orthogonal designs", *IEEE Trans. on Information Theory*, vol. 45, no. 5, pp. 1456–1467, jul. 1999.

[Tar99b] V. Tarokh, A. Naguib, N. Seshadri, and A. R. Calderbank, "Space-time codes for high data rate wireless communication: Performance criteria in the presence of channel estimation errors, mobility, and multiple paths", *IEEE Trans. on Communications*, vol. 47, no. 2, pp. 199—-207, feb. 1999.

[Tar09] V. Tarokh, H. Jafarkhani, and A. R. Calderbank, "Limited feedback beamforming over temporally-correlated channels", *IEEE Trans. on Signal Processing*, vol. 57, no. 5, pp. 1959–1975, may 2009.

[Tel99] I. E. Telatar, "Capacity of multi-antenna Gaussian channels", *European Trans. on Telecommunications*, vol. 10, no. 6, pp. 585–595, nov. 1999.

[Ten04] A. Tenenbaum, and R. S. Adve, "Joint multiuser transmit-receive optimization using linear processing", *Proc. IEEE Intl. Conf. on Communications*, pp. 588–592, jul. 2004.

[Vuc09] N. Vucić, H. Boche, and S. Shi, "Robust transceiver optimization in downlink multiuser MIMO systems", *IEEE Trans. on Signal Processing*, vol. 57, no. 9, pp. 3576–3587, set. 2009.

[Wan00] Z. Wang, and G. B. Giannakis, "Wireless multicarrier communications", *IEEE Signal Processing Magazine*, vol. 17, no. 3, pp. 29–48, may 2000.

[Wan10] J. Wang, and D. P. Palomar, "Robust MMSE precoding in MIMO channels with pre-fixed receivers", *IEEE Trans. on Signal Processing*, vol. 58, no. 11, pp. 5802–5818, nov. 2010.

[Wei06] H. Weingarten, Y. Steinberg, and S. Shamai, "The capacity region of the Gaussian multiple-input multiple-output broadcast channel", *IEEE Trans. on Information Theory*, vol. 52, no. 9, pp. 3936–3964, set. 2006.

[Wie08] A. Wiesel, Y. C. Eldar, and S. Shamai, "Linear transmit processing in MIMO communication systems", *IEEE Trans. on Signal Processing*, vol. 56, no. 9, pp. 4409–4418, set. 2008.

[Xia09] Y. Xiao, W. Miao, M. Zhao, S. Zhou, and J. Wang, "Limited-feedback modified block diagonalization for multiuser MIMO downlink with time-varying channels", *Proc. IEEE ICC'09*, jun. 2009.

[Yan94] J. Yang, and S. Roy, "On joint transmitter and receiver optimization for multiple-input-multiple-output (MIMO) transmission systems", *IEEE Trans. on Communications*, vol. 42, no. 12, pp. 3221–3231, dec. 1994.

[Yan07] J. Yang, and D. B. Williams, "Transmission subspace tracking for MIMO systems with low-rate feedback", *IEEE Trans. on Communications*, vol. 55, no. 8, pp. 1629–1639, aug. 2007.

[Yu04] W. Yu, and J. M. Cioffi, "Sum capacity of Gaussian vector broadcast channels", *IEEE Trans. on Information Theory*, vol. 50, no. 9, pp. 1875–1892, set. 2004.

[Zha08] X. Zhang, D. P. Palomar, and B. Ottersten, "Statistically robust design of linear MIMO transceivers", *IEEE Trans. on Signal Processing*, vol. 56, no. 8, pp. 3678–3689, aug. 2008.

[Zha09] H. Zhang, D. Yuan, H. Chen, and J. Nossek, "Effects of channel estimation error on array processing based QO-STBC coded OFDM systems", *IEEE Communications Letters*, vol. 13, no. 4, pp. 212 –214, apr. 2009.

[Zho11] B. Zhou, L. Jiang, L. Zhang, C. He, S. Zhao, and L. Lin, "Impact of imperfect channel state information on TDD downlink multiuser MIMO system", *Proc. IEEE Wireless Communications and Networking Conference (WCNC) 2011*, pp. 1823–1828, mar. 2011.